Discovering and Solving Fractional-Order Partial Differential Equations: Machine Learning and Monte Carlo Methods

by

Mamikon Armen Gulian

Sc.M., Brown University, 2015

B.S., University of Maryland, Baltimore Country, 2013

A dissertation submitted in partial fulfillment of the
requirements for the degree of Doctor of Philosophy
in the Department of Mathematics at Brown University

Providence, Rhode Island

2019

This dissertation by Mamikon Armen Gulian is accepted in its present form by the Department of Mathematics as satisfying the dissertation requirement for the degree of Doctor of Philosophy.

Date _____ _____

George Em Karniadakis, Ph.D., Director

Recommended to the Graduate Council

Date _____ _____

Mark Ainsworth, Ph.D., Reader

Date _____ _____

Wei Cai, Ph.D., Reader

Approved by the Graduate Council

Date _____ _____

Andrew G. Campbell, Dean of the Graduate School

Abstract of "Discovering and Solving Fractional-Order Partial Differential Equations: Machine Learning and Monte Carlo Methods" by Mamikon Armen Gulian, Ph.D., Brown University, 2019.

Fractional-order partial differential equations (FPDEs) describe macroscopic properties of systems driven by Lévy processes and, more generally, Continuous-Time Random Walks (CTRWs). CTRWs form a versatile family of abstract stochastic models for *anomalous* diffusion/transport, in which the "actors" at the microscopic scale – be they particles, organisms, or stock prices – do not obey *normal* or *Gaussian* statistics. The fractional-order operators that are required to describe such systems are nonlocal integral operators that pose novel conceptual, theoretical, and numerical challenges for modeling and solution. These challenges are compounded when considering boundary conditions.

Focusing on the most fundamental example – the fractional Laplacian – we consolidate several recent results for nonzero boundary conditions and organize a taxonomy in which the various fractional Laplacians on bounded domains correspond to different ways of imposing boundary conditions on isotropic α-stable Lévy motion. We prove and implement stochastic solution (or Feynman-Kac) formulas for elliptic and parabolic problems involving the spectral fractional Laplacian with Dirichlet boundary conditions. This yields an embarrassingly parallel Monte Carlo method that we demonstrate in solving 16-dimensional benchmark problems. We then develop a Path Integral Monte Carlo method for the many-body fractional Schrödinger equation with periodic boundary conditions. Our methodology opens the door to studying fractional Hamiltonians with arbitrarily complex potentials. We find that the fractional Laplacian strongly encourages particle delocalization, suggesting it may manifest atypical forms of condensation at low temperatures.

We then turn to the problem of data-driven discovery of FPDE models using machine learning. We develop fractional physics-informed Gaussian processes, compatible with Matérn covariance kernels, and demonstrate how they can be used to discover and interpolate a wide variety of linear integer-order and space-fractional PDEs from noisy data in multidimensions. Illustrating several themes of the thesis, we employ our methodology to describe relative stock performance in the S&P 500 by calibrating a fractional Fokker-Planck equation with empirical distribution data.

Curriculum Vitae

Mamikon Gulian graduated in 2009 from Paint Branch High School in Burtonsville, Maryland. He then worked as a research assistant at the Chapman University Advanced Physics Laboratory, assisting in experiments with fiber-optics and superconductors under the direction of his father, Dr. Armen Gulian. Concurrently, with Dr. Gurgen Melkonyan, he worked as a contractor for Honda Research Labs, performing Density-Functional Theory simulations for bulk materials and carbon nanotubes.

In 2010, he enrolled as a Meyerhoff Scholar at the University of Maryland, Baltimore Country (UMBC), majoring in Mathematics. During this time, he traveled to Texas A&M University and Brown University for research. He graduated from UMBC in 2013 as Outstanding Graduating Senior in Mathematics, and earned an NSF Graduate Research Fellowship to study in the Department of Mathematics at Brown University in the same year. Initially, he performed research on partial differential equations and geometric analysis, earning his Sc.M. in Mathematics in 2015. He then began working towards his Ph.D. with Dr. George Em Karniadakis of the Department of Applied Mathematics. He was selected as a Deans' Faculty Fellow at Brown University for 2018-2019, and defended his dissertation on December 21, 2018.

Research Publications and Preprints

(1) "'Stochastic Solution of Elliptic and Parabolic Boundary Value Problems for the Spectral Fractional Laplacian"

(with Guofei Pang).

Preprint, 45 pages.

(2) "Machine Learning of Space-Fractional Differential Equations"

(with Maziar Raissi, Paris Perdikaris, and George Karniadakis).

Submitted to SIAM Journal on Scientific Computing (2018), 25 pages.

(3) "What is the Fractional Laplacian?"

(with Anna Lischke, Guofei Pang, Fangying Song, Christian Glusa, Xiaoning Zheng, Zhiping Mao, Wei Cai, Mark M. Meerschaert, Mark Ainsworth, and George Em Karniadakis).

Submitted to Journal of Computational Physics (2018), 85 pages.

(4) "Fractional Path Integral Monte Carlo"

(with Haobo Yang and Brenda M. Rubenstein).

Submitted to Journal of Chemical Physics (2017), 18 pages.

(5) "Free boundary minimal surfaces in the unit ball with low cohomogeneity"

(with Peter McGrath and Brian Freidin).

Proceedings of the American Mathematical Society, **145** (2017), 1671-1683.

(6) "An ab-initio framework for discovering high-temperature superconductors", (with Gurgen Melkonyan and Sakthisundar Kasthurirengan).
Quantum Studies: Mathematics and Foundations (2017), 1-13.

(7) "Engineering room-temperature superconductors using ab-initio calculations", (with Armen Gulian and Gurgen Melkonyan).
Physics Proceedia, **67** (2015), 963-969.

Acknowledgments

I thank my advisor, George Em Karniadakis, for giving me the opportunity of a lifetime to work alongside him and the rest of his group, and for the valuable direction and help. I thank all my colleagues, past and present, in the CRUNCH group and especially those in the Fractional PDE club – Guofei Pang, Zhiping Mao, Anna Lischke, Xiaoning Zheng, Fangying Song, Christian Glusa, Mark Ainsworth, and many others. I learned a great deal from our discussions and collaborations. I am very grateful to Wei Cai and Mark Ainsworth for serving on my thesis committee along with George. I thank the Department of Applied Mathematics at Brown University for their hospitality in accommodating me while I completed this thesis. I thank Maziar Raissi and Paris Perdikaris for their patience during our collaboration and the invaluable training in machine learning that I gained by working with them. I also thank Mohsen Zayernouri for advice at the start of my research in applied mathematics. I thank the Department of Mathematics, the National Science Foundation, the Army Research Office, and the Graduate School for financial support.

I thank Brenda Rubenstein and Haobo (Jordan) Yang of the Department of Chemistry for our collaboration on the Fractional Path Integral Monte Carlo method. Brenda has provided guidance and help throughout almost the entirety of my research in applied mathematics. Our collaboration taught me many valuable lessons and was an exciting and fruitful start to my thesis research. We thank Jimmie Doll, who initially convened Brenda and I to brainstorm about this project, but did not

live to see the work to its fruition. We also thank Paul Dupuis, Matthew Harrison, and Bryan Clark for valuable discussions. Some of the simulations performed in Chapter 4 used computational resources and services at the Center for Computation and Visualization, Brown University.

I am extremely grateful to Mark M. Meerschaert of Michigan State University, who provided so many valuable and enjoyable discussions about the stochastic aspects of Fractional PDEs which have played such an important role in every chapter of this thesis. I also thank Harbir Antil, Wei Cai, Kavita Ramanan, and Rich Lehoucq for valuable discussions on these topics.

I thank my friends in the Department of Mathematics at Brown University. I extend particular thanks to Peter McGrath and Doreen Pappas, two constant and loyal friends who have never ceased to offer their help and humor. The graduate school at Brown deserves thanks for the many special programs that I participated in, such as the Deans' Fellowship, that contributed to the completion of this thesis. Finally, I thank the many students in the courses I taught for the Department of Mathematics – it was a privilege to be your teacher.

I thank my professors from my undergraduate studies at UMBC – Muddappa Gowda, Muruhan Rathinam, Jon Bell, Thomas Armstrong, Charles Toll, Osman Guler, and others – who helped me develop the mathematical skills which served as a foundation for the research in this thesis. My higher education would never have been possible without the support of the Meyerhoff scholarship program at UMBC. I thank all the founders, staff and fellow Meyerhoff scholars for guidance and support throughout my undergraduate years. I thank my previous research mentors: David Larson, Yunus Zeytuncu, Gurgen Melkonyan, and Justin Holmer. I also thank two high school teachers, David Zeleski and Lisa Blighton, for the education and the encouragement to always think for myself and seek understanding.

I thank my family for their patience and help in all things throughout my many years of education. I owe particular thanks to my father, Armen Gulian, the greatest teacher I have ever had. Finally, I thank God for the good fortune represented by this opportunity, and for the health that allowed me to take it. I dedicate this thesis to my grandmother Lena, who passed away during its writing.

Contents

CHAPTER 1

Introduction and Overview

1.1 The Need for Fractional-Order Partial Differential Equations

The past half-century has seen an exponential growth of data from economic, physical, biological, and social systems that shows signatures of *anomalous* transport and diffusion [**117, 206**]. This refers to systems in which the "actors" at the individual/microscopic level – such as particles, organisms or stock prices – do not obey *normal* or *Gaussian* statistics. For example, pioneering work by Mandelbrot [**141**] and Fama [**73**] in the 1960s demonstrated that changes in certain stock prices are not empirically distributed with Gaussian decay, but rather are distributed according to infinite-variance α-stable Lévy distributions featuring inverse power-law decay. In this case, such behavior can be understood in part as being due to the disproportionate impact of rare events, such as governmental macroeconomic announcements [**21, 222**]. Intuitively, the actors in such systems perform "long jumps" and can be modeled by a class of discontinuous random walks under the heading of *superdiffusion*. In another type of anomalous diffusion known as *subdiffusion*, memory [**64**] or traps (such as in porous media [**24**] or formations of eddies in a fluid [**215, 194, 220**]) may introduce random waiting times that slow down the actors. Many systems (see Table 1) may exhibit both long jumps *and* waiting times. The general stochastic model for such anomalous behavior is the Continuous Time Random Walk (CTRW), a versatile family of anomalous diffusions which satisfy generalized central limit theorems [**148**] that cement their validity in statistical applications.

Theoretical work over the past few decades has shown that Fractional-Order Partial Differential Equations (FPDEs) govern the macroscopic properties of CTRWs [**149**]. Roughly speaking, superdiffusive behavior corresponds to *space-fractional* operators; subdiffusive behavior corresponds to *time-fractional* operators. In the

language of functional analysis, fractional operators are *infinitesimal generators* of appropriate CTRWs; in the language of probability, fractional diffusion equations are Fokker-Planck equations for (non-Fickian) CTRWs [**137, 149**]. Thus, the relationship between CTRWs and FPDEs generalizes the fundamental theory of Einstein [**70**] and Bachelier [**15**] relating Brownian Motion to the (standard) heat equation.

Perhaps the most straightforward way to understand the relation of fractional calculus to stochastic processes is by writing the classical Lévy-Khinchtine theorem in *generator form*. This is discussed in more detail in Section 2.2.4; see also the introduction of Applebaum [**12**]. The Lévy-Khinchtine theorem relates to a general Lévy process, that is, a process X_t which satisfies $X_0 = 0$ and has independent, stationary increments that are continuous in probability. Such a processes is a natural generalization of Brownian motion, without the assumption of finite variance or samples from a normal distribution. With the theory of semigroups, the Lévy-Khinchtine theorem can be interpreted as follows: the Fokker-Planck equation governing such a process X_t must be of the form $\partial_t P = \mathcal{L}P$, where the operator $\mathcal{L}$ is given by a formula

$$Lf(x) = -a \cdot \nabla f(x) + \frac{1}{2}\nabla \cdot Q \nabla f(x) + \int \left(f(x-y) - f(x) + \frac{y \cdot \nabla f(x)}{1+|y|^2} \right) \phi(dy),$$

for a matrix Q and Lévy measure ϕ. This operator may be understood as combination of a first-order drift term, a second order diffusion term, and a *nonlocal* integro-differential operator. Of these, fractional-order operators, such as the fractional Laplacian discussed in this thesis, are the simplest and most fundamental examples. This basic theorem of probability already makes clear that integer-order PDEs, which have been the focus of centuries of mathematical work, are insufficient for describing such a natural class of processes, and that fractional and nonlocal calculus are required to do so.

Phenomena (microscopic)	**Stochastic Model**	**Fractional Model for macroscopic properties**
Long jumps (superdiffusion). Observed in finance [141, 73], econometrics [207], foraging [105], and epidemics [98].	α-stable Lévy flights, a parametrized family of random walks featuring heavy-tailed distributions for increments.	Space fractional: $\frac{\partial P}{\partial t} + (-\Delta)^{\alpha/2} P = 0$
Waiting times (subdiffusion). Observed in porous media [24], subsurface hydrology [152], and pollution [87].	Brownian Motion time-changed by the inverse stable subordinator, a non-decreasing random process with waiting times.	Time fractional: $\frac{\partial^\beta P}{\partial t^\beta} - \Delta P = 0$
Both long jumps and waiting times. Observed in plasmas [227, 84, 63, 53, 229, 19], turbulence [140, 179, 71], and nonequilibirum systems [215],	Continuous Time Random Walk (CTRW), which includes α-stable Lévy motion time changed by inverse stable subordinator.	Space and time fractional: $\frac{\partial^\beta P}{\partial t^\beta} + (-\Delta)^{\alpha/2} P = 0$

TABLE 1. *Left column:* Main feature of anomalous transport, with representative examples from economics, biology, or physical sciences. *Center column:* Stochastic model that simulates the behavior at the microscopic level. *Right column:* Representative fractional equation (in this case, a Fokker-Planck equation) that governs certain macroscopic properties of the stochastic model, hence serves as a model of the phenomena in the left column. These theoretical connections are more fully discussed in [149].

1.2 Monte Carlo Methods for FPDEs

Stochastic solution methods for FPDEs leverage their deep connection to Lévy processes and provide embarrassingly-parallel Monte Carlo algorithms for their solution. The resulting Monte Carlo methods are especially advantageous in high-dimensions and in problems that call for local solutions. Stochastic interpretations also represent a direct, physical approach to understanding and implementing reflecting boundary

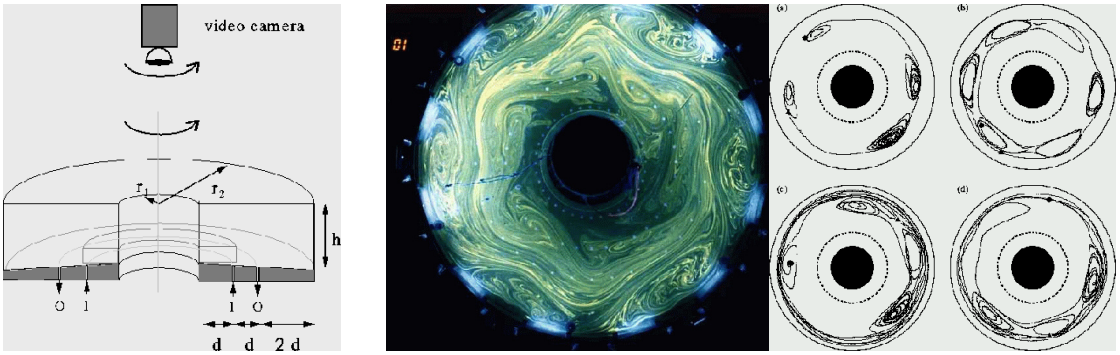

FIGURE 1. *Left:* diagram of the rotating annulus experiment of [194, 220], see also [215] for a discussion. Water flows in through inlets I and out through outlets O while the system rotates. *Center:* photo of fluid (with tracers) in motion. *Right:* illustration of the paths of four sample tracers in the experiment. Two anomalous features are visible: waiting times and long jumps, which are the two signatures of a Continuous Time Random Walk (CTRW). This suggests a *time-and-space-fractional* Fokker-Planck equation $\frac{\partial^\beta P}{\partial t^\beta} + (-\Delta)^{\alpha/2} P = 0$ with reflecting-type boundary conditions governing the transport.

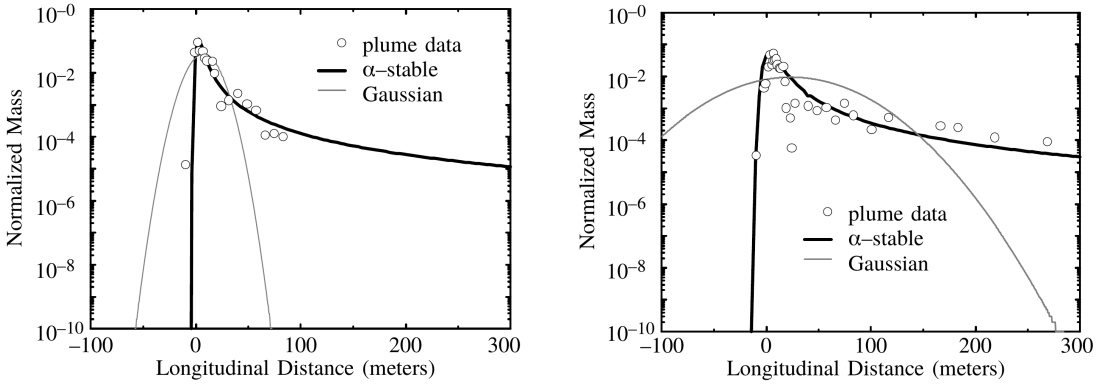

FIGURE 2. This figure is from [24], and shows the fitting of macrodispersion experiments (MADE) at the Columbus Air Force Base in Mississippi. The experiments measured the arrival of tritium tracers downstream from a source point through a highly heterogeneous aquifer consisting of "generally unconsolidated sands and gravels with smaller clay and silt components." Two time snapshots, at day 132 and day 328, are shown. The authors of [24] obtain a superior fit of this data using a space-fractional advection diffusion equation with fractional order $\alpha = 1.1$ (the α-stable model) versus a standard advection-diffusion equation (the Gaussian model).

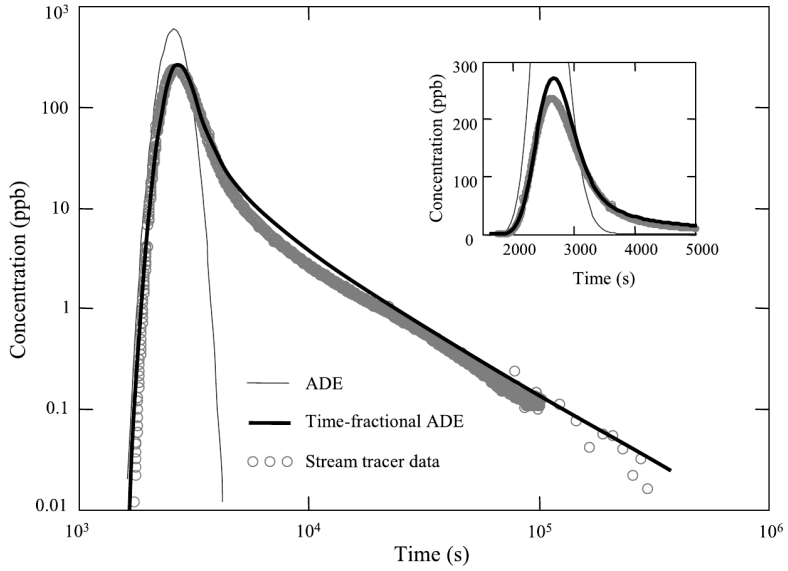

FIGURE 3. This figure is from [190], and shows the utility of time-fractional advection-diffusion in fitting the arrival in time of fluorescent dye 306.4 meters downstream of the injection point in a mountain stream. The stream tracer data is due to experiments reported in [97]. A far superior fit for long time compared to standard advection diffusion (ADE) is obtained for time-fractional order 0.3.

conditions for nonlocal and fractional operators, an area ripe with many open fundamental questions.

In 1944, Kakutani [109] showed that the solution to the classical Dirichlet problem for Laplace's equation at a given point is the expected value of the boundary data over the distribution of exit points of Brownian motion starting at that point. This has been an highly influential work in stochastic processes, and part of this thesis is concerned with developing analogues of these results for the Dirichlet problem for the spectral fractional Laplacian. Classically, such processes are related to Itô processes, but since FPDEs are related to stochastic differential equations (SDEs) driven by Lévy motion rather than Brownian motion, obtaining these stochastic solution formulas represents a fertile area for probability techniques. Such problems also raise

intriguing questions about imposing boundary conditions on Lévy processes, which is also explored in this thesis.

Historically, although high-dimensional partial differential equations frequently arise in finance, perhaps the biggest impact of Monte Carlo methods for partial differential equations is in quantum statistical mechanics. For realistic physical systems, the Schrödinger equation is inherently high-dimensional, rendering grid-based numerical methods useless. This has led to a broad family of widely studied and applicable methods known as Quantum Monte Carlo for studying the many-body problem. Monte Carlo methods based on path integrals for computing quantum mechanical observables, known as Path Integral Monte Carlo, have played an important role in numerical solutions for quantum statistical mechanics. Such methods are facilitated by the path integral formulation of quantum mechanics, in which observables are directly expressed in terms of stochastic integrals. They are based on computing the density matrix rather than the quantum mechanical wavefunction. It was for a related problem in computing thermodynamic equations of state that the term "Monte Carlo" was introduced [**151, 150**]. The Path Integral Monte Carlo method has been used in studies of the time-independent Schrödinger equation [**20, 41**]. It has achieved particular success in studies of liquid helium [**41**].

The fractional Schrödinger equation is no less challenging to solve for many-body systems than the integer-order counterpart. For this reason, despite years of debate about the implications and feasibility of fractional quantum mechanics, no studies have been made of the many-body fractional Schrödinger equation with realistic potentials. In the thesis, we address this problem by developing a Fractional Path Integral Monte Carlo method for studying observables in fractional quantum mechanics (governed by the fractional Schrödinger equation) that is compatible with such potentials.

1.3 Machine Learning of FPDE Models

The past decade has seen huge strides – theoretical and numerical – in the mathematical problems posed by FPDEs in bounded domains with corresponding fractional/nonlocal boundary conditions [**29, 68, 137**]. Yet, these mathematical advances have not been accompanied by a commensurate increase in the use of FPDE models in the many applications where anomalous transport or nonlocality/memory has been recognized. The difficulties of working with unfamiliar fractional operators that involve deep theory, additional parameters, singular integrals, and nonlocal discretizations pose serious challenges to researchers closer to applications. The development of machine learning frameworks for discovering FPDEs has the potential to ameliorate the challenges of deriving and calibrating FPDEs in practice and bridge the gap between mathematical advances in FPDEs and diverse applications.

The potential of machine learning for scientific breakthroughs is already being realized. In the field of inertial confinement fusion, for example, a deep learning algorithm applied to a very large, high-dimensional synthetic dataset by Lawrence Livermore National Laboratory researchers "...led to the discovery of asymmetric implosions that, in simulation, provide high yield and a greater robustness to perturbations than spherical implosions" [**198, 104, 164, 160**]. Across many application fields, given the rapidly increasing availability of data, the combination of machine learning and scientific computing is widely recognized as having strong potential for facilitating discoveries. As proof of this, the architecture of the first exascale supercomputer (*Aurora*) built in the United States, which will be deployed at Argonne National Laboratory in 2021, was developed with three recently designated "pillars" of leadership computing in mind: Simulation, Data, and Learning [**2, 1**].

1.4 Thesis Outline

Chapter 2 provides important theoretical material on fractional Laplacians in bounded domains and related theoretical topics. This material is used throughout the entire thesis. We begin by reviewing the fractional Laplacian in $\mathbb{R}^d$, which we write as $(-\Delta)^{\alpha/2}$ with $\alpha \in (0, 2)$. We briefly summarize the multiple equivalent characterizations of this operator on $\mathbb{R}^d$. This has been a very active area of research in the last decade. Our discussion aims to give a reasonably complete outline of the analytic and probabilistic aspects of this operator.

This sets up the discussion of fractional Laplacians on bounded domains that follows. The different fractional Laplacians on bounded domains arise due to the various characterizations of the fractional Laplacian on $\mathbb{R}^d$ no longer being equivalent, or having more than one generalization to bounded domains. We define these operators and compare how different boundary conditions are incorporated with them. Then, we discuss and compare well-posedness and regularity for the corresponding Poisson problems; many of these results are invoked in the theorems of Chapter 3. We focus on the Riesz and spectral fractional Laplacians, as well as the fractional Laplacian with periodic boundary conditions. These operators, together with the fractional Lapacian on $\mathbb{R}^d$, are the main fractional operators used in the thesis. For example, Monte Carlo methods for the spectral fractional Laplacian are the main focus of Chapter 3; the Riesz fractional Laplacian and periodic boundary conditions are used in the theory of fractional quantum mechanics discussed in Chapter 4; machine learning of equations involving the fractional Laplacian on $\mathbb{R}^d$ is explored in Chapter 5. We also provide very brief discussions of related fractional operators, such as the censored fractional Laplacian as well as alternative operators that arise in fractional vector calculus.

Motivated by the probabilistic connections of the fractional Laplacian to Lévy processes in $\mathbb{R}^d$, we spend a significant portion of this chapter discussing stochastic processes relating to fractional Laplacians on a bounded domain. The stochastic connections clarify the differences between these operators, such as the requirement of nonlocal boundary conditions for the Riesz fractional Laplacian versus the local boundary conditions for the spectral fractional Laplacian, or the harmonic lifting of boundary values for the spectral fractional Laplacian (using the Feynman-Kac formula). Another major focus of this chapter is the recent developments in defining the spectral fractional Laplacian with nonzero boundary conditions. The material relating to these two aspects of the spectral fractional Laplacian – probabilistic and analytic – are leveraged in Chapter 3.

This chapter contains several novel contributions. The stochastic processes relating to various fractional Laplacians on bounded domains have been assembled in one discussion and compared. This is lacking in other surveys in the numerical literature, and provides a physical basis for choosing between the operators in applications. Furthermore, following a review of recently proposed operators by Antil et al. [**11**] and Cusimano et al. [**55**] which generalize the spectral fractional Laplacian to nonzero boundary conditions, we show that both operators are equivalent. We then obtain a third characterization of this operator using the spectral theorem directly for the inverse fractional Laplacian together with a classical representation of the (integer-order) Laplacian. This characterization can be used to justify a weak formulation of boundary value problems for this operator based on nonharmonic lifting. Most of the content of this chapter has appeared in the article [**137**], joint with Anna Lischke, Guofei Pang, Fangying Song, Christian Glusa, Xiaoning Zheng, Zhiping Mao, Wei Cai, Mark M. Meerschaert, Mark Ainsworth, and George Em Karniadakis.

Chapter 3 focuses on Monte Carlo methods for the solution of boundary value problems involving the spectral fractional Laplacian $(-\Delta_{\Omega,g})^{\alpha/2}$ with nonzero Dirichlet boundary condition g. We prove and implement stochastic solution (or Feynman-Kac) formulas for such problems. The main tools used in the proofs are the abstract Cauchy problem for Feller semigroups together with Balakrishnan's theory of fractional powers. We show the operator $(-\Delta_{\Omega,g})^{\alpha/2}$ is the generator of an appropriate Feller semigroup for subordinate stopped Brownian motion

$$X_t^{\Omega,\alpha} = \sqrt{2}B_{T_{\alpha/2}(t)\wedge\tau_\Omega}, \quad \tau_\Omega = \inf\left\{t \;\middle|\; \sqrt{2}B_t \notin \Omega\right\},$$

and obtain a stochastic solution formula

$$u(t,x) = \mathbb{E}_{X_0^{\Omega,\alpha}=x}\left[f\left(X_t^{\Omega,\alpha}\right)\chi_{\tau_\Omega > T_{\alpha/2}(t)} + g\left(X_t^{\Omega,\alpha}\right)\chi_{\tau_\Omega \le T_{\alpha/2}(t)}\right] + \mathbb{E}_{X_0^{\Omega,\alpha}=x}\left[\int_0^t r\left(t-s, X_s^{\Omega,\alpha}\right)\chi_{\tau_\Omega > T_{\alpha/2}(s)}ds\right]$$

for the fractional heat equation in a bounded domain Ω,

$$\begin{cases} \partial_t u(t,x) + (-\Delta_{\Omega,g})^{\alpha/2}u(t,x) = r(x,t) \text{ for } t > 0, x \in \Omega \\ u(0,x) = f(x) \text{ for } x \in \Omega, \quad u(t,x) = g(x) \text{ for } x \in \partial\Omega. \end{cases}$$

Here, τ_Ω denotes (Brownian) exit time from Ω, and $T_{\alpha/2}$ is the standard $\alpha/2$-stable subordinator starting at zero. We then obtain precise regularity and steady-state convergence properties of the above parabolic (time-dependent) problem using the eigenfunction expansion of the classical solution, which leads to estimates for the survival probability of subordinate stopped Brownian motion. These results allow us to take $t \to \infty$ in the stochastic formula for the time-dependent problem to establish

a stochastic solution formula

$$u(x) = \mathbb{E}_{X_0^{\Omega,\alpha}=x}\left[g\left(X^{\Omega,\alpha}_{T^{-1}_{\alpha/2}(\tau_\Omega)}\right)\right] + \mathbb{E}_{X_0^{\Omega,\alpha}=x}\left[\int_0^{T^{-1}_{\alpha/2}(\tau_\Omega)} r\left(X_s^{\Omega,\alpha}\right) ds\right],$$

for the Dirichlet boundary value problem

$$\begin{cases} (-\Delta_{\Omega,g})^{\alpha/2} u(x) = r(x) \text{ for } x \in \Omega \\ u(x) = g(x) \quad \text{for } x \in \partial\Omega. \end{cases}$$

These stochastic solution formulas for the operator $(-\Delta_{\Omega,g})^{\alpha/2}$ (i.e., in the setting of nonzero boundary conditions) are novel, and allow for efficient, embarrassingly parallel local solution of the above boundary value problems. We discuss the discretization of these formulas, and verify them in multiple dimensions with benchmark examples. We study the effect of the number of path samples and the time step size for path discretization on the accuracy of the solution. We demonstrate the favorable scaling of the method with the dimension by computing solutions to time-dependent (parabolic) and time-independent (elliptic) benchmark problems in 16 dimensions. The results of this chapter have appeared in [92], joint with Guofei Pang.

Chapter 4 develops a Path Integral Monte Carlo method for the many-body fractional Schrödinger equation. This equation was introduced by Laskin [128, 129, 130, 131], following the early suggestions of Kac [108]. Starting from the Feynman path integral formulation of quantum mechanics, Laskin showed that replacing integrals over Brownian paths with integrals over α-stable Lévy paths yields a Schrödinger equation in which the ordinary Laplacian in the Hamiltonian is replaced by the Riesz fractional Laplacian. Laskin also showed that this equation enjoys many of the basic properties that allow the usual Schrödinger equation to serve as a foundation for quantum mechanics. For example, since $(-\Delta)^{\alpha/2}$ is self-adjoint, observables are real valued. The fractional Schrödinger equation has subsequently been derived

by Kleinert by taking an appropriate scale-invariant limit of the wave equation in quantum field theory [**119, 118**]. It has been also been suggested that fractional Hamiltonians may naturally arise from strong many body interactions [**119**], and a nonlinear fractional Schrödinger equation in $\mathbb{R}^d$ has been rigorously derived from a mathematical physics perspective as the continuum limit of a system of discrete nonlinear Schrödinger equations with increasingly long-range interactions [**116**].

To date, the fractional Schrödinger equation has been generated significant debate, but solutions have only been studied for a variety of simple, analytically tractable Hamiltonians. A robust algorithm for examining the properties of the many-body fractional Schrödinger equation for arbitrary potentials has been lacking. The Fractional Path Integral Monte Carlo algorithm that we propose can be used to study the finite temperature behavior of the time-independent Fractional Schrödinger equation with periodic boundary conditions.

In developing the algorithm, we derive an analytic form for the finite temperature fractional free particle density matrix and demonstrate how it can be sampled to acquire new sets of particle positions. We employ this algorithm to simulate both the free particle and ^{4}He (Aziz) Hamiltonians. We find that the fractional Laplacian strongly encourages particle delocalization, even in the presence of interactions, suggesting that fractional Hamiltonians may manifest atypical forms of condensation. The work in this chapter opens the door to studying fractional Hamiltonians with arbitrarily complex potentials that escape analytical solutions. This chapter is based on our article [**94**], joint with Haobo Yang and Brenda M. Rubenstein.

Chapter 5 discusses machine learning of space-fractional partial differential equations. Data-driven discovery of "hidden physics" – i.e., machine learning of differential equation models underlying observed data – has recently been approached by embedding the discovery problem into a Gaussian Process regression of spatial data, treating and discovering unknown equation parameters as hyperparameters

of a "physics informed" Gaussian Process kernel [**173**]. This kernel includes the parametrized differential operators applied to a prior covariance kernel. We extend this framework to the data-driven discovery of linear *space-fractional* differential equations. The methodology is compatible with a wide variety of space-fractional operators in $\mathbb{R}^d$ and stationary covariance kernels, including the Matérn class, and allows for optimizing the Matérn parameter during training. The main challenges to be addressed are a user-friendly way to perform fractional-order derivatives of covariance kernels, together with numerical methods that render such implementations feasible. Making use of the simple Fourier-space representation of space-fractional derivatives in $\mathbb{R}^d$, we provide a unified set of integral formulas for the resulting Gaussian Process kernels. The shift property of the Fourier transform results in formulas involving d-dimensional integrals that can be efficiently treated using generalized Gauss-Laguerre quadrature.

The implementation of fractional derivatives within a physics-informed Gaussian process machine learning framework has several benefits. First, the method allows for discovering models involving fractional-order PDEs for systems characterized by heavy tails or anomalous diffusion, while bypassing the analytical difficulty of fractional calculus. Data sets exhibiting such features are of increasing prevalence in physical and financial domains. Second, a single fractional-order archetype allows for a derivative term of arbitrary order to be learned, with the order itself being a parameter in the regression. As a result, even when used for discovering integer-order equations, the proposed method has several benefits compared to previous works on data-driven discovery of differential equations; the user is not required to assume a "dictionary" of derivatives of various orders, and directly controls the parsimony of the models being discovered. We illustrate our method on several examples, including fractional-order interpolation of advection-diffusion and modeling relative stock performance in the S&P 500 with α-stable motion via a fractional diffusion equation.

The results of this chapter have appeared in the article [**93**], joint with Maziar Raissi, Paris Perdikaris, and George Em Karniadakis.

CHAPTER 2

The Fractional Laplacian and Anomalous Diffusion

2.1 Introduction

The fractional Laplacian can be defined in $\mathbb{R}^d$ in many equivalent ways [**124**]; however, when these definitions are restricted to bounded domains, the associated boundary conditions lead to distinct operators. The purpose of this chapter is to give a comprehensive report of the commonly used definitions of the fractional Laplacian and examine their differences in bounded domains. The work in this chapter, especially the discussion of stochastic interpretations of the different operators, will be of use to practitioners looking to gain insight into which fractional Laplacian definition and associated numerical methods may be appropriate for their application.

A number of articles which include comparisons of the different fractional Laplacians on bounded domains have appeared recently, such as those of Bonito et al. [**29**], Duo et al. [**68**], and Čiegis et al. [**51**]. The discussion here differs from these in that there is a focus on recent advances in boundary value problems with *nonzero* boundary conditions and the *inhomogeneous* fractional operators that such problems entail. In addition to a review of the theoretical advances in this area, we include a number of new results. In Section 2.7, we show the equivalence of recently proposed definitions of [**11**] and [**55**] for the inhomogeneous spectral fractional Laplacian, and we provide a new equivalent characterization via the *inverse* Laplacian. The equivalence of these approaches allows us to conclude that the problem of defining the inhomogeneous *spectral* fractional Laplacian, and posing boundary value problems with it, has largely been solved. These results may be used to justify the method of nonharmonic lifting for the Poisson problem with nonzero boundary conditions for the spectral fractional Laplacian [**137**].

Another goal is to illuminate the physical meaning of the different definitions of the fractional Laplacian in bounded domains through their associated stochastic

processes. In particular, we discuss the fact that these differing definitions can be interpreted through different ways of applying boundary conditions to α-stable Lévy processes. We discuss this in Sections 2.2.4, 2.4.3, and 2.6.3, and compare the resulting stochastic processes and their operators in Section 2.9. This is most easily summarized for Dirichlet boundary conditions, where the stochastic picture involves two successive modifications of Brownian motion: stopping (when the motion exists the Ω) and subordination (a stochastic time change by the standard α-stable subordinator, a strictly increasing jump process). These modifications do not commute, leading to two distinct stochastic processes depending on the order in which the modifications are performed [**196, 197, 91**]. Each corresponds to a distinct fractional Laplacian operator. The spectral fractional Laplacian is the negative infinitesimal generator of subordinate stopped Brownian motion (Section 2.6.3). Since paths of Brownian motion are continuous, stopped Brownian paths stop at $\partial\Omega$, and therefore subordinate stopped Brownian paths also stop at $\partial\Omega$, despite being discontinuous in the interior of Ω. Thus, a local boundary condition prescribed only on $\partial\Omega$ is sufficient for a spectral Laplacian model of anomalous diffusion. In contrast, the Riesz fractional Laplacian is the negative infinitesimal generator of stopped subordinate Brownian motion (i.e., stopped α-stable Lévy motion; Sections 2.2.4 and 2.4.3), which represents particles that are stopped upon exiting the domain via a jump over the boundary. Hence, conditions prescribed merely on the boundary of Ω are not sufficient to describe the behavior of particles that are exiting the domain, and instead an *exterior condition* on the behavior of the process within Ω^c must be given to pose a physically meaningful model.

2.2 The Fractional Laplacian on $\mathbb{R}^d$

The fractional Laplacian on $\mathbb{R}^d$ is at the core of this thesis, and is used in machine learning experiments in Chapter 5. Moreover, the characterizations discussed in this section will lead to the definitions of the most commonly used fractional Laplacians (Riesz, directional, and spectral) in a bounded domain. Thus, this section serves as a cornerstone for the entire thesis. For proofs that the characterizations we consider in this chapter, as well as other characterizations, are equivalent in $\mathbb{R}^d$, see [**124**].

2.2.1 Spectral/Fourier Definition

We wish to construct a fractional power of the Laplacian, $(-\Delta)^{\alpha/2}$, for $0 < \alpha < 2$. A general approach to define the positive real powers L^ρ, with $\rho \in [-1, 1]$, of a positive self-adjoint linear operator L, such as $L = -\Delta$, is facilitated by the spectral theorem. This result states that for a self-adjoint, densely defined linear operator L (not necessarily bounded) on a Hilbert space $\mathcal{H}$,

$$L : \mathcal{D}(L) \to \mathcal{H}, \quad \mathcal{D}(L) \text{ a dense subspace of } \mathcal{H}, \tag{2.1}$$

there is a projection-valued measure E_λ such that

$$L = \int_{\lambda \in \sigma(L)} \lambda \, dE_\lambda \quad \text{on } \mathcal{D}(L) \subset \mathcal{H}. \tag{2.2}$$

Here, E_λ is the unique operator-valued spectral measure (resolution of the identity) associated to L, and $\sigma(L) \subset \mathbb{R}$ is the spectrum of L, which is the support of E_λ. See Reed & Simon ([**178**], p. 263) or Rudin ([**183**], p. 368) for a full discussion of the spectral theorem for self-adjoint operators. The dense domain $\mathcal{D}(L)$ is often referred to as a *core* for the operator L [**72**], and may be chosen to be smaller and more convenient space than a "maximal" domain of definition of L. Using the above

spectral representation, powers of the operator L of order $-1 \leq \alpha/2 \leq 1$ can be defined as the self-adjoint operator

$$L^{\alpha/2} = \int_{\lambda \in \sigma(L)} \lambda^{\alpha/2} dE_\lambda. \tag{2.3}$$

The domain of the operator $L^{\alpha/2}$ can then be extended to $\mathcal{H}$ by continuity.

We wish to consider $L = -\Delta$ on $\mathbb{R}^d$ on the Sobolev space $\mathcal{H} = H^2(\mathbb{R}^d)$, with domain the dense subspace $\mathcal{D}(-\Delta) = C_0^\infty(\mathbb{R}^d) \subset \mathcal{H}$ taken with the $\mathcal{H}$-norm. This gives $-\Delta = \int_{\sigma(-\Delta)} \lambda dE_\lambda$ from (2.1) and (2.2). For a regular domain Ω, the spectrum $\sigma(-\Delta)$ is a point spectrum, i.e., consisting entirely of eigenvalues [**178**], so one can think of dE_λ as being, for each λ, a projection operator onto the eigenspace of λ. Then, from (2.3), the fractional Laplacian on $\mathbb{R}^d$ is defined by

$$(-\Delta)^{\alpha/2} := \int_{\sigma(-\Delta)} \lambda^{\alpha/2} dE_\lambda. \tag{2.4}$$

Let us briefly discuss the use of $-\Delta$ instead of Δ above. Since $\Delta = \frac{\partial^2}{\partial x_1^2} + ... + \frac{\partial^2}{\partial x_d^2}$ has negative eigenvalues, if we were to push such an operator through the above machinery, the resulting fractional operator would have complex eigenvalues. For this reason, the spectral theorem is usually applied to positive-definite operators.

To make the definition (2.4) more explicit, the spectrum $\sigma(-\Delta)$ must be known exactly. On $\mathbb{R}^d$, this spectrum consists of eigenvalues $|\xi|^2$, where $\xi \in \mathbb{R}^d$, with corresponding generalized eigenfunctions $e^{-i\xi \cdot x}$. Thus, the projection valued measure is given on $\mathcal{D}(-\Delta)$ by

$$dE = \frac{1}{(2\pi)^d} (\cdot, e^{-i\xi \cdot x}) e^{i\xi \cdot x} d\xi,$$

where $(u, v) = \int uv dx$ denotes the L^2 inner product on $\mathbb{R}^d$. The scale factor $1/(2\pi)^d$ is required so that $\int dE_\lambda = I$ (where I is the identity). The fractional Laplacian in

$\mathbb{R}^d$ can therefore be written as

$$(2.5) \qquad (-\Delta)^{\alpha/2}u(x) = \frac{1}{(2\pi)^d}\int_{\mathbb{R}^d} |\xi|^\alpha (u, e^{-i\xi\cdot x})e^{i\xi\cdot x}d\xi = \mathcal{F}^{-1}\left\{|\xi|^\alpha \mathcal{F}\{u\}(\xi)\right\}(x),$$

where $\mathcal{F}$ and $\mathcal{F}^{-1}$ denote the Fourier and inverse Fourier transforms, respectively. Throughout this thesis, we use the convention

$$\mathcal{F}\{u\}(\xi) = \frac{1}{(2\pi)^{d/2}}\int_{\mathbb{R}^d} u(x)e^{-i\xi\cdot x}dx$$

and

$$\mathcal{F}^{-1}\{\hat{u}\}(x) = \frac{1}{(2\pi)^{d/2}}\int_{\mathbb{R}^d} \hat{u}(\xi)e^{i\xi\cdot x}d\xi.$$

Thus, we see that $(-\Delta)^{\alpha/2}$, defined by (2.4), is a *Fourier multiplier operator* with symbol $|\xi|^\alpha$, i.e.,

$$(2.6) \qquad \mathcal{F}\left\{(-\Delta)^{\alpha/2}u\right\}(\xi) = |\xi|^\alpha \mathcal{F}\{u\}(\xi),$$

which generalizes the well-known Fourier multiplier property of $-\Delta$.

An alternate statement of the spectral theorem can be made which involves representations of operators as multiplication operators. From that point of view, this result is not surprising, as $\mathcal{F}$ is precisely the unitary transformation $\mathcal{H} \to L^2$ specified in that theorem that diagonalizes the Laplacian, turning it into a multiplication operator ([**178**], p. 260).

Many authors use the property (2.6) to define the fractional Laplacian as a pseudodifferential operator [**200**]. The drawback of taking this as a starting point is that the Fourier transform is no longer available for bounded domains, although the functional calculus approach (2.4) using the spectral theorem is applicable for the case of zero boundary conditions. Of course, in that setting, the Hilbert space $\mathcal{H}$, spectrum $\sigma(-\Delta)$, and measure dE_λ must be taken accordingly, as discussed in Section 2.6.1.

2.2.2 Singular Integral Representation

The fractional Laplacian can be expressed directly as a singular integral in real space $\mathbb{R}^d$, rather than as a $2d$-integral in both real and frequency space, as in Equation (2.5). This thesis focuses on positive powers $0 \leq \alpha \leq 2$, but the negative α case bears mentioning in connection with this goal.

For $-d < \alpha < 0$, i.e., for fractional *inverse* Laplacians, the multiplier $|\xi|^\alpha$ is decaying and has a Fourier inverse in the sense of distributions: $\mathcal{F}^{-1}\{|\xi|^\alpha\} = C(d,\alpha)|x|^{-d-\alpha}$ (see Stein [**200**] or Landkof [**126**]). The constant $C(d,\alpha)$ is given by

$$C(d,\alpha) = \frac{2^\alpha \Gamma\left(\frac{\alpha}{2} + \frac{d}{2}\right)}{\pi^{d/2} |\Gamma\left(-\frac{\alpha}{2}\right)|}. \tag{2.7}$$

Then, (2.6) and the convolution property of the Fourier transform imply that the fractional inverse Laplacian is given, for $-2 < \alpha < 0$, by

$$\begin{aligned} (-\Delta)^{\alpha/2} u(x) &= C(d,\alpha)|x|^{-d-\alpha} * u(x) \\ &= C(d,\alpha) \int_{\mathbb{R}^d} \frac{u(y)}{|x-y|^{d+\alpha}} dy \\ &=: I_{-\alpha} u(x). \end{aligned} \tag{2.8}$$

This results in a well-defined function if $u(x)$ is, say, a smooth function with sufficient decay (Joshi & Freidlander [**78**] or Reed & Simon [**178**]). This operator $I_{-\alpha}$ is known as the Riesz potential, the properties of which (such as L^p boundedness) are discussed at length in Stein [**200**]. The Riesz potential is an important tool in harmonic analysis and the analysis of linear PDEs [**102**].

For $0 < \alpha < 2$ (the fractional Laplacians in which we are interested), the above derivation fails because the inverse Fourier transform of the symbol $|\xi|^\alpha$ no longer exists, even as a distribution. In addition, the representation (2.8) does not continue

for $\alpha > 0$, since the singularity would no longer be integrable. However, starting from the negative α case (2.8), a beautiful argument that can be found in Landkof ([**126**], p. 45) based on analytic continuation in α of $(-\Delta)^{\alpha/2}u(x)$, for fixed u and x, yields the following real-space formula for the fractional Laplacian:

$$(-\Delta)^{\alpha/2}u = C(d,\alpha)\ \text{p.v.}\int_{\mathbb{R}^d}\frac{u(x)-u(y)}{|x-y|^{d+\alpha}}dy. \tag{2.9}$$

The constant $C(d,\alpha)$ is the same as in Eq. (2.7), and "p.v." denotes the principal value of the integral:

$$\text{p.v.}\int_{\mathbb{R}^d}\frac{u(x)-u(y)}{|x-y|^{d+\alpha}}dy = \lim_{\epsilon\to 0}\int_{\mathbb{R}^d\setminus B_\epsilon(x)}\frac{u(x)-u(y)}{|x-y|^{d+\alpha}}dy,$$

where $B_\epsilon(x)$ is a ball of radius ϵ centered at x. The difference $u(x)-u(y)$ in the numerator of (2.9), which vanishes at the singularity, provides a regularization, which together with averaging of positive and negative parts allows the principal value to exist, e.g., for smooth u with sufficient decay.

The relation between the Riesz potential and the fractional Laplacian is discussed in detail in [**185**], Sections 5.25 and 5.26, where it is shown that

$$(-\Delta)^{\alpha/2}I_\alpha u = u.$$

This identity leads to the representation of the fractional Laplacian directly in terms of the Riesz potential:

$$(-\Delta)^{\alpha/2}u(x) = -\Delta I_{2-\alpha}u(x).$$

2.2.3 Via the standard Laplacian: Elliptic Extension, Heat Semigroup, & Balakrishnan Formula

Next, we summarize three representations of the fractional Laplacian $(-\Delta)^{\alpha/2}$ of a function $u(x)$ on $\mathbb{R}^d$ that require the solution of equations involving the standard Laplacian, albeit in the $(d+1)$-dimensional half-plane. The first is the *extension method*, or the *Dirichlet-to-Neumann map*, which requires the solution of a degenerate *elliptic* equation in the half-plane using $u(x)$ as the Dirichlet boundary data, followed by a type-of normal derivative of the solution. The second is the *heat semigroup method*, which requires the solution of a *parabolic* equation – the simple heat equation – in the half-plane with $u(x)$ as the intial condition, followed by long-time integration. The third is the Balakrishnan formula, which expresses the fractional Laplacian in terms of the resolvent $(sI - \Delta)^{-1}$.

The *extension method* is based on the following result. Given a function $u(x)$ on $\mathbb{R}^d$, consider the extension $\tilde{u}(x, y)$ on $\mathbb{R}^d \times [0, \infty)$ that solves

$$\begin{aligned} \Delta_x \tilde{u} + \frac{1-\alpha}{y} \partial_y \tilde{u} + \partial_y^2 \tilde{u} &= 0 \\ \tilde{u}(x, 0) &= u(x). \end{aligned} \tag{2.10}$$

Then

$$(-\Delta)^{\alpha/2} u(x) = c \lim_{y \to 0} \frac{u(x, y) - u(x, 0)}{y^\alpha}$$

for a certain constant c that depends on d and α.

The above statement is taken directly from Caffarelli and Silvestre [**38**], which is the most widely read source for the extension method. The extension method was reported as early as 1968 by Molchanov and Ostrovskii, in their studies of symmetric

stable processes [153]. The result was also used by other authors (e.g., [57]), before it was systematically addressed by Caffarelli and Silvestre.

The *heat semigroup representation* of the fractional Laplacian uses the solution of the heat equation in $\mathbb{R}^d \times [0, \infty)$:

$$(-\Delta)^{\alpha/2} u(x) = \frac{1}{\Gamma(-\alpha)} \int_0^\infty \left(e^{t\Delta} u(x) - u(x) \right) \frac{dt}{t^{1+\alpha/2}}. \tag{2.11}$$

Here, $e^{t\Delta}$ is the propagator of the heat equation, i.e., $w(x,t) = e^{t\Delta}u(x)$ is the solution of the problem

$$\partial_t w - \Delta w = 0 \text{ on } \mathbb{R}^d \times [0, \infty)$$

$$w(x, t = 0) = u.$$

The family $\{e^{t\Delta}\}$ is called the heat semigroup. See [202] and [203] for a full discussion. An implementation of the formula (2.11) on $\mathbb{R}^d$ was studied in [50].

The *Balakrishnan formula*, introduced in [18], is a result from spectral theory and the theory of semigroups. This formula for the fractional Laplacian is

$$(-\Delta)^{\alpha/2} u(x) = \frac{\sin(\alpha\pi/2)}{\pi} \int_0^\infty \Delta (sI - \Delta)^{-1} u(x) s^{\alpha/2 - 1} ds.$$

For a further discussion of these characterizations in $\mathbb{R}^d$, we refer to [124] and references therein. Although fractional Laplacians in bounded domains will be introduced in the next subsection, we preface that discussion by pointing out that analogues of these methods hold in bounded domains, depending on the fractional Laplacian being considered. In the case of the spectral fractional Laplacian for functions that satisfy zero Dirichlet boundary conditions, the characterization via an elliptic extension holds with the half-plane being replaced by a cylinder over the original domain [202, 203]. The Balakrishnan formula and the closely related Dunford-Taylor formula (for the inverse spectral fractional Laplacian) are valid and

have efficient numerical implementations [**32, 31**]. The heat kernel formula has been found to be valid even for nonzero boundary conditions [**55**]. See sections 2.6.2 and 2.7.4 for further discussion and references to proofs and implementations of these methods.

2.2.4 Relation to Lévy processes

The fractional Laplacian is connected to *anomalous* diffusion, which accounts for much of the interest in modeling with fractional equations. Just as the Laplacian is the negative generator of Brownian motion (scaled by $\sqrt{2}$), the fractional Laplacian is the infinitesimal generator of a standard isotropic α-stable Lévy motion X_t^α, which can be expressed by

$$-(-\Delta)^{\alpha/2} f(x) = \lim_{h \to 0} \frac{\mathbb{E}\left[f(x - X_h^\alpha) - f(x)\right]}{h}. \tag{2.12}$$

This connection is explained more fully in the last two paragraphs of this section. This process X_t^α is a Lévy process ([**149**], p. 100) in which the increments are drawn from a spherically-symmetric α-stable distribution ([**149**], Ex. 6.24). This process can be viewed as the long-time scaling limit of a random walk with power law jumps ([**149**], Theorem 6.17). For $\alpha = 2$, X_t^α reduces to scaled Brownian motion $X_t^2 = \sqrt{2}B_t$, with the 2-stable distribution being the normal distribution $\mathcal{N}(0, \sigma^2 = 2)$. For $\alpha < 2$, the $\alpha-$stable distribution exhibits heavy tails and infinite variance. Moreover, the mean is finite if and only if $\alpha > 1$. The Lévy process X_t^α has superdiffusive scaling $X_{ct}^\alpha \sim c^{1/\alpha} X_t^\alpha$, and exhibits long, infinite-variance jumps when $\alpha < 2$. As an example, a superdiffusing cloud of particles would spread in space like $t^{1/\alpha}$. In many ways, α-stable Lévy flights are the simplest generalization of Brownian motion. As a result of (2.12), the fractional Laplacian naturally appears in macroscopic governing equations of systems of particles undergoing α-stable Lévy motion, making it a powerful and

useful generalization [149]. In Figure 1, we include examples of 2D isotropic stable Lévy motion and standard Brownian motion.

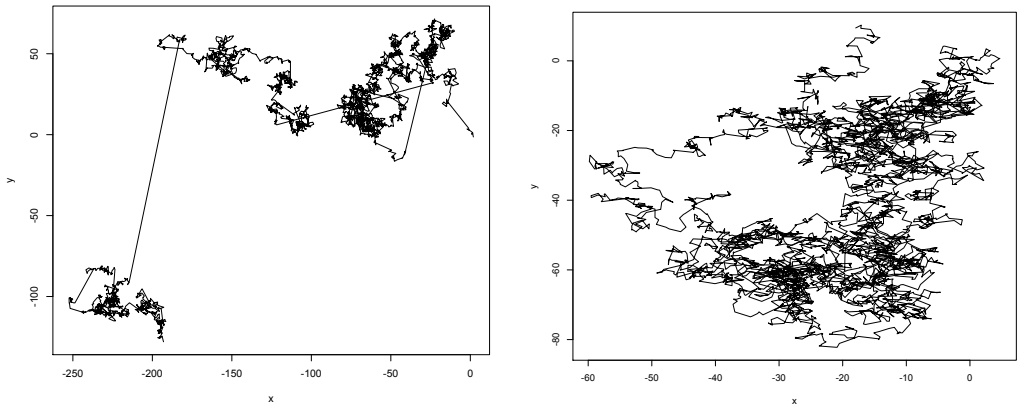

FIGURE 1. Comparison of Lévy motion and Brownian motion: *(left)* A 2D standard isotropic stable Lévy motion with $\alpha = 1.8$. *(right)* A 2D standard isotropic stable Lévy motion with $\alpha = 2.0$ (Brownian motion scaled by $\sqrt{2}$).

The heavy-tailed behavior of α-stable random variables is very much in demand for modeling, although the infinite variance property may sometimes be undesirable, for physical or numerical reasons. Recently, *tempered fractional calculus* has been developed to avoid this issue [147]. Tempered fractional diffusion equations model particles that undergo *tempered α-stable Lévy motion*, which is based on an exponentially tempered α-stable density [122]. Roughly, this density exhibits the power-law decay up to a certain argument, then decays exponentially. The generator of tempered α-stable Lévy motion, i.e., the tempered fractional Laplacian, was discussed in [230], where a Riesz basis Galerkin method was proposed to solve the Poisson problem with this operator.

The characterization of $(-\Delta)^{\alpha/2}$ as an infinitesimal generator of X_t^α also lends itself to the stochastic (Monte Carlo) solution of boundary value problems involving

the various fractional Laplacians in bounded domains. These formulas are typically referred to as Feynman-Kac (Dirichlet boundary conditions, [**107**]) or Brosamler (Neumann boundary conditions, after [**36, 136, 103**]) formulas. One such solution method for the Riesz fractional Laplacian, due to [**125**], is discussed in Section 2.4.3.

We now give a brief outline of the probabilistic theory behind the relation of the fractional Laplacian to Lévy processes. This will also result in the *generator form* of the fractional Laplacian, which is related to the directional representation in the next Section 2.2.5. Following the text [**149**], we review the classical Lévy-Khintchine formula for generators of Lévy processes and sketch how it results in the fractional Laplacian for the special case of isotropic α-stable processes. Given a Lévy process $\{Z_t : t > 0\}$, define the family of linear operators

$$T_t f(x) = \mathbb{E}[f(x - Z_t)], \quad t \geq 0,$$

for suitable functions f. Suppose that the characteristic function of the random variable Z_1 is $\mathbb{E}[e^{ik\cdot Z_1}] = e^{\psi(k)}$, where

$$\psi(k) = ik \cdot a - \frac{1}{2} k \cdot Bk + \int \left(e^{ik\cdot y} - 1 - \frac{ik \cdot y}{1 + |y|^2} \right) \phi(dy).$$

Then $T_t f(x)$ defines a C_0-semigroup on $C_0(\mathbb{R}^d)$ with generator ([**149**], Theorem 6.26)

(2.13)
$$Lf(x) = -a \cdot \nabla f(x) + \frac{1}{2} \nabla \cdot Q \nabla f(x) + \int \left(f(x - y) - f(x) + \frac{y \cdot \nabla f(x)}{1 + |y|^2} \right) \phi(dy),$$

where $\phi(dy)$ is some Lévy measure ([**149**], Eq. (6.20)). The domain of L contains $\{f : f, f', f'' \in C_0(\mathbb{R}^d)\}$ ([**149**], Theorem 6.26). This is the Lévy-Khintchine formula. The first order differential term in this operator can be understood as the "drift" term, the second order differential term can be understood as the standard diffusion, and the Lévy measure describes the jumps of the Lévy process ([**149**], p. 159).

As we will now see, if we choose Z_t to be the standard isotropic α-stable Lévy motion, then (2.13) reduces to the negative of the fractional Laplacian. The details of the following discussion can be found in [**149**], Examples 6.28 and 6.29. If $0 < \alpha < 1$ and Z_t is a Lévy process such that Z_1 has the characteristic function

$$\mathbb{E}[e^{ik\cdot Z_1}] = \exp\left[-C\Gamma(1-\alpha)\int_{|\boldsymbol{\theta}|=1}(-ik\cdot\boldsymbol{\theta})^{\alpha}M(d\boldsymbol{\theta})\right], \tag{2.14}$$

then the generator of the corresponding stable semigroup can be written in the form

$$Lf(x) = \int (f(x-y) - f(x))\phi(dy), \tag{2.15}$$

where

$$\phi(dy) = \alpha C r^{-\alpha-1}drM(d\boldsymbol{\theta}) \text{ with } y = r\boldsymbol{\theta},\ r > 0, \text{ and } |\boldsymbol{\theta}| = 1. \tag{2.16}$$

If $M(d\boldsymbol{\theta})$ is a uniform measure on the unit sphere, and if

$$C^{-1} = B\Gamma(1-\alpha), \text{ and } B = \cos(\pi\alpha/2)\int_{|\boldsymbol{\theta}|=1}|\theta_1|^{\alpha}M(d\boldsymbol{\theta}), \tag{2.17}$$

then the right-hand side of (2.14) reduces to $\exp[-|k|^{\alpha}]$, so that $Z_t = X_t^{\alpha}$, the standard isotropic α-stable Lévy motion[1], and $L = -(-\Delta)^{\alpha/2}$, the negative of the fractional Laplacian ([**149**], Example 6.24). Indeed, (2.15) reduces to (2.9) after a simple change of variables (see [**58**], Section 4). Now if $1 < \alpha < 2$, and Z_1 has the characteristic function

$$\mathbb{E}[e^{ik\cdot Z_1}] = \exp\left[C\frac{\Gamma(2-\alpha)}{\alpha-1}\int_{|\boldsymbol{\theta}|=1}(-ik\cdot\boldsymbol{\theta})^{\alpha}M(d\boldsymbol{\theta})\right], \tag{2.18}$$

[1]The general isotropic α-stable random variable has characteristic function $\exp[-c^{\alpha}|k|^{\alpha}]$, where c is the scale parameter. The standard α-stable random variable has scale parameter $c = 1$. Note that the standard isotropic 2-stable random variable corresponds to a normal random variable with characteristic function $\exp\left[\frac{-\sigma^2|k|^2}{2}\right]$ and variance $\sigma^2 = 2$.

then the generator of the corresponding stable semigroup can be written in the form

$$Lf(x) = \int (f(x-y) - f(x) + y \cdot \nabla f(x))\phi(dy), \tag{2.19}$$

where ϕ is defined as in (2.16), and the constants B and C are defined as in (2.17). In this case, if $M(d\boldsymbol{\theta})$ is a uniform measure on the unit sphere, then $L = (-\Delta)^{\alpha/2}$, which has a different sign than in the case $0 < \alpha < 1$. The sign change is due to the fact that $B > 0$ for $0 < \alpha < 1$, and $B < 0$ for $1 < \alpha < 2$. Equations (2.15) and (2.19) yield alternate forms of the fractional Laplacian (2.9), known as the generator forms, without using the principal value. The generator form (2.13) of the fractional Laplacian is useful for probabilists working in this area.

2.2.5 Directional Representation

Another integral characterization of the fractional Laplacian, which we refer to as the directional representation, can be found in [**185**] (Eq. (26.24)). The operator is written as

$$(-\Delta)^{\alpha/2} u(x) = C_{\alpha,d} \int_{|\boldsymbol{\theta}|=1} D^{\alpha}_{\boldsymbol{\theta}} u(x) d\boldsymbol{\theta}, \quad x, \boldsymbol{\theta} \in \mathbb{R}^d, \alpha \in (0,1) \cup (1,2], \tag{2.20}$$

where the scaling constant before the integral is [**185, 161**]

$$C_{\alpha,d} = \frac{\Gamma(\frac{1-\alpha}{2})\Gamma(\frac{d+\alpha}{2})}{2\pi^{\frac{1+d}{2}}}.$$

The Fourier transform of (2.20) corresponds to multiplication of the Fourier transform of u by (2.14) when $\alpha < 1$ and by (2.18) when $\alpha > 1$. Here, $D^{\alpha}_{\boldsymbol{\theta}}(\cdot)$ is the Riemann-Liouville fractional directional derivative [**146**] given by

$$D^{\alpha}_{\boldsymbol{\theta}}(\cdot) = (\boldsymbol{\theta} \cdot \nabla) I^{1-\alpha}_{\boldsymbol{\theta}}(\cdot) \quad \text{for } 0 < \alpha < 1; \quad D^{\alpha}_{\boldsymbol{\theta}}(\cdot) = (\boldsymbol{\theta} \cdot \nabla)^2 I^{2-\alpha}_{\boldsymbol{\theta}}(\cdot) \quad \text{for } 1 < \alpha < 2;$$

where $\boldsymbol{\theta}\cdot\nabla = \sum_{i=1}^{d} \theta_i \frac{\partial}{\partial x_i}$ is the directional derivative, thus $(\boldsymbol{\theta}\cdot\nabla)^2 = \sum_{j=1}^{d}\sum_{i=1}^{d} \theta_i\theta_j \frac{\partial^2}{\partial x_j \partial x_i}$, and the fractional directional integral $I_{\boldsymbol{\theta}}^{\beta}(\cdot)$ is defined by (for $\beta \in (0,1)$)

$$I_{\boldsymbol{\theta}}^{\beta} u(x) = \frac{1}{\Gamma(1-\beta)} \int_0^{+\infty} \varsigma^{-\beta} u(x - \varsigma\boldsymbol{\theta}) d\varsigma.$$

Note that (2.20) excludes the case $\alpha = 1$. When $\alpha = 1$, the directional representation is more complicated; for the one-dimensional case, see [**112**].

We now explicitly write out the directional representation (2.20) for one and two dimensions; these formulas provide important examples of this operator. In one dimension, using the identity $\Gamma(x)\Gamma(1-x) = \pi/\sin(\pi x)$, we have

$$\Gamma\left(\frac{1-\alpha}{2}\right)\Gamma\left(\frac{1+\alpha}{2}\right) = \Gamma\left(\frac{1-\alpha}{2}\right)\Gamma\left(1-\frac{1-\alpha}{2}\right) = \frac{\pi}{\sin\left(\pi\frac{1-\alpha}{2}\right)} = \frac{\pi}{\cos\left(\frac{\pi\alpha}{2}\right)},$$

and so

$$\begin{aligned}(-\Delta)^{\alpha/2} u(x) &= \frac{1}{2\cos\left(\frac{\pi\alpha}{2}\right)}\left[D_{\theta=-1}^{\alpha} u(x) + D_{\theta=1}^{\alpha} u(x)\right] \\ &= \frac{1}{2\cos\left(\frac{\pi\alpha}{2}\right)}\left[{}_{-\infty}^{RL}D_x^{\alpha} u(x) + {}_{x}^{RL}D_{\infty}^{\alpha} u(x)\right],\end{aligned}$$

where ${}_{-\infty}^{RL}D_x^{\alpha}$ and ${}_{x}^{RL}D_{\infty}^{\alpha}$ are the well-known one-dimensional left- and right-sided Riemann-Liouville fractional derivatives, respectively [**226**]. Note that, using the Fourier transforms of these operators, $\mathcal{F}[(-\Delta)^{\alpha/2}u] = \frac{1}{\cos(\alpha\pi/2)}\left[\frac{1}{2}(-i\xi)^{\alpha} + \frac{1}{2}(i\xi)^{\alpha}\right]\hat{u} = |\xi|^{\alpha}\hat{u}$ for $\alpha \neq 1$. In two dimensions and for $\alpha \neq 1$, the fractional Laplacian can be written in polar form as

$$(-\Delta)^{\alpha/2} u(x) = C_{\alpha,2} \int_0^{2\pi} D_{\theta}^{\alpha} u(x) d\theta,$$

where D_{θ}^{α} is a derivative along the direction $[\cos(\theta), \sin(\theta)]$.

Meerschaert et al. [**144**] extended the above operator (2.20) to an anisotropic version, which they called the general (asymmetric) fractional derivative operator

∇_M^α,

$$\nabla_M^\alpha u(x) = \int_{|\boldsymbol{\theta}|=1} D_{\boldsymbol{\theta}}^\alpha u(x) M(d\boldsymbol{\theta}), \quad x, \boldsymbol{\theta} \in \mathbb{R}^d, \alpha \in (0,1) \cup (1,2], \tag{2.21}$$

where $M(d\boldsymbol{\theta})$ is an arbitrary probability measure on the unit sphere $\{|\boldsymbol{\theta}| = 1\}$. The motivation for the definition extension is to generate "the full range of Lévy-stable motions". For more details, see Equation (2.14) and the corresponding discussion. The study of this more general operator is beyond the scope of this thesis. However, it is an interesting and pertinent topic for future extensions of many of the results and methods discussed in this work. It should be noted that the directional fractional Laplacian will be recovered if the measure $M(d\boldsymbol{\theta})$ is uniform, namely, $M(d\boldsymbol{\theta}) = d\boldsymbol{\theta}/S_d$ where $S_d = 2\pi^{d/2}/\Gamma(d/2)$ is the surface area of the unit sphere in $\mathbb{R}^d$. In this case, the two types of operators are related by

$$(-\Delta)^{\alpha/2} u(x) = \frac{\Gamma\left(\frac{d+\alpha}{2}\right)\Gamma\left(\frac{1-\alpha}{2}\right)}{\Gamma\left(\frac{d}{2}\right)\sqrt{\pi}} \nabla_M^\alpha u(x).$$

2.2.6 Fractional Vector Calculus

We touch briefly on the topic of fractional vector calculus and the relation to the fractional Laplacian. While the directional fractional Laplacian defined by (2.21) has been proposed as a basis for fractional vector calculus (in particular, for fractional advection-diffusion) by [**146**], Tarasov proposed a different formulation in terms of fractional gradient, divergence, and curl, and used this to introduce fractional Maxwell equations [**208**]. Consider the rectangle

$$W = \left\{ (x,y,z) \;\middle|\; a \le x \le b,\ c \le y \le d,\ g \le z \le h \right\}.$$

For functions f and vector fields $\boldsymbol{F} = (F_x, F_y, F_z)$ on W, Tarasov [208] introduced the fractional gradient and divergence operators by

(2.22)
$$\text{Grad}_W^\alpha \boldsymbol{F} = \boldsymbol{e}_1 \, {}^C D_W^\alpha[x] F_x(x,y,z) + \boldsymbol{e}_2 \, {}^C D_W^\alpha[y] F_y(x,y,z) + \boldsymbol{e}_3 \, {}^C D_W^\alpha[z] F_z(x,y,z),$$

and

$$\text{Div}_W^\alpha f = {}^C D_W^\alpha[x] f(x,y,z) + {}^C D_W^\alpha[y] f(x,y,z) + {}^C D_W^\alpha[z] f(x,y,z), \tag{2.23}$$

respectively, where $\boldsymbol{e_i}$ are the unit vectors, and the Caputo fractional derivatives

$${}^C D_W^\alpha[x] = {}_a^C D_b^\alpha[x], \quad {}^C D_W^\alpha[y] = {}_c^C D_d^\alpha[y], \quad {}^C D_W^\alpha[z] = {}_g^C D_h^\alpha[z]$$

are used (see [149] for a discussion of the Caputo derivative).

These definitions lead to a fractional generalization of the Laplacian via the formula $\Delta f = \text{Div Grad } f$ as

(2.24)
$$\text{Div}_W^{\alpha/2} \, \text{Grad}_W^{\alpha/2} f = \left({}^C D_W^{\alpha/2}[x]\right)^2 f(x,y,z) + \left({}^C D_W^{\alpha/2}[y]\right)^2 f(x,y,z) + \left({}^C D_W^{\alpha/2}[z]\right)^2 f(x,y,z).$$

This operator is distinct from the fractional Laplacian that is the focus of this chapter, and has the advantage that a system of fractional vector calculus can be established which largely mirrors ordinary vector calculus. Various identities, together with fractional versions of Green's, Stoke's, and Gauss's formulas, were shown to hold [208] with a definition of fractional curl analogous to the definitions (2.22) and (2.23).

We point out one important distinction between the fractional Laplacians studied in this thesis and the operator (2.24), as they relate to Lévy processes. For simplicity, assume that $f \in C_c^\infty(\text{ interior}(W))$, so that the Caputo derivatives above reduce to

Riemann-Louiville derivatives and the operator (2.24) reduces in Fourier space to

$$\mathcal{F}\left\{\mathrm{Div}_W^{\alpha/2}\ \mathrm{Grad}_W^{\alpha/2} f\right\} = \text{const.}\ [(\xi_1)^\alpha + (\xi_2)^\alpha + (\xi_3)^\alpha]\ \mathcal{F}\{f\}.$$

Except for the case $\alpha = 2$, the Fourier multiplier in this equation is not rotationally invariant. This is contrast to the multiplier $|\boldsymbol{\xi}|^\alpha$ of the fractional Laplacian in $\mathbb{R}^d$. The multiplier $|\boldsymbol{\xi}|^\alpha$ corresponds to a multivariate α-stable process with constant spectral measure, i.e., the *isotropic* multivariate stable process. In contrast, the multiplier $[(\xi_1)^\alpha + (\xi_2)^\alpha + (\xi_3)^\alpha]$ corresponds to a spectral measure supported on the basis vectors in three-dimensional space, i.e., to a multivariate stable process with *independent components*. Except for the case $\alpha = 2$, the isotropic multivariate α-stable process is *not* equivalent to the multivariate α-stable processes with independent components.

2.3 Fractional Laplacians on Bounded Domains

We have discussed several characterizations and formulas for the fractional Lapacian in $\mathbb{R}^d$, which are all equivalent in that setting. If we apply these different formulas on a bounded domain $\Omega \subset \mathbb{R}^d$, certain equivalences break down, which leads to the definition of several distinct fractional Laplacians in a bounded domain. Some researchers have defined other fractional Laplacians on a bounded domain directly, instead of restricting the definition for $\mathbb{R}^d$ [45]. Here, we survey the *Riesz* fractional Laplacian (sometimes called the *integral* fractional Laplacian), the *directional* fractional Laplacian, and the *spectral* fractional Laplacian. We focus on the following topics.

- Appropriate boundary conditions for the Poisson problem

$$(-\Delta)^{\alpha/2} u = f \text{ in } \Omega. \tag{2.25}$$

The spectral fractional Laplacian admits local boundary conditions on $\partial\Omega$; the regional fractional Laplacian has also been considered with local boundary conditions. On the other hand, the Riesz (and directional) fractional Laplacians require *exterior* boundary conditions on $\mathbb{R}^d \setminus \Omega$.

- Connection of each fractional Laplacian with given boundary conditions to a stochastic process. The standard Laplacian $-\Delta$ in a bounded domain is the generator of *stopped* [**121**] Brownian motion if taken with Dirichlet BCs [**167**, **77**], and *reflected* Brownian motion if taken with Neumann BCs [**36**, **103**, **23**]. Similarly, the fractional Laplacians are generators of certain stopped or reflected Lévy motions. This is useful for physical interpretation as well as stochastic solution methods.
- Well-posedness and regularity properties of the fractional Poisson problem (2.25) with appropriate boundary conditions.

REMARK 2.26. Many results in the probability literature (e.g., [**196**]) are stated and proved for *killed* processes rather than *stopped* processes. Without going into details here, we note that the resulting semigroups are equivalent when applied to functions f that vanish outside the domain, in the sense that $\mathbb{E}_x\left[f(X_t)\right]$ is the same whether X_t is the killed or the stopped process. Here, we are assuming that $f(\partial) = 0$ where ∂ is the cemetery point specified for the killed process.

2.4 Riesz Fractional Laplacian

2.4.1 Definition

One approach to defining the fractional Laplacian on a bounded domain Ω is to apply the real space formula (2.9) to functions on Ω. This leads to the *Riesz* fractional Laplacian in Ω. Let us first consider Dirichlet boundary conditions. Since formula

(2.9) requires values of u on all of $\mathbb{R}^d$, an *exterior* boundary condition

$$u = g \text{ in } \mathbb{R}^d \setminus \Omega \tag{2.27}$$

is required, even to define the Riesz Laplacian within Ω. For functions u that satisfy (2.27), the *Riesz* fractional Laplacian is defined for $x \in \Omega$ by

$$\begin{aligned}(-\Delta)^{\alpha/2}u(x) &= C(d,\alpha)\ \text{p.v.} \int_{\mathbb{R}^d} \frac{u(x)-u(y)}{|x-y|^{d+\alpha}}dy \\ &= C(d,\alpha)\left[\ \text{p.v.} \int_{\Omega} \frac{u(x)-u(y)}{|x-y|^{d+\alpha}}dy + \int_{\mathbb{R}^d\setminus\Omega} \frac{u(x)-g(y)}{|x-y|^{d+\alpha}}dy\right].\end{aligned}$$

The Riesz Laplacian depends directly on Ω and the exterior boundary values g.

2.4.2 Boundary Conditions: Dirichlet vs. Neumann

The Neumann condition for the Riesz Laplacian is, at the time of this writing, an area of active development. A type of exterior fractional normal derivative is needed to specify u on $\mathbb{R}^d\setminus\Omega$, but there is no widely studied or accepted definition. Recently, a fractional Neumann operator was proposed in [**65**], and the properties were studied in detail in [**60**]. Another approach to defining reflecting boundary conditions based on mass conservation for diffusion in one dimension was explored in [**16, 113**].

The Poisson problem with Dirichlet boundary conditions

$$\begin{aligned}(-\Delta)^{\alpha/2}u &= f \text{ in } \Omega\ , \\ u &= g \text{ in } \mathbb{R}^d \setminus \Omega\end{aligned} \tag{2.28}$$

has been extensively studied in the $g \equiv 0$ case [**5, 182, 9, 7, 88**], but literature based on the nonzero case is more recent and limited [**125**].

For the case of zero exterior Dirichlet condition $g \equiv 0$ in (2.28), finite element algorithms have been developed in [**5**], [**9**], and in particular the adaptive finite element scheme of [**7**] has been used for the computations in the work [**137**]. Moreover, in [**125**], a Monte Carlo method based on the Feynman-Kac formula for the problem (2.28) was developed and studied for general Dirichlet exterior conditions. This method is described in more detail in Section 3 of our article [**137**].

2.4.3 Stopped Lévy Motion

The Riesz fractional Laplacian with Dirichlet boundary conditions is the generator of the stopped α-stable Lévy motion. The stopped Lévy motion is defined as follows [**121**, **167**, **77**]. Given a stable Lévy motion X_t^α and a bounded domain Ω, we define the stopping time (or exit time)

$$\tau_\Omega = \inf\{t : X_t^\alpha \notin \Omega\}. \tag{2.29}$$

Then, the stopped Lévy process is defined as $X^\alpha_{t\wedge\tau_\Omega}$. Unlike stopped Brownian motion, which has almost surely continuous paths that are stopped at the boundary, the paths of α-stable Lévy motion are discontinuous and almost surely exit the domain by a jump. Thus, the paths of stopped α-stable Lévy motion pass into the exterior $\mathbb{R}^d \setminus \Omega$ where they are stopped immediately.

In [**125**], this stochastic connection was exploited to prove a Feynman-Kac for the Poisson problem.

$$\begin{aligned} (-\Delta)^{\alpha/2} u(x) &= f(x), \quad x \in \Omega \subset \mathbb{R}^d, \\ u(x) &= g(x), \quad x \in \mathbb{R}^d \setminus \Omega. \end{aligned} \tag{2.30}$$

Under mild conditions on f and g, the Feynman-Kac formula was proven:

$$u(x) = \mathbb{E}_x \left[g(X^\alpha_{\tau_\Omega}) \right] + \mathbb{E}_x \left[\int_0^{\tau_\Omega} f(X^\alpha_s) ds \right], \ x \in \Omega, \tag{2.31}$$

where X^α_t is the symmetric α-stable process, $\mathbb{E}_x(\cdot)$ denotes the expectation with respect to all the sample paths with the initial location x, and $\tau_\Omega = \inf\{t > 0 : X_t \notin \Omega\}$ is the first exit time of the sample path.

In addition to a proof, in [**125**] a walk-on-spheres (WOS) method for faster computation of (2.31) was introduced and analyzed. This speeds up the implementation of (2.31) by replacing the simulation of exact stopped paths in Ω by a series of maximal inscribed spheres. Conceptually, the WOS method is based on the isotropy of the problem (2.30) as well as the analytic formula for mean-exit time of X^α_t on a sphere [**85**]. In the Brownian motion case, the center of each sphere is chosen by sampling a uniform distribution on the boundary of the previous sphere, and the procedure terminates when the process comes within some tolerance ε of the boundary of Ω. In the α-stable case, the center of each sphere is chosen by sampling a distribution on the exterior of the previous sphere, due to the discontinuity of α-stable Lévy paths. Thus, in the α-stable case, the sample path may exit the sphere by a jump, instead of by passing through the boundary. The WOS terminates when the process jumps outside the domain Ω. The convergence in finite steps for $\alpha \neq 2$ was proven in [**125**].

2.4.4 Well-posedness and Regularity

In this section, we consider the problem

$$\begin{aligned} (-\Delta)^{\alpha/2} u &= f \text{ in } \Omega, \\ u &= 0 \text{ in } \mathbb{R}^d \setminus \Omega. \end{aligned} \tag{2.32}$$

Using the Lax-Milgram Lemma, for a bounded Lipschitz domain Ω, it is easy to show that this problem is well-posed if $f(x) \in \mathbb{H}^{-\alpha/2}(\Omega)$ and the resulting solution $u(x) \in \mathbb{H}^{\alpha/2}(\Omega)$. See, for example, [**9**, **29**, **5**]. For the definitions of the Sobolev space $\mathbb{H}^s$, which will also feature in the following regularity results, see Appendix B.

As for regularity, our intention is not to give a complete survey of all the known regularity results for the fractional Laplacian. Instead, we mention two results that give an indication of the regularity for the Riesz fractional Laplacian, for the case of the zero boundary condition. These properties should be compared with the regularity of the spectral fractional Laplacian (see Section 2.7.5). The regularity up to the boundary is a key difference between the two definitions.

The Hölder regularity for the solution of the problem 2.32 was studied in [**182**]. The authors were motivated by the exact solution for $f \equiv 1$ in the ball $B_r(x_0)$ centered at x_0 of radius r:

$$\begin{aligned} (-\Delta)^{\alpha/2} u &= 1 \text{ in } B_r(x_0), \\ u &= 0 \text{ in } \mathbb{R}^d \setminus B_r(x_0), \end{aligned} \tag{2.33}$$

which has solution

$$u(x) = \frac{2^{-\alpha}\Gamma(n/2)}{\Gamma\left(\frac{n+\alpha}{2}\right)\Gamma(1+\alpha/2)} \left(r^2 - |x - x_0|^2\right)^{\alpha/2} \text{ in } B_r(x_0).$$

This solution exhibits strict $C^{\alpha/2}$ regularity up the boundary. The authors proved the following result. Let Ω be a bounded $C^{1,1}$ domain and $\delta(x) = d(x, \partial\Omega)$ denote the distance to the boundary. Then $g \in L^\infty(\Omega)$ implies that $u/\delta^{\alpha/2}$ can be extended to a $C^r(\overline{\Omega})$ function for some $r < \min(\alpha/2, 1 - \alpha/2)$, and

$$\|u/\delta^{\alpha/2}\|_{C^r(\overline{\Omega})} \leq C\|g\|_{L^\infty(\Omega)}.$$

This result is sharp for the problem (2.33).

The following theorem relates to the Sobolev regularity of (2.32). This form is presented nicely in [7] and is based on the results of [88] and [4].

THEOREM 2.34. [7, 88, 4] *Let* $\partial\Omega \in C^\infty$, $f \in H^s(\Omega)$ *for* $s \geq -\alpha/2$ *and* $u \in \mathbb{H}^{\alpha/2}(\Omega)$ *be the solution of the fractional Poisson problem* (2.32). *Then*

$$u \in \begin{cases} H^{\alpha+s}(\Omega) & \text{if } 0 < \alpha/2 + s < 1/2, \\ H^{\alpha/2+1/2-\varepsilon}(\Omega) \ \forall \varepsilon > 0 & \text{if } 1/2 \leq \alpha/2 + s. \end{cases}$$

An interesting feature of the Sobolev regularity for the Riesz fractional Laplacian is that if $\alpha/2+s \geq 1/2$, the global regularity of u need not improve if s, the regularity of f, is increased. Rather, s merely improves the interior regularity of u. This was proven in [88], where it was shown that for a smooth boundary $\partial\Omega$, $f \in H^s(\Omega)$ implies that $u \in H^{\alpha+s}_{\text{loc}}(\Omega)$. Therefore, the global regularity (i.e., regularity up to the boundary) for the Riesz fractional Laplacian is in contrast to the global regularity for the spectral fractional Laplacian (see Section 2.7.5). In the case when $f \in L^2(\Omega)$ for the spectral Laplacian, $u \in \mathbb{H}^\alpha(\Omega)$ for all $\alpha \in (0, 2)$, while this is only true if $\alpha < 1$ for the Riesz fractional Laplacian. In the case when $f \in H^s(\Omega)$ and $s > 1/2$, $u \in \mathbb{H}^{s+\alpha}(\Omega)$ for the spectral fractional Laplacian provided $f \equiv 0$ on the boundary $\partial\Omega$, while for the Riesz definition, $u \in H^{\alpha/2+1/2-\varepsilon}(\Omega)$, independent of s. Even if $f \not\equiv 0$ on $\partial\Omega$, the regularity of u for the spectral definition improves as $\alpha + 1/2 - \varepsilon$, while in the Riesz case, it improves as $\alpha/2 + 1/2 - \varepsilon$.

2.5 Directional Fractional Laplacian

We can also apply the directional fractional Laplacian $(-\Delta)^{\alpha/2}_M$ to functions on Ω with an exterior boundary condition, which is applied in the same way as for the Riesz definition. Although the directional characterization was motivated in [144] by

the desire to capture anisotropic anomalous diffusion, in this work, we always choose $M(d\boldsymbol{\theta}) = d\boldsymbol{\theta}/S_d$ where $S_d = 2\pi^{d/2}/\Gamma(d/2)$ is the surface area of the unit sphere in $\mathbb{R}^d$, so that our computational results for this definition can be compared to those of the Riesz definition. With this choice of measure, the associated Lévy process is symmetric stable motion that is stopped upon exiting the domain Ω, which is the same process as the one associated with the Riesz fractional Laplacian. A proof of this equivalence can be found in [**47**], Lemma 4.1. Hence the discussions of Section 2.4.3 and 2.4.4 also apply to the directional fractional Laplacian with our choice of integration measure.

2.6 Spectral Fractional Laplacian

In this chapter, we have split the discussion of the spectral fractional Laplacian into two: the case of zero boundary condition and the case of nonzero boundary conditions. This is due to the vast body of work that considers only the homogeneous spectral fractional Laplacian (i.e., the zero boundary condition case), as only recently was the inhomogeneous version considered. In deference to the fact that many results in the literature apply only to the homogeneous case, we have taken this approach to avoid misleading the reader. The results reported in Sections 2.6.1 and 2.7.5 on the homogeneous spectral fractional Laplacian should not be taken to apply in the case of nonzero boundary conditions without modification.

The inhomogeneous spectral fractional Laplacian has been considered by Antil et al. [**11**] (see Section 2.7.1) and Cusimano et al. [**55**] (see Section 2.7.4). In Section 2.7.4, we point out that the definitions considered in [**11**] and [**55**] are the same, and are essentially a harmonic lifting to the homogeneous spectral fractional Laplacian. Moreover, we show that this amounts to another natural definition in terms of the inverse spectral fractional Laplacian.

2.6.1 Zero Boundary Condition

The spectral approach to defining the factional Laplacian in Ω is to start with the standard negative Laplacian $-\Delta$ on that domain and take the spectral power defined by (2.4). Let us first consider the case of zero boundary conditions. We will take $\mathcal{D}(-\Delta)$ to be the subspace of $H^2(\Omega)$ consisting of smooth functions with zero Dirichlet or zero Neumann boundary values[2], depending on the choice of boundary condition.

The spectrum $\sigma(-\Delta)$, which is now discrete, depends on the domain Ω and on whether Dirichlet or Neumann conditions are used. The spectrum of the Laplacian in the Dirichlet case is defined by the problem,

$$\begin{aligned} -\Delta e_k &= \lambda_k e_k \text{ in } \Omega \\ e_k &= 0 \text{ on } \partial\Omega, \end{aligned} \tag{2.35}$$

and in the Neumann case by

$$\begin{aligned} -\Delta e_k &= \lambda_k e_k \text{ in } \Omega \\ \frac{\partial e_k}{\partial n} &= 0 \text{ on } \partial\Omega. \end{aligned}$$

The λ_k are the eigenvalues, and e_k the eigenfunctions, of $-\Delta$ with zero Dirichlet or Neumann boundary condition, respectively. The spectral decomposition (2.2) then reads

$$-\Delta u(x) = \sum_{k=1}^{\infty} \lambda_k (u, e_k)_{L^2_\Omega} e_k(x). \tag{2.36}$$

[2]We remind the reader that, for using the spectral theorem as in Section 2.2.1, $\mathcal{D}(-\Delta)$ need not be all of $\mathcal{H}$, or even a "maximal" domain of definition of $-\Delta$ within $\mathcal{H}$, but rather a more convenient, dense subspace of $\mathcal{H}$ (a *core* for $-\Delta$) .

We remark that this identity is valid on $\mathcal{D}(-\Delta)$, and can be extended by continuity to $H_0^2(\Omega)$ in the Dirichlet case, or $H^2_{\partial u/\partial n=0}(\Omega) = \left\{u \in H^2(\Omega) \ : \ \frac{\partial u}{\partial n}\Big|_{\partial\Omega} = 0\right\}$ in the Neumann case. It is not in general true for functions u with nonzero boundary values (Dirichlet or Neumann). For example, in one dimension with $-\Delta = -\frac{\partial^2}{\partial x^2}$, and (λ_k, e_k) from (2.35) on $[0, 2\pi]$ and $u = \cos(x)$, the equation (2.36) does not hold. In fact, the series on the right-hand side diverges.

Thus, on $\mathcal{D}(-\Delta)$, in accordance with (2.4), the *spectral fractional Laplacian* is defined by

$$(-\Delta)^{\alpha/2}u(x) := \sum_{k=1}^{\infty} \lambda_k^{\alpha/2}(u, e_k)_{L^2_\Omega} e_k(x). \tag{2.37}$$

As usual, by continuity, this can be extended to an operator on $\mathbb{H}^\alpha(\Omega)$ (see Appendix B). The spectral fractional Laplacian is nonlocal on the interior of Ω for noninteger $\alpha \in (0, 2)$. We see that to compute the inner product $(u, e_k)_{L^2_\Omega}$, it suffices for u to be defined on the interior of Ω. Unlike the Riesz fractional Laplacian, the spectral fractional Laplacian requires no information about u on the exterior $\mathbb{R}^d \setminus \Omega$. Thus, from a conceptual viewpoint, in boundary value problems the spectral fractional Laplacian admits the same type of boundary conditions as the standard, local Laplacian $-\Delta$. Precise conditions and references for rigorous proofs for well-posedness of boundary value problems for the spectral fractional Laplacian with such local boundary conditions (Dirichlet and Neumann) are discussed in Section 2.7.5.

2.6.2 Other representations

In this section, we merely point out the analogues of the characterizations in Section 2.2.3 which have been proven (and implemented) for the spectral fractional Laplacian. Unless otherwise stated, these are not applicable without modification in the case of

nonzero boundary conditions. We do not use these characterizations in our numerical comparisons, but each has its advantages and disadvantages.

The analogue of the extension method (2.10) for the homogeneous spectral fractional Laplacian on a bounded domain was derived in [**203**]. In this characterization, a degenerate elliptic equation is solved in the extruded domain ("cylinder") over Ω, followed by a similar Neumann-type trace. Further studies include [**80, 39, 202**] As this higher-dimensional formulation involves only integer-order operators, standard discretization approaches may be applied, as in [**158, 82, 8**].

The heat semigroup formula on a bounded domain Ω was studied and implemented in [**55**], where the heat semigroup was used to define the spectral fractional Laplacian. This approach can also be carried out for nonzero boundary conditions, and is discussed at length in Section 2.7.4.

The Balakrishnan formula was implemented in, e.g., [**32**]. More recently, in [**31**], a rapidly convergent sinc quadrature was developed for this formula, which is used together with a finite-element approximation to the resolvent $(sI - \Delta)^{-1}$.

Yet another approach in [**213**] considered a reformulation of the spectral fractional Poisson equation with zero Robin boundary conditions as an integer-order (time-dependent) pseudo-parabolic equation that could be solved with standard FEMs in space and finite difference methods in time. The solution of the pseudo-parabolic equation at time $t = 1$ turns out to be the inverse spectral fractional Laplacian applied to the source function, which yields the solution to the fractional Poisson problem.

2.6.3 Subordinate Stopped/Reflected Brownian Motion

It is well known that the Laplacian in a bounded domain is the generator of stopped Brownian motion for Dirichlet boundary conditions, and reflected Brownian motion

for Neumann boundary conditions [**228**]. The construction of stopped Brownian motion uses the same procedure as in (2.29), while the construction of reflected Brownian motion involves the solution of the Skorokhod problem [**103**]. The corresponding processes for the spectral fractional Laplacian can be obtained by means of subordination. Subordination of a process X_t results in a process $X_{T(t)}$, in which time t is replaced by "operational time" $T(t)$, itself a stochastic process – more specifically, an increasing Lévy process. In $\mathbb{R}^d$, an isotropic α-stable Lévy motion can be constructed by subordinating the isotropic Brownian motion with the stable subordinator (see [**52**], Section 4.4). The same time change gives a way of converting Brownian paths that are stopped at the boundary into α-stable Lévy paths that are stopped at the boundary.

The spectral fractional Laplacian with Dirichlet boundary conditions is the generator of subordinate stopped Brownian motion [**196**], i.e., stopped Brownian motion that is then subordinated by the standard stable subordinator. The spectral fractional Laplacian with Neumann boundary conditions is the generator of subordinate reflected Brownian motion. These are both results from the semigroup theory of Markov processes (reviewed in [**228**], Chapter IX; a detailed discussion may be found in Chapter 3 of the present thesis). Thus, one imposes the boundary condition on the process first, before subordinating and turning the stopped/reflected Brownian motion into what resembles a Lévy motion on the interior of the domain. It is important to note the order of the modifications; the reverse order corresponds to the *Riesz* fractional Laplacian in Ω, see Section 2.4.3. For illustrations and further details of subordinate stopped Brownian motion, see Chapter 3, which largely focuses on this process.

2.7 Inhomogeneous Spectral Fractional Laplacian

The construction of the spectral power (2.37) cannot simply be repeated for the case of nonzero boundary conditions. This is because subsets of $C^\infty(\Omega)$ that satisfy a fixed nonzero boundary condition are no longer linear spaces, which prohibits the use of the spectral theorem. However, in the case of the standard Laplacian $-\Delta$ on a bounded domain, using a lifting technique, a spectral series can be derived (see eq. (2.40)). The generalization of this approach can be used to derive a suitable series representation[3] for the inhomogeneous spectral fractional Laplacian, namely

$$(-\Delta_{\Omega,g})^{\alpha/2}u = \sum_{i=1}^{\infty}\left(\lambda_i^{\alpha/2}(u,e_i)_{L^2(\Omega)} - \lambda_i^{\alpha/2-1}\left(u,\frac{\partial e_i}{\partial n}\right)_{L^2(\partial\Omega)}\right)e_i,$$

where g is the nonzero Dirichlet boundary condition for u. This approach was taken by Antil et al. [11] and is discussed in Section 2.7.1. The same authors show that under suitable regularity conditions, the inhomogeneous spectral fractional Laplacian can be written as

$$(-\Delta_{\Omega,g})^{\alpha/2}u = (-\Delta_{\Omega,0})^{\alpha/2}[w-v], \tag{2.38}$$

where $-\Delta v = 0$ in the weak sense, and $v\big|_{\partial\Omega} = g$. This essentially reduces the inhomogeneous operator to the well-studied homogeneous spectral fractional Laplacian. The details of the harmonic lifting are discussed in Section 2.7.2. Nonharmonic lifting functions may also be used; this is discussed in Section 2.7.3.

A different approach was taken by Cusimano et al. [55] where the heat operator was used to define the inhomogeneous spectral fractional Laplacian, for which they

[3]We use the notations $(u,e_i)_{L^2(\Omega)}$ and $\left(u,\frac{\partial e_i}{\partial n}\right)_{L^2(\partial\Omega)}$ as shorthand for $\int_\Omega ue_i$ and $\int_{\partial\Omega} u\frac{\partial e_i}{\partial n}$, respectively.

used the notation $\mathcal{L}_{\Omega,g}^{\alpha/2}$:

$$\mathcal{L}_{\Omega,g}^{\alpha/2}u = -\frac{1}{\Gamma(-\alpha/2)}\int_0^\infty \left(e^{t\Delta_{\Omega,g}}u(x) - u(x)\right)\frac{dt}{t^{1+\alpha/2}}. \tag{2.39}$$

This approach is discussed in Section 2.7.4. A lifting characterization equivalent to (3.4) was obtained for this operator $\mathcal{L}_{\Omega,g}^{\alpha/2}$; thus both the operator $(-\Delta_{\Omega,g})^{\alpha/2}$ defined my Antil et al. [**11**] and the operator $\mathcal{L}_{\Omega,g}^{\alpha/2}$ defined by Cusimano et al. [**55**] are the same. Hence, we use the symbol $(-\Delta_{\Omega,g})^{\alpha/2}$ in the remainder of this work. We compare numerical methods that can be applied to both approaches in our article [**137**].

2.7.1 Series Representation

We motivate the approach in [**11**] by discussing the spectral representation of the standard Laplacian $-\Delta u = -\frac{\partial^2 u}{\partial x_1^2} - ... - \frac{\partial^2 u}{\partial x_d^2}$ on a bounded domain Ω for arguments u with nonzero boundary values. Given a function u such that $u|_{\partial\Omega} = g$, where g need not be zero, subtract from u a harmonic function v inside Ω with the same boundary values:

$$-\Delta v = 0, \quad v|_{\partial\Omega} = g.$$

We refer to this as a *harmonic lifting* of u. Then

$$-\Delta u = -\Delta(u - v), \quad (u - v)|_{\partial\Omega} = 0.$$

In other words, this does not change the Laplacian, and since the boundary value for $u - v$ is zero, we can use it in formula (2.36):

$$\begin{aligned} -\Delta u &= -\Delta(u - v) \\ &= \sum \lambda_k (u - v, e_k)_{L^2(\Omega)} e_k \\ &= \sum \lambda_k (u, e_k)_{L^2(\Omega)} e_k - \lambda_k (v, e_k)_{L^2(\Omega)} e_k. \end{aligned}$$

Let us rewrite the second inner product in the sum, which involves the harmonic function v:

$$\begin{aligned} (v, e_k) &= (v, -\Delta(-\Delta)^{-1} e_k)_{L^2(\Omega)} \\ &= (v, -\Delta\lambda^{-1} e_k)_{L^2(\Omega)} && \text{(by the eigenfunction property)} \\ &= \lambda^{-1} \int_\Omega -\Delta v e_k + \lambda^{-1} \int_{\partial\Omega} v \frac{\partial e_k}{\partial n} - \lambda^{-1} \int_{\partial\Omega} e_k \frac{\partial v}{\partial n} && \text{(Green's second identity)} \\ &= \lambda^{-1} \int_{\partial\Omega} v \frac{\partial e_k}{\partial n} && \text{(since } -\Delta v = 0 \text{ on } \Omega \text{ and } e_k = 0 \text{ on } \partial\Omega) \\ &= \lambda^{-1} \int_{\partial\Omega} u \frac{\partial e_k}{\partial n} && \text{(since } u - v = 0 \text{ on } \partial\Omega). \end{aligned}$$

This gives us the spectral expansion of $-\Delta$ which is now valid for *any* smooth function u on Ω, regardless of boundary values:

$$-\Delta u = \sum_{k=1}^{\infty} \left(\lambda_k \int_\Omega u e_k - \int_{\partial\Omega} u \frac{\partial e_k}{\partial n} \right) e_k. \tag{2.40}$$

This is a key result for defining the inhomogeneous spectral fractional Laplacian. However, before we can proceed, the operator $(-\Delta)^{-1}$ that appeared in the derivation above requires clarification. *A priori*, it is a multiple-valued operator, since $(-\Delta)^{-1} f$ is only specified up to a harmonic function in Ω. However, owing to the uniqueness of the (standard) Poisson problem, this arbitrariness may be removed by requiring $(-\Delta)^{-1} f$ to have fixed boundary value g on $\partial\Omega$. Thus, $u = (-\Delta_g)^{-1} f$ is defined as

the function such that $-\Delta u = f$ and $u = g$ on $\partial\Omega$. Regardless of the fixed boundary condition, this will result in a single-valued operator $(-\Delta_g)^{-1}$ such that

$$-\Delta(-\Delta_g)^{-1} = \mathrm{Id}_{H^{-2}}, \tag{2.41}$$

and

$$(-\Delta_g)^{-1}(-\Delta) = \mathrm{Id}_{\{u\in H^2 \text{ such that } u|_{\partial\Omega}=g\}}. \tag{2.42}$$

For definiteness, and to obtain an identity operator on a linear subset of H^2 in (2.42), the zero boundary value $g \equiv 0$ is chosen. We sometimes refer to this as the *zero gauge* inverse Laplacian, and simply write $(-\Delta)^{-1}$ rather than $(-\Delta_0)^{-1}$. The series expansion is then the spectral power

$$(-\Delta)^{-1} f = \sum_{i=1}^{k} \lambda^{-1} (f, e_i)_{L^2(\Omega)} e_i,$$

which defines an operator from $H^{-2}(\Omega)$ to $L^2(\Omega)$. We remark that, even with the choice of a zero gauge, (2.41) is valid on functions with arbitrary boundary values.

Using the result (2.40), a natural approach to defining the spectral fractional Laplacian with nonzero boundary conditions is to write

$$(-\Delta)^{\alpha/2} u := (-\Delta)^{\alpha/2-1}(-\Delta)u$$

and use the series (2.40) above. At first glance, this merely shifts the problem to defining the *inverse* spectral fractional Laplacian with nonzero boundary conditions. However, defining this inverse inhomogeneous operator is considerably easier. By the above discussion of $(-\Delta)^{-1}$, the spectral power

$$(-\Delta)^{\alpha/2-1} := \sum_{i=1}^{\infty} \lambda_i^{\alpha/2-1} (-\Delta u, e_i)_{L^2(\Omega)} e_i$$

is a convergent, single valued operator on $H^{-s}(\Omega)$, regardless of boundary conditions. For $\alpha = 2$, we understand the operator $(-\Delta)^{-1}u$ to be the projection onto the zero-boundary value functions $H_0^2(\Omega)$ of all functions v such that $-\Delta v = u$. Thus, the zero-boundary condition is used to eliminate multi-valuedness of $(-\Delta)^{-1}$, but the operator may take as argument a function with arbitrary boundary values.

As a result of these definitions, using the spectral expansion of the inhomogeneous (integer-order) Laplacian (2.40), we obtain

$$\begin{aligned}
(-\Delta)^{\alpha/2}u &= (-\Delta)^{\alpha/2-1}(-\Delta)u \\
&= \sum_{i=1}^{\infty} \lambda_i^{\alpha/2-1}(-\Delta u, e_i)_{L^2(\Omega)} e_i \\
&= \sum_{i=1}^{\infty} \lambda_i^{\alpha/2-1} \left(\sum_{j=1}^{\infty} \left(\lambda_j \int_\Omega u e_j - \int_{\partial\Omega} u \frac{\partial e_j}{\partial n} \right) e_j, e_i \right)_{L^2(\Omega)} e_i \\
&= \sum_{i=1}^{\infty} \lambda_i^{\alpha/2-1} \left(\lambda_i \int_\Omega u e_i - \int_{\partial\Omega} u \frac{\partial e_i}{\partial n} \right) e_i \\
&= \sum_{i=1}^{\infty} \lambda_i^{\alpha/2} \left(\int_\Omega u e_i \right) e_i - \lambda_i^{\alpha/2-1} \left(\int_{\partial\Omega} u \frac{\partial e_i}{\partial n} \right) e_i.
\end{aligned}$$

This is the definition in [11] of a general inhomogeneous spectral fractional Laplacian. This can be considered the fractional analogue of (2.40). In their paper, Antil et al. also proved a similar formula for nonzero Neumann boundary conditions. Furthermore, they developed an integration-by-parts formula for these formulations, proved regularity results, introduced finite element discretizations, derived the associated error estimates, and included numerical experiments.

2.7.2 Harmonic Lifting

Taking the series representation of the operator $(-\Delta_{\Omega,g})^{\alpha/2}$ as a definition, Antil et al. [11] considered the inhomogeneous spectral fractional Poisson problem:

$$\begin{aligned}(-\Delta_{\Omega,g})^{\alpha/2}u(x) &= f(x), \quad x \in \Omega, \quad \alpha \in (0,2),\\ u(x) &= g(x), \quad x \in \partial\Omega.\end{aligned}$$

By linearity, the solution u can be written as

$$u(x) = a(x) + b(x), \tag{2.43}$$

where a solves

$$\begin{aligned}(-\Delta_{\Omega,g})^{\alpha/2}a = (-\Delta_{\Omega,0})^{\alpha/2}a &= f \quad \text{in } \Omega,\\ a\Big|_{\partial\Omega} &= 0 \quad \text{on } \partial\Omega,\end{aligned} \tag{2.44}$$

and the component b solves the equation

$$\begin{aligned}(-\Delta_{\Omega,g})^{\alpha/2}b &= 0 \quad \text{in } \Omega,\\ b\Big|_{\partial\Omega} &= g \quad \text{on } \partial\Omega.\end{aligned} \tag{2.45}$$

However, this "fractional harmonic" function b, under certain conditions on the regularity of g, is simply the solution to the standard Laplace equation

$$\begin{aligned}-\Delta b &= 0 \quad \text{in } \Omega,\\ b\Big|_{\partial\Omega} &= g \quad \text{on } \partial\Omega.\end{aligned} \tag{2.46}$$

The simple intuition behind this equivalence involves the characterization of the operator $(-\Delta_{\Omega,g})^{\alpha/2}$ as $(-\Delta)^{\alpha/2-1}(-\Delta)$ and our choice of the zero gauge inverse Laplacian, so that $(-\Delta)^{\alpha/2-1}0 = 0$. From this,

$$-\Delta b = 0 \implies (-\Delta_{\Omega,g})^{\alpha/2}b = 0.$$

Indeed, the authors of [11] show that Equation (2.45) is, for boundary functions $g \in L^2(\partial\Omega)$, equivalent to the *very weak variational form* of Equation (2.46):

$$\int_\Omega b(-\Delta)\phi = \int_{\partial\Omega} g\frac{\partial\phi}{\partial n}, \text{ for all } \phi \in H_0^1(\Omega) \cap H^2(\Omega). \tag{2.47}$$

The phrase "very weak" refers to the transfer of all derivatives of v to the test function ϕ via fractional integration-by-parts, a result of the same work [11]. Of course, if the boundary data g is sufficiently regular, then b may be sought as a solution to the weak (rather than very weak) variational form of Equation (2.46):

$$\int_\Omega \nabla b \cdot \nabla\phi = \int_{\partial\Omega} g\frac{\partial\phi}{\partial n}, \text{ for all } \phi \in H_0^1(\Omega).$$

For the precise regularity estimate for the problem (2.47) in terms of the boundary function g, we refer to Lemma 4.1 and the surrounding discussion in the article [11]. We point out the simplest case, in which $g \in H^{1/2}(\partial\Omega)$ implies that $b \in H^1(\Omega)$ and b satisfies (2.46) in the weak sense.

2.7.3 Nonharmonic Lifting

While Antil et al. [11] used a fractional harmonic lifting in their approach, it is possible to obtain a variational form with an arbitrary (i.e., nonharmonic) lifting function. In this section, we describe a lifting approach in which the lifting function $v \in H^1(\Omega)$ need only satisfy the boundary condition $v\big|_{\partial\Omega} = u\big|_{\partial\Omega}$. Again, we wish to solve the spectral fractional Poisson problem

$$\begin{aligned} (-\Delta)^{\alpha/2}u &= f, \quad \text{in } \Omega \\ u\big|_{\partial\Omega} &= g, \quad \text{on } \partial\Omega. \end{aligned} \tag{2.48}$$

The unknown function u can be decomposed as $u = w - v$, where v is the lifting function. This function v need not be unique, and the fractional harmonic function v described above is also admissible.

To derive the variational form of Equation (2.48), we need the following integration-by-parts formula for the inverse spectral fractional Laplacian $(-\Delta)^{\alpha/2-1}$.

THEOREM 2.49. *Let* $0 \leq \alpha \leq 2$ *and* $f, \phi \in L^2(\Omega)$. *Then*

$$((-\Delta)^{\alpha/2-1} f, \phi) = (f, (-\Delta)^{\alpha/2-1} \phi).$$

PROOF. We use the notation $\hat{f}_i = (f, e_i)$ and $\hat{\phi}_i = (\phi, e_i)$.

$$\begin{aligned}
((-\Delta)^{\alpha/2-1} f, \phi) &= \left(\sum_{i=1}^{\infty} \lambda_i^{\alpha/2-1} \hat{f}_i e_i, \sum_{j=1}^{\infty} \hat{\phi}_j e_j \right) \\
&= \sum_{i=1}^{\infty} \sum_{j=1}^{\infty} \lambda_i^{\alpha/2-1} \hat{f}_i \hat{\phi}_j (e_i, e_j) \\
&= \sum_{i=1}^{\infty} \lambda_i^{\alpha/2-1} \hat{f}_i \hat{\phi}_i \\
&= \sum_{i=1}^{\infty} \sum_{j=1}^{\infty} \lambda_j^{\alpha/2-1} \hat{f}_i \hat{\phi}_j (e_i, e_j) \\
&= \left(\sum_{i=1}^{\infty} \hat{f}_i e_i, \sum_{j=1}^{\infty} \lambda_j^{\alpha/2-1} \hat{\phi}_j e_j \right) \\
&= (f, (-\Delta)^{\alpha/2-1} \phi).
\end{aligned}$$

□

This formula is valid regardless of the boundary values of the functions f and ϕ. This is due to our choice of zero gauge for the definition of $(-\Delta)^{\alpha/2-1}$. Then, the variational form of the problem is written as follows: find the function $w \in \mathbb{H}^{\alpha}$ such

that for any $\phi \in L^2(\Omega)$,

$$((-\Delta)^{\alpha/2}(w+v), \phi) = (f, \phi).$$

Now we can define the inhomogeneous spectral fractional Laplacian of v in weak form by integrating-by-parts in the v term on the left-hand-side.

$$\begin{aligned}((-\Delta)^{\alpha/2}v, \phi) &= (-\Delta v, (-\Delta)^{\alpha/2-1}\phi) \\ &= (\nabla v, \nabla(-\Delta)^{\alpha/2-1}\phi),\end{aligned}$$

which is our (weak sense) definition of the inhomogeneous spectral fractional Laplacian.

Finally, we can solve for w by solving the variational equation

$$((-\Delta)^{\alpha/2}w, \phi) = (f, \phi) - (\nabla v, \nabla((-\Delta)^{\alpha/2-1}\phi)), \tag{2.50}$$

where all the fractional operators that appear are now applied to functions satisfying zero boundary conditions. Note that this (standard) weak form (2.50) requires that $v \in H^1(\Omega)$, which by $v|_{\partial\Omega} = g$ and the trace theorem B.3, requires the boundary data $g \in H^{1/2}(\Omega)$. While other weak variational forms leading to less regular solution spaces may be studied to treat rougher boundary data, for the purposes of this chapter, (2.50) will suffice. We recover the solution to Equation (2.48) using the relation $u = w+v$. These lifting approaches were compared using numerical examples in [**137**].

2.7.4 Heat Operator

The authors of [**55**] proposed an extension of the heat semigroup method to define an inhomogeneous spectral fractional Laplacian. In their work, only discretizations of their newly-defined operator are considered, not the solution of the Poisson problem

using this operator. Cusimano et al. define their inhomogeneous spectral fractional Laplacian as in Equation (2.39), in which $e^{t\Delta_{\Omega,g}}$ is the propagator of the heat equation. Next, the authors use a splitting for $w(x,t)$, which allows one to relate $\mathcal{L}^{\alpha/2}_{\Omega,g}$ to $(-\Delta_{\Omega,0})^{\alpha/2}$, the homogeneous spectral fractional Laplacian. The unknown function $w(x,t)$ can be expressed as $w(x,t) = v(x,t) + z(x)$, where $z(x)$ is a harmonic function, i.e.,

$$\begin{aligned} -\Delta z &= 0 \quad \text{in } \Omega, \\ z &= g \quad \text{on } \partial\Omega, \end{aligned} \tag{2.51}$$

and $v(x,t)$ solves a zero boundary value heat equation:

$$\begin{aligned} \partial_t v - \Delta v &= 0 \quad \text{in } \Omega \times [0,+\infty), \\ v(x,t=0) &= u(x) - z(x), \\ v(x,t) &= 0 \quad \text{on } \partial\Omega \times [0,+\infty). \end{aligned}$$

We notice that $w(x,0) = v(x,0) + z(x) = u(x) - z(x) + z(x) = u(x)$. Then, using the definition of $w(x,t)$ and Equation (2.39), we see that

$$\begin{aligned} \mathcal{L}^{\alpha/2}_{\Omega,g} u &= \frac{1}{\Gamma(-\alpha/2)} \int_0^\infty (w(x,t) - w(x,0)) \frac{dt}{t^{1+\alpha/2}} \\ &= \frac{1}{\Gamma(-\alpha/2)} \int_0^\infty ([v(x,t) + z(x)] - [v(x,0) + z(x)] \frac{dt}{t^{1+\alpha/2}} \\ &= \frac{1}{\Gamma(-\alpha/2)} \int_0^\infty (v(x,t) - v(x,0)) \frac{dt}{t^{1+\alpha/2}} \\ &= \frac{1}{\Gamma(-\alpha/2)} \int_0^\infty (e^{t\Delta_{\Omega,g}}[u-z](x) - [u-z](x)) \frac{dt}{t^{1+\alpha/2}} \\ &= (-\Delta_{\Omega,0})^{\alpha/2}[u-z](x). \end{aligned}$$

Given this information, we can see that the two formulations of the spectral fractional Laplacians in works [11] and [55] are equivalent. We know that the heat

operator approach leads to the relation

$$\mathcal{L}_{\Omega,g}^{\alpha/2}u = (-\Delta_{\Omega,0})^{\alpha/2}[u - z],$$

where z is the harmonic function given by Equation (2.51). We can also obtain a similar formula for the operator of Antil et al. From Equations (2.45) and (3.7), we know

$$(-\Delta_{\Omega,g})^{\alpha/2}u = (-\Delta_{\Omega,0})^{\alpha/2}b.$$

Inserting $b = u - a$ from the splitting (3.6), we have

$$(-\Delta_{\Omega,g})^{\alpha/2}u = (-\Delta_{\Omega,0})^{\alpha/2}[u - a].$$

This shows that the inhomogeneous spectral fractional Laplacian $(-\Delta_{\Omega,g})^{\alpha/2}$ is just the standard homogeneous operator applied to the lifting $u - a$. Since a is also a harmonic function in Ω with $a\Big|_{\partial\Omega} = g$, by uniqueness, $a = z$. Therefore

$$(-\Delta_{\Omega,g})^{\alpha/2}u = (-\Delta_{\Omega,0})^{\alpha/2}[u - z] = \mathcal{L}_{\Omega,g}^{\alpha/2}u.$$

This fact is demonstrated numerically in the article [**137**].

2.7.5 Well-posedness and Regularity

We begin by discussing well-posedness (existence and uniqueness) of the spectral fractional Poisson problem. We consider the general case of nonzero boundary conditions. Thus, the fractional Laplacian that is used in the two problems below is the inhomogeneous operator that has been reviewed in this section. We have transcribed the existence and uniqueness theorems proven in [**11**]. These results have been abbreviated by considering $\alpha/2 \geq 1/2$, resulting in minimal regularity of boundary data $g \in L^2(\partial\Omega)$ in the Dirichlet case, and $g \in H^{-1}(\partial\Omega)$ for the Neumann case; the

full theorems in [11] actually allow for $\alpha/2 < 1/2$ and rougher boundary data. The Sobolev space notations used in this section are defined in Appendix B.

For the Dirichlet boundary condition, let Ω be a bounded quasi-convex domain. If $f \in \mathbb{H}^{-\frac{\alpha}{2}}(\Omega)$ and $g \in H^{\frac{\alpha}{2}-\frac{1}{2}}(\partial\Omega)$ for $\alpha/2 \geq 1/2$, then there exists a unique solution $u \in H^{\frac{\alpha}{2}}(\Omega)$ to

$$(-\Delta)^{\alpha/2} u = f \text{ in } \Omega, \quad u|_{\partial\Omega} = g,$$

which satisfies

$$\|u\|_{H^{\frac{\alpha}{2}}(\Omega)} \leq C \left(\|f\|_{\mathbb{H}^{-\frac{\alpha}{2}}(\Omega)} + \|g\|_{H^{\frac{\alpha}{2}-\frac{1}{2}}(\partial\Omega)} \right).$$

For $\alpha/2 = 1/2$, the convention is $H^0(\partial\Omega) = L^2(\partial\Omega)$. This statement is a special case of Theorem 4.5 in [11].

For the Neumann boundary condition, again let Ω be a bounded quasi-convex domain. Let $1/2 \leq \alpha/2 \leq 1$. If $f \in H^{\frac{\alpha}{2}}(\Omega)^*$ (the dual of $H^{\frac{\alpha}{2}}(\Omega)$; for $\alpha/2 > 1/2$ this is distinct from $\mathbb{H}^{-\frac{\alpha}{2}}(\Omega)$) and $g \in H^{\frac{\alpha}{2}-\frac{3}{2}}(\partial\Omega)$ satisfy the compatibility condition

$$\int_\Omega f + \int_{\partial\Omega} g = 0,$$

then there exists a unique solution $u \in H^{\frac{\alpha}{2}}(\Omega)$ such that $\int_\Omega u = 0$ to

$$(-\Delta)^{\alpha/2} u = f \text{ in } \Omega, \quad \partial u/\partial n|_{\partial\Omega} = g,$$

which satisfies

$$|u|_{H^{\frac{\alpha}{2}}(\Omega)} \leq C \left(\|f\|_{H^{\frac{\alpha}{2}}(\Omega)^*} + \|g\|_{\mathbb{H}^{\frac{\alpha}{2}-\frac{3}{2}}(\partial\Omega)} \right).$$

This statement is a special case of Theorem 5.4 in [11].

Next, we discuss regularity for the spectral fractional Poisson equation. Unlike the well-posedness results discussed above, we now focus exclusively on the case of *zero* boundary conditions. This is because almost all regularity results that have been published at the time of this writing have been presented in this form. Various extensions to nonzero boundary conditions can be made by considering these results in combination with the harmonic lifting property discussed in 2.7.2 and 2.7.4.

For the standard homogeneous spectral fractional Laplacian, we state only the simplest case of the Sobolev regularity results in [89], and direct the reader to that article for a full discussion. First, we consider the Dirichlet problem, using the zero Dirichlet boundary value fractional Sobolev space $\mathbb{H}^{\alpha/2}(\Omega)$. Let Ω be a bounded, C^∞-smooth subset of $\mathbb{R}^d$. Let u satisfy the equation

$$(-\Delta)^{\alpha/2}u = f \text{ in } \Omega, \quad u|_{\partial\Omega} = 0 \tag{2.52}$$

for $0 < \alpha < 2$. Then

(1) If $s < 1/2$, then $f \in H^s(\Omega)$ implies $u \in \mathbb{H}^{s+\alpha}(\Omega)$.
(2) If $s = 1/2$, then $f \in H^s_{00}(\Omega)$ implies $u \in \mathbb{H}^{s+\alpha}(\Omega)$.
(3) If $1/2 < s < 2 + 1/2$, then $f \in H^s(\Omega)$ implies only that $u \in \mathbb{H}^{1/2-\epsilon+\alpha}(\Omega)$, and we have the stronger result $u \in \mathbb{H}^{s+\alpha}(\Omega)$ if and only if $f = 0$ on $\partial\Omega$.

We illustrate that this last result is sharp with a simple example. Note that the Sobolev norm in $H^s(I)$ of a Fourier sine series is given by

$$\left\|\sum a_k \sin(kx)\right\|_{H^s(I)} = \sum (1+k^2)^s |a_k^2|.$$

Consider the interval $[0, 2\pi]$, where the eigenvalues of the (Dirichlet) Laplacian are $\lambda_k = k^2$, with corresponding eigenfunctions $e_{\lambda_k} = \sin(kx)$. Let us begin by constructing a low regularity $f \in L^2$:

$$f = \sum_{k=1}^{\infty} \frac{1}{\sqrt{k}\log(k+1)} \sin(kx). \tag{2.53}$$

Then, $f \in L^2$ since

$$\begin{aligned}
\sum_{k=1}^{\infty} \frac{1}{k\log^2(k+1)} &\leq \int_1^{\infty} \frac{dx}{x\log^2(x+1)} \\
&= \int_1^{\infty} \frac{dx}{(x+1)\left(\log^2(x+1) - \frac{\log^2(x+1)}{x+1}\right)} \\
&= \int_{\log 2}^{\infty} \frac{dx}{x^2(1-e^{-x})} \\
&\leq 2.
\end{aligned}$$

But $f \notin H^s$ for any $s > 0$ since

$$\|f\|_{H^s} \sim \sum_{k=1}^{\infty} \frac{(1+k^2)^s}{k(\log^2(k+1))} \geq \sum_{k=1}^{\infty} \frac{k^{2s}}{k\log^2(k+1)} \geq \sum_{k=1}^{\infty} \frac{1}{k} = \infty.$$

Now, the solution to the fractional Poisson problem with zero Dirichlet boundary conditions and f given by (2.53) is

$$u = \sum_{k=1}^{\infty} \frac{k^{-\alpha}}{\sqrt{k}\log(k+1)} \sin(kx).$$

We see $\|u\|_{H^{s+\alpha}} \sim \|f\|_{H^s}$, so u has strict H^α regularity: $u \in H^\alpha$ and $u \notin H^{\alpha+\epsilon}$. *Thus, the α-gain in regularity as stated in the result above is sharp.*

Next, we consider the Neumann problem, and for $s > 3/2$ we define the zero Neumann boundary value fractional Sobolev space

$$H^s_{\partial u/\partial n=0}(\Omega) = \left\{ u \in H^s(\Omega) \text{ such that } \frac{\partial u}{\partial n} \bigg|_{\partial\Omega} = 0 \right\}.$$

If $s < 3/2$, we define $H^s_{\partial u/\partial n=0}(\Omega) = H^s(\Omega)$. Let Ω be a bounded, C^∞-smooth subset of $\mathbb{R}^d$. Let u satisfy the equation

$$(-\Delta)^{\alpha/2} u = f \text{ in } \Omega, \quad \partial u/\partial n|_{\partial\Omega} = 0. \tag{2.54}$$

Then,

(1) If $s < 3/2$, then $f \in H^s(\Omega)$ implies $u \in H^{s+\alpha}_{\partial u/\partial n=0}(\Omega)$.
(2) If $3/2 < s < 7/2$, then $f \in H^s(\Omega)$ implies $u \in H^{s+\alpha}_{\partial u/\partial n=0}(\Omega)$ if and only if $\partial f/\partial n = 0$ on $\partial\Omega$.

Among additional results, [89] discusses the extension by induction of the above points to higher $H^s(\Omega)$ regularity of f.

Regularity in the Hölder spaces $C^{k,r}$ for the spectral fractional Poisson problem was studied extensively in [39]. In that work, an array of results were obtained, for both interior and boundary regularity of the solution u in the Dirichlet problem (2.52) and in the Neumann problem (2.54), with conditions of the form $f \in C^{0,r}(\Omega)$ or of the form $f \in L^p(\Omega)$, under fairly general conditions on the domain Ω. The results also allow for powers of more general, variable-coefficient elliptic operators. We transcribe just one of these results for the fractional Laplacian, namely, the interior regularity for $f \in C^{0,r}(\Omega)$ of the Poisson problem, which is the same for both zero Dirichlet or zero Neumann boundary condition:

Assume that Ω is a bounded Lipschitz domain and that $f \in C^{0,r}(\Omega)$, for some $0 < r < 1$. Let u be a solution to (2.52) or (2.54).

(1) If $0 < r + \alpha < 1$, then $u \in C^{0,r+\alpha}(\Omega)$ and

$$[u]_{C^{0,r+\alpha}(\Omega)} \leq C\Big(\|u\|_{L^2(\Omega)} + [u]_{H^{\alpha/2}(\Omega)} + \|f\|_{C^{0,r}(\Omega)}\Big).$$

(2) If $1 < r + \alpha < 2$, then $u \in C^{1,r+\alpha-1}(\Omega)$ and

$$[u]_{C^{1,r+\alpha-1}(\Omega)} \leq C\Big(\|u\|_{L^2(\Omega)} + [u]_{H^{\alpha/2}(\Omega)} + \|f\|_{C^{0,r}(\Omega)}\Big).$$

The constants C depend only on d, Ω, r, and α. For the proof of this and other regularity results, see [**39**]. Similar results have also been obtained for the equation $(-\epsilon\Delta)^{1/2}u + u = f$ with zero Neumann boundary condition in [**204**].

As indicated by the above theorem, the results of Caffarelli and Stinga [**39**] hold for quite general assumptions on the boundary $\partial\Omega$, but are limited to Hölder spaces of low order. It is far from straightforward to extend them to $C^{k,r}$ for $r \geq 2$ (given appropriate assumptions). Higher order Hölder regularity was studied in Grubb [**89**] under the assumption that the domain Ω has smooth boundary. Below, we transcribe one such theorem, Corollary 3.6 in [**89**], for the case of the spectral fractional Laplacian with zero Dirichlet boundary conditions. We use the notation for Hölder spaces discussed in Appendix A, with $C^r(\Omega) = C^{\lfloor r \rfloor,\rho}(\Omega)$ for real $r > 0$, $r = \lfloor r \rfloor + \rho$. Suppose that u is a solution to (2.52), and that

(1) $f \in C^r(\overline{\Omega})$;
(2) For the integer k such that $2k < r < 2k+2$, $(-\Delta)^l f = 0$ for all nonnegative integers $l \leq k$.

Then for any $\epsilon > 0$,

$$u \in C^{r+\alpha-\epsilon}(\Omega) \text{ and } \begin{cases} (-\Delta)^l u = 0 \text{ for } l \leq k, \text{ if } r + \alpha \leq 2k + 2, \\ (-\Delta)^l u = 0 \text{ for } l \leq k + 1, \text{ if } r + \alpha > 2k + 2. \end{cases}$$

2.8 The Fractional Laplacian with Periodic Boundary Conditions

The fractional Laplacian with periodic boundary conditions (i.e., on the torus $\mathbb{T}^d$) is also a widely-studied operator. One way to define it follows the construction of the fractional Laplacian in $\mathbb{R}^d$ using the spectral theorem in Section 2.2.1 except that the spectrum is discrete, so the operator is given by a Fourier series. For a basic discussion, see, e.g., [**100**], and for discussions of extension characterizations as well as well-posedness and regularity, see [**181, 180**]. This operator is discussed in more detail in Chapter 4 of this thesis, in reference to the fractional Schrödinger equation with periodic boundary conditions for Path Integral Monte Carlo. Importantly, the same representation in terms of a Fourier series is formally in agreement with (2.6) when applied to periodic functions. Thus, the definition of the spectral fractional Laplacian is unambiguous. In other words, the disagreement between various definitions when considering the fractional Laplacian on bounded domains with, say, Dirichlet boundary conditions, does not occur for periodic boundary conditions. Both the restriction of definition of the fractional Laplacian in $\mathbb{R}^d$ via the Fourier transform and the construction of the operator directly in terms of periodic eigenfunctions (trigonometric functions) lead to the same operator.

2.9 Summary

In Table 1, we have summarized the fundamental properties and stochastic interpretations of the Riesz and spectral fractional Laplacians, as they were discussed in this chapter. From the stochastic perspective, these operators differ in that the

$(-\Delta)^{\alpha/2}u$	Definition	Domain	BC type	Stopped process for Dirichlet BC	Reflected process for zero Neumann BC
Spectral	$\sum \lambda_i^{\alpha/2}(u, e_i)e_i$, where (λ_i, e_i) is the spectrum of $-\Delta$ on Ω.	Functions on Ω	Local ($\partial\Omega$)	Subordinate stopped Brownian Motion [228, 196, 92]	Subordinate reflected Brownian Motion [228, 92]
Regional	C p.v. $\int_\Omega \frac{u(x)-u(y)}{\lvert x-y\rvert^{n+2\alpha}}dy$, for $C = \frac{2^\alpha \Gamma\left(\frac{\alpha}{2}+\frac{d}{2}\right)}{\pi^{d/2}\lvert\Gamma\left(-\frac{\alpha}{2}\right)\rvert}$.	Functions on Ω	Local ($\partial\Omega$)	Censored Stable Process [25]	Reflected Stable Process [91]
Riesz	C p.v. $\int_{\mathbb{R}^d} \frac{u(x)-u(y)}{\lvert x-y\rvert^{d+\alpha}}dy$ for $C = \frac{2^\alpha \Gamma\left(\frac{\alpha}{2}+\frac{d}{2}\right)}{\pi^{d/2}\lvert\Gamma\left(-\frac{\alpha}{2}\right)\rvert}$.	Functions on $\mathbb{R}^d$.	Ext. (Ω^c)	Stopped α-stable motion [125].	Various conditions/ processes proposed [65, 60]

TABLE 1. Comparison of the Riesz and spectral fractional Laplacians in a bounded domain $\Omega \subset \mathbb{R}^d$.

Riesz Laplacian is associated to processes that leave the domain, while the spectral Laplacian is associated to processes that are confined in the domain.

REMARK 2.55. The Riesz and the spectral fractional Laplacians are merely the two most commonly used definitions. Another fractional Laplacian that has been studied is the *regional* definition:

$$(-\Delta_{\text{regional}})^{\alpha/2}u(x) = C(d,\alpha) \text{ p.v.} \int_\Omega \frac{u(x)-u(y)}{|x-y|^{d+\alpha}}dy,$$

where $C(d,\alpha)$ is given by (2.7). Note that the domain of this operator consists of functions defined on Ω, rather than $\mathbb{R}^d$. The regional definition differs from the Riesz

definition, even if $u(x) \equiv 0$ for $x \in \mathbb{R}^d \setminus \Omega$:

$$\begin{aligned}(-\Delta_{\text{Riesz}})^{\alpha/2}u(x) &= C(d,\alpha)\ \text{p.v.} \int_{\mathbb{R}^d} \frac{u(x)-u(y)}{|x-y|^{d+\alpha}}\ dy \\ &= C(d,\alpha)\ \text{p.v.} \int_{\Omega} \frac{u(x)-u(y)}{|x-y|^{d+\alpha}}\ dy - u(x) \int_{\mathbb{R}^d\setminus\Omega} \frac{C(d,\alpha)}{|x-y|^{d+\alpha}}\ dy \\ &= (-\Delta_{\text{regional}})^{\alpha/2}u(x) - u(x) \int_{\mathbb{R}^d\setminus\Omega} \frac{C(d,\alpha)}{|x-y|^{d+\alpha}}\ dy.\end{aligned}$$

The well-posedness of the fractional Poisson problem involving the regional Laplacian was studied using the Feynman-Kac formula [**90**]. For a further discussion of the regional Laplacian and the relation to reflected and censored α-stable processes, see [**91**]. Neumann and Robin boundary conditions for the regional Laplacian have been discussed in [**219**].

Other notions of fractional Laplacians that arise from related processes are discussed in [**114**]. In general, the probabilistic literature on stable-type processes in bounded domains and related notions of fractional Laplacians is very rich [**26**]. For example, estimates for eigenvalues of the spectral Laplacian were derived using probabilistic techniques in [**48**].

CHAPTER 3

Stochastic Solution of Elliptic and Parabolic Boundary Value Problems for the Spectral Fractional Laplacian

3.1 Introduction.

The deep connection [**149, 152, 121**] between continuous-time random walks (CTRWs) and fractional-order partial differential equations (FPDEs) discussed in Chapter 1 can be utilized to establish stochastic solution formulas, or Feynman-Kac formulas, for FPDEs. Such formulas forge direct connections between stochastic processes at a microscopic level and an FPDE at a macroscopic level, providing a physical basis for using fractional-order models. At the same time, they provide simple, embarrassingly parallel methods for computing solutions of FPDEs locally at a point without having to generate a grid or otherwise solve for the solution at other points. Monte Carlo method based on stochastic solution formulas scale favorably to high dimensions. In general, various methods can be considered to accelerate numerical implementation of such Feynman-Kac formulas, such as walk-on-spheres [**155, 225, 233, 232**], as discussed in Section 2.4.3, or quasi-Monte Carlo sampling [**154**].

In [**145**] and [**17**], such stochastic solution formulas were studied for a general time-fractional equations involving generators of Feller semigroups. Stochastic solutions of equations involving both first-order and fractional-order time derivatives were studied in [**46**]. As regards fractional Laplacians in bounded domains, stochastic solution formulas for the regional fractional Laplacian were studied [**90**] and [**91**]; formulas for the time-fractional Cauchy problem for this operator have recently been obtained in [**210**]. In [**47**], a stochastic solution formula for the time fractional Cauchy problem for Riesz fractional Laplacian with zero (exterior) boundary condition was proven. In [**125**] and [**192**], stochastic solution formulas for the Dirichlet problem for the Riesz fractional Laplacian were obtained and walk-on-spheres algorithms were developed. For a discussion of these different fractional Laplacians and their connections to stochastic processes, see [**137**]. Finally, we mention that this line

of research is not limited to FPDEs; stochastic connections for nonlocal equations have been studied, e.g., in [66]. Recently, [67] gave stochastic representations for a general, nonlocal-in-time evolution equation.

This chapter is motivated by recent advances [11, 55, 137] in defining the spectral fractional Laplacian with nonzero boundary conditions, including Dirichlet, Neumann, and Robin. Reviewed in Chapter 2, these advances have made clear the appropriate definition for the operator, and have established well-posedness of the associated fractional elliptic boundary value problems and fractional parabolic initial-boundary value problems. Thus, in this chapter, we develop and implement stochastic solution formulas for such problems for Dirichlet boundary conditions.

We now outline the main points of this chapter. In Section 3.2, we review the definition and basic properties of the spectral fractional Laplacian with nonzero Dirichlet boundary conditions. In Section 3.3, we review the theory of Feller semigroups, culminating in the abstract Cauchy problem, that will provide the setup for proving stochastic solution formulas. In Section 3.4, we introduce a technique based on subordination and a result of Balakrishnan for obtaining fractional stochastic solution formulas from classical ones, and use this technique to prove the Feynman-Kac formula for the fractional Laplacian $(-\Delta)^{\alpha/2}$ on $\mathbb{R}^d$. This formula itself is well-known and can be shown using the Lévy-Khinchtine formula or other techniques, but the proof presented here serves an illustration of the method. In Section 3.5, we extend this result to equations with nonzero forcing term using Duhamel's principle. Following this blueprint, in Sections 3.6 and 3.7 we prove the first main result of the chapter. For the fractional parabolic mixed initial-boundary value problem in Ω,

$$\begin{cases} \partial_t u(t,x) + (-\Delta_{\Omega,g})^{\alpha/2} u(t,x) = r(x,t) \text{ for } t > 0, x \in \Omega \\ u(0,x) = f(x) \text{ for } x \in \Omega, \quad u(t,x) = g(x) \text{ for } x \in \partial\Omega, \end{cases}$$

we obtain the stochastic solution formula

$$u(t,x) = \mathbb{E}_{X_0^{\Omega,\alpha}=x}\left[f(X_t^{\Omega,\alpha})\chi_{\tau_\Omega > T_{\alpha/2}(t)} + g(X_t^{\Omega,\alpha})\chi_{\tau_\Omega \le T_{\alpha/2}(t)}\right] + \mathbb{E}_{X^{\Omega,\alpha_0}=x}\left[\int_0^t r(t-s, X_s^{\Omega,\alpha})\chi_{\tau_\Omega > T_{\alpha/2}(t-s)} ds\right].$$

This formula involves the process $X_t^{\Omega,\alpha}$, which is constructed by first stopping standard isotropic 2-stable motion X_t^2 at the boundary of Ω at sample exit time τ_Ω, then subordinating by the standard $\alpha/2$-stable subordinator:

$$X_t^{\Omega,\alpha} = X^{\Omega,2}_{T_{\alpha/2}(t)}, \quad X_t^{\Omega,2} = X^2_{t\wedge\tau_\Omega}, \quad \tau_\Omega = \inf\{s : X_s^2 \notin \Omega\}.$$

As discussed in Section 2.2.4, standard isotropic 2-stable motion X_t^2 is equivalent to $\sqrt{2}B_t$, i.e., Brownian motion scaled by $\sqrt{2}$, which is why we refer to the process $X_t^{\Omega,\alpha}$ as "subordinate stopped Brownian motion" throughout this thesis. The process is illustrated in Figure 1.

For the same problem above, in Section 3.8, we then study a classical solution formula, smoothness for $t > 0$, convergence as $t \to 0+$ to the initial condition and convergence as $t \to \infty$ to a steady state which satisfies a fractional elliptic equation. This is the second main result of this chapter. From this analytical result and the stochastic solution formula for the parabolic problem proved in the previous section, we obtain exponential decay in time of the "survival probability" of subordinate stopped Brownian paths $X_t^{\Omega,\alpha}$ – that is, the probability that such a path has not reached the boundary $\partial\Omega$ (being stopped there) within a given time. These results will are then used to prove the stochastic solution formula for the time-independent problem in the Section 3.9, where, for the fractional elliptic boundary value problem

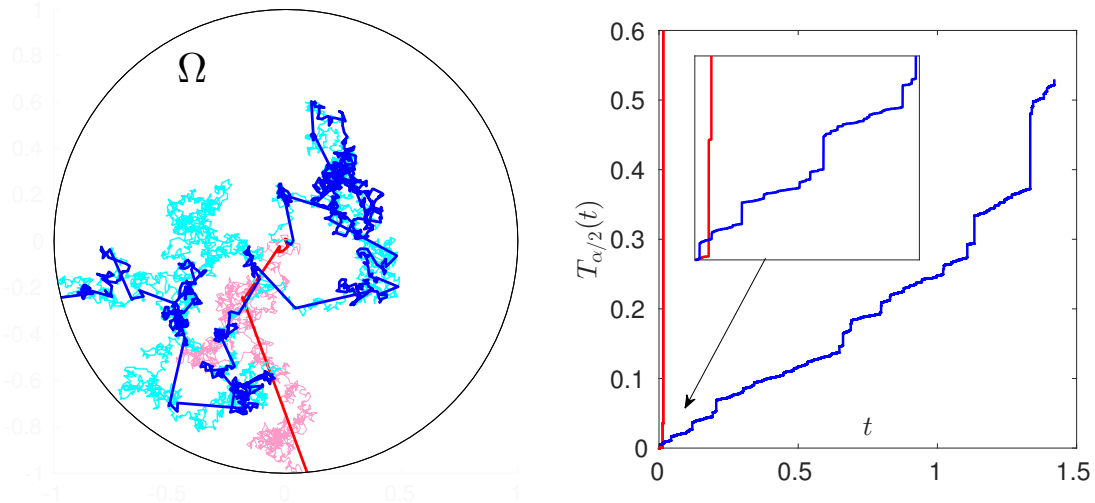

FIGURE 1. Illustration of two sample paths of $X_t^{\Omega,\alpha}$ on the unit disk Ω. In the left subfigure, the cyan/pink curves are two samples of $X_t^{\Omega,2} = X^2_{t\wedge\tau_\Omega} = \sqrt{2}B_{t\wedge\tau_\Omega}$. The right subfigure shows two samples of $T_{\alpha/2}(t)$ that run until they exceed the respective exit times τ_Ω of these two samples of $X_t^{\Omega,2}$. The blue/red curves on the left subfigure are two resulting samples of $X_t^{\Omega,\alpha} = X^{\Omega,2}_{T_{\alpha/2}(t)}$.

in Ω

$$\begin{cases} (-\Delta_{\Omega,g})^{\alpha/2}u(x) = r(x) \text{ for } x \in \Omega \\ u(x) = g(x) \quad \text{for } x \in \partial\Omega, \end{cases}$$

we establish the stochastic solution formula

$$u(x) = \mathbb{E}_{X_0^{\Omega,\alpha}=x}\left[g\left(X^{\Omega,\alpha}_{T^{-1}_{\alpha/2}(\tau_\Omega)}\right)\right] + \mathbb{E}_{X_0^{\Omega,\alpha}=x}\left[\int_0^{T^{-1}_{\alpha/2}(\tau_\Omega)} r(X_s^{\Omega,\alpha})ds\right].$$

This is the third main result of the chapter. Finally, in Section 3.10, we discuss the implementation of these formulas and provide numerical simulations that verify them for benchmark problems on the 2-dimensional unit square, the 3-dimensional unit cube, and the 16-dimensional unit hypercube. We discuss how to discretize the

process $X_t^{\Omega,\alpha}$ and study the convergence of the stochastic solution formula both with the number of paths and the time step size dt used in the discretization.

There is a rich literature on the potential theory of subordinate killed Brownian motion from the probabilistic perspective [**196**, **115**, **114**, **197**]. In [**196**], it is mentioned that the generator of subordinate killed Brownian motion is the spectral fractional Laplacian with zero Dirichlet boundary conditions. To the best of our knowledge, there have been no studies or reported stochastic solution formulas in this literature for the recently introduced spectral fractional Laplacian $(-\Delta_{\Omega,g})^{\alpha/2}$ with nonzero boundary conditions. This represents a novel contribution of our thesis.

3.2 The Spectral Fractional Laplacian with Nonzero Dirichlet Boundary Conditions.

Denoting the Dirichlet eigenvalues and eigenfunctions of $(-\Delta)$ by λ_i and e_i , respectively, the spectral fractional Laplacian[1] for zero Dirichlet boundary values is defined as

$$(-\Delta_{\Omega,0})^{\alpha/2}u = \sum_{i=1}^{\infty} \lambda_i^{\alpha/2}(u, e_i)_{L^2(\Omega)}e_i, \tag{3.1}$$

for $0 < \alpha < 2$. See Appendix A for the basic properties of (λ_i, e_i). This operator has attracted significant attention, both theoretical and numerical, in the past decade; for discussions of the many works relating to this operator, see [**137**, **203**, **29**, **30**] and references therein. However, the generalization of this operator to the case of nonzero boundary conditions was until recently an open problem.

[1]This section contains the minimal definitions and results related to the spectral fractional Laplacian required to state and prove the results of this chapter, and is included to keep the chapter self-contained. The reader who has thoroughly read the more detailed Sections 2.6 and 2.7 on the same topic may choose to skip this section.

In 2017, the spectral fractional Laplacian with nonzero boundary conditions (Dirichlet and Neumann) was introduced and studied [**11**, **55**]. For functions u on $\overline{\Omega}$ satisfying $u|_{\partial\Omega} = g$, Antil, Pfefferer, and Rogovs [**11**] proposed the operator defined by the spectral expansion

$$(-\Delta_{\Omega,g})^{\alpha/2}u = \sum_{i=1}^{\infty}\left(\lambda_i^{\alpha/2}(u,e_i)_{L^2(\Omega)} - \lambda_i^{\alpha/2-1}\left(u,\frac{\partial e_i}{\partial n}\right)_{L^2(\partial\Omega)}\right)e_i, \tag{3.2}$$

On the other hand, Cusimano, Del Teso, Gerardo-Giorda, and Pagnini [**55**] defined an operator in the case of nonzero Dirichlet boundary conditions as

$$(-\Delta_{\Omega,g})^{\alpha/2}u = -\frac{1}{\Gamma(-\alpha/2)}\int_0^{\infty} t^{-\alpha/2-1}(e^{t\Delta_{\Omega,g}} - I)u(x)dt, \tag{3.3}$$

where I denotes the identity operator and $e^{t\Delta_{\Omega,g}}$ is the heat operator with boundary condition g, i.e., $w(x,t) = e^{t\Delta_{\Omega,g}}u(x)$ is defined as the solution to the problem

$$\begin{cases} \partial_t w - \Delta w = 0 \text{ for } x \in \Omega, t > 0 \\ w(t,x) = g(x) \text{ for } x \in \partial\Omega, t > 0 \\ w(0,x) = u(x) \text{ for } x \in \Omega. \end{cases}$$

In Chapter 2, (see also [**137**]), it was pointed out that the proposed operators (3.2) and (3.3) are essentially the same, as the same characterization in terms of (standard) harmonic lifting was proven by their respective authors of [**11**, **55**]. More specifically,

$$(-\Delta_{\Omega,g})^{\alpha/2}u = (-\Delta_{\Omega,0})^{\alpha/2}[u - v], \tag{3.4}$$

where v solves

$$\begin{cases} -\Delta v = 0 \\ v\Big|_{\partial\Omega} = g. \end{cases} \tag{3.5}$$

Moreover, it was shown in Chapter 2 that the same operator can be obtained by first taking the spectral power of the inverse fractional Laplacian

$$(-\Delta)^{-\beta}u = \sum_{i=1}^{\infty} \lambda^{-\beta}(u, e_i)_{L^2(\Omega)} e_i, \quad \beta > 0.$$

then defining $(-\Delta_{\Omega,g})^{\alpha/2} = (-\Delta)^{\alpha/2-1}(-\Delta)u$, noting that $\alpha/2 - 1 < 0$, and using the classical formula

$$(-\Delta)u = \sum_{i}^{\infty} \left(\lambda_i (u, e_i)_{L^2(\Omega)} - \left(u, \frac{\partial e_i}{\partial n} \right)_{L^2(\partial\Omega)} \right) e_i,$$

which is valid for any $C^2(\Omega)$ function u, regardless of boundary values. Thus, there is no ambiguity in the use of the symbol $(-\Delta_{\Omega,g})^{\alpha/2}$.

The solutions of boundary value problems involving the operator $(-\Delta_{\Omega,g})^{\alpha/2}$ have corresponding harmonic lifting characterizations as well. From [**11**], the solution of

$$\begin{cases} (-\Delta_{\Omega,g})^{\alpha/2} u(x) = f(x), & x \in \Omega, \quad \alpha \in (0,2), \\ u(x) = g(x), & x \in \partial\Omega. \end{cases}$$

can be written as

$$u(x) = w(x) + v(x), \tag{3.6}$$

where v again solves (3.5) and w solves the problem

$$\begin{cases} (-\Delta_{\Omega,0})^{\alpha/2} w = f & \text{in } \Omega, \\ w\big|_{\partial\Omega} = 0 & \text{on } \partial\Omega, \end{cases} \tag{3.7}$$

provided the problem (3.5) for v has a classical solution. In fact, [**11**] showed that this decomposition holds even if the problem (3.5) admits a solution in the *very weak variational sense*. However, in this chapter, we will only deal with classical solutions.

In the following sections, we will prove Feynman-Kac formulas for parabolic and elliptic problems posed with $(-\Delta_{\Omega,g})^{\alpha/2}$ and Dirichlet boundary conditions.

3.3 Markov Semigroups, Generators, Feller Processes, and the Abstract Cauchy Problem.

The following is setup of Feller semigroup theory needed for the main result, distilled from the first two chapters of Mark Freidlin's book [77]. Let Ω be a locally compact subset of $\mathbb{R}^d$; this includes open and closed subsets of $\mathbb{R}^d$. Let $X_t : \mathbb{R}^+ \to \Omega$ be a Markov process in Ω. Define the one-parameter family of operators $\mathcal{T}_t$ for $t \geq 0$, acting on functions $f : \Omega \to \mathbb{R}$, as follows:

$$\mathcal{T}_t f : \Omega \to \mathbb{R}, \quad \mathcal{T}_t f(x) = \mathbb{E}_{X_0=x}\left[f(X_t)\right]$$

Then $\mathcal{T}_t$ satisfies the semigroup properties in t, and is linear in f:

$$\mathcal{T}_0 f(x) = f(x) \tag{3.8}$$

$$\mathcal{T}_t \mathcal{T}_s f(x) = \mathcal{T}_{t+s} f(x) \tag{3.9}$$

$$\mathcal{T}_t[f + \tilde{f}](x) = \mathcal{T}_t f(x) + \mathcal{T}_t \tilde{f}(x) \tag{3.10}$$

Here $t, s > 0$. Property (3.8) is obvious. Property (3.9) follows from the Markov property of X_t. Property (3.10) is a property of mathematical expectation. If, in addition, X_t is a *Feller Process*, then the semigroup is *contractive* and *right continuous*:

$$\|\mathcal{T}_t f\|_{C_0(\Omega)} \leq \|f\|_{C_0(\Omega)} \tag{F1}$$

$$\lim_{t \to 0} \|\mathcal{T}_t f - f\|_{C_0(\Omega)} = 0 \tag{F2}$$

Here, $C_0(\Omega)$ denotes the space of continuous functions vanishing at infinity, i.e., real-valued continuous functions f on Ω with the property that for every $\epsilon > 0$, there exists a compact subset $K \subset \Omega$ such that $|f(x)| < \epsilon$ for all x outside of K. The norm of $C_0(\Omega)$ is the sup-norm on Ω:

$$\|f\|_{C_0(\Omega)} = \sup_{x\in\Omega} |f(x)|.$$

Thus, $\{\mathcal{T}_t\}$ is a family of (uniformly) bounded linear operators from $C_0(\Omega)$ to itself. We refer to $\{\mathcal{T}_t f\}$ as the *Feller semigroup* of the process X_t. We note that Lévy Processes are Feller (Theorem 3.1.9, [12]).

Associated to every Markov semigroup $\mathcal{T}_t$ is an *infinitesimal generator* or *infinitesimal operator* $\mathcal{A}$, again acting on functions $f : \Omega \to \mathbb{R}$, defined by

$$\mathcal{A}f : \Omega \to \mathbb{R}, \quad \mathcal{A}f(x) = \lim_{t\to 0+} \frac{\mathcal{T}_t f(x) - f(x)}{h}, \tag{3.11}$$

where the limit is taken in $C_0(\Omega)$, i.e.,

$$\left\| \frac{\mathcal{T}_t f(x) - f(x)}{h} - \mathcal{A}f(x) \right\|_{C_0(\Omega)} \to 0 \text{ as } t \to 0+. \tag{3.12}$$

The domain $\mathrm{Dom}(\mathcal{A})$ is the space of all functions f where the above limit exists.

In some works, the semigroup is jumped over, and one speaks of $\mathcal{A}$ as the *infinitesimal generator* of the process X_t without introducing the notation $\mathcal{T}_t$. However, the semigroup is the key to proving stochastic solution formulas. It features in the following important result:

LEMMA 3.13. *Let X_t be a Feller Process. The function $u(t,x) = \mathcal{T}_t f(x)$ solves the* ***abstract Cauchy problem****,*

$$\begin{cases} \frac{d}{dt}u(t,x) = \mathcal{A}u(t,x) \text{ for } t > 0, \\ \lim_{t\to 0} u(t,x) = f(x), f \in \mathrm{Dom}(\mathcal{A}). \end{cases} \tag{3.14}$$

It is the unique solution in the class of functions that grow at most exponentially, i.e., those solutions $u(t,x)$ for which there exist constants P, k such that $\|u(t,\cdot)\|_{C_0(\Omega)} \leq Pe^{kt}$.

REMARK 3.15. We understand the statement of problem (3.14) to mean: the limit in $C_0(\Omega)$ of $\frac{1}{h}\left[u(t+h,\cdot) - u(t,\cdot)\right]$ as $h \to 0$ exists and is equal to $\mathcal{A}u(\cdot,x)$. This convergence in $C_0(\Omega)$ (i.e., uniform convergence) of the limit quotient defining $\frac{d}{dt}u(t,x)$ is a stronger requirement than is typically understood when seeking a classical solution of a differential equation. It must be met to apply the uniqueness result in the lemma.

Lemma 3.13 is transcribed from the book of Mark Freidlin [**77**]. For full details of this theory, the reader should consult that text and references therein; below, we provide a sketch of the proof of the lemma. It is obvious from (F2) that $\mathcal{T}_t f$ satisfies the initial condition in (3.14). The next step is to that see the ordinary differential equation is satisfied for $t > 0$. That is, we wish to prove

$$\lim_{h\to 0} \frac{\mathcal{T}_{t+h}f(x) - \mathcal{T}_t f(x)}{h} = \mathcal{A}\mathcal{T}_t f(x) \text{ in } C_0(\Omega)\ . \tag{3.16}$$

We do this by proving it for the right-sided and left-sided cases separately. For $h > 0$, we write

$$\frac{\mathcal{T}_h\left[\mathcal{T}_t f(x)\right] - \mathcal{T}_t f(x)}{h} = \frac{\mathcal{T}_{t+h}f(x) - \mathcal{T}_t f(x)}{h} = \mathcal{T}_t \frac{\mathcal{T}_h f(x) - f(x)}{h}$$

The rightmost ratio converges in $C_0(\Omega)$ as $h \to 0+$ to $\mathcal{T}_t\mathcal{A}f(x)$ by the contractive property (F1), the definition (3.11), (3.12) of the generator $\mathcal{A}$, and $f \in \mathrm{Dom}(\mathcal{A})$. Therefore, the other two ratios also converge, and to the same limit. The center ratio is a one-sided derivative, while the convergence of the leftmost ratio implies

$\mathcal{T}_t f \in \mathrm{Dom}(\mathcal{A})$, so that it also converges to $\mathcal{A}\mathcal{T}_t f(x)$. Thus,

$$\mathcal{A}\mathcal{T}_t f(x) = \lim_{h\to 0+} \frac{\mathcal{T}_{t+h} f(x) - \mathcal{T}_t f(x)}{h} = \mathcal{T}_t \mathcal{A} f(x) \tag{3.17}$$

The first equality is (3.16) when $h \to 0+$.

Next, we consider the left-sided derivative. By the equality in (3.17) of $\mathcal{A}\mathcal{T}_t f(x)$ and $\mathcal{T}_t \mathcal{A} f(x)$, we have

$$\begin{aligned}
&\left\| \frac{\mathcal{T}_t f - \mathcal{T}_{t-h} f}{h} - \mathcal{A}\mathcal{T}_t f \right\|_{C_0(\Omega)} \\
&\qquad = \left\| \frac{\mathcal{T}_t f(x) - \mathcal{T}_{t-h} f(x)}{h} - \mathcal{T}_t \mathcal{A} f \right\|_{C_0(\Omega)} \\
&\qquad = \left\| \frac{\mathcal{T}_t f(x) - \mathcal{T}_{t-h} f}{h} - \mathcal{T}_{t-h}\mathcal{A} f(x) + \mathcal{T}_{t-h}\mathcal{A} f - \mathcal{T}_t \mathcal{A} f \right\|_{C_0(\Omega)} \\
&\qquad \le \left\| \mathcal{T}_{t-h} \left[\frac{\mathcal{T}_h f - f(x)}{h} - \mathcal{A} f(x) \right] \right\|_{C_0(\Omega)} + \| \mathcal{T}_{t-h}\mathcal{A} f - \mathcal{T}_t \mathcal{A} f \|_{C_0(\Omega)} \\
&\qquad \le \left\| \frac{f(x) - \mathcal{T}_h f}{h} - \mathcal{A} f(x) \right\|_{C_0(\Omega)} + \| \mathcal{T}_{t-h}\mathcal{A} f - \mathcal{T}_t \mathcal{A} f \|_{C_0(\Omega)} .
\end{aligned}$$

In obtaining the final line, we used the contraction property (F1). In the limit as $h \to 0+$, the first term vanishes by the definition of the generator (3.11), (3.12) and $f \in \mathrm{Dom}(\mathcal{A})$, while the second term vanishes by right continuity (F2) of $\mathcal{T}_t$. Thus,

$$\lim_{h\to 0+} \frac{\mathcal{T}_t f(x) - \mathcal{T}_{t-h} f(x)}{h} = \mathcal{A}\mathcal{T}_t f(x) \text{ in } C_0(\Omega)$$

which together with (3.17) implies that the ODE (3.16) is satisfied.

Finally, as Freidlin [**77**] points out, uniqueness follows from a general uniqueness theorem for solutions of normal type (satisfying the exponential bound) of the abstract Cauchy problem for closed operators the point spectrum of which is not dense in the right half-plane. See p. 619 of Hille and Phillips [**101**]. This proves the lemma.

3.4 Subordination, Balakrishnan's Theorem, and the fractional Feynman-Kac formula on $\mathbb{R}^d$.

In this section, we introduce background material on subordination of processes together with results of Balakrishnan that connect this to concept to fractional calculus. Rather than listing these results in isolation, we introduce them as steps used in a proof of the Feynman-Kac formula for the fractional Laplacian $(-\Delta)^{\alpha/2}$ in $\mathbb{R}^d$ by leveraging the Feynman-Kac formula for the classical Laplacian $(-\Delta)$. This will mirror our approach for obtaining our main results with the operator $(-\Delta_{\Omega,g})^{\alpha/2}$ in later sections. The formula itself (3.22) in $\mathbb{R}^d$ is well-known; for example it appears in [47] where it is obtained by appealing to Dirichlet form theory [79].

We consider the following problem

$$\begin{cases} \partial_t u(t,x) = -(-\Delta)^{\alpha/2} u(t,x) \text{ for } t > 0, x \in \mathbb{R}^d \\ u(0,x) = f(x). \end{cases} \tag{3.18}$$

We prove the following

THEOREM 3.19. *Let $u(t,x)$ be a solution to (3.18) such that*

$$\text{for every } t \geq 0,\ u(t,\cdot) \in C_x^2(\mathbb{R}^d), \text{ and} \tag{3.20}$$

$$\partial_t u(\cdot,\cdot) \text{ is uniformly continuous in spacetime } [0,\infty) \times \mathbb{R}^d. \tag{3.21}$$

Then

$$u(t,x) = \mathcal{T}_t^\alpha f(x) := \mathbb{E}_{X_0^\alpha = x}\left[f(X_t^\alpha)\right] \tag{3.22}$$

where X_t^α is standard isotropic α-stable Lévy motion in $\mathbb{R}^d$.

To prove the theorem, we will show that the assumption (3.20) implies that $u(t,\cdot) \in \mathrm{Dom}(\mathcal{A}^\alpha)$ and

$$-(-\Delta)^{\alpha/2} u = \mathcal{A}^\alpha u, \tag{3.23}$$

where $\mathcal{A}^\alpha$ is the generator of α-stable Lévy motion X_t^α:

$$\mathcal{A}^\alpha f(x) = \lim_{t \to 0+} \frac{\mathcal{T}_t^\alpha f(x) - f(x)}{h}.$$

Since X_t^α is a Feller process, this result (3.23) together with equation (3.18) and the assumption (3.21) will imply that u satisfies the abstract Cauchy problem (3.14) of the operator $\mathcal{A}^\alpha$. By the uniqueness asserted in Lemma 3.13, $u(t,x)$ must then be given by the semigroup (3.22), which is Theorem 3.19.

Now, the result (3.23) is classical in the case $\alpha = 2$, where it can be shown using Itô's rule as follows [77]. Noting that X_t^2 is scaled Brownian motion $\sqrt{2}B_t$, for $u \in C^2(\mathbb{R}^d)$ we have

$$u(X_t^2) - u(x) = \int_0^t \sum_{i=1}^n \frac{\partial u}{\partial x_i}(X_s)(dX_s^2)_i + \int_0^t \Delta u(X_s^2) ds.$$

Taking expectations,

$$\mathbb{E}[u(X_t^2)] - u(x) = \int_0^t \Delta u(X_s^2) ds.$$

Dividing by t and taking $t \to 0$ gives

$$\mathcal{A}^2 u(x) = \Delta u(x), \quad (u \in C^2) \tag{3.24}$$

This suggests one way to prove Theorem 3.19 is to prove (3.23) using some sort of Itô rule for Lévy processes. However, we will instead use *subordination* to upgrade the classical $\alpha = 2$ result (3.24) to general $\alpha < 2$.

We shall use the fact that α-stable Lévy motion X_t^α is equivalent to *subordinate* Brownian motion, i.e.,

$$X_t^\alpha = X^2_{T_{\alpha/2}(t)}, \tag{3.25}$$

where $T_\beta(t)$ is the standard β-stable subordinator starting at zero, an increasing Lévy process which can most easily be described as having a probability density function $h_\beta(t)$ with Laplace transform

$$\mathcal{L}\left\{h_\beta\right\}(s) = e^{-s^\beta} \tag{3.26}$$

See (see Meerschaert and Sikorskii [**149**] p. 156 or Sato [**187**] p. 198). Then from (3.22) and (3.25), a conditioning argument yields

$$\begin{aligned}
\mathcal{T}_t^\alpha f(x) &= \mathbb{E}_{X_0^2=x}\left[f(X^2_{T_{\alpha/2}(t)})\right] \\
&= \mathbb{E}_{X_0^2=x}\left[\int \mathbb{P}\{T_{\alpha/2}=s\} f(X_s^2) ds\right] \\
&= \int \mathbb{P}\{T_{\alpha/2}=s\}\mathbb{E}_{X_0^2=x}\left[f(X_s^2)\right] ds \\
&= \int \mathbb{P}\{T_{\alpha/2}=s\}\mathcal{T}_s^2 f(x) ds \\
&= \int h_{\alpha/2}(s)\mathcal{T}_s^2 f(x) ds.
\end{aligned} \tag{3.27}$$

We require the following theorem of Balakrishnan [**18**]. The notion of *equicontinuous semigroup of class* C_0 is a semigroup $\mathcal{T}_t$ that satisfies (3.8) and (3.9), as well as the condition

$$\lim_{t\to t_0} \|\mathcal{T}_t f - \mathcal{T}_{t_0} f\|_{C_0} = 0.$$

We note that a Feller semigroup is equicontinuous of class C_0, as for $h > 0$, the contraction property (F1) gives

$$\|\mathcal{T}_{t+h}f - \mathcal{T}_t f\|_{C_0} \leq \|\mathcal{T}_t[\mathcal{T}_h f - f]\|_{C_0} \leq \|\mathcal{T}_h f - f\|_{C_0};$$
$$\|\mathcal{T}_{t-h}f - \mathcal{T}_t f\|_{C_0} \leq \|\mathcal{T}_{t-h}[f - \mathcal{T}_h f]\|_{C_0} \leq \|f - \mathcal{T}_h f\|_{C_0}.$$

As $h \to 0$, the right continuity property (F2) implies that both of the above bounds tend to zero. The following lemma is taken from Yosida [**228**], pages 259 & 264, with a slight change in notation:

LEMMA 3.28. *(Balakrishnan [**18**]) Let $\mathcal{T}_t$ be an equicontinuous semigroup of class C_0. Let*

$$g_{t,\beta}(\lambda) = \begin{cases} \frac{1}{2\pi i}\int_{\sigma-i\infty}^{\sigma+i\infty} e^{t\lambda - tz^\beta} dz; & \sigma > 0, t > 0, \lambda \geq 0, 0 < \beta < 1. \\ 0 \quad \textit{(when } \lambda < 0\textit{)} \end{cases} \tag{3.29}$$

Then the operators $\widehat{\mathcal{T}}_t^\alpha$ defined by

$$\widehat{\mathcal{T}}_t^\alpha g = \begin{cases} \int_0^\infty g_{t,\alpha/2}(s)\mathcal{T}_s f ds & (t > 0) \\ f \qquad (t = 0) \end{cases} \tag{3.30}$$

constitute an equicontinuous semigroup of class C_0. Moreover, the infinitesimal generator of $\widehat{\mathcal{T}}_t^\alpha$, denoted $\widehat{\mathcal{A}}^\alpha$, is given for $f \in \mathrm{Dom}(\mathcal{A})$ by the two equivalent formulas

$$\begin{aligned} \widehat{\mathcal{A}}^\alpha f &= \frac{\sin(\alpha\pi/2)}{\pi}\int_0^\infty \lambda^{\alpha/2-1}(\lambda I - \mathcal{A})^{-1}(-\mathcal{A}f)d\lambda \\ &= \frac{1}{\Gamma(-\alpha/2)}\int_0^\infty \lambda^{-\alpha/2-1}(\mathcal{T}_\lambda - I)f d\lambda. \end{aligned} \tag{3.31}$$

Since Feller semigroups are equicontinuous, we may apply this result to the semigroup $\mathcal{T}_t^2$ generated by Brownian motion X_t^2, in which case we know that

$$\mathcal{A}^2 u = \Delta u, \quad \text{if } u(t,\cdot) \in C^2,$$

which is the classical result (3.24). Next, the function $g_{t,\beta}$ in equation (3.29) with parameters $t = 1$ and $\beta = \alpha/2$ is simply the inverse Laplace transform of (3.26); thus, it coincides with h_β. By the derivation (3.27), we see that the semigroup $\widehat{\mathcal{T}}_t^\alpha$ in equation (3.30) coincides with the semigroup $\mathcal{T}_t^\alpha$.

Now the lemma says that the generator $\mathcal{A}^\alpha$ of $\mathcal{T}_t^\alpha$ is given by the formulas (3.31),

$$\mathcal{A}^\alpha u(t,\cdot) = \widehat{\mathcal{A}}^\alpha u(t,\cdot) = \frac{\sin(\alpha\pi/2)}{\pi} \int_0^\infty \lambda^{\alpha/2-1}(\lambda I - \Delta)^{-1}(\Delta u(t,\cdot))d\lambda$$

whenever $u(t,\cdot) \in C^2$. However, we recognize the expression on the right-hand side as the usual Balakrishnan formula, which is equivalent to the standard fractional Laplacian on $\mathbb{R}^d$ (Kwasnicki [**124**]). Therefore,

$$\mathcal{A}^\alpha u(t,x) = -(-\Delta)^\alpha u(t,x) \text{ when } u(t,\cdot) \in C^2.$$

This proves (3.23), and completes the proof of Theorem 3.19.

Remark 3.32. The same technique may apply for the fractional power $\mathcal{L}^\alpha$ of a constant coefficient elliptic operator

$$\mathcal{L} = \frac{1}{2}\sum_{i,j=1}^n a^{ij}\frac{\partial^2}{\partial x_i}\partial x_j + \sum_{i=1}^n b^i(x)\frac{\partial}{\partial x_i},$$

In the book of Freidlin [**77**] a result corresponding to (3.24) for such operators is proven, leading to a Feynman-Kac formula

$$u(t,x) = \mathcal{T}_t^\alpha f(x) := \mathbb{E}_{X_0=x}\left[f(X_t)\right],$$

where X_t is now the Itô process

$$dX_t = \sigma(X_t)dB_t + b(X_t)dt, \quad X_0 = x, \quad a^{ij}(x) = \sigma(x)\sigma^*(x).$$

Since spectral powers can be constructed for such operators $\mathcal{L}$ and they can also be expressed by Balakrishnan formulas, we would obtain a subordinated formula

$$u(t,x) = \mathbb{E}_{X_0=x}\left[f(X_{T_{\alpha/2}(t)})\right] = \mathbb{E}_{Z_0=x}\left[f(X_{Z_t})\right]$$

for solutions to the Cauchy problem of L^α. Here $Z_t = X_{T_{\alpha/2}(t)}$ would be a Lévy process with measure defined by the coefficients of L and α. Thus the solution would be given by nonisotropic Lévy process. For example, if the a^{ij} are constant, we expect $Z_t = X_{T_{\alpha/2}(t)}$ to be an elliptically-contoured stable Lévy process. Furthermore, it may be possible to prove Feynman-Kac formulas for fractional equations with an additional zero-order term $c(x)u(x,t)$, which Freidlin [77] treats by comparison to an auxillary semigroup, to obtain a formula

$$u(x,t) = \mathbb{E}_{X_0^\alpha=x}\left[f(X_t)\right]\exp\int_0^t c(X_s)ds.$$

Neither of these results are pursued here, but would be a worthwhile extensions of the results of this section.

3.5 The Inhomogeneous Fractional Cauchy Problem on $\mathbb{R}^d$.

In this section, we show how a stochastic solution formula for the Cauchy problem with nonzero forcing term can be obtained from the results in the previous sections

using Duhamel's principle. We consider the following problem

$$\begin{cases} \partial_t u(t,x) + (-\Delta)^{\alpha/2} u(t,x) = r(x,t) \text{ for } t > 0 \\ u(0,x) = f(x). \end{cases} \tag{3.33}$$

which differs from Problem (3.18) by the presence of the inhomogeneity $r(x,t)$.

Let us write the solution to (3.33) as $u(t,x) = u_1(t,x) + u_2(t,x)$, where $u_1(t,x)$ solves

$$\begin{cases} \partial_t u_1(t,x) + (-\Delta)^{\alpha/2} u_1(t,x) = 0 \text{ for } t > 0 \\ u_1(0,x) = f(x) \end{cases} \tag{3.34}$$

and $u_2(t,x)$ solves

$$\begin{cases} \partial_t u_2(t,x) + (-\Delta)^{\alpha/2} u_2(t,x) = r(t,x) \text{ for } t > 0 \\ u_2(0,x) = 0. \end{cases}$$

Then by Theorem 3.19, provided the regularity assumptions hold,

$$u_1 = \mathbb{E}_{X_0^\alpha = x} \left[f(X_t^\alpha) \right]. \tag{3.35}$$

As for u_2, by Duhamel's principle,

$$u_2(x,t) = \int_0^t [P^s r](x,t) ds,$$

where $[P^s r]$ solves, for fixed s,

$$\begin{cases} \partial_t u(t,x) + (-\Delta)^{\alpha/2} u(t,x) = 0 \text{ for } t > s \\ u(s,x) = r(s,x) \text{ for } x \in \mathbb{R}^d. \end{cases}$$

Letting $\tilde{u}(t-s,x) = u(t,x)$, this problem becomes

$$\begin{cases} \partial_t \tilde{u}(t,x) + (-\Delta)^{\alpha/2}\tilde{u}(t,x) = 0 \text{ for } t > 0 \\ \tilde{u}(0,x) = r(s,x) \text{ for } x \in \mathbb{R}^d. \end{cases} \tag{3.36}$$

Again, by Theorem 3.19, provided the regularity assumptions hold,

$$\tilde{u}(x,t) = \mathbb{E}_{X_0^\alpha = x}\left[r(s, X_t^\alpha)\right].$$

so that

$$[P^s r](x,t) = \tilde{u}(x, t-s) = \mathbb{E}_{X_0^\alpha = x}\left[r(s, X_{t-s}^\alpha)\right],$$

and therefore

$$u_2(x,t) = \int_0^t \mathbb{E}_{X_0^\alpha = x}\left[r(s, X_{t-s}^\alpha)\right] ds = \mathbb{E}_{X_0^\alpha = x}\left[\int_0^t r(s, X_{t-s}^\alpha) ds\right]. \tag{3.37}$$

Adding (3.37) and (3.35) gives the following result.

THEOREM 3.38. *Let $u(t,x)$ solve (3.33). Suppose that f and $r(s,\cdot)$, for every $s \geq 0$, are such that the problems (3.34) and (3.36) each admit a solution that satisfies the regularity conditions (3.20) and (3.21). Then*

$$\begin{aligned} u(t,x) &= \mathbb{E}_{X_0^\alpha = x}\left[f(X_t^\alpha)\right] + \mathbb{E}_{X_0^\alpha = x}\left[\int_0^t r(s, X_{t-s}^\alpha) ds\right] \\ &= \mathbb{E}_{X_0^\alpha = x}\left[f(X_t^\alpha)\right] + \mathbb{E}_{X_0^\alpha = x}\left[\int_0^t r(t-s, X_s^\alpha) ds\right] \end{aligned}$$

where X_t^α is standard isotropic α-stable Lévy motion in $\mathbb{R}^d$.

We persue analogues of this result in bounded domains with the operator $-(\Delta_{\Omega,g})^{\alpha/2}$.

3.6 The Homogeneous Spectral Fractional Cauchy Problem on a Bounded Domain, with Dirichlet Boundary Conditions.

Let $\Omega \subset \mathbb{R}^d$ be an open domain with Lipschitz boundary $\partial\Omega$. We consider the Cauchy problem on Ω, with both initial and boundary conditions,

$$\begin{cases} \partial_t u(t,x) = -(-\Delta_{\Omega,g})^{\alpha/2} u(t,x) \text{ for } t > 0, x \in \Omega \\ u(0,x) = f(x) \quad \text{for } x \in \Omega. \\ u(t,x) = g(x) \quad \text{for } x \in \partial\Omega. \end{cases} \tag{3.39}$$

We require that f and g are continuous, and for any $x_0 \in \partial\Omega$

$$\lim_{\Omega \ni x \to x_0} f(x) = g(x_0). \tag{3.40}$$

We prove the following

THEOREM 3.41. *Let $u(t,x)$ be a solution to (3.39), (3.40) such that*

for every $t \geq 0$, $u(t,\cdot) \in C^2_x(\Omega)$, and (3.42)

$\partial_t u(\cdot,\cdot)$ is uniformly continuous in spacetime $[0,\infty) \times \Omega$. (3.43)

Then

$$u(t,x) = \mathbb{E}_{X^{\Omega,\alpha}_0 = x} \left[f(X^{\Omega,\alpha}_t) \chi_{\tau_\Omega > T_{\alpha/2}(t)} + g(X^{\Omega,\alpha}_t) \chi_{\tau_\Omega \leq T_{\alpha/2}(t)} \right] \tag{3.44}$$

where $X^{\Omega,\alpha}_t$ is standard $\alpha/2$-subordinate stopped isotropic Brownian (or rather, standard 2-stable) motion in Ω:

$$X^{\Omega,\alpha}_t = X^{\Omega,2}_{T_{\alpha/2}(t)}, \quad X^{\Omega,2}_t = X^2_{t \wedge \tau_\Omega}, \quad \tau_\Omega = \inf\{s : X^2_s \notin \Omega\}. \tag{3.45}$$

Thus, paths of $X_t^{\Omega,\alpha}$ are simply paths of Brownian motion (scaled by $\sqrt{2}$) that are stopped upon reaching the boundary $\partial\Omega$, then time-changed by the standard $\alpha/2$ stable subordinator. To prove the theorem, the same strategy is used as in Section 3.4. We start with proven results for the standard Laplacian/Brownian motion. Then, we use the subordination lemma of Balakrishnan to obtain the result for the fractional equation.

Define the semigroup $\mathcal{T}_t^{\Omega,\alpha}$ on $C_0(\overline{\Omega})$ by

$$\mathcal{T}_t^{\Omega,\alpha} F(x) = \mathbb{E}_{X_0^{\Omega,\alpha}=x}\left[F(X_t^{\Omega,\alpha})\right], \quad F \in C_0(\overline{\Omega}). \tag{3.46}$$

This is well defined, since the process $X_t^{\Omega,\alpha}$ remains in $\overline{\Omega}$ for all time. Moreover, $\mathcal{T}_t^{\Omega,\alpha}$ is the Feller semigroup of the same process. The reason for introducing this semigroup is that the condition (3.40) imples that the initial condition f can be extended to the $C_0(\overline{\Omega})$ function $\overline{f}$ on $\overline{\Omega}$:

$$\overline{f}(x) = \begin{cases} f(x), x \in \Omega \\ g(x) = \lim_{\Omega \ni x \to x_0} f(x), x \in \partial\Omega \end{cases} \implies \overline{f} \in C_0(\overline{\Omega}).$$

Then the proposed solution (3.44) can be written as the Feller semigroup

$$u(t,x) = \mathcal{T}_t^{\Omega,\alpha}\overline{f}(x). \tag{3.47}$$

We shall now prove that $u(t,x)$ in this form satisfies the problem. First, we prove the following

LEMMA 3.48. *The generator $\mathcal{A}^\alpha$ of the semigroup $\mathcal{T}_t^{\Omega,\alpha}$ on $C_0(\overline{\Omega})$ defined by (3.46) agrees with the operator $-(-\Delta_{\Omega,g})^{\alpha/2}$ on*

$$C_0(\overline{\Omega}) \cap C^2(\Omega) \equiv \left\{u \in C_0(\overline{\Omega}) \text{ such that } u|_\Omega \in C^2(\Omega)\right\}.$$

To prove this lemma, we begin by referring to Chung and Zhao [49], Theorem 2.13, p. 56, where it is shown under more general conditions for the case $\alpha = 2$. In that case, the operator $-(-\Delta_{\Omega,g})^{\alpha/2}$ reduces to the standard Laplacian Δ and the process $X_t^{2,\Omega}$ to stopped standard isotropic 2-stable motion. Thus,

$$C_0(\overline{\Omega}) \cap C^2(\Omega) \subset \mathrm{Dom}(\mathcal{A}^2), \text{ and } \mathcal{A}^2 = \Delta \text{ on } C_0(\overline{\Omega}) \cap C^2(\Omega).$$

Then, the result of Balakrishnan (Lemma 3.28) tells us that the semigroup

$$\widehat{\mathcal{T}}_t^{\Omega,\alpha} F = \begin{cases} \int_0^\infty h_{\alpha/2}(s) \mathcal{T}_s^{\Omega,2} F ds & (t > 0) \\ F & (t = 0) \end{cases}$$

has infinitesimal generator, for $F \in \mathrm{Dom}(\mathcal{A})$, and in particular, $F \in C_0(\overline{\Omega}) \cap C^2(\Omega)$,

$$\mathcal{A}^\alpha F(x) = \frac{1}{\Gamma(-\alpha/2)} \int_0^\infty \lambda^{-\alpha/2-1} (\mathcal{T}_\lambda^{\Omega,2} - I) F(x) d\lambda.$$

We begin with the right-hand side of this equation. In Freidlin [77], formula (3.47) is shown to satisfy Problem (3.39) when $\alpha = 2$. In other words,

$$\mathcal{T}_t^{\Omega,2} \overline{f}(x) = e^{t\Delta_{\Omega,g}} f(x), x \in \Omega, \tag{3.49}$$

Therefore, for $F \in C_0(\overline{\Omega}) \cap C^2(\Omega)$ and $x \in \Omega$, by (3.49), we have

$$\begin{aligned} \mathcal{A}^\alpha F(x) &= \frac{1}{\Gamma(-\alpha/2)} \int_0^\infty \lambda^{-\alpha/2-1} (e^{t\Delta_{\Omega,g}} - I) F(x) d\lambda \\ &= -(-\Delta_{\Omega,g})^{\alpha/2} F(x). \end{aligned}$$

It remains to show that $\widehat{\mathcal{T}}_t^{\Omega,\alpha} = \mathcal{T}_t^{\Omega,\alpha}$. In order to do this, we will use the definition (3.45) of the stopped process $X_t^{\Omega,\alpha}$ as subordinate stopped Brownian motion, and

the tower property:

$$\begin{aligned}
\mathcal{T}_t^{\Omega,\alpha}F(x) &= \mathbb{E}_{X_0^2=x}\left[F(X_t^{\Omega,\alpha})\right] \\
&= \mathbb{E}_{X_0^2=x}\left[F\left(X^{\Omega,2}_{T_{\alpha/2}(t)}\right)\right] \\
&= \mathbb{E}_{X_0^2=x}\left[\int \mathbb{P}\{T_{\alpha/2}=s\}F(X_s^{\Omega,2})ds\right] \\
&= \int \mathbb{P}\{T_{\alpha/2}=s\}\mathbb{E}_{X_0^2=x}\left[F(X_s^{\Omega,2})\right]ds \\
&= \int \mathbb{P}\{T_{\alpha/2}=s\}\mathcal{T}_s^2F(x)ds \\
&= \int h_{\alpha/2}(s)\mathcal{T}_s^2F(x)ds \\
&= \widehat{\mathcal{T}}_t^{\Omega,\alpha}F(x).
\end{aligned}$$

The proof of the lemma is complete.

Let us now prove Theorem 3.41. We know by Lemma 3.13 that $\mathcal{T}_t^{\Omega,\alpha}\overline{f}(x)$ is the unique solution to the abstract Cauchy problem

$$\begin{cases} \frac{d}{dt}u(t,x) = \mathcal{A}^\alpha u(t,x) \text{ for } x\in\overline{\Omega}, t>0 \\ \lim_{t\to 0} u(t,x) = \overline{f}(x). \end{cases}$$

For any path starting at $x\in\partial\Omega$, $\tau_\Omega = 0$, so that $X_t^{\Omega,\alpha} = x$, and therefore

$$\mathcal{T}_t^{\Omega,\alpha}\overline{f}(x) = \mathbb{E}_{X_0^{\Omega,\alpha}=x}\left[\overline{f}(x)\right] = \mathbb{E}_{X_0^{\Omega,\alpha}=x}\left[g(x)\right] = g(x).$$

This shows that

$$\frac{d}{dt}\mathcal{T}_t^{\Omega,\alpha}\overline{f}(x) = 0 \text{ for } x\in\partial\Omega.$$

Therefore, an equivalent statement is that $\mathcal{T}_t^{\Omega,\alpha}\overline{f}$ is the unique solution to the problem

$$\begin{cases} \frac{d}{dt}u(t,x) = \mathcal{A}^\alpha u(t,x) \text{ for } x \in \Omega, t > 0 \\ \frac{d}{dt}u(t,x) = 0 \text{ for } x \in \partial\Omega, t > 0 \\ \lim_{t\to 0} u(t,x) = \overline{f}(x) \end{cases} \tag{3.50}$$

On the other hand, we note that, by Lemma 3.48,

$$u(t,\cdot) \in C_0(\overline{\Omega}) \cap C^2(\Omega) \subset \text{Dom}(\mathcal{A}^\alpha).$$

and the differential equation in the problem (3.39) together with the regularity condition (3.43) is equivalent to the first differential equation in the problem (3.50). Also, $u(t,x)$ clearly satisfies the remaining two equations in (3.50), so by uniqueness,

$$u(t,x) = \mathcal{T}_t^{\Omega,\alpha}\overline{f}(x).$$

This completes the proof.

3.7 The Inhomogeneous Spectral Fractional Cauchy Problem on a Bounded Domain, with Dirichlet Boundary Conditions.

We consider, on bounded domain $\Omega \subset \mathbb{R}^d$, the mixed problem with both initial and boundary conditions:

$$\begin{cases} \partial_t u(t,x) + (-\Delta_{\Omega,g})^{\alpha/2} u(t,x) = r(x,t) \text{ for } t > 0, x \in \Omega \\ u(t,x) = g(x) \quad \text{for } t > 0, x \in \partial\Omega \\ u(0,x) = f(x) \quad \text{for } x \in \Omega. \end{cases} \tag{3.51}$$

Again, we require that f and g are continuous, and for any $x_0 \in \partial\Omega$

$$\lim_{\Omega \ni x \to x_0} f(x) = g(x_0).$$

Let us write the solution to (3.51) as $u(t,x) = u_1(t,x) + u_2(t,x)$, where $u_1(t,x)$ solves

$$\begin{cases} \partial_t u_1(t,x) + (-\Delta_{\Omega,g})^{\alpha/2} u_1(t,x) = 0 \text{ for } t > 0, x \in \Omega \\ u_1(t,x) = g(x) \quad \text{for } t > 0, x \in \partial\Omega \\ u_1(0,x) = f(x) \quad \text{for } x \in \Omega \end{cases} \tag{3.52}$$

and $u_2(t,x)$ solves

$$\begin{cases} \partial_t u_2(t,x) + (-\Delta_{\Omega,0})^{\alpha/2} u_2(t,x) = r(t,x) \text{ for } t > 0, x \in \Omega \\ u_2(t,x) = 0 \quad \text{for } t > 0, x \in \partial\Omega \\ u_2(0,x) = 0 \quad \text{for } x \in \Omega. \end{cases}$$

Then by Theorem 3.41, provided the regularity assumptions hold,

$$u_1 = \mathbb{E}_{X_0^{\Omega,\alpha}=x} \left[f(X_t^{\Omega,\alpha}) \chi_{\tau_\Omega > T_{\alpha/2}(t)} + g(X_t^{\Omega,\alpha}) \chi_{\tau_\Omega \le T_{\alpha/2}(t)} \right]. \tag{3.53}$$

By Duhamel's principle,

$$u_2(x,t) = \int_0^t [P^s r](x,t) ds,$$

where $[P^s r]$ solves, for fixed s,

$$\begin{cases} \partial_t u(t,x) + (-\Delta_{\Omega,0})^{\alpha/2} u(t,x) = 0 \text{ for } t > 0, x \in \Omega \\ u(t,x) = 0 \quad \text{for } t > 0, x \in \partial\Omega \\ u(s,x) = r(s,x) \text{ for } x \in \Omega. \end{cases}$$

Letting $\tilde{u}(t-s,x) = u(t,x)$, this problem becomes

$$\begin{cases} \partial_t \tilde{u}(t,x) + (-\Delta_{\Omega,0})^{\alpha/2}\tilde{u}(t,x) = 0 \text{ for } t > 0, x \in \Omega \\ u(t,x) = 0 \quad \text{for } t > 0, x \in \partial\Omega. \\ \tilde{u}(0,x) = r(s,x) \text{ for } x \in \Omega. \end{cases} \tag{3.54}$$

Again, by Theorem 3.41, provided the regularity assumptions hold,

$$\tilde{u}(x,t) = \mathbb{E}_{X_0^{\Omega,\alpha}=x}\left[r(s, X_t^{\Omega,\alpha})\chi_{\tau_\Omega > T_{\alpha/2}(t)}\right]$$

so that

$$[P^s r](x,t) = \tilde{u}(x,t-s) = \mathbb{E}_{X_0^{\alpha}=x}\left[r(s, X_{t-s}^{\Omega,\alpha})\chi_{\tau_\Omega > T_{\alpha/2}(t-s)}\right],$$

and therefore

$$\begin{aligned} u_2(x,t) &= \int_0^t \mathbb{E}_{X_0^{\alpha}=x}\left[r(s, X_{t-s}^{\Omega,\alpha})\chi_{\tau_\Omega > T_{\alpha/2}(t-s)}\right] ds \\ &= \mathbb{E}_{X_0^{\Omega,\alpha}=x}\left[\int_0^t r(s, X_{t-s}^{\Omega,\alpha})\chi_{\tau_\Omega > T_{\alpha/2}(t-s)} ds\right]. \end{aligned} \tag{3.55}$$

Adding (3.55) and (3.53) gives the following result.

THEOREM 3.56. *Let $u(t,x)$ solve (3.51). Suppose that f and $r(s,\cdot)$ for every $s \geq 0$, are such that the problems (3.52) and (3.54) each admit a solution that satisfies the regularity conditions (3.42) and (3.43). Then*

$$\begin{aligned} u(t,x) = \mathbb{E}_{X_0^{\Omega,\alpha}=x}&\left[f(X_t^{\Omega,\alpha})\chi_{\tau_\Omega > T_{\alpha/2}(t)} + g(X_t^{\Omega,\alpha})\chi_{\tau_\Omega \leq T_{\alpha/2}(t)}\right] \\ &+ \mathbb{E}_{X_0^{\alpha}=x}\left[\int_0^t r(s, X_{t-s}^{\Omega,\alpha})\chi_{\tau_\Omega > T_{\alpha/2}(t-s)} ds\right]; \end{aligned}$$

or, by a change of variables,

$$u(t,x) = \mathbb{E}_{X_0^{\Omega,\alpha}=x}\left[f(X_t^{\Omega,\alpha})\chi_{\tau_\Omega > T_{\alpha/2}(t)} + g(X_t^{\Omega,\alpha})\chi_{\tau_\Omega \le T_{\alpha/2}(t)}\right] + \mathbb{E}_{X_0^{\alpha}=x}\left[\int_0^t r(t-s, X_s^{\Omega,\alpha})\chi_{\tau_\Omega > T_{\alpha/2}(s)} ds\right].$$

where $X_t^{\Omega,\alpha}$ is subordinate stopped standard isotropic 2-stable Lévy motion in Ω.

3.8 Regularity and Steady-State for the Spectral Fractional Heat Equation in a Bounded Domain and Survival Probability of Subordinate Stopped Brownian Motion.

The previous section contains stochastic solution formulas for the fractional Cauchy problem that are contingent upon the regularity of the solutions to problems (3.52) and (3.54) . The latter can be reduced to the case of zero boundary value by harmonic lifting [**55, 11**]. We now investigate regularity for such problems, together with convergence to a steady state. Our results allow us to obtain exponential decay of the survival probability of subordinate stopped Brownian motion, and obtain a stochastic solution formulas for the Dirichlet problem by applying the formula in the previous section to a related Cauchy problem and taking the limit as $t \to \infty$. We proceed by working with a classical solution formula (eigenfunction expansion) directly and adapting the proof in [**127**]. The classical solution formula (3.59) appears, e.g., in [**30**], but we did not find a precise statement of the results below in the literature. Appendix A contains background material used in this section.

Consider the fractional heat equation, for bounded and smooth domain Ω,

$$\begin{cases} \partial_t w + (-\Delta_{\Omega,0})^{\alpha/2} w = 0 \text{ for } x \in \Omega \\ w(x,t) = 0 \quad \text{for } x \in \partial\Omega \\ w(x,0) = w_0 \in L^2 \quad \text{for } x \in \Omega. \end{cases} \tag{3.57}$$

THEOREM 3.58. *Define*

$$w(t,x) = \sum_{j=1}^{\infty} e^{-t\lambda_j^{\alpha/2}} (w_0, e_j)_{L^2(\Omega)} e_j(x). \tag{3.59}$$

Then,

(1) For any $t > 0$, integers $K, \ell \geq 0$, and $\mu < 1$, there exists $C > 0$ such that

$$\|\partial_t^\ell w(t,\cdot)\|_{H^K(\Omega)} \leq C t^{-\ell - K/\alpha} e^{-\mu \lambda_1^{\alpha/2} t} \|w_0\|_{L^2(\Omega)}.$$

The convention is that $H^0(\Omega) = L^2(\Omega)$.

(2) For any $t > 0$, integers $r, \ell > 0$, and $\mu < 1$, there exists $C > 0$ such that

$$\|\partial_t^\ell w(t,\cdot)\|_{C^r(\Omega)} \leq t^{-\ell - \lceil \frac{d}{2} + r \rceil/\alpha} e^{-\mu \lambda_1^{\alpha/2} t} \|w_0\|_{L^2(\Omega)}.$$

where $\lceil x \rceil$ is the smallest integer $\geq x$. Therefore, w is smooth in $(0,\infty) \times \Omega$.

(3) $\lim_{t \to 0} w(t,x) = w_0$ in $L^2(\Omega)$.

(4) The series w given by (3.59) is the unique classical solution to the problem (3.57).

To prove this, we define

$$S^{\ell,J} = (-1)^\ell \sum_{j=J}^{\infty} \lambda_j^{\ell\alpha/2} e^{-\lambda_j^{\alpha/2} t} (w, e_j) e_j(x).$$

Note that $S^{\ell,J=1}$ corresponds to term-by-term differentiation of the function $w(t,x)$. However, since the validity of term-by-term differentiation is not known *a priori*, we

must establish it by studying $S^{\ell,J}$ for $J \to \infty$. We begin by proving the following lemma:

LEMMA 3.60. *For $t > 0$ and any integers $k, \ell \geq 0$,*

$$(-\Delta)^k S^{\ell,J} = (-1)^\ell \sum_{j=J}^{\infty} \lambda_j^{\ell\alpha/2+k} e^{-\lambda_j^{\alpha/2} t} (w, e_j) e_j(x). \tag{3.61}$$

For any $\mu < 1$, there exists C such that

$$\|(-\Delta)^k S^{\ell,J}\|_{L^2(\Omega)} \leq C t^{-\ell-k(2/\alpha)} e^{-\mu \lambda_J^{\alpha/2} t} \|w_0\|_{L^2(\Omega)}. \tag{3.62}$$

Moreover, $(-\Delta)^k S^{\ell,J} \in H_0^1(\Omega)$, and for any $\mu < 1$, there exists C such that

$$\left[(-\Delta)^k S^{\ell,J}\right]_{H_0^1(\Omega)} = \|\nabla(-\Delta)^k S^{\ell,J}\|_{L^2(\Omega)} \leq C t^{-\ell-(k+1/2)(2/\alpha)} e^{-\mu \lambda_J^{\alpha/2} t} \|w_0\|_{L^2(\Omega)}. \tag{3.63}$$

We prove the lemma by induction. For $k = 0$, the representation (3.61) is just the definition of $S^{\ell,J}$. To prove the L^2 bound (3.62), we note

$$\begin{aligned} (S^{\ell,J}, e_j)_{L^2}^2 &= \left((-1)^\ell \sum_{\tilde{j}=J}^{\infty} \lambda_{\tilde{j}}^{\ell\alpha/2} e^{-\lambda_{\tilde{j}}^{\alpha/2} t} (w_0, e_{\tilde{j}}) e_{\tilde{j}}(x), e_j \right)_{L^2}^2 \\ &= \lambda_j^{\ell\alpha} e^{-2\lambda_j^{\alpha/2} t} (w_0, e_j)^2, \end{aligned} \tag{3.64}$$

and write

$$\begin{aligned} \|S^{\ell,J}\|_{L^2(\Omega)}^2 &= \sum_{j=1}^{\infty} (S^{\ell,J}, e_j)_{L^2}^2 \\ &= \sum_{j=J}^{\infty} \lambda_j^{\ell\alpha} e^{-2\lambda_j^{\alpha/2} t} (w_0, e_j)^2. \end{aligned}$$

Next, we need the following fact:

(3.65) For any $\theta \geq 0$ and $\mu < 1$, there exists a constant C such that $s^\theta e^{-2s} \leq Ce^{-2\mu s}$ for all $s \in [0, \infty)$.

Using the fact (3.65), we can write, for any $\mu < 1$,

$$\lambda_j^{\ell\alpha} e^{-2\lambda_j^{\alpha/2} t} = t^{-2\ell} \left(\lambda_j^{\alpha/2} t\right)^{2\ell} e^{-2\lambda_j^{\alpha/2} t} \leq Ct^{-2\ell} e^{-2\mu\lambda_j^{\alpha/2} t}.$$

Therefore,

$$\begin{aligned} \|S^{\ell,J}\|_{L^2(\Omega)}^2 &\leq Ct^{-2\ell} \sum_{j=J}^{\infty} e^{-2\mu\lambda_j^{\alpha/2} t} (w_0, e_j)^2 \\ &\leq Ct^{-2\ell} e^{-2\mu\lambda_J^{\alpha/2} t} \sum_{j=J}^{\infty} (w_0, e_j)^2 \\ &\leq Ct^{-2\ell} e^{-2\mu\lambda_J^{\alpha/2} t} \|w_0\|^2. \end{aligned}$$

Taking the square-root yields (3.62) with $k = 0$:

$$\|S^{\ell,J}\|_{L^2(\Omega)} \leq Ct^{-\ell} e^{-\mu\lambda_J^{\alpha/2} t} \|w_0\|_{L^2(\Omega)}.$$

Next, we have $S^{\ell,J} \in H_0^1(\Omega)$ if and only if $\sum_{j=1}^{\infty} \lambda_j (S^{\ell,J}, e_j)_{L^2(\Omega)}^2$ converges, and

$$\left[S^{\ell,J}\right]_{H_0^1(\Omega)}^2 = \|\nabla S^{\ell,J}\|_{L^2(\Omega)}^2 = \sum_{j=1}^{\infty} \lambda_j (S^{\ell,J}, e_j)_{L^2(\Omega)}^2.$$

See Theorem A.5 in Appendix A. From (3.64), have

$$\left[S^{\ell,J}\right]_{H_0^1(\Omega)}^2 = \sum_{J=1}^{\infty} \lambda_j^{\ell\alpha+1} e^{-2\lambda_j^{\alpha/2} t} (w_0, e_j)^2.$$

Using the fact (3.65) again, we can write, for any $\mu < 1$,

$$\lambda_j^{\ell\alpha+1} e^{-2\lambda_j^{\alpha/2} t} = t^{-2(\ell+1/\alpha)} \left(\lambda_j^{\alpha/2} t\right)^{2(\ell+1/\alpha)} e^{-2\lambda_j^{\alpha/2} t} \leq Ct^{-2(\ell+1/\alpha)} e^{-2\mu\lambda_j^{\alpha/2} t}.$$

Therefore,

$$\begin{aligned}\left[S^{\ell,J}\right]^2_{H^1_0(\Omega)} &\leq Ct^{-2(\ell+1/\alpha)}\sum_{j=J}^{\infty} e^{-2\mu\lambda_j^{\alpha/2}t}(w_0,e_j)^2\\ &\leq Ct^{-2(\ell+1/\alpha)}e^{-2\mu\lambda_J^{\alpha/2}t}\sum_{j=J}^{\infty}(w_0,e_j)^2\\ &\leq Ct^{-2(\ell+1/\alpha)}e^{-2\mu\lambda_J^{\alpha/2}t}\|w_0\|^2_{L^2(\Omega)}.\end{aligned}$$

Taking the square-root yields (3.63) with $k=0$:

$$\left[S^{\ell,J}\right]_{H^1_0(\Omega)} \leq Ct^{-(\ell+1/\alpha)}e^{-\mu\lambda_J^{\alpha/2}t}\|w_0\|_{L^2(\Omega)}.$$

This completes the proof of the lemma for $k=0$.

Now we perform the induction step. Suppose the lemma is true for a certain k; we show that this implies it is true for $k+1$. We know that $(-\Delta)^k S^{\ell,J} \in H^1_0(\Omega)$, i.e., $(-\Delta)^k S^{\ell,J}$ is zero on $\partial\Omega$. Therefore, the representation

$$(-\Delta) = \sum_{j=1}^{\infty}\lambda_j(\cdot,e_j)_{L^2}e_j$$

is valid on $(-\Delta)^k S^{\ell,J}$. Since we also have (3.61), we see that

$$\begin{aligned}\left((-\Delta)^k S^{\ell,J},e_j\right)_{L^2} &= \left((-1)^\ell\sum_{\tilde{j}=J}^{\infty}\lambda_{\tilde{j}}^{\ell\alpha/2+k}e^{-\lambda_{\tilde{j}}^{\alpha/2}t}(w_0,e_{\tilde{j}}),e_{\tilde{j}}\right)_{L^2}\\ &= (-1)^\ell\lambda_j^{\ell\alpha/2+k}e^{-\lambda_j^{\alpha/2}t}(w_0,e_j).\end{aligned}$$

Therefore,

$$(-\Delta)^{k+1}S^{\ell,J} = (-\Delta)(-\Delta)^k S^{\ell,J} = (-1)^\ell\sum_{j=J}^{\infty}\lambda_j^{\ell\alpha/2+k+1}e^{-\lambda_j^{\alpha/2}t}(w_0,e_j)e_j.$$

This is (3.61) for the case $k+1$. We can use it to obtain the L^2 bound as before; first we note that the representation implies

$$\begin{aligned}\left((-\Delta)^{k+1}S^{\ell,J},e_j\right)_{L^2}^2 &= \left((-1)^\ell\sum_{\tilde{j}=J}^{\infty}\lambda_{\tilde{j}}^{\ell\alpha/2+k+1}e^{-\lambda_{\tilde{j}}^{\alpha/2}t}(w_0,e_{\tilde{j}})e_{\tilde{j}}\right)_{L^2}^2 \\ &= \lambda_j^{\ell\alpha+2(k+1)}e^{-2\lambda_j^{\alpha/2}t}(w_0,e_j)_{L^2(\Omega)}^2.\end{aligned} \tag{3.66}$$

Therefore, using the fact (3.65),

$$\begin{aligned}\|(-\Delta)^{k+1}S^{\ell,J}\|_{L^2(\Omega)}^2 &= \sum_{j=1}^{\infty}\left((-\Delta)^{k+1}S^{\ell,J},e_j\right)_{L^2}^2 \\ &= \sum_{j=J}^{\infty}\lambda_j^{\ell\alpha+2(k+1)}e^{-2\lambda_j^{\alpha/2}t}(w_0,e_j)_{L^2}^2 \\ &= \sum_{j=J}^{\infty}t^{-2\ell-2(k+1)(2/\alpha)}\left(\lambda_j^{\alpha/2}t\right)^{2\ell+2(k+1)(2/\alpha)}e^{-2\lambda_j^{\alpha/2}t}(w_0,e_j)_{L^2}^2 \\ &\le Ct^{-2\ell-2(k+1)(2/\alpha)}\sum_{j=J}^{\infty}e^{-2\mu\lambda_j^{\alpha/2}t}(w_0,e_j)_{L^2}^2 \\ &\le Ct^{-2\ell-2(k+1)(2/\alpha)}e^{-2\mu\lambda_J^{\alpha/2}t}\sum_{j=J}^{\infty}(w_0,e_j)_{L^2}^2 \\ &\le Ct^{-2\ell-2(k+1)(2/\alpha)}e^{-2\mu\lambda_J^{\alpha/2}t}\|w_0\|_{L^2}^2.\end{aligned}$$

Taking the square-root yields (3.62) for $k+1$:

$$\|(-\Delta)^{k+1}S^{\ell,J}\|_{L^2(\Omega)}^2 \le Ct^{-\ell-(k+1)(2/\alpha)}e^{-\mu\lambda_J^{\alpha/2}t}\|w_0\|_{L^2}.$$

Next, we have $(-\Delta)^{k+1}S^{\ell,J}\in H_0^1(\Omega)$ if and only if $\sum_{j=1}^{\infty}\lambda_j((-\Delta)^{k+1}S^{\ell,J},e_j)_{L^2(\Omega)}^2$ converges, and

$$\left[(-\Delta)^{k+1}S^{\ell,J}\right]_{H_0^1(\Omega)}^2 = \|\nabla(-\Delta)^{k+1}S^{\ell,J}\|_{L^2(\Omega)}^2 = \sum_{j=1}^{\infty}\lambda_j\left((-\Delta)^{k+1}S^{\ell,J},e_j\right)_{L^2(\Omega)}^2.$$

From (3.66), have

$$\left[(-\Delta)^{k+1}S^{\ell,J}\right]^2_{H^1_0(\Omega)} = \sum_{j=J}^{\infty} \lambda_j^{\ell\alpha+2(k+1)+1} e^{-2\lambda_j^{\alpha/2}t}(w_0,e_j)^2_{L^2(\Omega)}$$

Therefore, using the fact (3.65),

$$\begin{aligned}
\left[(-\Delta)^{k+1}S^{\ell,J}\right]^2_{H^1_0(\Omega)} &= \sum_{j=J}^{\infty} \lambda_j^{\ell\alpha+2(k+1)+1} e^{-2\lambda_j^{\alpha/2}t}(w_0,e_j)^2 \\
&= \sum_{j=J}^{\infty} t^{-2\ell-\left(2(k+1)+1\right)(2/\alpha)} \left(\lambda_j^{\alpha/2}t\right)^{2\ell+\left(2(k+1)+1\right)(2/\alpha)} e^{-2\lambda_j^{\alpha/2}t}(w_0,e_j)^2 \\
&\le Ct^{-2\ell-\left(2(k+1)+1\right)(2/\alpha)} \sum_{j=J}^{\infty} e^{-2\mu\lambda_j^{\alpha/2}t}(w_0,e_j)^2 \\
&\le Ct^{-2\ell-\left(2(k+1)+1\right)(2/\alpha)} e^{-2\mu\lambda_J^{\alpha/2}t} \sum_{j=J}^{\infty}(w_0,e_j)^2 \\
&\le Ct^{-2\ell-\left(2(k+1)+1\right)(2/\alpha)} e^{-2\mu\lambda_J^{\alpha/2}t}\|w_0\|^2_{L^2}.
\end{aligned}$$

Taking the square-root yields (3.63) for $k+1$:

$$\left[(-\Delta)^{k+1}S^{\ell,J}\right]_{H^1_0(\Omega)} \le Ct^{-\ell-\left((k+1)+1/2\right)(2/\alpha)} e^{-\mu\lambda_J^{\alpha/2}t}\|w_0\|_{L^2(\Omega)}.$$

This completes the proof of the lemma.

Now that Lemma 3.60 has been proven, to prove the theorem we invoke elliptic regularity (Theorem A.2 in Appendix A) to obtain, for $\delta = 0$ or 1,

$$\|S^{\ell,J}\|_{H^{2k+\delta}(\Omega)} \le C\|(-\Delta)^k S^{\ell,J}\|_{H^\delta(\Omega)}. \tag{3.67}$$

The two estimates in Lemma 3.60 can be wrapped into one estimate, again for $\delta = 0$ or 1,

$$\begin{aligned}\|(-\Delta)^k S^{\ell,J}\|_{H^\delta(\Omega)} &\le \|(-\Delta)^k S^{\ell,J}\|_{L^2(\Omega)} + \delta \left[(-\Delta)^k S^{\ell,J}\right]_{H_0^1(\Omega)} \\ &\le C\left[t^{-\ell-k(2/\alpha)} + \delta t^{-\ell-(k+1/2)(2/\alpha)}\right] e^{-\mu\lambda_J^{\alpha/2}t}\|w_0\|_{L^2(\Omega)}.\end{aligned} \tag{3.68}$$

Together, (3.67) and (3.68) yield

$$\|S^{\ell,J}\|_{H^{2k+\delta}(\Omega)} \le C\left[t^{-\ell-k(2/\alpha)} + \delta t^{-\ell-(k+1/2)(2/\alpha)}\right] e^{-\mu\lambda_J^{\alpha/2}t}\|w_0\|_{L^2(\Omega)}.$$

If an integer K is even, we can take $K = 2k$ and $\delta = 0$ in the above estimate; the second term in the square brackets vanishes, and the first term involves a factor $t^{-\ell-K/\alpha}$. If K is odd, we can take $K = 2k+1$, $\delta = 1$ in the above estimate. In this case, the second term in the square brackets can be written $t^{-\ell-K/\alpha}$, and dominates the first term for small t; for large t, by adjusting C and μ, the first term can be dropped. Thus, for any integer K, we obtain

$$\|S^{\ell,J}\|_{H^K(\Omega)} \le Ct^{-\ell-K/\alpha}e^{-\mu\lambda_J^{\alpha/2}t}\|w_0\|_{L^2(\Omega)} \tag{3.69}$$

This is a direct analogue of Eq. 8.17 in [**127**]. From Theorem A.1, we obtain that for all integers $r, l \ge 0$, there exists C such that

$$\|S^{\ell,J}\|_{C^r(\Omega)} \le C\|S^{\ell,J}\|_{H^{\lceil \frac{d}{2}+r\rceil}(\Omega)} \le Ct^{-\ell-\lceil \frac{d}{2}+r\rceil/\alpha}e^{-\mu\lambda_J^{\alpha/2}t}\|w_0\|_{L^2(\Omega)}. \tag{3.70}$$

From (3.69) and (3.70), considering the particular case $r = 0$, and taking the supremum over $[t_1, t_2]$ with $0 < t_1 < t_2 < \infty$, we have

$$\|S^{\ell,J}(\cdot, x)\|_{C^0([t_1,t_2])} \le \|S^{\ell,J}\|_{C^0([t_1,t_2]\times\Omega)} \le Ce^{-\lambda_J^{\alpha/2}t_1}.$$

This tends to zero as $J \to \infty$, which shows that $S^{\ell,J=1}$ for any $\ell \geq 0$ is uniformly convergent for $t > 0$. Hence, for any ℓ,

$$\partial_t^\ell w(t,x) = S^{\ell,J=1}(t,x).$$

This, together with (3.69) and (3.70), gives parts (1) and (2) of Theorem 3.58.

To prove part (3) of Theorem 3.58, we let $\epsilon > 0$. By the assumption $w_0 \in L^2(\Omega)$, there exists an integer N such that

$$\sum_{j=N+1}^{\infty} (w_0, e_j)^2_{L^2(\Omega)} \leq \frac{\epsilon}{2}.$$

Since $0 < e^{-t\lambda_j^{\alpha/2}} < 1$, we have

$$\sum_{j=N+1}^{\infty} \left(1 - e^{-t\lambda_j^{\alpha/2}}\right)^2 (w_0, e_j)^2_{L^2(\Omega)} \leq \frac{\epsilon}{2}.$$

For the same N, for all t sufficiently small,

$$\sum_{j=1}^{N} \left(1 - e^{-t\lambda_j^{\alpha/2}}\right)^2 (w_0, e_j)^2_{L^2(\Omega)} \leq \frac{\epsilon}{2}.$$

Therefore,

$$\begin{aligned} \|w_0 - w(t,x)\|^2_{L^2(\Omega)} &= \sum_{j=1}^{N} \left(1 - e^{-t\lambda_j^{\alpha/2}}\right)^2 (w_0, e_j)^2_{L^2(\Omega)} + \sum_{j=N+1}^{\infty} \left(1 - e^{-t\lambda_j^{\alpha/2}}\right)^2 (w_0, e_j)^2_{L^2(\Omega)} \\ &\leq \epsilon \end{aligned}$$

for all t sufficiently small. This completes the proof of part (3) of Theorem 3.58. Part (4) of that theorem is a consequence of parts (1) – (3).

Using the regularity results in Theorem 3.58, we can show

THEOREM 3.71. *Define, for $t \geq 0$ and $x \in \Omega$, the survival probability*

$$w(t,x) = \mathbb{P}\left\{X_t^{\Omega,\alpha} \in \Omega\right\} = 1 - \mathbb{P}\left\{X_t^{\Omega,\alpha} \in \partial\Omega\right\}. \tag{3.72}$$

Here, $X_t^{\Omega,\alpha}$ is a sample path of subordinate stopped Brownian motion that begins at $x \in \Omega$. Then, $w(t,x)$ satisfies

$$\begin{cases} \partial_t w + (-\Delta_{\Omega,0})^{\alpha/2} w = 0 \text{ for } x \in \Omega, t > 0 \\ w(x,t) = 0 \quad \text{for } x \in \partial\Omega \\ w(x,0) = 1 \quad \text{for } x \in \Omega. \end{cases} \tag{3.73}$$

This implies that the survival probability satisfies all of the estimates in Theorem 3.58.

Note that this result is precisely what would follow from the stochastic representation in Theorem 3.56 for the solution of (3.73):

$$w(t,x) = \mathbb{E}_{X_0^{\Omega,\alpha}=x}\left[1 \cdot \chi_{\tau_\Omega > T_{\alpha/2}(t)} + 0 \cdot \chi_{\tau_\Omega \leq T_{\alpha/2}(t)}\right] = \mathbb{P}\left\{X_t^{\Omega,\alpha} \in \Omega\right\}.$$

The matter is that the theorem does not directly apply, since the initial condition on $\overline{\Omega}$ is not continuous (i.e., the limit of the initial condition at the boundary is not consistent with the boundary conditions). However, we will use a the regularity results just obtained for the problem (3.73) to prove the desired representation.

Note that (3.72) clearly satisfies the initial condition and the boundary condition of problem (3.73); the initial condition is satisfied since $X_{t=0}^{\Omega,\alpha} = x$, and the boundary condition is satisfied since for $x \in \partial\Omega$, we have $\tau_\Omega = 0$. Thus, it remains to show that the solution $w(t,x)$ of problem (3.73) satisfies (3.72) for $t > 0, x \in \Omega$. By uniqueness, Theorem 3.71 will follow.

Let $t, \epsilon > 0$. Put

$$w_\epsilon(t,x) = w(t+\epsilon, x),$$

where $w(t,x)$ is the solution of (3.73). Then w_ϵ solves

$$\begin{cases} \partial_t w_\epsilon + (-\Delta_{\Omega,0})^{\alpha/2} w_\epsilon = 0 \text{ for } x \in \Omega \\ w_\epsilon(x,t) = 0 \quad \text{for } x \in \partial\Omega \\ w_\epsilon(x,0) = w(\epsilon, x) \quad \text{for } x \in \Omega. \end{cases}$$

Since $w(t,x) \in C^\infty((0,\infty)\times\Omega)$, w_ϵ satisfies

$$w_\epsilon(t,x) = \mathbb{E}_{X_0^{\Omega,\alpha}=x}\left[w(\epsilon, X_t^{\Omega,\alpha}) \cdot \chi_{\tau_\Omega > T_{\alpha/2}(t)}\right]$$

In other words, for $t > 0$ and $x \in \Omega$,

$$w(t+\epsilon, x) = \mathbb{E}_{X_0^{\Omega,\alpha}=x}\left[w(\epsilon, X_t^{\Omega,\alpha}) \cdot \chi_{\tau_\Omega > T_{\alpha/2}(t)}\right] \tag{3.74}$$

For any x, as $\epsilon \to 0$, the left-hand side $w(t+\epsilon, x) \to w(t,x)$. To evaluate the limit of the right-hand side, consider

$$\mathbb{E}_{X_0^{\Omega,\alpha}=x}\left[1 \cdot \chi_{\tau_\Omega > T_{\alpha/2}(t)} - w(\epsilon, X_t^{\Omega,\alpha}) \cdot \chi_{\tau_\Omega > T_{\alpha/2}(t)}\right]. \tag{3.75}$$

This may be written

$$\int_\Omega \left[1 - w(\epsilon, y)\right] P(t,x;y)dy \tag{3.76}$$

where $P(t,x;y)$ is the transition density of $X_t^{\Omega,\alpha}$, giving the probability of starting at x and hitting y:

$$P(t,x;y)dy = \mathbb{P}\left\{X_t^{\Omega,\alpha} \in [y, y+dy]\right\}, \quad X_0^{\Omega,\alpha} = x.$$

By construction, for $y \in \Omega$, $P(t,x;y)$ is less than the transition density of standard isotropic α-stable Lévy motion starting at x. The latter is bounded uniformly by some constant C (depending on α). Thus, we may bound (3.76) by

$$\begin{aligned}\int_\Omega \Big|1-w(\epsilon,y)\Big|P(t,x;y)dy &\leq \|1-w(\epsilon,y)\|_{L^2(\Omega)}\sqrt{\int_\Omega P^2(t,x;y)dy} \\ &\leq \|1-w(\epsilon,y)\|_{L^2(\Omega)}C\sqrt{m(\Omega)}\end{aligned}$$

Since $w(\epsilon,x) \to 1$ in $L^2(\Omega)$ as $\epsilon \to 0$, we obtain that (3.75) also tends to zero as $\epsilon \to 0$. In the same limit, equation (3.74) therefore becomes

$$w(t,x) = \mathbb{E}_{X_0^{\Omega,\alpha}=x}\left[1 \cdot \chi_{\tau_\Omega > T_{\alpha/2}(t)}\right].$$

3.9 The Spectral Fractional Dirichlet Problem.

THEOREM 3.77. *Let Ω be a C^∞ domain. Let $r \in C^2(\Omega)$ and g (defined on $\partial\Omega$) be continuous. Then the solution to*

$$\begin{cases} (-\Delta_{\Omega,g})^{\alpha/2}u(x) = r(x) \text{ for } x \in \Omega \\ u(x) = g(x) \quad \text{for } x \in \partial\Omega \end{cases} \tag{3.78}$$

is given by

$$u(x) = \mathbb{E}_{X_0^{\Omega,\alpha}=x}\left[g\left(X^{\Omega,\alpha}_{T^{-1}_{\alpha/2}(\tau_\Omega)}\right)\right] + \mathbb{E}_{X_0^\alpha=x}\left[\int_0^{T^{-1}_{\alpha/2}(\tau_\Omega)} r(X_s^{\Omega,\alpha})ds\right] \tag{3.79}$$

According to (3.6), the solution u to problem (3.78) can be written as $u = u_1 + u_2$ where u_1 solves

$$\begin{cases} (-\Delta_{\Omega,0})^{\alpha/2}u_1(x) = r(x) \text{ for } x \in \Omega \\ u_1(x) = 0 \quad \text{for } x \in \partial\Omega \end{cases} \tag{3.80}$$

and u_2 solves

$$\begin{cases} \Delta u_2(x) = 0 \text{ for } x \in \Omega \\ u_2(x) = g(x) \quad \text{for } x \in \partial\Omega \end{cases} \tag{3.81}$$

The classical theory of the Dirichlet problem [**106, 86**] implies $u_2 \in C^2(\Omega)$, so by the Feynman-Kac formula, it can be written

$$u_2(x) = \mathbb{E}_{X_0^{\Omega,2}=x}\left[g(X_{\tau_\Omega}^{\Omega,2})\right] = \mathbb{E}_{X_0^{\Omega,\alpha}=x}\left[g\left(X_{T_{\alpha/2}^{-1}(\tau_\Omega)}^{\Omega,\alpha}\right)\right]$$

on account of $X_{\tau_\Omega}^{\Omega,2} = X_{T_{\alpha/2}^{-1}(\tau_\Omega)}^{\Omega,\alpha}$. This is the first term in (3.79). It remains to show that u_1 coincides with the second term.

We begin by noting, from Corollary 3.6 in [**89**] (this is transcribed in Section 2.7.5), that the solution u_1 in (3.80) is $C^2(\Omega)$. Next, we consider the equation

$$\begin{cases} \partial_t w + (-\Delta_{\Omega,0})^{\alpha/2} w = r \text{ for } x \in \Omega \\ w(x,t) = 0 \quad \text{for } x \in \partial\Omega \\ w(x,0) = 0 \quad \text{for } x \in \Omega \end{cases}$$

The solution w to this equation can be written $w = w_{\text{trans}} + u_1$, where u_1 is the same as in equation (3.80) and therefore the transient part w_{trans} solves

$$\begin{cases} \partial_t w_{\text{trans}} + (-\Delta_{\Omega,0})^{\alpha/2} w_{\text{trans}} = 0 \text{ for } x \in \Omega \\ w_{\text{trans}}(x,t) = 0 \quad \text{for } x \in \partial\Omega \\ w_{\text{trans}}(x,0) = -u_1(x) \quad \text{for } x \in \Omega \end{cases}$$

Since $u_1 \in C^2$, we have from Theorem 3.58 that $w_{\text{trans}}(t,\cdot) \in C^2$ for $t \geq 0$ and therefore $w(t,\cdot) \in C^2$ for $t \geq 0$. From Theorem 3.56, we obtain

$$w(t,x) = \mathbb{E}_{X_0^\alpha = x}\left[\int_0^t r(X_s^{\Omega,\alpha})\chi_{\tau_\Omega > T_{\alpha/2}(s)} ds\right]$$

Next, we show, for each $x \in \Omega$,

(1) $w(t,x) \to u_1(x)$ as $t \to \infty$; equivalently, $w_{\text{trans}}(t,x) \to 0$. This follows directly from Theorem 3.58.

(2) As $t \to \infty$,

$$\mathbb{E}_{X_0^\alpha = x}\left[\int_0^t r(X_s^{\Omega,\alpha})\chi_{\tau_\Omega > T_{\alpha/2}(s)} ds\right] \to \mathbb{E}_{X_0^\alpha = x}\left[\int_0^{T_{\alpha/2}^{-1}(\tau_\Omega)} r(X_s^{\Omega,\alpha}) ds\right].$$

Items (1) and (2) imply

$$u_1(x) = \left[\int_0^{T_{\alpha/2}^{-1}(\tau_\Omega)} r(X_s^{\Omega,\alpha}) ds\right],$$

yielding the second term in (3.79) and completing the proof of the theorem. To prove (2), we write using the law of total expectation,

$$\begin{aligned}\mathbb{E}_{X_0^\alpha = x}\left[\int_0^t r(X_s^{\Omega,\alpha})\chi_{\tau_\Omega > T_{\alpha/2}(s)} ds\right] &= \mathbb{E}_{X_0^\alpha = x}\left[\int_0^t r(X_s^{\Omega,\alpha}) ds \;\middle|\; \tau_\Omega > T_{\alpha/2}(t)\right] \mathbb{P}\left\{\tau_\Omega > T_{\alpha/2}(t)\right\} \\ &+ \mathbb{E}_{X_0^\alpha = x}\left[\int_0^{T_{\alpha/2}^{-1}(\tau_\Omega)} r(X_s^{\Omega,\alpha}) ds \;\middle|\; \tau_\Omega \leq T_{\alpha/2}(t)\right] \mathbb{P}\left\{\tau_\Omega \leq T_{\alpha/2}(t)\right\}.\end{aligned}$$

From Theorem 3.71, we have $\mathbb{P}\left\{\tau_\Omega > T_{\alpha/2}(t)\right\} \sim e^{-\lambda_1^{\alpha/2} t}$, so the first term in the above equation tends to zero as $t \to \infty$. Consequently, in the second term, $\mathbb{P}\left\{\tau_\Omega \leq T_{\alpha/2}(t)\right\} \to$

1 as $t \to \infty$. By martingale convergence, the second term therefore tends to

$$\mathbb{E}_{X_0^\alpha = x}\left[\int_0^{T_{\alpha/2}^{-1}(\tau_\Omega)} r(X_s^{\Omega,\alpha})ds\right].$$

This completes the proof.

REMARK 3.82. Note that to obtain $u_2 \in C^2$ in equation (3.81), it is only required that Ω satisfy, e.g., the exterior sphere condition [**106**]. The condition that Ω is C^∞ is used in two places. First, to invoke the regularity results of article [**89**] (Corollary 3.6) that the solution u_1 in Eq. (3.80) is $C^2(\Omega)$. This assumption on Ω is required due the techniques utilized in that article; we do not believe it is essential for obtaining $u_1 \in C^2(\Omega)$. For example, regularity results in Hölder spaces for the same equation (3.80) were obtained in [**39**] assuming that Ω is Lipschitz, but only for the spaces $C^{0,r}$; this is discussed in Section 2.7.5 of the thesis. If regularity in higher order $C^{2,r}$ spaces were proven with weaker conditions on Ω, then the requirement that Ω is C^∞ in Theorem 3.77 could be relaxed accordingly. We believe this to be possible, but are not aware of such results in the literature. The second place where the smoothness of the domain is used is in the proof of Theorem 3.58, to invoke elliptic regularity (Theorem A.2) without restriction on k and obtain smoothness of the solution $u(t,x)$. Full smoothness of the solution to the Cauchy problem is not required in the above proof, and may also be relaxed in a way that depends on the dimension d. For simplicity, we have not done so. Numerical simulations in Section 3.10 verify both the time-dependent and time-independent stochastic solution formulas in the unit square and unit cube in benchmark examples.

3.10 Numerical Examples.

3.10.1 Implementation Details.

We now verify the stochastic solution formulas proved in this chapter. Namely, for the parabolic time-dependent problem (3.51) with initial condition f, boundary condition g, and time-independent right-hand side r, we study the formula

$$u(t,x) = \mathbb{E}_{X_0^{\Omega,\alpha}=x}\left[f(X_t^{\Omega,\alpha})\chi_{\tau_\Omega > T_{\alpha/2}(t)} + g(X_t^{\Omega,\alpha})\chi_{\tau_\Omega \le T_{\alpha/2}(t)}\right] + \mathbb{E}_{X_0^{\alpha}=x}\left[\int_0^t r(X_s^{\Omega,\alpha})\chi_{\tau_\Omega > T_{\alpha/2}(s)} ds\right]. \tag{3.83}$$

For the elliptic problem (3.78) with boundary condition g and right-hand side r, we study the formula

$$u(x) = \mathbb{E}_{X_0^{\Omega,\alpha}=x}\left[g\left(X^{\Omega,\alpha}_{T^{-1}_{\alpha/2}(\tau_\Omega)}\right)\right] + \mathbb{E}_{X_0^{\Omega,\alpha}=x}\left[\int_0^{T^{-1}_{\alpha/2}(\tau_\Omega)} r\left(X_s^{\Omega,\alpha}\right) ds\right].$$

We start by discussing the direct discretization of the process $X_t^{\alpha,\Omega} \equiv X^{2,\Omega}_{T_{\alpha/2}(t)} = X^2_{T_{\alpha/2}(t)\wedge\tau_\Omega}$. A short MATLAB implementation of method described below is included in Appendix C.

(1) **Generation of Discrete Stopped Brownian Motion $X_t^{2,\Omega}$.** A starting point $X_0^{2,\Omega} \in \Omega$ is specified. A discrete time step dt is chosen, and we generate the path at times $t = 0, dt, 2dt, ...$ using

$$X^{2,\Omega}_{t+dt} = X_t^{2,\Omega} + \sqrt{2}dt^{1/2}\texttt{mvnrnd}(\mathbf{0}, \mathbf{Id}) \tag{3.84}$$

where $\texttt{mvnrnd}(\mathbf{0}, \mathbf{Id})$ denotes the multivariate normal random variable with mean vector $\mathbf{0} = [0\ 0\ ...\ 0]^T$ and covariance matrix

$$\mathbf{Id} = \begin{bmatrix} 1 & 0 & ... & 0 \\ 0 & 1 & ... & 0 \\ \vdots & \vdots & ... & \vdots \\ 0 & 0 & ... & 1 \end{bmatrix}$$

in dimension d where $\Omega \subset \mathbb{R}^d$. Equation (3.84) is used to generate new points of the path while $X_t^{2,\Omega} \in \Omega$. Once we obtain a position $X_{t+\Delta t}^{2,\Omega} \notin \Omega$, we replace this last position by the point $X_{\tau_\Omega}^{2,\Omega}$ nearest to it on the boundary, and end. The full path is stored and used in the next steps. The exit time τ_Ω rounded up to the nearest dt, denoted $\lceil \tau_\Omega \rceil_{dt}$, is saved as well.

(2) **Generation of Discrete Subordinator $T_{\alpha/2}(t)$ starting at zero.** We generate the subordinator at times $t = 0, dt, 2dt, ...$ with $T_{\alpha/2}(0) = 0$ and

$$T_{\alpha/2}(t + dt) = T_{\alpha/2}(t) + dt^{1/a}\ \texttt{stblrnd}(a, \texttt{skewness}, \texttt{scale}, \texttt{center}) \tag{3.85}$$

with parameters $a = \alpha/2$, $\texttt{skewness} = 1$, $\texttt{scale} = (\cos(\pi a/2))^{1/a}$, and $\texttt{center} = 0$. For simplicity, we use the same value of dt as used to discretize the Brownian motion, although this is not required. The parameter values of `skewness`, `scale`, and `center` are the parameters in the Samorodnitsky and Taqqu parametrization of the one-dimensional stable process that yield the standard stable subordinator [**186**]. The function `stblrnd`, written by Mark Veillette [**214**], uses the methods of [**221, 43**] to generate samples of the one-dimensional stable random variable in the Samorodnitsky and Taqqu parametrization. The resulting samples from `stblrnd` are positive;

for these parameters, the stable distribution is supported on $\mathbb{R}^+$, as shown in Figure 2. Using (3.85), the subordinator is updated while $T_{\alpha/2}(t) < \tau_\Omega$. When $T_{\alpha/2}(t+dt)$ is greater than or equal to τ_Ω for the first time, we replace it by τ_Ω and end.

(3) **Subordination of Discrete Stopped Brownian Motion $X_t^{2,\Omega}$.** We now wish to insert the values of the subordinators $T_{\alpha/2}$ into the respective Brownian paths. However, since the positions of the Brownian paths are only available at times $0, dt, 2d, ...$, we round the subordinators up to the nearest multiple of dt. We denote this by $\lceil T_{\alpha/2} \rceil_{dt}$. The discretized process $X_t^{\alpha,\Omega}$ is obtained as $X^{2,\Omega}_{\lceil T_{\alpha/2} \rceil_{dt}}$. This step is illustrated in Table 1, and the process is illustrated with some example paths in Figures 3 and 4.

(4) **Integration for parabolic solution** (3.83) **in time**. To calculate the first term in the solution at time Ndt, if a sample path of $X_t^{\Omega,\alpha}$ has hit the boundary at time Ndt, the boundary condition g is evaluated at $X^{\Omega,\alpha}_{Ndt}$; otherwise, the initial condition f is evaluated at $X^{\Omega,\alpha}_{Ndt}$. The second term (the path integral) is discretized as

$$\left[\int_0^{Ndt} r(X_s^{\Omega,\alpha})\chi_{\tau_\Omega > T_{\alpha/2}(s)} ds\right] \sim dt \sum_{n=1}^{N \wedge \lceil T^{-1}_{\alpha/2}(\tau_\Omega)\rceil_{dt}/dt} r(X^{\Omega,\alpha}_{ndt}). \tag{3.86}$$

Importantly, the integration does not repeat over the exit point. Once a path hits the boundary, the path integral over that path no longer evolves. This is illustrated in Figure 5.

(5) **Integration for elliptic solution.** The boundary condition g is evaluated at the endpoints of each path, and for the path integral, the same discretization (3.86) is used except that all sums run to $\lceil T^{-1}_{\alpha/2}(\tau_\Omega)\rceil_{dt}/dt$, rather than $N \wedge \lceil T^{-1}_{\alpha/2}(\tau_\Omega)\rceil_{dt}/dt$.

REMARK 3.87. Unlike in the classical $\alpha = 2$ case, computing the solution for the time-dependent problem (using the direct approach above) even for a short time t requires generating Brownian paths all the way to the boundary. This is because the subordinator $T_{\alpha/2}$ may advance time significantly beyond the specified time t. The vast majority of computation time is spent generating paths, so once the paths are stored, we recommend computing the entire solution curve in time as well as the solution to the time independent problem.

REMARK 3.88. The true subordinator $T_{\alpha/2}(t)$ is strictly increasing. However, because we have to round the subordinator values to nearest multiple of dt, the discrete subordinator $\lceil T_{\alpha/2} \rceil_{dt}$ is merely nondecreasing, and frequently "waits" at the same time value for several increments.

$\boldsymbol{t}$	$\boldsymbol{X}_t^{\Omega,2}$
0	X_0
dt	X_{dt}
$2dt$	X_{2dt}
$\vdots$	$\vdots$
ndt	X_{ndt}
$\vdots$	$\vdots$
$\lceil \tau_\sigma \rceil_{dt}$	$X_{\lceil \tau_\sigma \rceil_{dt}}$
$\vdots$	$X_{\lceil \tau_\sigma \rceil_{dt}}$

$\rightarrow$

$\boldsymbol{t}$	$\boldsymbol{T}_{\alpha/2}(t)$	$\boldsymbol{X}_t^{\Omega,\alpha}$
0	0	X_0
dt	$\lceil T_{\alpha/2}(dt) \rceil_{dt}$	$X_{\lceil T_{\alpha/2}(dt) \rceil_{dt}}$
$2dt$	$\lceil T_{\alpha/2}(2dt) \rceil_{dt}$	$X_{\lceil T_{\alpha/2}(2dt) \rceil_{dt}}$
$\vdots$	$\vdots$	$\vdots$
ndt	$\lceil T_{\alpha/2}(ndt) \rceil_{dt}$	$X_{\lceil T_{\alpha/2}(ndt) \rceil_{dt}}$
$\vdots$	$\vdots$	$\vdots$
$\lceil T_\alpha^{-1}(\tau_\sigma) \rceil_{dt} = Ndt$	$\lceil T_{\alpha/2}(Ndt) \rceil_{dt}$	$X_{\lceil T_{\alpha/2}(Ndt) \rceil_{dt}}$
$\vdots$	$\vdots$	$X_{\lceil T_{\alpha/2}(Ndt) \rceil_{dt}}$

TABLE 1. *Left:* The output of Step 1 discussed above, in which a discrete stopped Brownian motion path is generated and stored. The process remains at the boundary point $X_{\lceil \tau_\Omega \rceil_{dt}}$ for all time greater than $\lceil \tau_\Omega \rceil_{dt}$, so the path need only be stored up to that point. *Right:* Illustration of Steps 2 and 3, in which the discrete subordinator $\lceil T_{\alpha/2}(Ndt) \rceil_{dt}$ is generated (center column) and used to subordinate a discrete stopped Brownian motion path stored in Step 1 to yield discrete subordinate stopped Brownian motion path (right column).

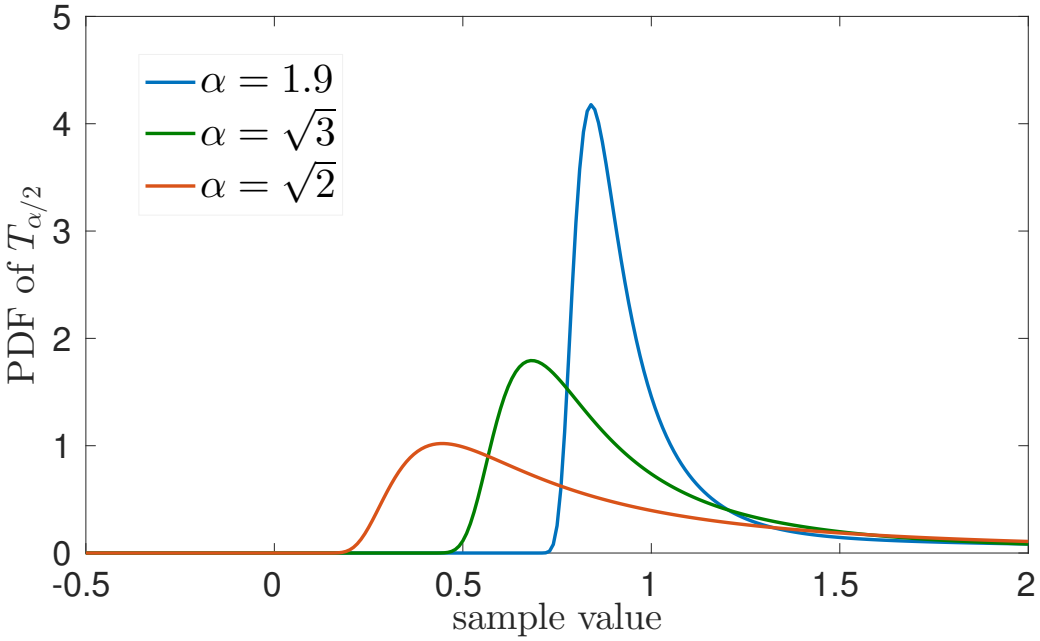

FIGURE 2. Probability density function of the standard stable subordinator $T_{\alpha/2}$ for various α, with the other parameters fixed as discussed above.

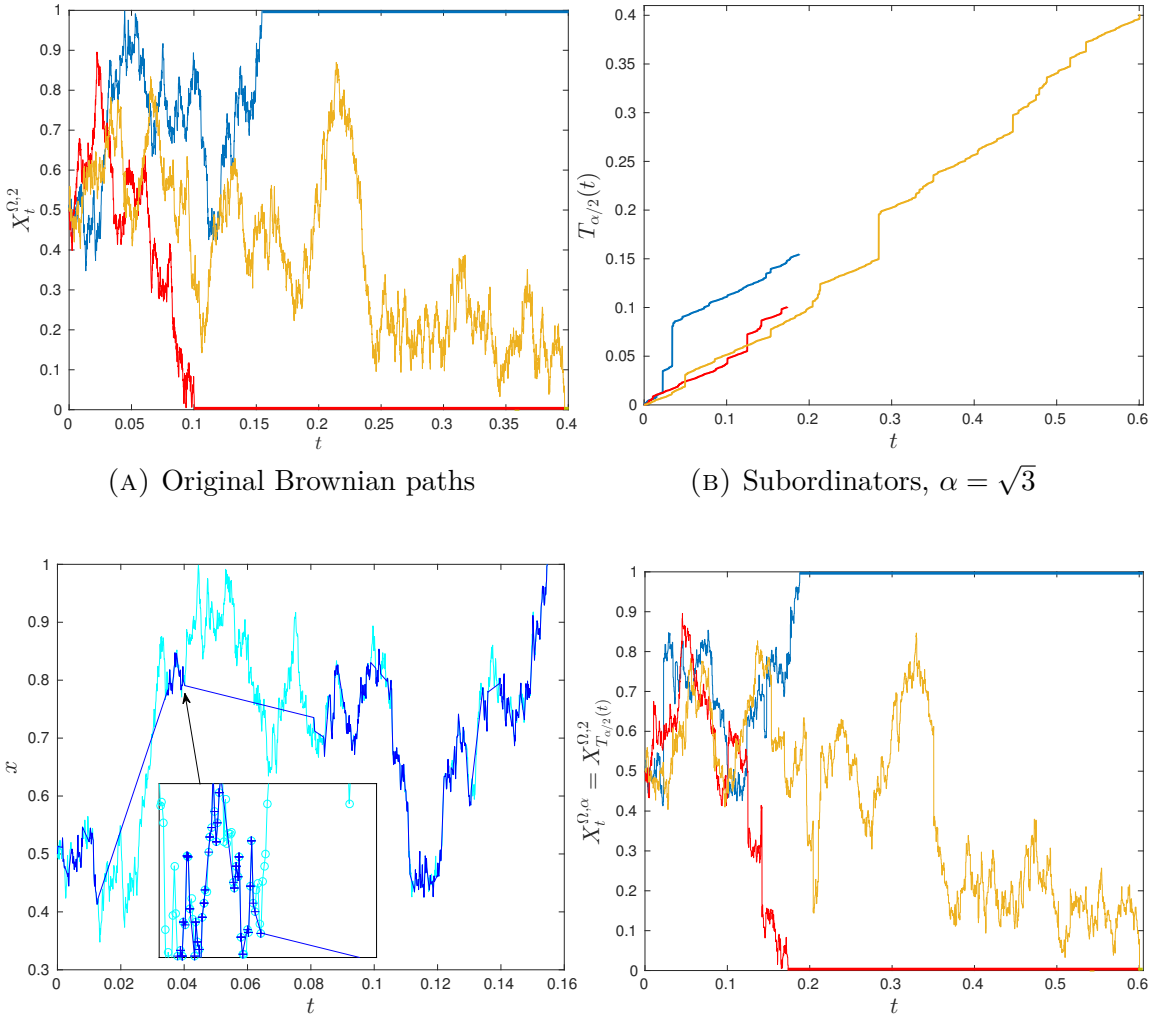

(A) Original Brownian paths

(B) Subordinators, $\alpha = \sqrt{3}$

(C) A subordinated path as sub-path of original path

(D) Final subordinated Paths from original BM paths

FIGURE 3. *Top left:* Three time series of stopped Brownian paths $X^{\Omega,2}$ in the unit interval $[0, 1]$. *Top right:* Three samples of the standard α-stable subordinator $T_{\alpha/2}$ for $\alpha = \sqrt{3}$, run until the exit time of the respective stopped Brownian path shown to the left. *Bottom Left:* The cyan process is an original BM (the blue one) from the top left plotted versus standard time t. The dark blue process shows the subordinated process plotted versus subordinated time $T_{\alpha/2}$. Some of the locations of the original process are skipped, and others are kept. *Bottom right:* Final subordinated paths plotted versus standard time t.

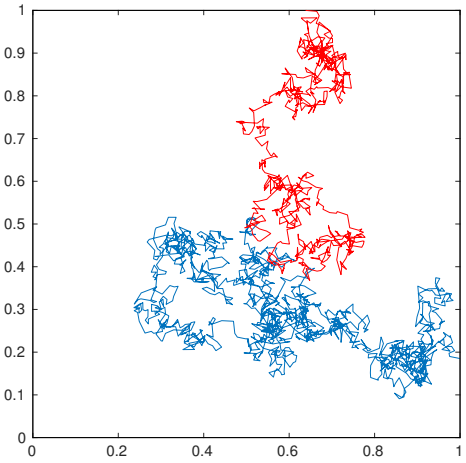

Stopped 2D Brownian paths in the unit square

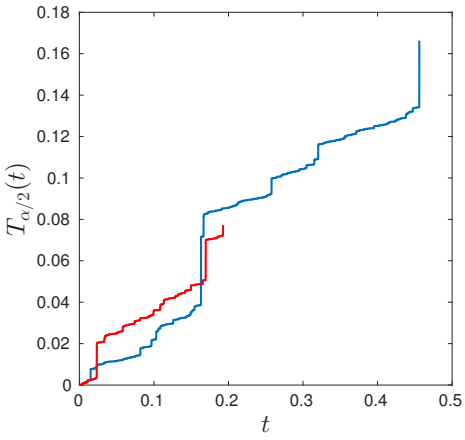

Subordinators, $\alpha = \sqrt{2}$

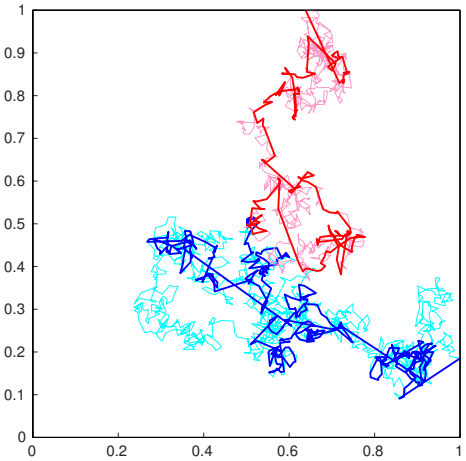

Subordinated paths as subpaths of original paths

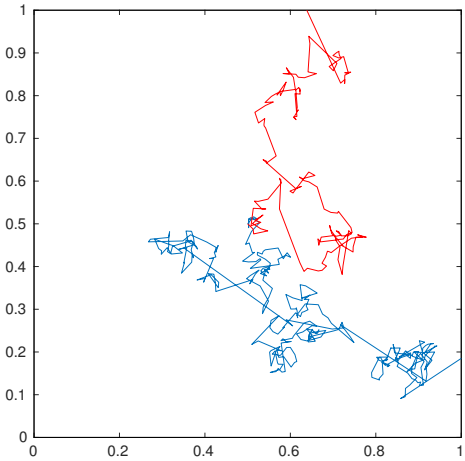

Final subordinated paths from original BM paths

FIGURE 4. *Top left:* Two stopped Brownian paths $X_t^{\Omega,2}$ in the unit square $[0,1] \times [0,1]$. *Top right:* Two samples of the standard α-stable subordinator $T_{\alpha/2}$ for $\alpha = \sqrt{2}$, run until the exit times of the respective stopped Brownian paths shown to the left are exceeded. *Bottom Left:* The light-colored paths are original stopped BM from the top left; the dark-colored paths are subordinated paths $X^{\Omega,2}_{T_{\alpha/2}(t)}$. The subordinated process is seen to be a subprocess of the stopped BM. *Bottom right:* Final subordinated paths.

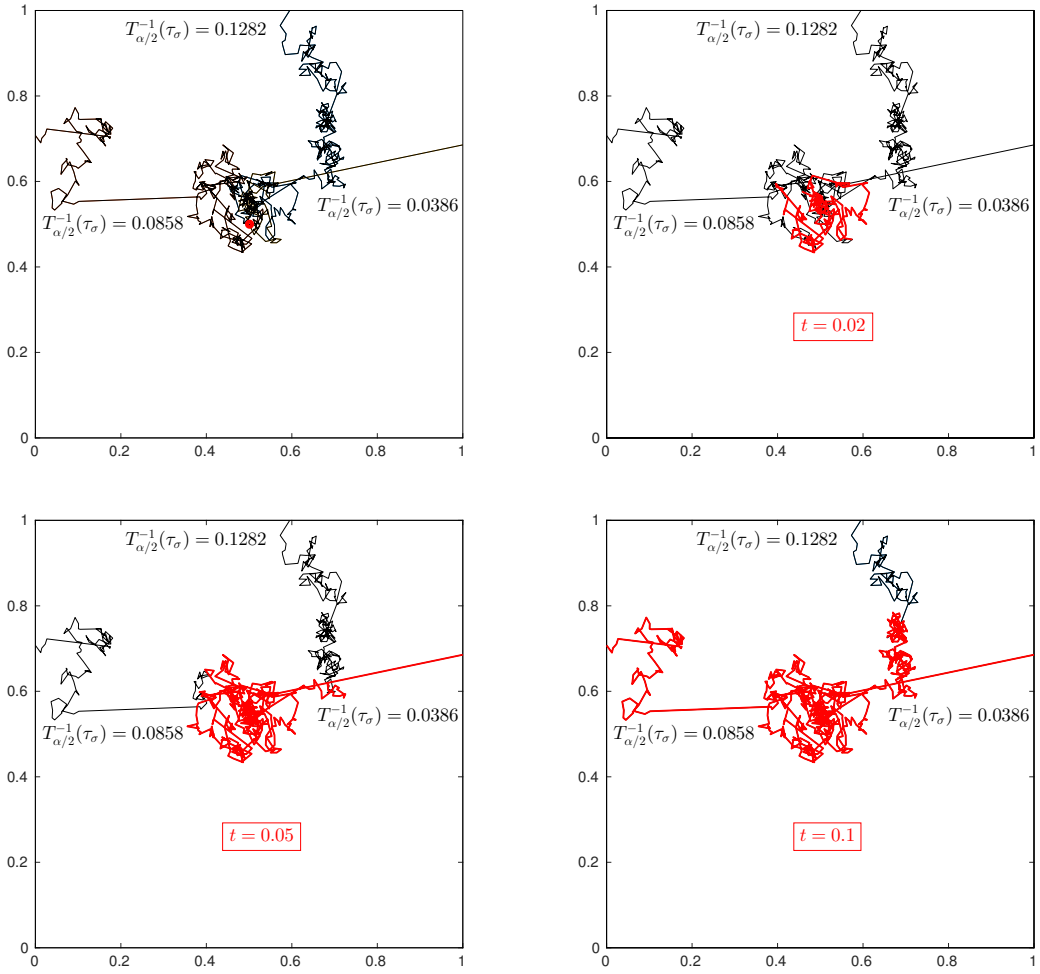

FIGURE 5. Illustration of path integration in the unit square $[0,1] \times [0,1]$ for the stochastic solution in time. First, several paths of the subordinate stopped process are generated and stored in memory. *Top left:* Three sample paths of the subordiante stopped process $X_t^{\Omega,\alpha}$ (black) for $\alpha = \sqrt{3}$ starting at $(x, y) = (0.5, 0.5)$ – shown as a red dot – with indicated stopping times. *Top right, bottom left, bottom right:* The red tracings show the paths of integration (running along the stopped paths for specified time t) for computing the solution to the parabolic problem $u(t, x = 0.5, y = 0.5)$ at increasing t.

3.10.2 2-Dimensional Benchmark Example (Unit Square).

First, we test the parabolic solution formula. Consider the two-dimensional unit square $R = [0,1] \times [0,1]$. Define $g : \partial R \to \mathbb{R}$ by

$$\begin{cases} g(x, y = 0) & = 0 \\ g(x, y = 1) & = 1 \\ g(x = 0, y) & = y \\ g(x = 1, y) & = y \end{cases} \tag{3.89}$$

and consider the problem, for $\alpha = \sqrt{3}$,

$$\begin{cases} \partial_t u + (-\Delta_{R,g})^{\alpha/2} u & = \sin(\pi x)\sin(\pi y) \\ u\big|_{\partial R} & = g \\ u(t = 0, x) & = y + \frac{1}{(\pi^2+\pi^2)^{\alpha/2}} \sin(\pi x)\sin(\pi x). \end{cases}$$

In this problem,

- the boundary condition (BC) function g is defined by (3.89).
- the right-hand side (RHS) is $r(x, y) = \sin(\pi x)\sin(\pi y)$, and
- the initial condition (IC) is

$$f(x, y) = y + \frac{1}{(\pi^2 + \pi^2)^{\alpha/2}} \sin(\pi x)\sin(\pi y) + \sin(2\pi x)\sin(2\pi y).$$

The exact solution is

$$u(t, x) = y + \frac{1}{(\pi^2 + \pi^2)^{\alpha/2}} \sin(\pi x)\sin(\pi y) + e^{-\left(4\pi^2+4\pi^2\right)^{\alpha/2} t} \sin(2\pi x)\sin(2\pi y).$$

In the top of Figure 6, we consider the time trajectory of the stochastic solution $u(t, 1/3, 2/3)$ at the fixed point $(1/3, 2/3) \in R$. The discretized Brownian motion/-subordinator time step is fixed at $dt = 10^{-4}$. The mean of 100 stochastic solutions,

computed using 100 or 1,000 paths (as indicated) starting from $(1/3, 2/3)$, is plotted and compared to the exact solution. The "Mean $\pm$ Standard Deviation" illustrates the expected variation of a stochastic solution computed using 100 or 1,000 paths, respectively, as it oscillates about the respective mean. Further, the means of the 100-path and 1000-path solutions *also* represent stochastic solutions for $u(t, 1/3, 2/3)$ computed using $100 \times 100 = 10,000$ paths and $100 \times 1000 = 100,000$ paths, respectively. We see that both are well-converged to the exact solution curve, although the 100,000 path solution is smoother when viewed more closely in the inset.

The next example illustrates the role of the Brownian motion/subordinator time step dt when the stochastic solution formula is used near the boundary. At the bottom of Figure 6, we consider the time trajectory of the stochastic solution $u(t, 9/10, 9/10)$ at the fixed point $(9/10, 9/10)$ near the top-right corner of R. In both the main figure and the insets, the 10,000 path solution using $dt = 0.0001$ has significant discrepancy from the true solution. Increasing the number of paths (as in the top figure) to $100,000$ does not improve the accuracy the solution; in fact, it remains mostly unchanged from the 10,000 path solution. However, in this case, refining dt by decreasing it one order of magnitude to 10^{-5} improves the solution significantly, even when using only 10,000 paths. This can be attributed to the closeness of the point $(9/10, 9/10)$ to the boundary. Because the paths have a high probability of exiting very close to the starting point in a few number of steps, using too high a dt results in under-resolved Brownian motion that looks more like ballistic motion, bottlenecking the convergence of the solution.

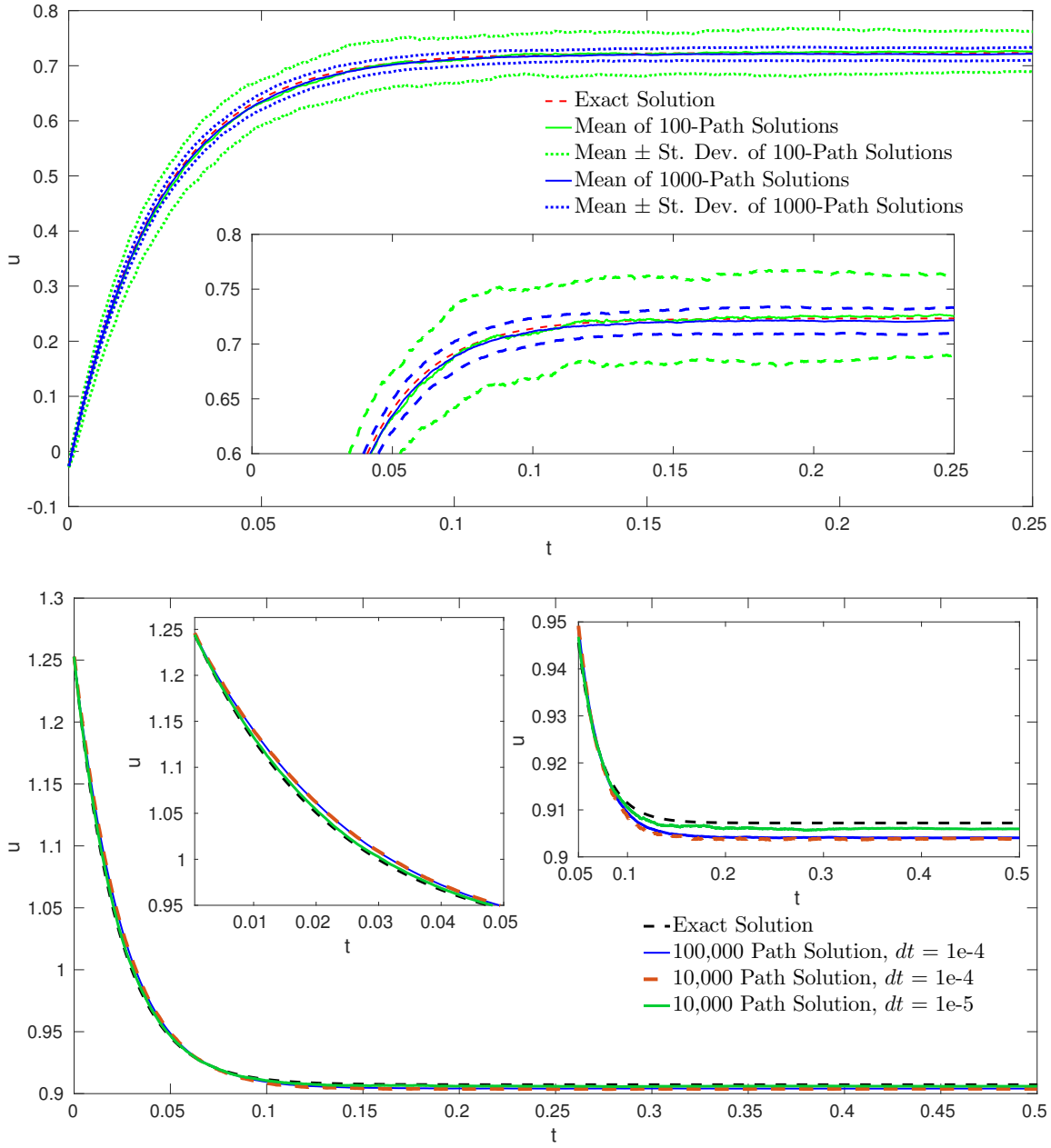

FIGURE 6. Convergence of stochastic solutions for the 2D problem with right-hand side $r(x, y) = \sin(\pi x)\sin(\pi y)$. *Top, main:* Convergence with respect to number of paths of the stochastic solution at (1/3, 2/3), with $dt = 10^{-4}$. *Top, inset:* Zoomed-in view of the main plot. *Bottom, main:* Bottlenecking of the convergence of the stochastic solution at (9/10,9/10), and improvement with refinement of dt from 10^{-4} to 10^{-5}. *Bottom, insets:* Zoomed-in views of the main plot.

Next, we consider the elliptic problem on the unit square $R = [0,1] \times [0,1]$:

$$\begin{cases} (-\Delta_{R,g})^{\alpha/2} u & = 137 \sin(2\pi x) \sin(3\pi y) \\ u\Big|_{\partial R}(x,y) & = y \end{cases}$$

In this problem, the BC function $g = y$ as before and the RHS is $r(x) = 137 \sin(2\pi x) \sin(3\pi y)$. The exact solution is

$$u(x,y) = y + \frac{137}{[(2\pi)^2 + (3\pi)^2]^{\alpha/2}} \sin(2\pi x) \sin(3\pi y);$$

For $\alpha = \sqrt{3}$, we study the elliptic solution formula along the diagonal line $D = \{(s,s) \;\big|\; s \in [0,1]\} \subset R$. Thus, D runs from the bottom left corner of the square to the top right corner. We take 100 equispaced points on this line, and compute the solution at each of the points using 100, 1,000, and 10,000 paths. The discretized Brownian motion/subordinator time step is fixed at $dt = 10^{-4}$. The solutions are compared to the exact solution in Figure 7. We see that they converge to the true solution as the number of paths is increased.

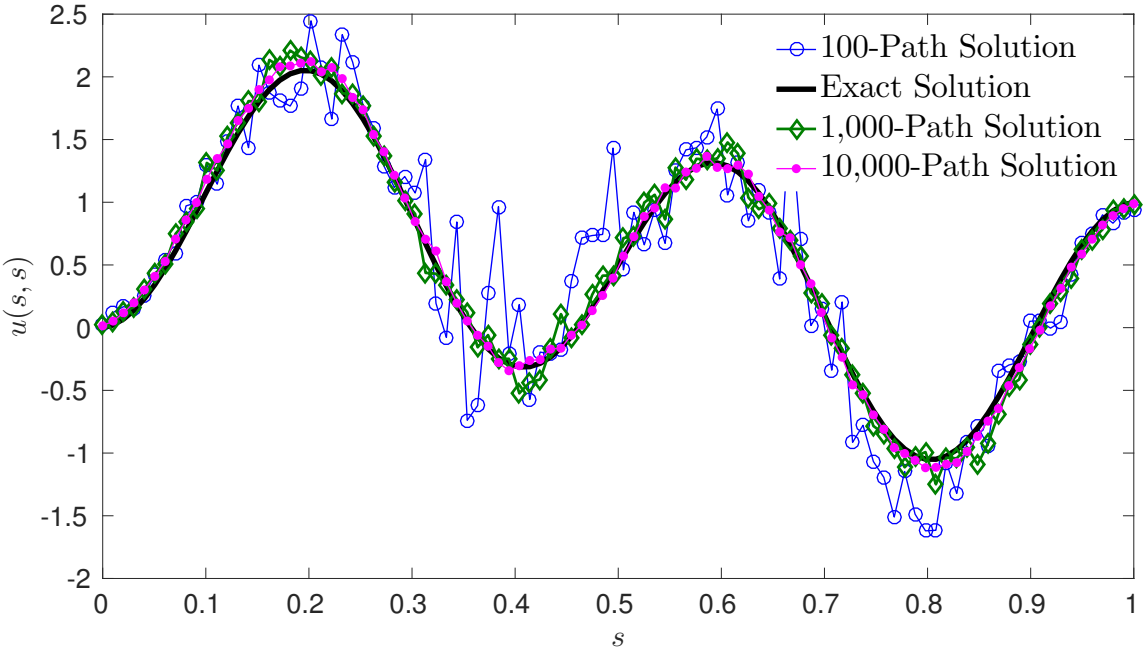

FIGURE 7. Stochastic solution of problem in the 2D unit square with right-hand side $r(x,y) = 137\sin(2\pi x)\sin(3\pi y)$ at 100 equispaced points along the line $D = \{(s,s) \mid s \in [0,1]\}$, using 100, 1,000, and 10,000 paths starting from each point.

3.10.3 3-Dimensional Benchmark Example (Unit Cube).

Consider the three-dimensional unit cube $Q = [0,1]^3$. Define $g \equiv 1$ on ∂Q. We study the equation

$$
\begin{cases}
\partial_t u + (-\Delta_{Q,g})^{\alpha/2} u &= \sin(\pi x)\sin(\pi y)\sin(\pi z) \\
u\big|_{\partial Q} &= g \\
u(t=0,x,y,z) &= 1 + \frac{1}{(\pi^2+\pi^2+\pi^2)^{\alpha/2}}\sin(\pi x)\sin(\pi y)\sin(\pi z) \\
&\qquad + \sin(2\pi x)\sin(2\pi y)\sin(2\pi z).
\end{cases} \tag{3.90}
$$

In this problem,

- the boundary condition (BC) function $g \equiv 1$,

- the right-hand side (RHS) is $r(x, y, z) = \sin(\pi x)\sin(\pi y)\sin(\pi z)$, and
- the initial condition (IC) is

$$f(x, y, z) = 1 + \frac{1}{(\pi^2 + \pi^2 + \pi^2)^{\alpha/2}} \sin(\pi x)\sin(\pi y)\sin(\pi z) + \sin(2\pi x)\sin(2\pi y)\sin(2\pi z).$$

The exact solution is

$$u(t, x, y, z) = 1 + \frac{1}{(\pi^2 + \pi^2 + \pi^2)^{\alpha/2}} \sin(\pi x)\sin(\pi y)\sin(\pi z) + e^{-\left(4\pi^2+4\pi^2+4\pi^2\right)^{\alpha/2} t} \sin(2\pi x)\sin(2\pi y)\sin(2\pi z).$$

We fix $\alpha = \sqrt{2}$ and $dt = 10^{-4}$. We start by testing the parabolic solution formula in Figure 8. We approximate the solution $u(t, x, y, z)$ as a function of t at two different points: $(x, y, z) = (1/3, 2/3, 1/3)$ and $(x, y, z) = (3/5, 2/5, 3/5)$. The mean of 100 stochastic solutions, computed using 100 or 1,000 paths (as indicated) starting from (x, y, z) is plotted and compared to the exact solution. The"Mean ± Standard Deviation" illustrates the expected variation of a stochastic solution computed using 100 or 1,000 paths, respectively, as it oscillates about the respective mean. Further, the means of the 100-path and 1000-path solutions *also* represent stochastic solutions for $u(t, x, y, z)$ computed using $100 \times 100 = 10,000$ paths and $100 \times 1000 = 100,000$ paths, respectively. We see that these are well-converged to the true solution.

Next, we study the stochastic solution in spacetime along line diagonal line $D = \{(s, s, s) \mid s \in [0, 1]\} \subset R$. We take 100 equispaced points on D, and compute the solution at each of the points using 100, 1,000, and 10,000 paths. In Figures 9 and 10, we show surface plots in (s, t) of these solutions and compare to the exact solution; in Figure 11, we plot the absolute error $u_{\text{stochastic}}(t, s, s, s) - u_{\text{exact}}(t, s, s, s)$ as a surface plot in (s, t). We observe a decrease in the maximum value of the absolute error by a factor of roughly $\sqrt{10}$ each time the number of paths is increased by a factor of 10.

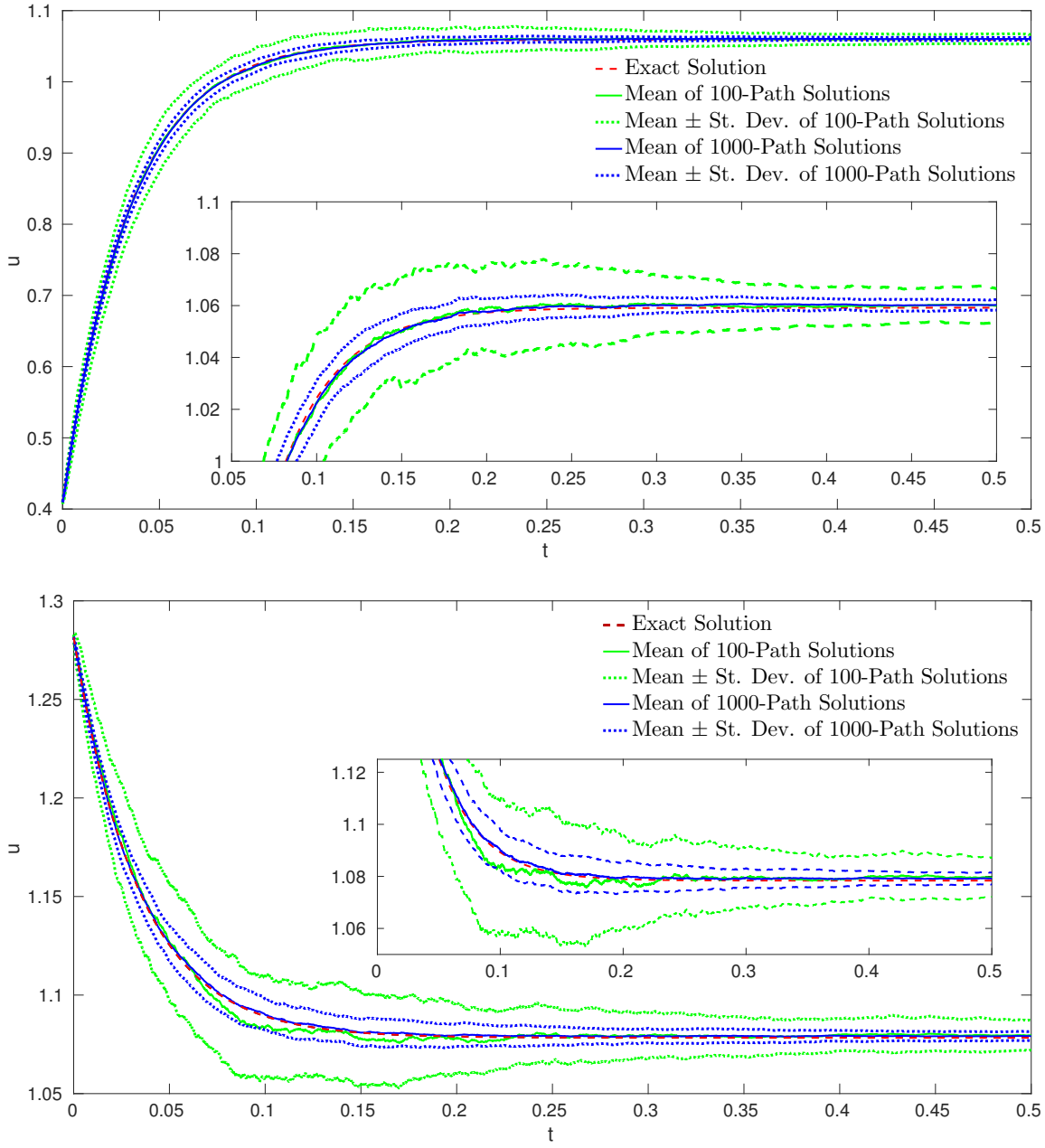

FIGURE 8. Convergence of stochastic solutions for the 3D problem with boundary condition $g \equiv 1$ and right-hand side $r(x, y, z) = \sin(\pi x)\sin(\pi y)\sin(\pi z)$. *Top, main:* Convergence with respect to number of paths of the stochastic solution at (1/3, 2/3, 1/3), with $dt = 10^{-4}$. *Top, inset:* Zoomed-in view of the main plot. *Bottom, main:* Convergence with respect to number of paths of the stochastic solution at (3/5, 2/5, 3/5), with $dt = 10^{-4}$. *Bottom, inset:* Zoomed-in view of the main plot.

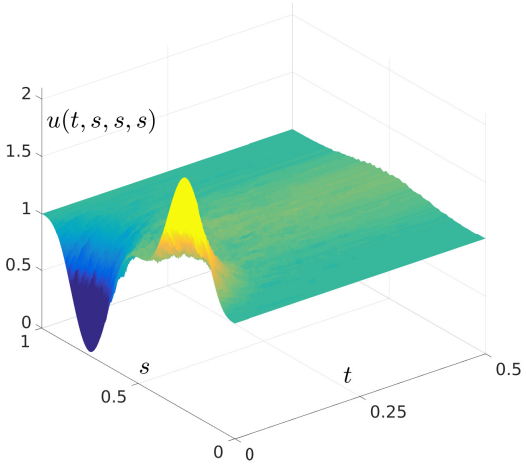

Stochastic solution computed using 100 paths for $t \in [0, 0.5]$.

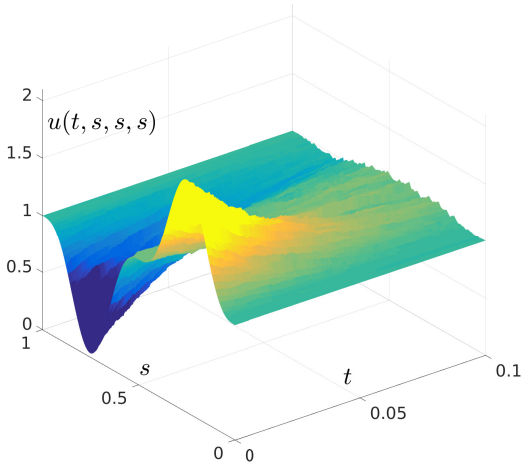

Stochastic solution computed using 100 paths zoomed in to a shorter time $t \in [0, 0.1]$.

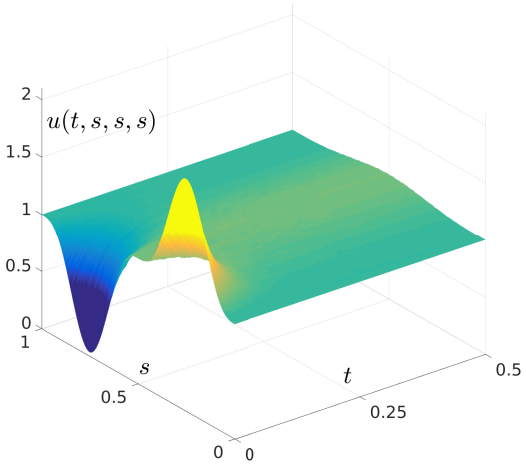

Stochastic solution computed using 1,000 paths for $t \in [0, 0.5]$.

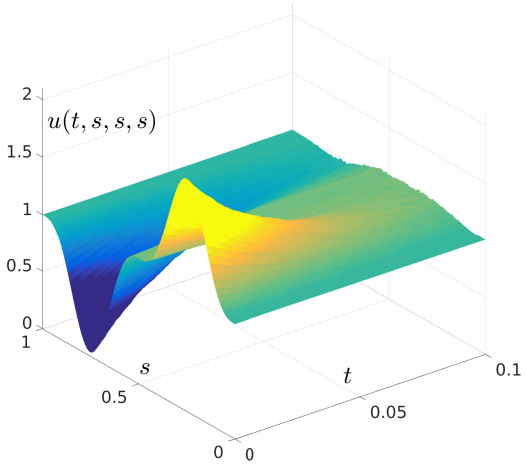

Stochastic solution computed using 1,000 paths zoomed in to a shorter time $t \in [0, 0.1]$.

FIGURE 9. Stochastic solution using 100 paths (*top*) and 1,000 paths (*bottom*) of problem (3.90) in time t on the diagonal $D = \{s, s, s\}$ in the unit cube.

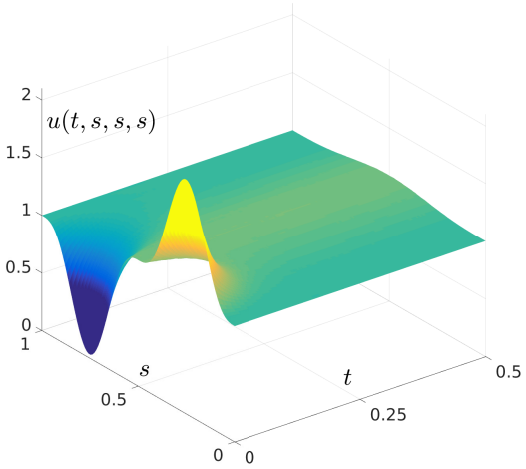

Stochastic solution computed using 10,000 paths for $t \in [0, 0.5]$.

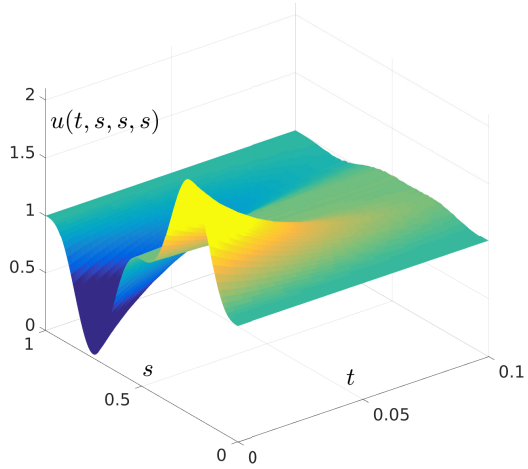

Stochastic solution computed using 10,000 paths zoomed in to a shorter time $t \in [0, 0.1]$.

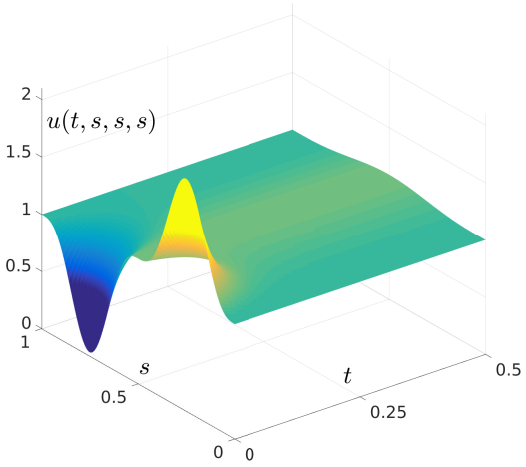

Exact solution for $t \in [0, 0.5]$.

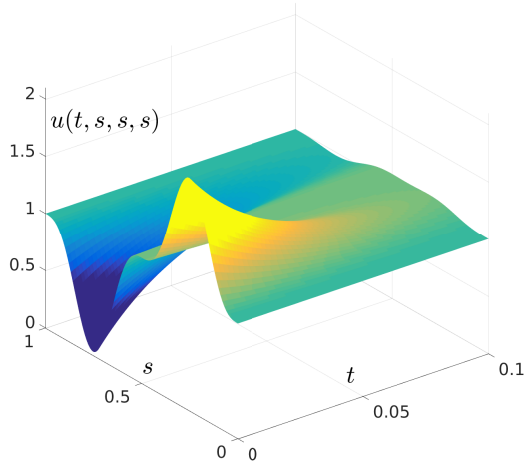

Exact solution zoomed in to a shorter time $t \in [0, 0.1]$.

FIGURE 10. Stochastic solution (using 10,000 paths, *top*) and exact solution (*bottom*) of problem the 3D problem with boundary condition $g \equiv 1$ and right-hand side $r(x, y, z) = \sin(\pi x) \sin(\pi y) \sin(\pi z)$ in time t on the diagonal $D = \{s, s, s\}$ in the unit cube.

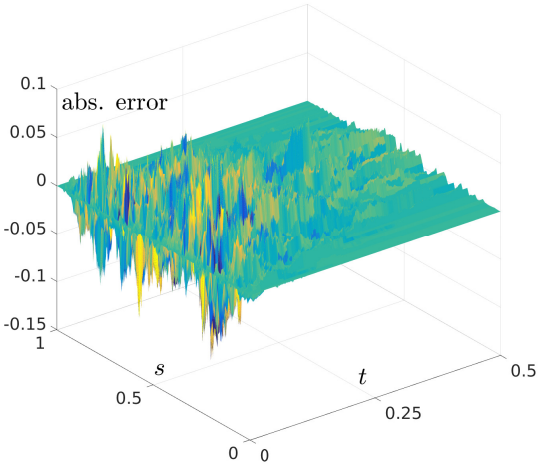

100 paths for the stochastic solution.

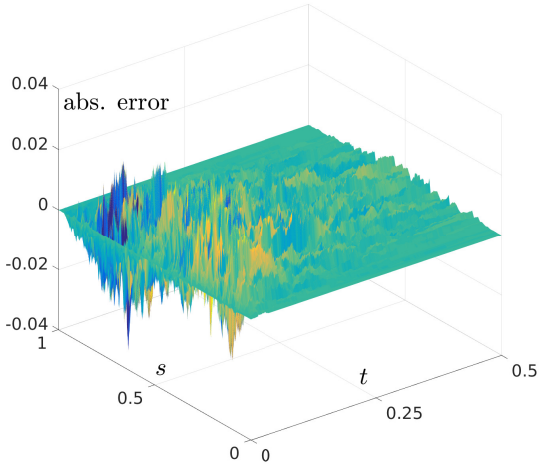

1,000 paths for the stochastic solution.

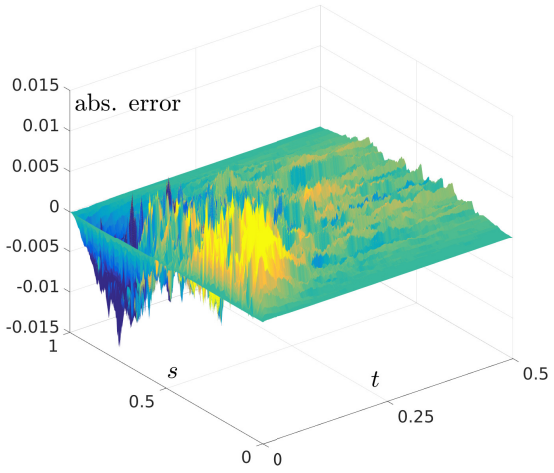

10,000 paths for the stochastic solution.

FIGURE 11. Convergence of the absolute error $u_{\text{stochastic}}(t,s,s,s) - u_{\text{exact}}(t,s,s,s)$ for the solution of the 3D problem with boundary condition $g \equiv 1$ and right-hand side $r(x,y,z) = \sin(\pi x)\sin(\pi y)\sin(\pi z)$ in spacetime for time $t \in [0, 0.5]$ and position $s \in [0,1]$ along the diagonal (s,s,s). 100, 1,000, and 10,000 paths are used in the stochastic solution.

Next, we test the elliptic solution formula for the example consisting of the steady state to problem (3.90), i.e.,

$$\begin{cases} (-\Delta_{Q,g})^{\alpha/2} u &= \sin(\pi x)\sin(\pi y)\sin(\pi z) \\ u\big|_{\partial Q} &= 1 \end{cases} \tag{3.91}$$

which has exact solution

$$u(x,y,z) = 1 + \frac{1}{(\pi^2+\pi^2+\pi^2)^{\alpha/2}} \sin(\pi x)\sin(\pi y)\sin(\pi z).$$

We keep $\alpha = \sqrt{2}$ and $dt = 10^{-4}$, and illustrate convergence by computing the solution $u(s,s,s)$ using 100, 1,000, and 10,000 paths from each of the 100 equispaced points on $D = \{(s,s,s) \mid s \in [0,1]\}$. This is shown in Figure 12. In fact, the same exact sets of stopped paths are used to produce Figures 9 and 10 are used to evaluate the stochastic solution formula for this elliptic problem.

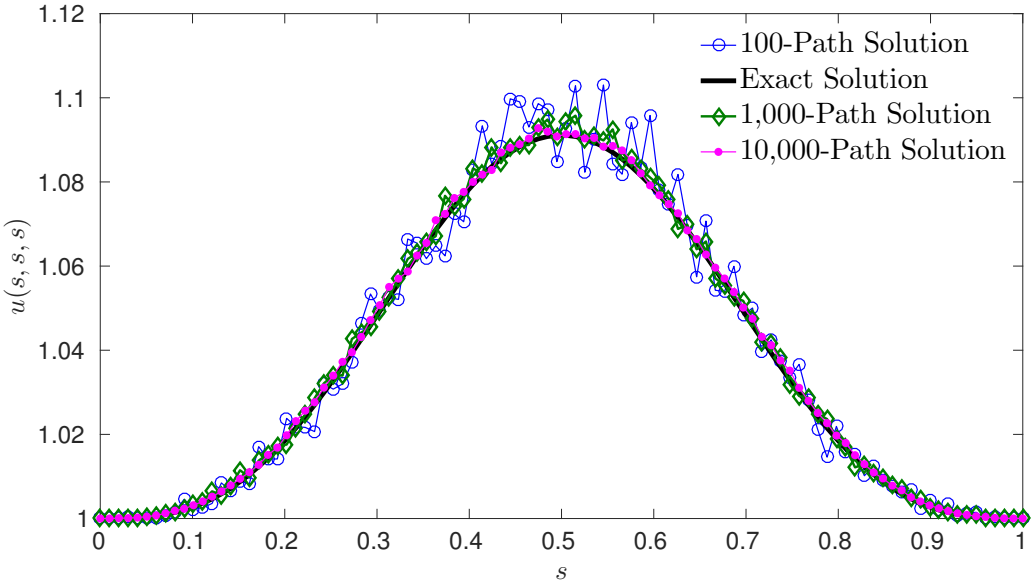

FIGURE 12. Stochastic solution of problem (3.91) in the 3D unit cube at 100 equispaced points along the line $D = \{(s,s,s) \mid s \in [0,1]\}$, using 100, 1,000, and 10,000 paths starting from each point.

3.10.4 16-Dimensional Benchmark Example (Unit Hypercube).

Finally, we demonstrate the utility of the stochastic solution formulas of this chapter in a 16-dimensional benchmark problem, where grid-based methods would not be feasible due to the curse of dimensionality. For the time-independent problem on the unit hypercube $Q \subset \mathbb{R}^{16}$ with $\alpha = \sqrt{3}$,

$$\begin{cases} (-\Delta_{Q,g})^{\alpha/2} u(\boldsymbol{x}) = (16\pi^2)^{\alpha/2} \prod_{i=1}^{16} \sin(\pi x_i) \\ u\big|_{\partial Q}(\boldsymbol{x}) = g(\boldsymbol{x}) \equiv 1 + \dfrac{1}{32} \sum_{i=1}^{16} x_i, \end{cases}$$

we show in Figure 13 the stochastic solutions computed on the diagonal $(s, s, ..., s)$ of the hypercube compared to the exact solution

$$u(\boldsymbol{x}) = 1 + \frac{1}{32} \sum_{i=1}^{16} x_i + \prod_{i=1}^{16} \sin(\pi x_i).$$

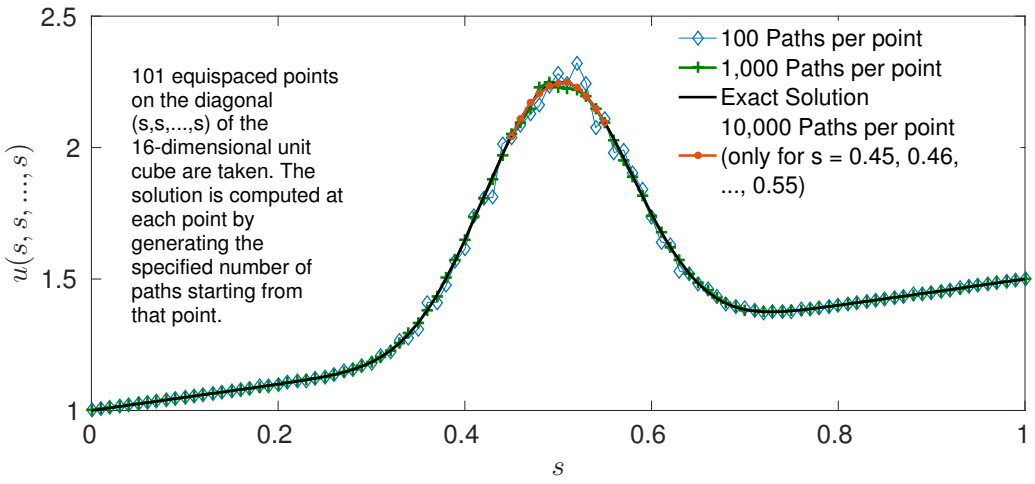

FIGURE 13. Stochastic solutions to the time-independent 16-dimensional benchmark problem on the diagonal of the unit hypercube.

The wall times were roughly 10 minutes for the 100-path solution, and 100 minutes for the 1,000-path solution using one core (i7-6700K processor). Then, 10,000 paths were used to refine the numerical solution near the peak ($s = 0.45, 0.46, ..., 0.55$), where the 1,000 path solution still had significant noise. The wall time to compute the solution at these 11 points using 10,000 paths was roughly 270 minutes.

For the time-dependent problem on the same unit hypercube $Q \subset \mathbb{R}^{16}$,

$$\begin{cases} \partial_t u(t, \boldsymbol{x}) + (-\Delta_{Q,g})^{\alpha/2} u(t, \boldsymbol{x}) = (16\pi^2)^{\alpha/2} \prod_{i=1}^{16} \sin(\pi x_i) \\ u\big|_{\partial Q}(t, \boldsymbol{x}) = g(\boldsymbol{x}) \equiv 1 + \dfrac{1}{32} \sum_{i=1}^{16} x_i \\ u(t = 0, \boldsymbol{x}) = 1 + \dfrac{1}{32} \sum_{i=1}^{16} x_i + \prod_{i=1}^{16} \sin(\pi x_i) + \prod_{i=1}^{16} \sin(2\pi x_i), \end{cases}$$

the same sample of paths may be used to compute the dynamics on the diagonal, and compared with the exact solution solution

$$u(t, \boldsymbol{x}) = 1 + \frac{1}{32} \sum_{i=1}^{16} x_i + \prod_{i=1}^{16} \sin(\pi x_i) + e^{-\left(16 \times 4\pi^2\right)^{\alpha/2} t} \prod_{i=1}^{16} \sin(2\pi x_i).$$

This is shown in Figure 14 for $0 \leq t \leq 0.03$.

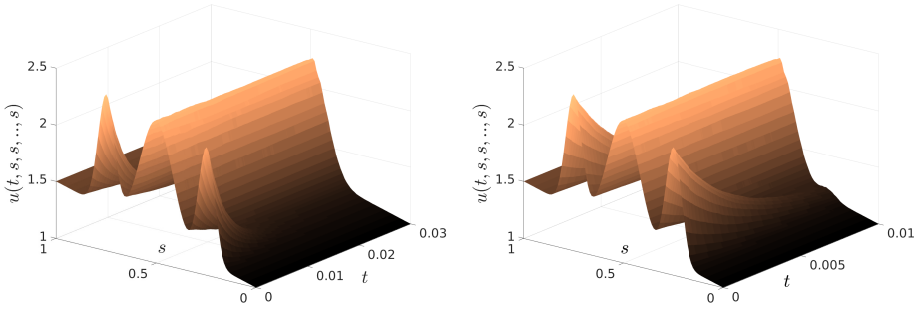

FIGURE 14. Stochastic solution $u(t, s, s, ..., s)$ to the time-dependent 16-dimensional problem on the diagonal of the unit hypercube in 16 dimensions, for $t \in [0, 0.03]$ (left) and zoomed in to $t \in [0, 0.01]$ (right), using 1000 paths for each point. Max abs. error on $(t, s) \in [0, 0.03] \times [0, 1] = 0.033$.

3.11 Chapter Conclusion

We have proven, implemented, and verified stochastic solution (Feynman-Kac) formulas for Cauchy and Dirichlet problems for the spectral fractional Laplacian $(-\Delta_{\Omega,g})^{\alpha/2}$ with nonzero Dirichlet boundary conditions. This operator was introduced recently in [11] and [55], and our work represents a novel probabilistic approach to this topic. The formulas, which involve subordinate stopped Brownian motion, were verified by considering a number of benchmark examples in two, three, and sixteen dimensions, and convergence with respect to the number of paths and time step parameter dt was studied. This work validates the proposed operator $(-\Delta_{\Omega,g})^{\alpha/2}$ from a stochastic perspective.

Stochastic solution formulas provide an attractive method to both understand fractional operators and compute solutions to associated boundary value problems. Such formulas for Neumann boundary value conditions, which involve boundary local time, are a worth exploring in this regard [36, 22, 136, 23]. Further numerical studies may explore Monte Carlo solution of boundary value problems in complex domains. The direct SDE discretization discussed in this chapter is an alternative to the work of [195], as implementation requires only an efficient subroutine to determine if the process is in the domain or not. Moreover, Monte Carlo methods based on such formulas can provide efficient solutions in high dimensions, a fertile area for applications. Walk-on-spheres [155, 225, 233, 232] and quasi-Monte Carlo [154] approaches may be explored to accelerate such solution methods.

CHAPTER 4

Fractional Path Integral Monte Carlo

4.1 Introduction

As discussed in Chapter 1, space- and time-fractional differential equations have emerged as the correct way to model many types of anomalous diffusion [**117, 149**], nonlocal phenomena [**133**], memory effects [**64**], and many non-equilibrium [**215**] and turbulent [**140, 179**] systems. Recall from Section 2.2.4 that anomalous diffusion is any diffusion in which the mean square displacement is not linear in time, i.e., $\langle X_t^2 \rangle \not\sim t$, and can include processes characterized by heavy tails, infinite variance, time-change by stochastic processes, and inhomogeneity in space and time. Diffusion is characterized by a space-time scaling relationship, such as

$$X_{ct} \sim c^{1/\alpha} X_t, \text{ where } \alpha > 0,$$

for time t and positive scaling factor c. When $\alpha = 2$, this scaling corresponds to Brownian motion, or *normal* diffusion. Otherwise, it describes two anomalous regimes: *subdiffusion* for $\alpha > 2$, and *superdiffusion* for $\alpha < 2$. One can think of superdiffusion for $1 < \alpha < 2$ as a regime between normal diffusion and ballistic motion, for which $\alpha = 1$.

An example of a physical system that may exhibit superdiffusion is a plasma (a fluid of charged particles) in which the particles favor ballistic motion in the presence of a magnetic field [**53, 215**]. Experimental evidence of anomalous diffusion [**227, 84**] in plasmas has prompted theoretical discussions on how the equations of magnetohydrodynamics can drive anomalous diffusion [**63, 53, 229**] and applications of CTRWs to plasma physics [**19**]. Anomalous diffusion has moreover been observed in percolation clusters [**110**], which has since been explained theoretically [**83**]. Inspired by this finding, the role of anomalous diffusion in disordered superconductors (and other disordered media) has also been elucidated [**34**].

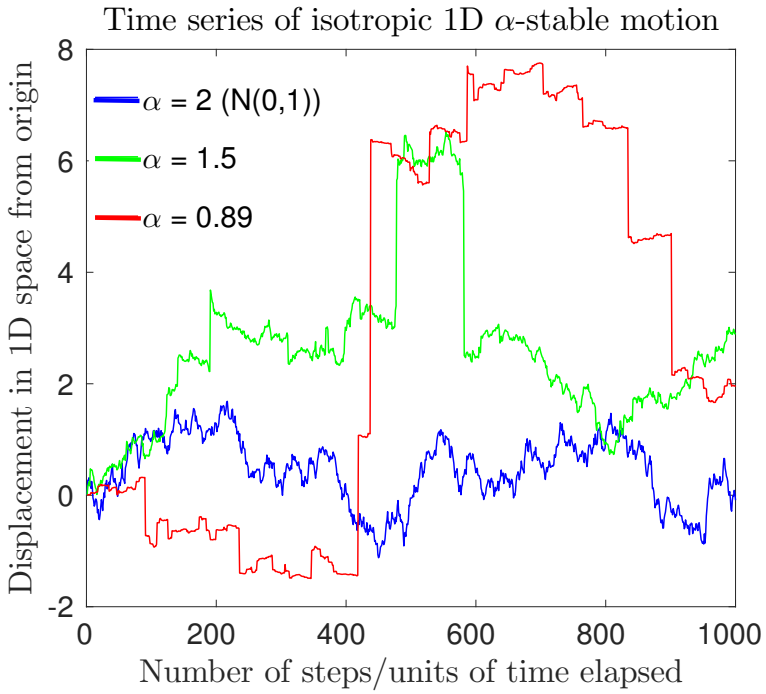

FIGURE 1. Time series illustrations (plots of displacement versus time) of an idealized particle undergoing superdiffusive, isotropic α-stable motion and comparison with the normal, $\alpha = 2$ case. The position parameter is set to 0 and the scale parameter to $1/\sqrt{2}$, giving a variance of 1 in the normal case $\alpha = 2$. For $0 < \alpha < 2$, the motion is discontinuous in time and has infinite variance; for $\alpha < 1$, the mean itself diverges.

Recently, a nonlinear fractional Schrödinger equation in $\mathbb{R}^d$ has been rigorously derived from a mathematical physics perspective as the continuum limit of a system of discrete nonlinear Schrödinger equations with increasingly long-range interactions [**116**]. Laskin [**128**, **129**, **130**, **131**] first developed fractional quantum mechanics, following the early considerations of Kac [**108**]. Starting from the Feynman path integral formulation of quantum mechanics, Laskin replaced integrals over Brownian paths with integrals over α-stable Lévy paths. He showed that this amounts to replacing the standard Laplacian by the (Riesz) fractional Laplacian in the Schrödinger

equation, leading to

$$i\hbar\frac{\partial\psi(\boldsymbol{r},t)}{\partial t} = D_\alpha(-\hbar^2\Delta)^{\alpha/2}\psi(\boldsymbol{r},t) + V(\boldsymbol{r})\psi(\boldsymbol{r},t), \tag{4.1}$$

with the Riesz fractional Laplacian defined by the momentum space representation

$$\mathcal{F}_\hbar\left[(-\hbar^2\Delta)^{\alpha/2}\psi\right] = |\boldsymbol{p}|^\alpha\,\mathcal{F}_\hbar\left[\psi\right],$$

where $\mathcal{F}_\hbar$ denotes the Fourier transform,

$$\mathcal{F}_\hbar\left[\psi\right] = \int_{\mathbb{R}^d} e^{-i\frac{\langle \boldsymbol{p},\boldsymbol{r}\rangle}{\hbar}}\psi(\boldsymbol{r},t)d\boldsymbol{r}.$$

This equation is called the space-fractional Schrödinger equation.

We distinguish the Riesz fractional Laplacian from other forms because, as discussed in great detail in Chapter 2 and [**137**], there are several ways to define the fractional Laplacian. Although the various notions of fractional Laplacian agree with each other in $\mathbb{R}^d$, they no longer agree on a bounded domain. The use of the Riesz fractional Laplacian $(-\Delta)^{\alpha/2}$, defined as the Fourier multiplier with symbol $|\boldsymbol{p}|^\alpha$, is required in all cases by the derivation of fractional quantum mechanics. See [**100**] for further discussion.

Laskin showed that Equation 4.1 enjoys many of the basic properties that allow the usual Schrödinger equation to serve as a foundation for quantum mechanics. For example, since $(-\Delta)^{\alpha/2}$ is self-adjoint, observables are real valued [**131**]. The fractional Schrödinger equation was subsequently derived by Kleinert by taking the scale-invariant limit of the wave equation in quantum field theory [**119, 118**].

To date, solutions to the fractional Schrödinger equation given by Equation (4.1) have been derived for a variety of analytically tractable Hamiltonians, including the delta potential [**56**], the fractional hydrogen atom [**129**], the fractional oscillator [**129**], and the fractional square well [**95, 62, 191, 74**]. More recently, it has been

suggested that fractional Hamiltonians may naturally arise from strong many body interactions, which prompted a mean field exploration of fractional Bose-Einstein condensation [**119**]. Nevertheless, no robust algorithm for examining the properties of the fractional Schrödinger equation for arbitrary potentials has yet been proposed, limiting the study of potentially rich fractional mathematics and physics.

In this chapter, we introduce a new fractional Path Integral Monte Carlo (PIMC) method capable of modeling the finite temperature physics of a wide variety of space-fractional Hamiltonians. The method computes finite temperature observables using the PIMC algorithm popularly employed to characterize boson and Boltzmannon phase diagrams [**41, 42, 166**] to sample the many body fractional partition function. Key to being able to use the PIMC algorithm in this context is being able to express *and sample* the free finite temperature fractional density matrix. Therefore, after establishing the theory in Sections 4.2.1–4.2.3, we derive several forms for the density matrix in Section 4.2.4, including a Hankel transform representation that allows for efficient computation through quadrature. Then, a sampling method based on a numerical inverse transformation is given in Section 4.2.5. How PIMC simulations based on the new fractional density matrix proceed is then briefly discussed in Sections 4.2.6 and 4.2.7.

Section 4.3 includes observations about the new methodology and the results of benchmark simulations. Interestingly, we find that the probability distribution function that represents the fractional density matrix manifests dramatically different asymptotic behaviors depending upon the fractional exponent present in the Hamiltonian. Whereas for fractional exponent $\alpha = 2$ the distribution reduces to the usual Gaussian case, for $\alpha < 2$, the distribution possesses heavy tails, and for $\alpha > 2$, the distribution becomes negative. Setting aside the $\alpha > 2$ case (this case is typically excluded in discussions of the fractional Laplacian because there is no α-stable process for $\alpha > 2$), in the remainder of section 4.3, we illustrate how our algorithm may be

used to compute finite temperature observables including energies and radii of gyration for two illustrative Hamiltonians: 1) the free particle Hamiltonian; and the ^{4}He Hamiltonian using the Aziz [14] potential. We end with a discussion of the general applicability of our method and the intriguing fractional physics it may reveal.

4.2 Theory and Algorithms

4.2.1 Overview of the Path Integral Monte Carlo Method

Since our method may be viewed as a generalization of the conventional PIMC algorithm, we begin this section with a review of PIMC. As described in significantly more detail by Ceperley [41], the finite temperature equilibrium expectation values of an observable, $\hat{O}$, in the position basis may be expressed as

$$\langle \hat{O} \rangle = Z^{-1} \int d\boldsymbol{R} d\boldsymbol{R}' \rho(\boldsymbol{R}, \boldsymbol{R}'; \beta) \langle \boldsymbol{R} | \hat{O} | \boldsymbol{R}' \rangle, \tag{4.2}$$

where Z denotes the system's partition function

$$Z = \int d\boldsymbol{R} \rho(\boldsymbol{R}, \boldsymbol{R}; \beta) \tag{4.3}$$

at inverse temperature $\beta = 1/(k_B T)$. In the above, $\boldsymbol{R} = \{\boldsymbol{r}_1, \boldsymbol{r}_2, ..., \boldsymbol{r}_N\}$ is the position vector of all N particles' coordinates, where $\boldsymbol{r}_i$ represents the position of the ith particle. One of the key quantities present in both Equations (4.2) and (4.3) is $\rho(\boldsymbol{R}, \boldsymbol{R}'; \beta)$, the finite temperature density matrix. In position space, the density matrix may be expanded into

$$\begin{aligned} \rho(\boldsymbol{R}, \boldsymbol{R}'; \beta) &= \langle \boldsymbol{R} | e^{-\beta \hat{H}} | \boldsymbol{R}' \rangle \\ &= \sum_i \psi_i^*(\boldsymbol{R}) \psi_i(\boldsymbol{R}') e^{-\beta E_i}, \end{aligned}$$

where $\hat{H}$ is the Hamiltonian that describes the system, and E_i and ψ_i respectively denote its eigenvalues (energies) and eigenfunctions (wave functions). Although obtaining an exact expression for the density matrix at an arbitrary temperature would require diagonalizing the many body Hamiltonian, a task generally beyond current computational capabilities, the density matrix may be simplified into more tractable expressions via Trotter factorization. In general, the convolution of two density matrices remains a density matrix such that

$$\rho(\boldsymbol{R}_1, \boldsymbol{R}_3; \beta_1 + \beta_2) = \int d\boldsymbol{R}_2 \; \rho(\boldsymbol{R}_1, \boldsymbol{R}_2; \beta_1)\rho(\boldsymbol{R}_2, \boldsymbol{R}_3; \beta_2), \tag{4.5}$$

which implies that the expression for the density matrix at inverse temperature, β, may be expressed as the convolution of M density matrices at inverse temperature $\tau = \beta/M$:

$$\rho(\boldsymbol{R}_0, \boldsymbol{R}_M; \beta) = \int ... \int d\boldsymbol{R}_1 d\boldsymbol{R}_2 ... d\boldsymbol{R}_{M-1} \; \rho(\boldsymbol{R}_0, \boldsymbol{R}_1; \tau) \\ \rho(\boldsymbol{R}_1, \boldsymbol{R}_2; \tau) ... \rho(\boldsymbol{R}_{M-1}, \boldsymbol{R}_M; \tau).$$

The $M + 1$ different N-particle position vectors represent the particle positions at $M+1$ different so-called "imaginary times." Because $\boldsymbol{R}_0$ is the same as $\boldsymbol{R}_M$ in the expression for the partition function, according to the quantum-classical isomorphism, the particles may be thought of as polymers constructed of M different beads linked together. If τ is sufficiently small, assuming the system Hamiltonian may be split into kinetic ($\hat{K}$) and potential pieces ($\hat{V}$), $\hat{H} = \hat{K} + \hat{V}$, the Suzuki-Trotter factorization [**211**, **111**] may be used to break up the exponential of the Hamiltonian into corresponding kinetic and potential exponentials

$$e^{-\tau\hat{H}} = e^{-\tau(\hat{K}+\hat{V})} \approx e^{-\tau\hat{K}} e^{-\tau\hat{V}}$$

such that the density matrices may also be broken into

$$\rho(\boldsymbol{R}_0, \boldsymbol{R}_2; \tau) \equiv \int d\boldsymbol{R}_1 \langle \boldsymbol{R}_0 | e^{-\tau \hat{K}} | \boldsymbol{R}_1 \rangle \langle \boldsymbol{R}_1 | e^{-\tau \hat{V}} | \boldsymbol{R}_2 \rangle.$$

Because potential operators are generally diagonal in the position representation, evaluating the position density matrix is trivial:

$$\langle \boldsymbol{R}_1 | e^{-\tau \hat{V}} | \boldsymbol{R}_2 \rangle = e^{-\tau \hat{V}(\boldsymbol{R}_1)} \delta(\boldsymbol{R}_2 - \boldsymbol{R}_1).$$

The evaluation of the kinetic density matrix is less trivial and requires finding the eigenvalues and eigenfunctions of $\hat{K}$. We assume periodic boundary conditions and the $\alpha = 2$, non-fractional form for the kinetic operator

$$\hat{K} = \frac{-\hbar^2}{2m} \nabla^2 = \lambda(-\Delta),$$

in which Δ denotes the Laplacian, ∇ denotes the gradient, and the constant $\lambda = \hbar^2/(2m)$. The eigenvalues of the three-dimensional kinetic operator are λK_n^2 and the eigenfunctions are $L^{-3N/2} e^{i \boldsymbol{K}_n \cdot \boldsymbol{R}}$, with $\boldsymbol{K}_n = 2\pi \boldsymbol{n}/L$ and $K_n = |\boldsymbol{K}_n|$. The kinetic density matrix may therefore be expressed as

$$\begin{aligned} \langle \boldsymbol{R}_0 | e^{-\tau \hat{K}} | \boldsymbol{R}_1 \rangle &= \sum_{\boldsymbol{n}} L^{-3N} e^{-\tau \lambda K_n^2 - i \boldsymbol{K}_n \cdot (\boldsymbol{R}_0 - \boldsymbol{R}_1)} \\ &= (4\pi\lambda\tau)^{-3N/2} e^{\frac{-|\boldsymbol{R}_0 - \boldsymbol{R}_1|^2}{4\lambda\tau}}. \end{aligned}$$

As discussed in more detail in Section 4.2.6, the finite temperature partition function may then be sampled via Monte Carlo. Foreshadowing the subsequent discussion, it should be noted that Equation (4.6), and the eigenvalues and eigenfunctions used to evaluate it, is only valid for the negative Laplacian $(-\Delta)$. If the differential operator is of a different power, the Suzuki-Trotter factorization is still valid (see Appendix

D), but new expressions for the density matrix are required. These expressions are derived and discussed below.

4.2.2 The Many-Body Fractional Schrödinger Equation

As first presented by Laskin [**128**, **129**, **130**, **131**], the fractional Schrödinger equation is a generalization of the Schrödinger equation in which the Hamiltonian is generalized to a fractional form, $\hat{H}_\alpha$, that contains a fractional Laplacian, $(-\Delta)^{\alpha/2}$. In one dimension, $\hat{H}_\alpha$, may be expressed as

$$\hat{H}_\alpha = D_\alpha(-\hbar^2\Delta)^{\alpha/2} + \hat{V}(\boldsymbol{r}). \tag{4.7}$$

In the above, $\hat{V}(\boldsymbol{r})$ denotes the potential and $D_\alpha = (1/2m)^{\alpha/2}$ denotes the constant that falls in front of the Laplacian. In general, D_α must have SI units of

$$[D_\alpha] = \frac{m^{2-\alpha}kg^{1-\alpha}}{s^{2-\alpha}}.$$

The fractional exponent, α, may in principle assume any positive value, including non-integer, fractional values, as its name implies [**128**, **129**, **130**, **131**]. For reference, the fractional Hamiltonian reduces to the conventional case when $\alpha = 2$.

A discussion of the fractional Schrodinger equation in the many-body case is required, as a choice must be made of the appropriate fractional operators. We have found very little discussion in the literature on this issue. The many-body kinetic Hamiltonian for N particles is classically given by

$$\hat{K} = -\sum_{i=1}^{N} \frac{\hbar^2}{2m_i}\Delta_i,$$

the sum of kinetic energies of each particle [**142**]. Here, m_i is the mass of the i-th particle, and Δ_i is the Laplacian in the $3i-2, 3i-1$, and $3i$ coordinates of a

$3N$-dimensional state space:

$$\Delta_i = \frac{\partial^2}{\partial r_{3i-2}^2} + \frac{\partial^2}{\partial r_{3i-1}^2} + \frac{\partial^2}{\partial r_{3i}^2}, \quad i = 1, 2, ..., N.$$

One choice for the $\alpha/2$-power of the many-body kinetic Hamiltonian is

$$\left(-\sum_{i=1}^{N} \frac{h^2}{2m_i} \Delta_i \right)^{\alpha/2},$$

which would result in a kinetic energy proportional to

$$(p_1^2 + ... + p_N^2)^{\alpha/2}.$$

However, this involves an unphysical nonlinear interaction among the individual fractional kinetic energies of the particles in the system. For this reason, we instead define the $\alpha/2$-fractional kinetic energy as

$$\begin{aligned} \hat{K}_\alpha &= \sum_{i=1}^{N} \left(-\frac{\hbar^2}{2m_i} \Delta_i \right)^{\alpha/2} \\ &= \sum_{i=1}^{N} D_{\alpha,i} (-\hbar^2 \Delta_i)^{\alpha/2}. \end{aligned} \tag{4.8}$$

This leads to a more physical, linear relation between the fractional kinetic energy and the momenta of the particles in the system

$$K_\alpha \propto p_1^\alpha + ... + p_N^\alpha.$$

Thus, in what follows, we will take the many-body fractional kinetic energy to always be given by Equation (4.8).

4.2.3 Spectrum of $(-\Delta)^\alpha$ with Periodic Boundary Conditions

In order to generalize PIMC to fractional Hamiltonians, expressions for the fractional density matrix amenable to sampling must be obtained. The standard boundary conditions used in condensed phase simulations are periodic boundary conditions, and the density matrix can be expressed in terms of the eigenvalues and eigenfunctions of the single-particle fractional Laplacian in a d-dimensional periodic domain. These eigenfunctions are tensor products of the one-dimensional periodic eigenfunctions

$$\begin{aligned}\psi_{\boldsymbol{k}}^{\mathrm{per},L}(\boldsymbol{r}) &= \sqrt{\frac{1}{L}}e^{-iC_{k_1}r_1} \times ... \times \sqrt{\frac{1}{L}}e^{-iC_{k_d}r_d} \\ &= \frac{1}{L^{n/2}}e^{-i\langle \boldsymbol{C},\boldsymbol{r}\rangle}.\end{aligned}$$

Here, $\boldsymbol{r} = (r_1, r_2, ..., r_d)$ denotes position in d-dimensional physical space, k_i denotes the wavenumber in each dimension, which can only take integer values (due to periodicity), $\boldsymbol{k} = (k_1, ..., k_d)$, and we have introduced the notation

$$C_{k_i} \;=\; \left(\frac{2\pi k_i}{L}\right),$$

such that

$$\boldsymbol{C} = \boldsymbol{C_k} = (C_{k_1}, ..., C_{k_d}).$$

The corresponding eigenvalue of $\psi_{\boldsymbol{k}}^{\mathrm{per},L}$ is

$$\begin{aligned}\lambda_{\boldsymbol{k}} &= -\left[\left(\frac{2\pi k_1}{L}\right)^2 + ... + \left(\frac{2\pi k_d}{L}\right)^2\right]^{\alpha/2} \\ &= -|C_{k_1}^2 + ... + C_{k_d}^2|^{\alpha/2} \\ &= -|\boldsymbol{C}|^\alpha.\end{aligned}$$

Inserting these expressions into Equation (4.7), the final Hamiltonian eigenvalues (energies) may be obtained:

$$\begin{aligned} D_\alpha \hbar^\alpha (-\Delta)^{\alpha/2} \psi_{\boldsymbol{k}}^{\mathrm{per},L}(\boldsymbol{r}) &= D_\alpha \hbar^\alpha |\boldsymbol{C}|^\alpha \frac{1}{L^{n/2}} e^{-i\langle \boldsymbol{C},\boldsymbol{r}\rangle} \\ &= E_{\boldsymbol{k}}^{\mathrm{per},L} \psi_{\boldsymbol{k}}^{\mathrm{per},L}(\boldsymbol{r}), \end{aligned}$$

where

$$\begin{aligned} E_{\boldsymbol{k}}^{\mathrm{per},L} &= D_\alpha \hbar^\alpha |\boldsymbol{C}|^\alpha \\ &= D_\alpha \hbar^\alpha \left[\left(\frac{2\pi k_1}{L} \right)^2 + ... + \left(\frac{2\pi k_d}{L} \right)^2 \right]^{\alpha/2}. \end{aligned}$$

4.2.4 Derivation of the Fractional Density Matrix

We begin with the single-particle case. Following Ceperley and Krauth [**41, 123**], the kinetic density matrix may be obtained along the same lines as in Equation (4.6) by summing over the Hamiltonian's eigenvalues and eigenfunctions

$$\begin{aligned} \rho^{\mathrm{per},L}(\boldsymbol{r},\boldsymbol{r'},\tau) &= \sum_{k_1=-\infty}^{\infty} ... \sum_{k_d=-\infty}^{\infty} \psi_{\boldsymbol{k}}^{\mathrm{per},L}(\boldsymbol{r}) e^{-\tau E_{\boldsymbol{k}}^{\mathrm{per},L}} \psi_{\boldsymbol{k}}^{*,\mathrm{per},L}(\boldsymbol{r'}) \\ &= \frac{1}{L^d} \sum_{k_1=-\infty}^{\infty} ... \sum_{k_d=-\infty}^{\infty} e^{-i\langle \boldsymbol{C},\boldsymbol{r}-\boldsymbol{r'}\rangle} e^{-\tau D_\alpha \hbar^\alpha |\boldsymbol{C}|^\alpha}. \end{aligned} \tag{4.11}$$

As usual, these sums may be turned into integrals by replacing the implied $1 = \Delta k_1 ... \Delta k_d$ in the summation with $\Delta k_1 ... \Delta k_d = \frac{\Delta C_1 L}{2\pi} ... \frac{\Delta C_d L}{2\pi}$, yielding

$$\begin{aligned}\rho^{\mathrm{per},L}(\boldsymbol{r},\boldsymbol{r'},\tau) &= \frac{1}{L^d} \sum_{C_1=...,-\frac{2\pi}{L},0,\frac{2\pi}{L},...} \cdots \sum_{C_d=...,-\frac{2\pi}{L},0,\frac{2\pi}{L},...} \\ &\qquad \left(\frac{\Delta C_1 L}{2\pi}\right) ... \left(\frac{\Delta C_d L}{2\pi}\right) e^{-i\langle \boldsymbol{C}, \boldsymbol{r}-\boldsymbol{r'}\rangle} e^{-\tau D_\alpha \hbar^\alpha |\boldsymbol{C}|^\alpha} \\ &= \frac{1}{(2\pi)^d} \sum_{C_1=...,-\frac{2\pi}{L},0,\frac{2\pi}{L},...} \cdots \sum_{C_d=...,-\frac{2\pi}{L},0,\frac{2\pi}{L},...} \\ &\qquad e^{-i\langle \boldsymbol{C}, \boldsymbol{r}-\boldsymbol{r'}\rangle} e^{-\tau D_\alpha \hbar^\alpha |\boldsymbol{C}|^\alpha} \Delta C_1 ... \Delta C_d\end{aligned} \tag{4.12}$$

and letting the box size, L, go to infinity

$$\rho^{\mathrm{per},L}(\boldsymbol{r},\boldsymbol{r'},\tau) = \frac{1}{(2\pi)^d} \int_{\mathbb{R}^d} e^{-i\langle \boldsymbol{C}, \boldsymbol{r}-\boldsymbol{r'}\rangle} e^{-\tau D_\alpha \hbar^\alpha |\boldsymbol{C}|^\alpha} d\boldsymbol{C}. \tag{4.13}$$

This integral is identical to the probability density function of an isotropic multivariate α-stable random variable in three dimensions with scale parameter $(\tau D_\alpha)^{1/\alpha}\hbar$ [**149**]. If $\alpha = 2$, this integral boils down to the usual Gaussian case in which completing the square yields the final line of Equation (4.6). For $\alpha \neq 2$, it is not possible to compute this integral in closed form. In one dimension, the integral may be expressed in terms of a Fox-Wright function [**165**] (see Appendix E for a full derivation), although we are not aware of an extension to the multivariate case.

Since it is necessary to evaluate Equation (4.13) using quadrature, it is important to note that it can be reduced to a one-dimensional integral known as the Hankel transform [**201**]. The following identity is valid for any radial function $f(\boldsymbol{C}) = f(|\boldsymbol{C}|)$:

$$\int_{\mathbb{R}^d} e^{-i\langle \boldsymbol{C}, \boldsymbol{r}\rangle} f(\boldsymbol{C}) d\boldsymbol{C} = (2\pi)^{\frac{d}{2}} |\boldsymbol{r}|^{-\frac{d-2}{2}} \int_0^\infty f(s) s^{\frac{d}{2}} J_{\frac{d-2}{2}}(|\boldsymbol{r}|s) ds.$$

Here J_ν is the Bessel function of first kind, and s a one-dimensional variable of integration. Applying this formula to the density matrix given by Equation (4.13), we obtain the representation

$$\rho^{\mathrm{per},L}(\boldsymbol{r},\boldsymbol{r'},\tau) = (2\pi)^{-\frac{d}{2}} |\boldsymbol{r}-\boldsymbol{r}|^{-\frac{d-2}{2}} \times \int_0^\infty e^{-\tau D_\alpha \hbar^\alpha s^\alpha} s^{\frac{d}{2}} J_{\frac{d-2}{2}}(|\boldsymbol{r}-\boldsymbol{r'}|s) ds. \tag{4.14}$$

This, rather than Equation (4.13), is the representation that will be used in computing the density matrix.

Next, we discuss the many-body fractional kinetic density matrix. The density matrix is then a function of $2d \times N$ coordinates $(\boldsymbol{r_1},...,\boldsymbol{r_N},\boldsymbol{r'_1},...,\boldsymbol{r'_N})$, where N is the number of particles. According to Equation (4.8), the eigenfunctions for the many-body kinetic energy operator are tensor products of the three-dimensional eigenfunctions

$$\Psi_{\boldsymbol{k_1},...,\boldsymbol{k_N}}(\boldsymbol{r}_1,...,\boldsymbol{r}_N) = \psi_{\boldsymbol{k_1}}(\boldsymbol{r_1})...\psi_{\boldsymbol{k}_N}(\boldsymbol{r}_N)$$

with eigenvalues

$$\Lambda_{\boldsymbol{k_1},...,\boldsymbol{k_N}} = \lambda_{\boldsymbol{k_1}} + ... + \lambda_{\boldsymbol{k_N}}.$$

The resulting kinetic energy of the system is

$$\begin{aligned} E^{\mathrm{per},L}_{\boldsymbol{k_1},...,\boldsymbol{k_N}} &= D_\alpha \hbar^\alpha (\lambda_{\boldsymbol{k_1}} + ... + \lambda_{\boldsymbol{k_N}}) \\ &= E^{\mathrm{per},L}_{\boldsymbol{k}_1} + ... + E^{\mathrm{per},L}_{\boldsymbol{k}_N}. \end{aligned}$$

Since

$$e^{-\tau E^{\mathrm{per},L}_{\boldsymbol{k_1},...,\boldsymbol{k_N}}} = e^{-\tau E^{\mathrm{per},L}_{\boldsymbol{k}_1}} ... e^{-\tau E^{\mathrm{per},L}_{\boldsymbol{k}_1}},$$

applying the same procedure as outlined by Equations (4.11), (4.12), and (4.13), and manipulating the sums results in the following factorization of the many-body density matrix

$$\rho^{\mathrm{per},L}(\boldsymbol{r}_1,...,\boldsymbol{r}_N,\boldsymbol{r'}_1,...,\boldsymbol{r'}_N,\tau) = \rho^{\mathrm{per},L}(\boldsymbol{r}_1,\boldsymbol{r'}_1,\tau)...\rho^{\mathrm{per},L}(\boldsymbol{r}_N,\boldsymbol{r'}_N,\tau), \tag{4.15}$$

where the single particle density $\rho^{\text{per},L}$ is given by Equation (4.14). This shows that the N particles are independent; more specifically, the pairs of variables $(\boldsymbol{r}_i, \boldsymbol{r}_i')$ are mutually independent and sampling the N-particle density matrix is reduced to sampling the single-particle density matrix. This aspect remains unchanged from standard PIMC methodology. Therefore, in the following, we need only develop a methodology to compute and sample (4.14).

4.2.5 Sampling the Fractional Density Matrix

From this point on, we consider only particles in three-dimensional physical space. Thus, we set $d = 3$ in Equations (4.13) and (4.14) and use the abbreviation ρ for the density matrix $\rho^{\text{per},L}$.

As can be seen from (4.14), the density matrix ρ depends only on $|\boldsymbol{r} - \boldsymbol{r}'|$. It is natural therefore to sample in spherical coordinates, which requires an appropriate transformation of the density function. Denote

$$\boldsymbol{v} = \boldsymbol{r} - \boldsymbol{r}' \text{ and } R = |\boldsymbol{v}|.$$

Consider the transformation from 3-dimensional rectangular coordinates $\boldsymbol{v}$ to standard spherical coordinates (R, ϕ, θ). The Jacobian of this map is $R^2 \sin\phi$, for $0 \leq \phi \leq \pi$. By the definition of the probability density function and following a change of variables,

$$\begin{aligned} P(\boldsymbol{v} \in A) &= \int_A \rho(|\boldsymbol{v}|) d\boldsymbol{v} \\ &= \int_A \rho(R) R^2 \sin(\phi) dR d\phi d\theta. \end{aligned} \tag{4.16}$$

Since we wish to sample the variables R, θ, and ϕ separately, we derive their individual probability density functions (PDFs) and cumulative density functions (CDFs) by considering different regions A in Equation (4.16).

First, let $A = \{\boldsymbol{v} : a \leq |\boldsymbol{v}| \leq b\}$ for fixed $a < b$. Then,

$$\begin{aligned} P(\boldsymbol{v} \in A) &= P(a \leq R \leq b) \\ &= \int_0^{2\pi} \int_0^{\pi} \int_a^b \rho(R) R^2 \sin(\phi) dR d\phi d\theta \\ &= 4\pi \int_a^b \rho(R) R^2 dR. \end{aligned}$$

Therefore, the PDF of the radial variable $R = |\boldsymbol{v}|$ is

$$\mathrm{PDF}_R = 4\pi R^2 \rho(R).$$

That is, we multiply $\rho(R)$ by the surface area of the sphere of radius R. The corresponding CDF may be computed by quadrature

$$\mathrm{CDF}_R(x) = 4\pi \int_0^x R^2 \rho(R) dR. \tag{4.17}$$

This integral cannot be computed (nor inverted) in closed form. Therefore, we discretize it by evaluating the density ρ using the quadrature described above, followed by another numerical quadrature for the outer integral.

To obtain the PDF_ϕ for ϕ, we write

$$\begin{aligned} P(a \leq \phi \leq b) &= \int_0^{\infty} \int_a^b \int_0^{2\pi} \rho(R) R^2 \sin(\phi) dR d\phi d\theta \\ &= \left(2\pi \int_0^{\infty} \rho(R) R^2 dR \right) \int_a^b \sin\phi d\phi. \\ &= \frac{1}{2} \int_a^b \sin\phi d\phi. \end{aligned} \tag{4.18}$$

The prefactor above is understood to be $1/2$ by noting that the integral of the density, as in Equation (4.16), over all space must equal 1:

$$\begin{aligned} 1 &= \int_0^{\infty}\int_0^{\pi}\int_0^{2\pi} \rho(R)R^2\sin(\phi)dRd\phi d\theta \\ &= \left(2\pi\int_0^{\infty}\rho(R)R^2dR\right)\int_0^{\pi}\sin(\phi)d\phi \\ &= 2\left(2\pi\int_0^{\infty}\rho(R)R^2dR\right) \end{aligned}$$

An alternative way to express Equation (4.18) is

$$\mathrm{PDF}_{\phi} = \frac{1}{2}\sin(\phi).$$

Then, CDF_{ϕ} can be directly computed as

$$y = \mathrm{CDF}_{\phi}(x) = -\frac{1}{2}\cos(\phi)|_0^x = \frac{1}{2}\left(1-\cos(x)\right),$$

and inverted analytically to yield

$$\mathrm{CDF}_{\phi}^{-1}(y) = \arccos\left(1-2y\right).$$

Finally, it is seen from Equation (4.16) that the PDF for θ is constant, so θ is uniformly distributed in $[0, 2\pi]$. Denoting by $\mathcal{U}[a, b]$ the uniform random variable in $[a, b]$, the sampling algorithm may be summarized as:

(1) Sample $\theta \sim \mathcal{U}[0, 2\pi]$.

(2) Sample $\phi \sim \arccos(1 - 2 \times \mathcal{U}[0, 1])$.

(3) Sample r according to $\mathrm{PDF}_R{=}4\pi R^2\rho(R)$, where ρ is given by Equation (4.14), $R = |\boldsymbol{v}|$, and

$$\sigma = (\hbar^{\alpha} D_{\alpha}\tau)^{1/\alpha}$$

is temporarily assumed to equal 1 for now. This can be accomplished via one-dimensional inverse transform sampling after the CDF in R (4.17) is discretized; see below.

(4) Transform the sample (R, ϕ, θ) in spherical coordinates obtained from the first three steps to a sample of $\boldsymbol{v} = \boldsymbol{r} - \boldsymbol{r'}$ in rectangular coordinates using

$$\boldsymbol{v} = (R\sin(\phi)\cos(\theta), R\sin(\phi)\sin(\theta), R\cos(\phi)).$$

(5) Multiply $\boldsymbol{v}$ by σ to rescale.

The only technical detail that remains to implement this strategy is the computation of Equation (4.14), which is required to discretize CDF (4.17) in R. The advantage of this Hankel representation formula is that it requires a one-dimensional, radial quadrature. For that formula, we note that in dimension $d = 3$, the Bessel $J_{\frac{d-2}{2}}$ reduces to

$$J_{\frac{1}{2}}(t) = \sqrt{\frac{2}{\pi t}}\sin(|t|).$$

Roughly speaking, the integrand is an exponentially damped oscillatory function, with $|\boldsymbol{r} - \boldsymbol{r'}|$ being the frequency, α controlling the power of the exponential factor, and the prefactor $-\tau D_\alpha \hbar^\alpha$ scaling the argument of the exponential. An illustration of the various regimes in $|\boldsymbol{r} - \boldsymbol{r'}|$ is given in Figure 2.

Based on this analysis of the integrand, the numerical procedure we use to evaluate Equation (4.14) is as follows. A tolerance of 10^{-8} is specified and the integration is truncated to a region where the exponential factor in the integrand is greater than this tolerance. On the integration range, the integral is divided into integrals between each root of the Bessel function; i.e., each of the positive and negative contributions are integrated individually. Finally, for each such positive/negative "bump", the integration is again divided into intervals of length < 1, and 10-point Gauss-Legendre

quadrature is performed on each interval. The subdivision into intervals of length < 1 ensures an accurate evaluation in the first case ($|\boldsymbol{r} - \boldsymbol{r'}| << 1$) described in Figure 2.

We note such a procedure will take longer to evaluate in the highly oscillatory case ($|\boldsymbol{r} - \boldsymbol{r'}| >> 1$), due to the larger number of bumps, despite the final answer being very small. Stationary phase analysis and quadrature based on asymptotic expansions may leverage the highly oscillatory nature of the integrand to speed (rather than slow down) computations. It was not necessarily to do so in this work, although this may be explored in future implementations.

In summary, the efficient Hankel transform representation (4.14) is used to compute the fractional density matrix, which is then sampled using numerical inverse transform sampling in spherical coordinates. Plots of the fractional density matrix are analyzed in section 4.3.1. Alternate methods for sampling may involve the use of subordinators and the use of the Chambers-Mallows-Stuck method, which is an exact sampling method for the one-dimensional stable random variable [**43**]. However, we have based the entire discussion of computation and sampling around the Hankel transform (4.14) for brevity.

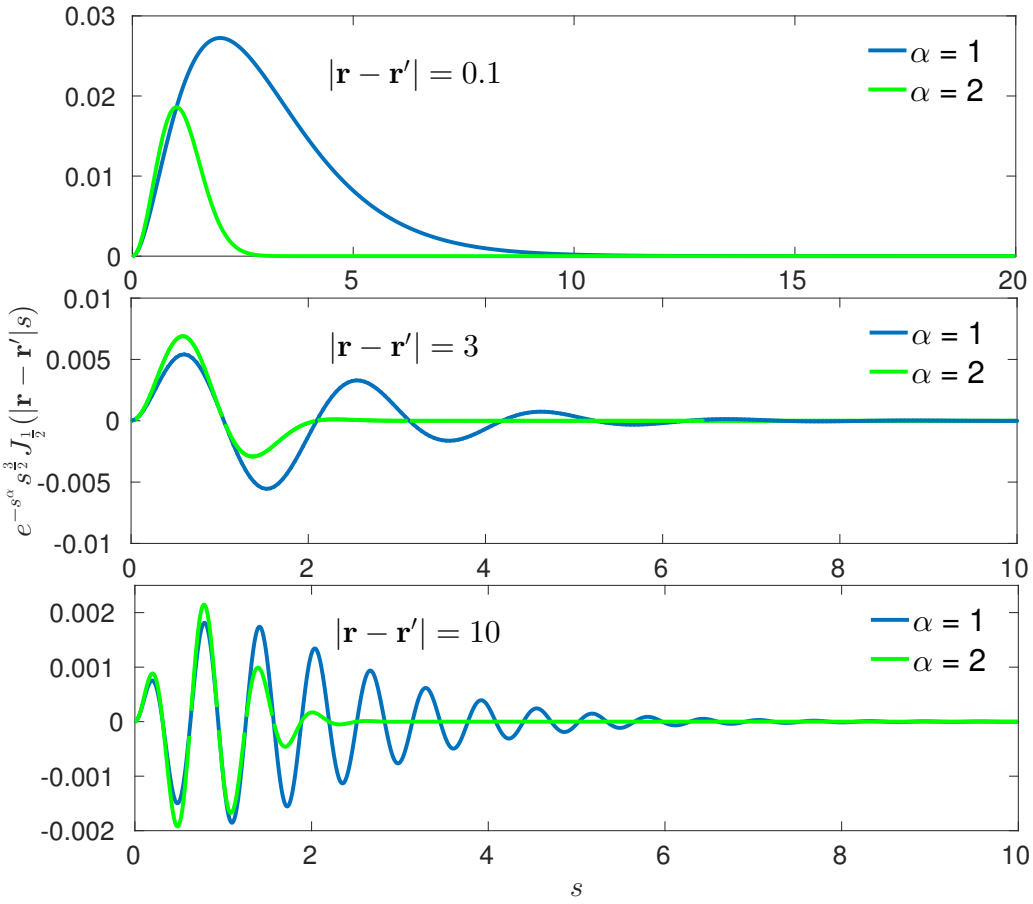

FIGURE 2. Three different regimes of the integrand in Equation (4.14). The scaling constant $-\tau D_\alpha \hbar^\alpha$ is fixed to be unity. (**Top**) For $|\boldsymbol{r} - \boldsymbol{r'}| << 1$, the frequency is so low that the integrand is a smooth bump. (**Middle**) For $|\boldsymbol{r} - \boldsymbol{r'}| \approx O(1)$, the integrand is a damped wave. In this case, a few oscillations in the integrand are present despite the exponential factor. However, the integrand is not highly oscillatory, so the integral is not expected to be very small. (**Bottom**) For $|\boldsymbol{r} - \boldsymbol{r'}| >> 1$, the integrand is a highly oscillatory damped wave, and the integral can be expected to be very small due to cancellation.

4.2.6 Performing PIMC Moves Using the Fractional Density Matrix

As described in greater detail elsewhere [28], in Path Integral Monte Carlo, a random walk is performed through the space of N-particle paths at the M different time slices, $\{\boldsymbol{R}_1, \boldsymbol{R}_2, ..., \boldsymbol{R}_M\}$. A random walk may be constructed by randomly displacing the positions of the different beads within the particles. While many different move possibilities exist, one of the simplest moves is to displace a subset of the beads in the M-bead path of a given particle. Let the portion of a particle i's path to be updated be denoted by $\boldsymbol{r}_{i,k+1}...\boldsymbol{r}_{i,k+s-1}$, where s is the number of beads in the path to be displaced and $\boldsymbol{r}_{i,k}$ and $\boldsymbol{r}_{i,k+s}$ are held fixed. Let $\boldsymbol{X} = \{\boldsymbol{R}_0, \boldsymbol{R}_1, ..., \boldsymbol{R}_M\}$ denote the old set of particle bead coordinates and let $\boldsymbol{X}' = \{\boldsymbol{R}_0, ...\boldsymbol{R}_k, \boldsymbol{R}'_{k+1}...\boldsymbol{R}'_{k+s-1}, \boldsymbol{R}_{k+s}, ..., \boldsymbol{R}_M\}$ denote the updated (new) set of particle bead coordinates. Then, based upon Equation (4.3), the probability, P, that this displacement will be accepted from sampling the partition function is

$$\begin{aligned} P &= \frac{\prod_{j=0}^{s-1} \rho(\boldsymbol{R}'_{k+j}, \boldsymbol{R}'_{k+j+1}, \tau)}{\prod_{j=0}^{s-1} \rho(\boldsymbol{R}_{k+j}, \boldsymbol{R}_{k+j+1}, \tau)} \\ &\quad \times \frac{e^{-\Delta \sum_{j=1}^{s-1} V(\boldsymbol{R}'_{k+j})}}{e^{-\Delta \sum_{j=1}^{s-1} V(\boldsymbol{R}_{k+j})}} \frac{T(\boldsymbol{X}' \rightarrow \boldsymbol{X})}{T(\boldsymbol{X} \rightarrow \boldsymbol{X}')}. \end{aligned}$$

Here, $T(\boldsymbol{X}' \rightarrow \boldsymbol{X})$ represents the transition probability, which can be selected with great freedom. The most convenient choice for the transition probability is to set it equal to the product of the kinetic density matrices, so that it can be evaluated using the expressions derived above and can cancel out other contributions to P. If this choice is made,

$$T(\boldsymbol{X} \rightarrow \boldsymbol{X}^{'}) = \prod_{j=0}^{s-1} \rho(\boldsymbol{R}'_{k+j}, \boldsymbol{R}'_{k+j+1}, \tau),$$

and Equation (4.19) reduces to

$$P = e^{-\tau \sum_{j=1}^{s-1} (V(\boldsymbol{R}^{'}_{k+j}) - V(\boldsymbol{R}_{k+j}))}.$$

These equations imply that, in a practical PIMC simulation, coordinates should first be sampled from the product of the kinetic density matrices (the length of that product depends upon the number of beads to be moved) and then the move should be accepted/rejected based upon the ratio of the potential energy in the new configuration to the potential energy in the old configuration. There are many ways to sample the transition probability and construct multiple bead moves [**199**, **41**, **61**]. One of the most common ways to propose multi-bead moves in the $\alpha = 2$ case is to use the staging algorithm [**199**], which samples a hierarchy of position moves based upon the fact that a product of Gaussians is a Gaussian. Because the single-particle fractional kinetic density matrix, given by Equation (4.14), is not Gaussian for $\alpha < 2$ and cannot be neatly broken into a product of fractional density matrices of the same form, the staging algorithm cannot be straightforwardly adapted to this formalism. For the purpose of this work, we therefore use single-bead and center of mass moves, despite the ergodicity problems single-bead moves may cause at low temperatures, particularly for strong interactions. For center of mass moves, all beads in each particle are moved at once, as usual. For single-bead moves, a bead on a particle is randomly selected. New unscaled x', y', and z' coordinates are then independently sampled as described in Section 4.2.4 by sampling (r, θ, ϕ) coordinates, transforming

them back to Cartesian, and rescaling them by

$$\sigma^{\alpha} = \frac{\hbar \tau^{1/\alpha}}{2^{1/\alpha} m^{1/\alpha}}$$

to yield coordinates of the correct dimensions. The resulting potential energy from this move is lastly determined and used to accept/reject the proposed move.

4.2.7 Computing Observables in Fractional PIMC

The fundamental purpose of performing PIMC simulations in most cases is to obtain measures of different systems' finite temperature observables, such as their energies, radial distribution functions, and radii of gyration. Because such observables as the potential energy and radial distribution functions are diagonal in the position representation and therefore do not directly depend upon the fractional exponent, they can be measured as in the $\alpha = 2$ case.

Computing quantities based upon derivatives of the partition function, such as the kinetic energy, is less straightforward. The thermodynamic estimator of the kinetic energy per link i connecting beads i and $i-1$ may be expressed as [41]

$$\langle \hat{K} \rangle_{\text{link}} = \left\langle \frac{m}{\tau \rho(\tau)} \frac{\partial \rho(\tau)}{\partial m} \right\rangle_{\text{link}} = \left\langle \frac{m}{\tau} \frac{\partial \ln \rho(\tau)}{\partial m} \right\rangle_{\text{link}}, \tag{4.20}$$

in the free particle case where ρ_i denotes the short-time density matrix at link, i, and $\langle \rangle_{\text{link}}$ denotes an ensemble average over all links i. In the $\alpha = 2$ case, the free Gaussian density matrix can be differentiated analytically to yield

$$\langle \hat{K} \rangle_{\text{link}} = \frac{3N}{2\tau} - \frac{m \langle |\boldsymbol{r} - \boldsymbol{r}'|^2 \rangle_{\text{link}}}{2\tau^2 \hbar^2}, \quad \alpha = 2.$$

As ρ itself does not have a closed form expression for $\alpha < 2$, derivatives with respect to m cannot be computed analytically. One alternative is to pass the differential operator through the integral in Equation (4.14), leading to a new integrand which

can be treated with quadrature. However, the most convenient option is to evaluate either of the derivatives within Equation (4.20) using a difference formula in m. We use a four-point forward difference formula with $h = 10^{-3}$:

$$\frac{\partial \rho}{\partial m}(m_0) = \frac{1}{h}\left(\frac{-11}{6}\rho(m_0) + 3\rho(m_0 + h) - \frac{3}{2}\rho(m_0 + 2h) + \frac{1}{3}\rho(m_0 + 3h)\right). \tag{4.22}$$

The behavior of the unaveraged quantity $\frac{m}{\tau\rho_i(\tau)}\frac{\partial \rho_i(\tau)}{\partial m}$ is studied in 4.3.2.

4.3 Results and Discussion

4.3.1 Fractional Density Matrix Distributions

In this section, we compute the density to analyze its behavior and to verify the accuracy of our sampling technique. For all of the figures in this section, ρ denotes the density matrix with $\tau = D_\alpha = \hbar = 1$. The density matrix for nonunitary constants may be rescaled by a change of variables in (4.13) to this case. In Figure 3, we illustrate the overall behavior of the probability density function that represents the unidimensional fractional density matrix, ρ. The density exhibits "heavy" inverse power-law tails for fractional order $\alpha < 2$. Compared to the normal case, the fractional cases exhibit a larger probability of both small and large jumps, and a lower probability for medium jumps. In Figure 4, we look more closely at the tail behavior. As α decreases, the related probability density functions exhibit heavier and heavier tails.

In Figures 3 and 4, we have also plotted the density ρ for $\alpha = 2.25$ as a curiosity. Of course, α-stable distributions are only defined for $0 < \alpha \leq 2$; this illustration shows that for $\alpha > 2$, ρ takes negative values and is therefore not a density at all. In particular, it should be noted that while $\alpha < 2$ corresponds to superduffision, $\alpha > 2$

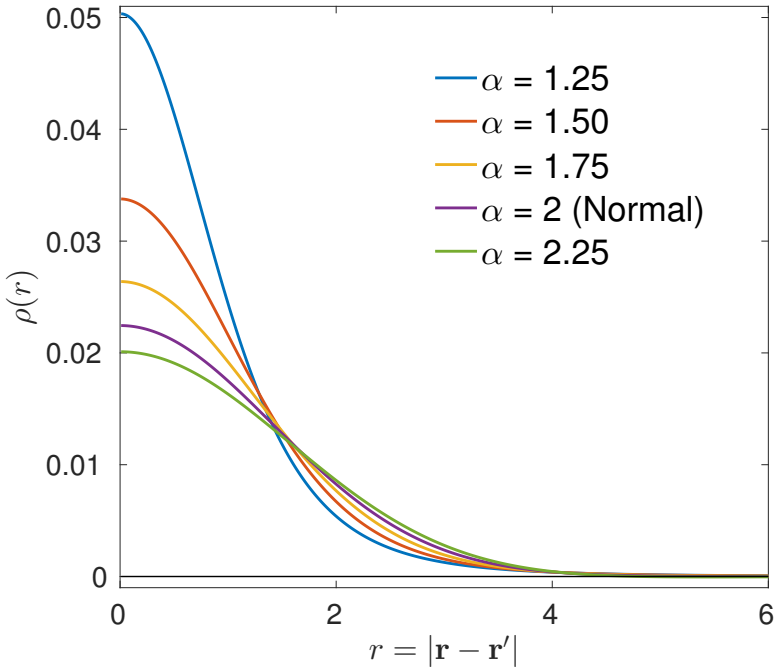

FIGURE 3. Illustration of the fractional density matrix distribution as a function of the scalar interbead distance, $|\boldsymbol{r}-\boldsymbol{r}'|$, for different α.

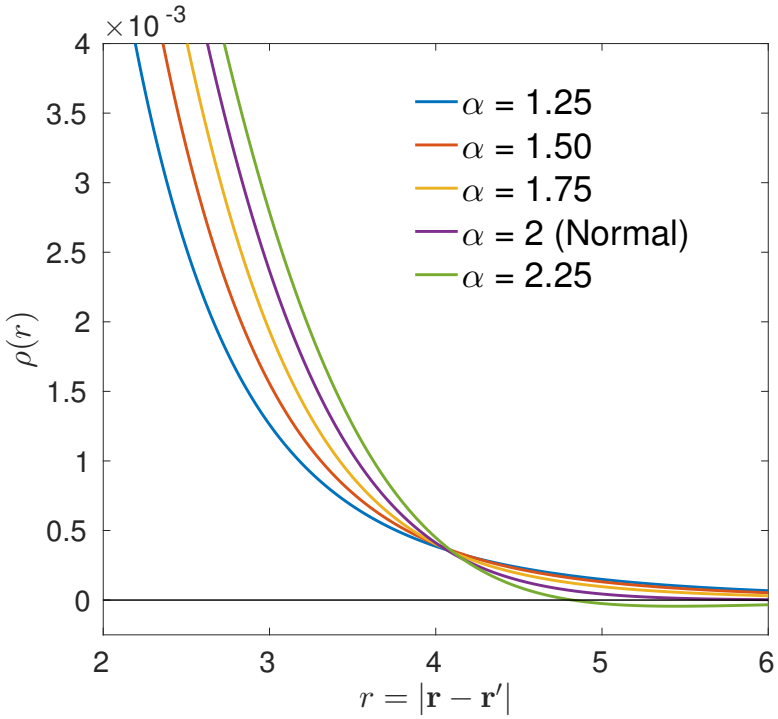

FIGURE 4. Illustration of the tail behavior of the fractional density matrix with the scalar interbead distance, $|\boldsymbol{r} - \boldsymbol{r}'|$, for different α. Heavier tails are visible for fractional α. The case $\alpha = 2.25$, which becomes negative, clearly cannot be a probability density function. This issue occurs for all $\alpha > 2$, in which case ρ has no meaning as a probability density function.

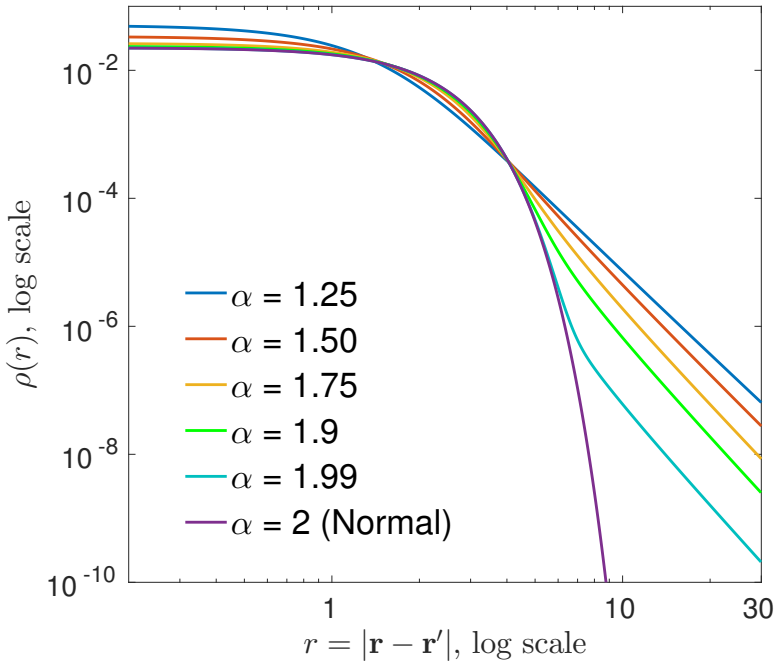

FIGURE 5. Illustration, in log-log scale, of the fractional density matrix distribution as a function of the scalar interbead distance, $|\boldsymbol{r} - \boldsymbol{r}'|$, for different α. In this scale, it becomes clear that ρ quickly enters into a power-law regime for fractional α.

does not correspond to subdiffusion. In Figure 5, we plot the same densities on a log-log scale to better understand their tail behavior. We see that for $\alpha < 2$, as $|\boldsymbol{r} - \boldsymbol{r}'|$ increases, the density in log-log scale exhibits linear behavior, implying that the density itself enters a power-law regime. This happens fairly early, for $|\boldsymbol{r} - \boldsymbol{r}'| \sim 10$, even for $\alpha = 1.99$.

4.3.2 Fractional Kinetic Energy

Using the forward difference scheme described in 4.2.7, we analyze the form of the kinetic energy as a function of the interbead distance squared for a range of α's. Interestingly, whereas the kinetic energy decreases linearly with interbead distance for $\alpha = 2$, for certain $\alpha < 2$ it first decreases, then increases, and finally plateaus, as depicted in Figure 6. Similar functional forms are observed for varying τ in Figure 7.

The plateaus observed in the kinetic energy may be understood by writing

$$\begin{aligned}\rho^{\mathrm{per},L}(\boldsymbol{r}-\boldsymbol{r'},\beta) &= \frac{1}{(2\pi)^d}\int_{\mathbb{R}^d} e^{-i\langle \boldsymbol{C},\boldsymbol{r}-\boldsymbol{r'}\rangle} e^{-\tau D_\alpha \hbar^\alpha |\boldsymbol{C}|^\alpha} d\boldsymbol{C} \\ &= \frac{1}{(2\pi)^d}\frac{1}{(\tau D_\alpha \hbar^\alpha)^{d/\alpha}}\int_{\mathbb{R}^d} e^{i\left\langle \boldsymbol{C},\left[(\tau D_\alpha \hbar^\alpha)^{1/\alpha}(\boldsymbol{r}-\boldsymbol{r'})\right]\right\rangle} e^{-|\boldsymbol{C}|^\alpha} d\boldsymbol{C} \\ &= \frac{1}{(\tau D_\alpha \hbar^\alpha)^{d/\alpha}}\rho^{\mathrm{per},L}\left((\beta D_\alpha \hbar^\alpha)^{1/\alpha}(\boldsymbol{r}-\boldsymbol{r'}), \tau = D_\alpha = \hbar = 1\right).\end{aligned}$$

and noting the power-law tail behavior of the fractional density matrix visible from Figure 5. Based upon this power-law behavior, we can write, for large $|\boldsymbol{r}-\boldsymbol{r}'|$,

$$\begin{aligned}\rho^{\mathrm{per},L}(\boldsymbol{r}-\boldsymbol{r'},\tau) &\sim \frac{1}{(\tau D_\alpha \hbar^\alpha)^{d/\alpha}}\left[(\tau D_\alpha \hbar^\alpha)^{1/\alpha}|\boldsymbol{r}-\boldsymbol{r}'|\right]^{-P} \\ &\sim \frac{1}{m^{d/2}}\left[m^{1/2}|\boldsymbol{r}-\boldsymbol{r}'|\right]^{-P} \\ &= m^{\frac{-P-d}{2}}|\boldsymbol{r}-\boldsymbol{r}'|^{-P}.\end{aligned}$$

In the first equality, we used $D_\alpha = \left(\frac{1}{2m}\right)^{\alpha/2}$. Thus,

$$\frac{m}{\tau\rho}\frac{\partial \rho}{\partial m} \sim \frac{m}{m^{\frac{-P-d}{2}}} \times m^{\frac{-P-d}{2}-1} \sim 1.$$

In other words, the above quantity is constant for large $|\boldsymbol{r}-\boldsymbol{r'}|$.

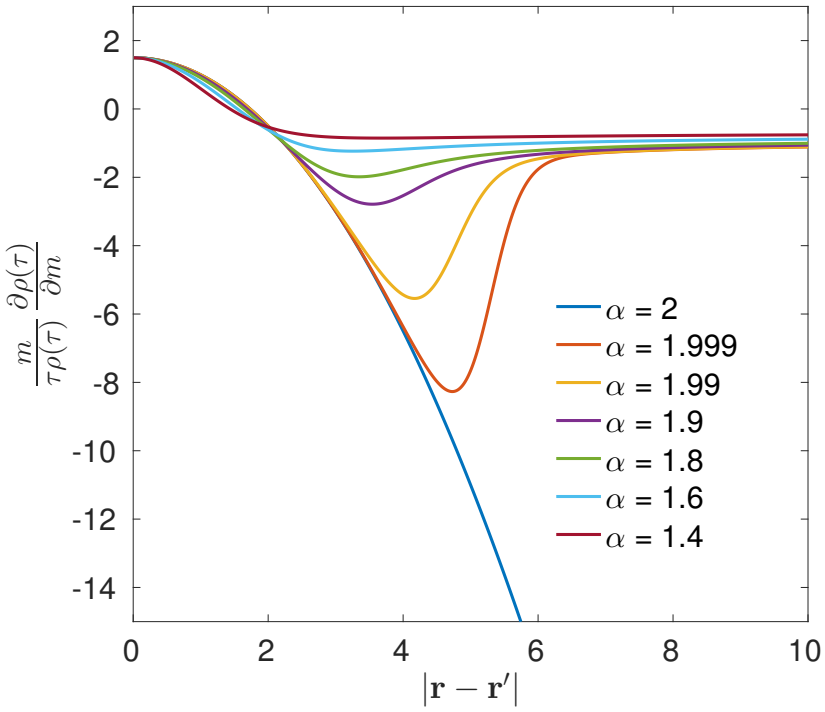

FIGURE 6. Comparison of the single link kinetic energy (the unaveraged quantity in the formula (4.20) for kinetic energy) as a function of the interbead distance for different α. The parameters $\tau, D_\alpha, \hbar$ are set to 1 for illustration.

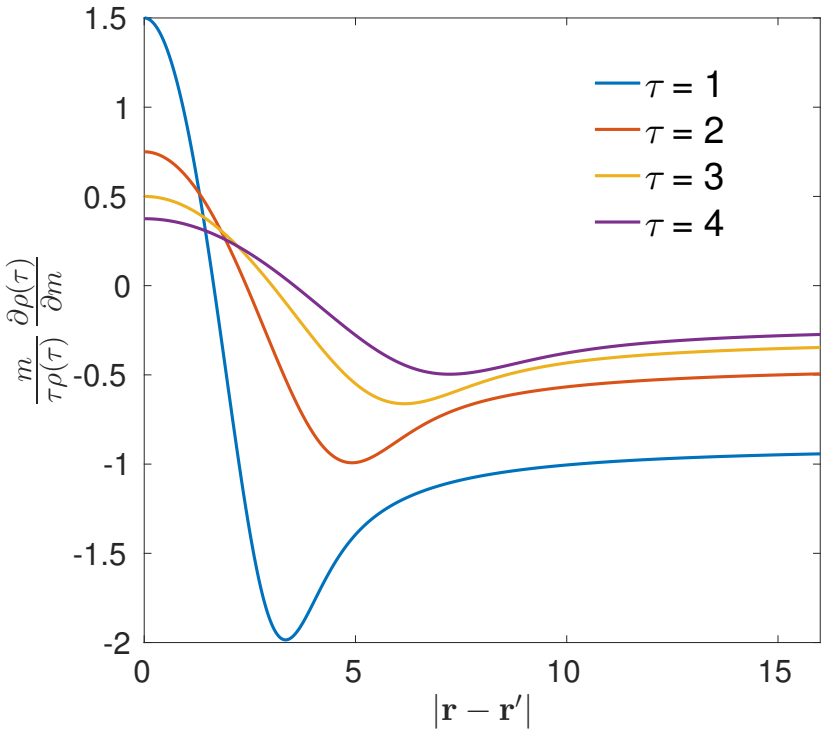

FIGURE 7. Comparison of the single link kinetic energy (the unaveraged quantity in the formula (4.20) for kinetic energy) as a function of the interbead distance for different τ, using a fixed $\alpha = 1.8$. The parameters $D_\alpha, \hbar$ are set to 1 for illustration.

As may be expected on a conceptual basis and is confirmed in the above plots, the average interbead distance for which the kinetic energy reaches its minimum shifts to larger values with decreasing α and increasing τ. This is because smaller values of α imply more diffuse paths, while larger τ correspond to lower temperatures and therefore larger de Broglie wave lengths. The presence of a minimum in the kinetic energy is a strictly fractional feature which appears for a range of α infinitesimally smaller than two and suggests that fractional particles may exhibit intriguing behavior as they attempt to minimize their potential and kinetic energies – which have competing minima – at once.

4.3.3 Fractional Free Particle PIMC Results

We first demonstrate our algorithm by simulating the free-particle Hamiltonian. Our interest in the free-particle Hamiltonian stems from the fact that it is amenable to analytic solutions and free-particle PIMC serves as the bedrock for interacting simulations. As such, if our algorithm is to be useful in simulation, it must first be demonstrated to work for the free particle Hamiltonian. More specifically, we consider the Hamiltonian

$$\hat{H}_{\text{free},\alpha} = \frac{-\hbar^\alpha}{(2m)^{\alpha/2}}\nabla^\alpha = \hbar^\alpha D_\alpha(-\Delta)^{\alpha/2}.$$

In order to make direct comparisons with our helium results presented in the next section, we set our mass equal to that of helium. In both sections, we moreover simulate a two particle system for simplicity at a density of $\rho = .00323$ bohr^{-3} at all of the temperatures and α values presented. Atomic units are employed in all of the following results.

As a qualitative check on our simulations and underlying theory, we first consider the conformations of the polymers representing our particles. One of the principle

motivations for this work was the fact that a fractional Laplacian for $\alpha < 2$ should lead to significantly more diffuse particles than in the typical $\alpha = 2$ case. Figure 8 demonstrates that this is indeed the case: as α decreases, the average square of the interbead distance, $\langle(\boldsymbol{R}_i - \boldsymbol{R}_{i+1})^2\rangle$, for fixed β and number of beads steadily increases. As may be expected, this increase is most dramatic at the low temperatures at which, in the absence of a potential, increased delocalization should be favored. Similar trends may be observed in the average square of the interbead distance as a function of temperature, as depicted in Figure 9, and the particles' average radii of gyration, $R_G = \langle(\boldsymbol{R}_i - \boldsymbol{R}_{cm})^2\rangle$, as depicted in Figure 10. Example paths illustrating these features for varying temperatures and fractional exponents are depicted in Figure 11.

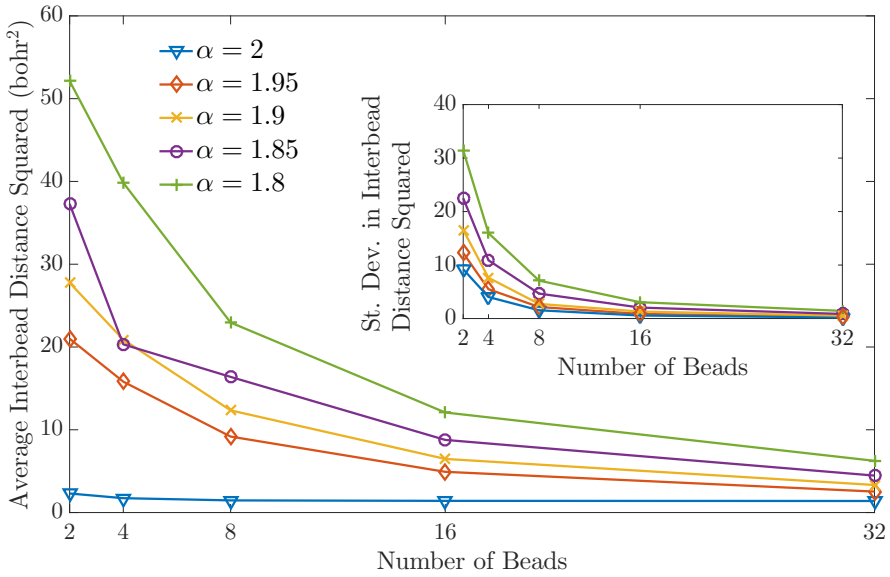

FIGURE 8. The average interbead distance squared as a function of the number of beads at temperature 2 K for free particles. The interbead distance steadily increases for the same number of beads as α decreases. *Inset:* Standard deviation of the same quantity.

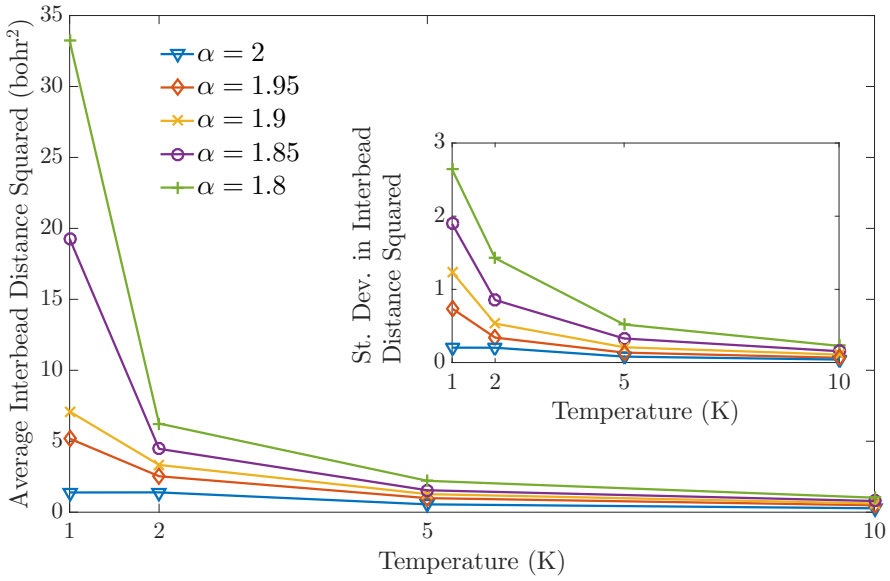

FIGURE 9. The average interbead distance squared a function of temperature for free particles (32 beads). The interbead distance steadily increases as α decreases. *Inset:* Standard deviation of the same quantity.

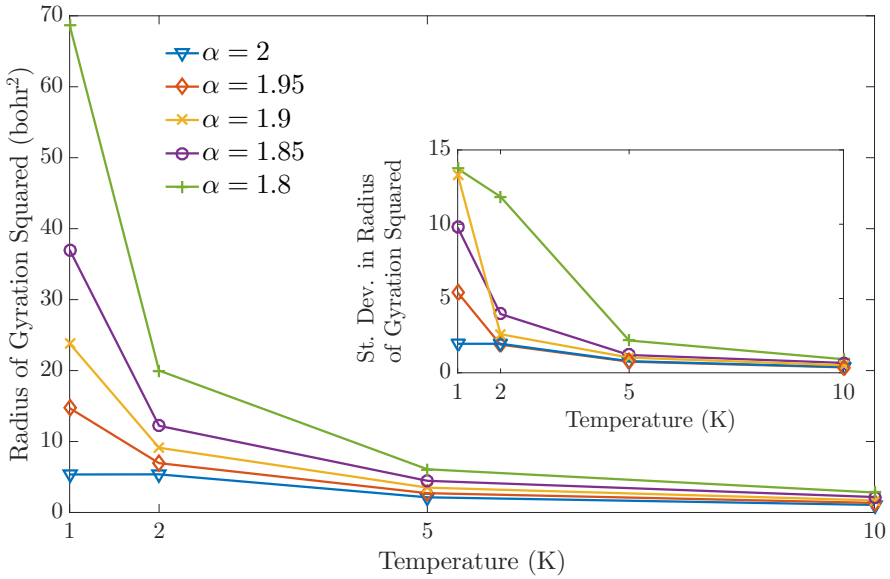

FIGURE 10. The average radius of gyration squared as a function of the temperature for free particles (32 beads). The radius of gyration also steadily increases as α decreases. *Inset:* Standard deviation of the same quantity.

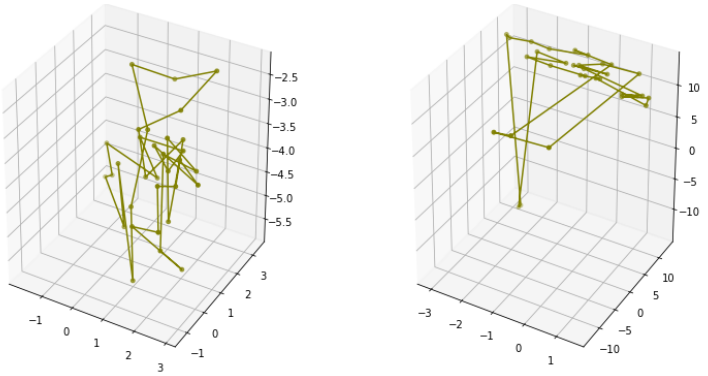

(A) $\alpha = 2$, radius of gyration 1.86 (left) and 9.18 (right).

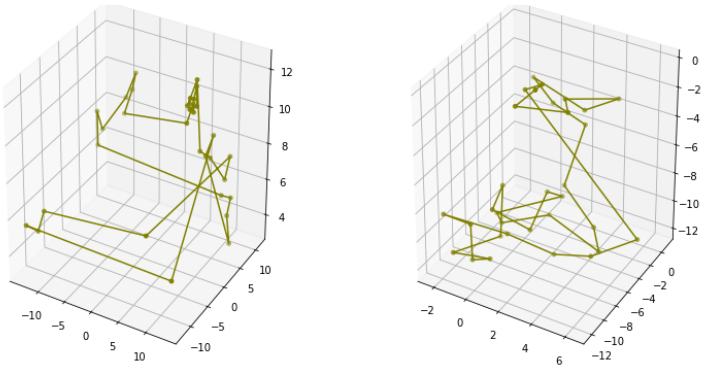

(B) $\alpha = 1.7$, radius of gyration 11.94 (left) and 5.51 (right).

FIGURE 11. Two representative paths with indicated radii of gyration sampled from the free particle $T = 2$ K distributions with 32 beads for two different values of α. *Top:* two illustrative paths from an $\alpha = 2$ simulation. *Bottom:* two illustrative paths from a fractional $\alpha = 1.7$ simulation. Scale units are in bohr.

What can be gleaned from the insets of Figures 8, 9, and 10 is that measures of both the average interbead distance and the radius of gyration are accompanied by increasingly large standard deviations as α decreases. This can be expected as the variance of an α-stable law is infinite for $0 < \alpha < 2$, with the mean itself becoming infinite for $\alpha < 1$ (we only consider the $1 < \alpha < 2$ case).

The bead-sampling algorithm together with the numerical scheme for the per-link kinetic energy (4.22) may now be used to compute the average kinetic energy $\langle \hat{K} \rangle$ as in (4.20). Some computed values of $\langle \hat{K} \rangle$ for α near 2 at various temperatures using 32 beads are shown in Table 1. Our findings suggest that the fractional regime exhibits kinetic energies similar to the ordinary regime except at low temperatures. Roughly speaking, this would suggest that the effect of the fractional density matrix (Figures 3 – 5), which manifests in the paths that are sampled (Figure 11), is roughly balanced by the behavior of the fractional per-link kinetic energy (Figure 6). However, while we have verified that the values of $\langle \hat{K} \rangle$ in the fractional regime converge to the values of $\langle \hat{K} \rangle$ for the ordinary $\alpha = 2$ regime as $\alpha \to 2$, we currently lack a benchmark that can be used to verify the results of our algorithm for general α. An example of this for the $\alpha = 2$ case would be $\langle \hat{K} \rangle = 3Nk_BT/2$ for high temperature according to the equipartition theorem [**41**]. While in one-dimension, a fractional analogue of this may be derived using the representations in Appendix E, it is not clear how to proceed in the relevant case of physical dimension three. Thus, while the results for the kinetic energy in our simulations are reasonable and consistent with the ordinary $\alpha = 2$ case, we believe it is worthwhile to explore theoretical predictations that can serve as a robust test of our kinetic energy routines.

α	Temperature (K)			
	1	**2**	**5**	**10**
2.00	1.495155	3.011902	7.737682	14.796637
1.95	1.469983	3.036802	7.60732	14.578588
1.90	1.21939	3.029805	7.49339	14.99152

TABLE 1. The free particle kinetic energy as a function of temperature for varying α. 32 beads are used. A noticable relative difference occurs only at low temperature $T = 1$ K.

4.3.4 Fractional He-4 PIMC Results

Building upon our free particle simulations, we also simulate fractional ^{4}He, the prototypical quantum liquid for which PIMC algorithms were initially designed and therefore a prime target for our technique, to demonstrate the utility of our PIMC algorithm in the presence of interactions. ^{4}He is a particularly illuminating example because, even in the $\alpha = 2$ case, its particle paths become so diffuse at low temperatures that it can form a superfluid [**42, 166**]. In the following, we model ^{4}He with the Aziz potential [**14**]. Irrespective of the increased localization due to the potential, the overarching trend that delocalization is favored with decreasing α persists. Interestingly, for ^{4}He, we do not observe a pronounced competition between minimizing the kinetic and potential energies. This competition may be more pronounced, leading to more intriguing behavior, for interparticle potentials with deeper minima.

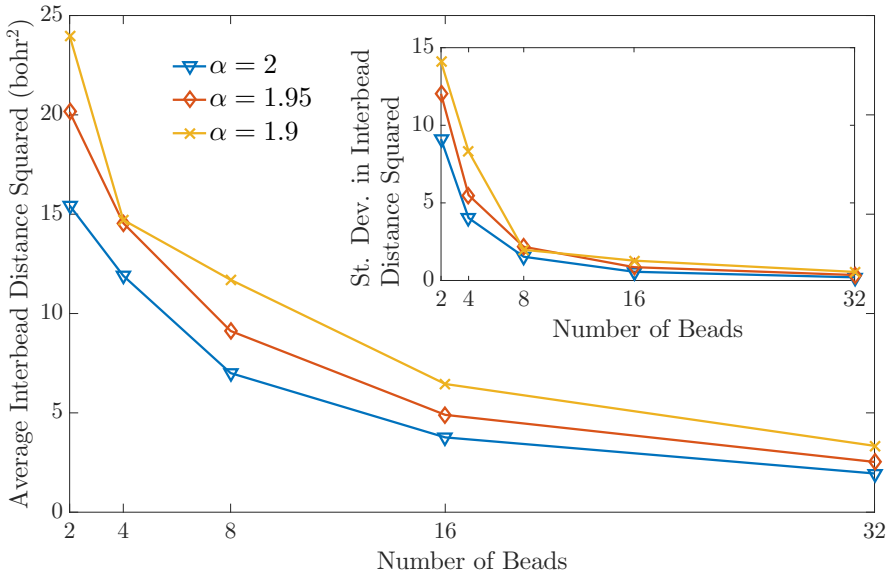

FIGURE 12. The average interbead distance squared vs. the number of beads for ^{4}He at 2 K. *Inset:* Standard deviation of the same quantity.

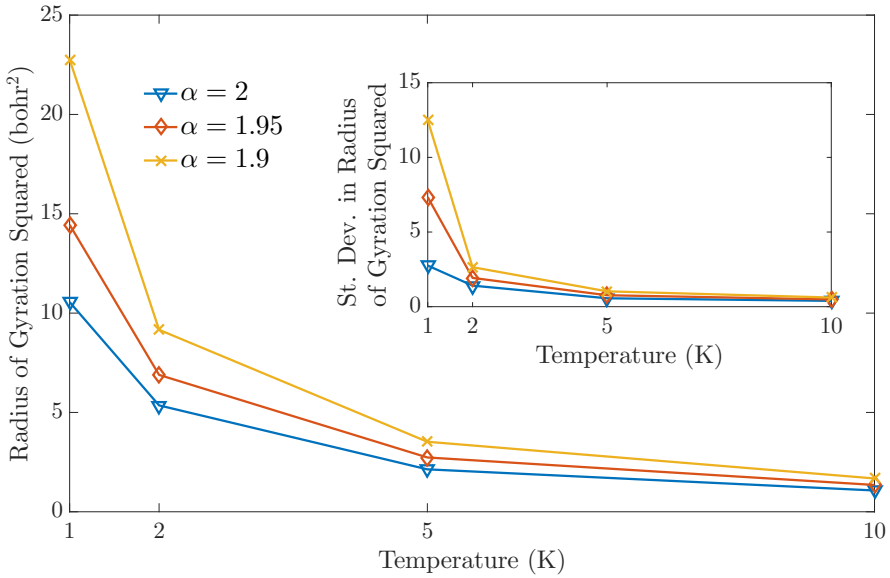

FIGURE 13. The average radius of gyration squared vs. the temperature for ^{4}He (32 beads). *Inset:* Standard deviation of the same quantity.

4.4 Chapter Conclusion

We have presented a methodology that generalizes the Path Integral Monte Carlo algorithm to fractional Hamiltonians, thereby enabling the computational exploration of fractional Hamiltonians with potentials that are not readily amenable to analytical treatments. We have furthermore employed our algorithm to explore the impact of a fractional Laplacian on free-particle and ^{4}He path observables, such as the radius of gyration and the average interbead distance. We have identified novel properties of the fractional kinetic energy such as its asymptotic behavior and the existence of a pronounced minimum for fractional exponents less than two ($\alpha < 2$). Fractional particles become increasingly more diffuse as a consequence of sampling a fractional density matrix distribution with heavier tails than the usual Gaussian distribution. Because the onset of phenomena related to condensation heavily depends on the diffusivity of particle paths, our findings suggest that fractional Hamiltonians may manifest intriguing superfluid and Wigner crystallization phase transitions. Such transitions have only previously been studied for the fractional Schrödinger equation based upon mean field theories [**119**]. Fractional Path Integral Monte Carlo will enable a more complete understanding of such phenomena.

To further enable the exploration of fractional condensation phenomena, several complications revealed by our work should be addressed. First and foremost, because the conventional staging algorithm [**41, 199**] cannot readily be applied to non-Gaussian distributions, we sampled our partition functions using inefficient single bead moves. While, for the potentials explored, we verified that our simulations were able to converge to their equilibrium distributions, this may not be the case for more general potentials. Single bead moves are furthermore suboptimal for sampling permutations among particles with quantum statistics. Future work will therefore

focus on the development of generalized multi-bead moves. Fourier path sampling may permit the generality we require [**61, 76, 123**].

As Figures 3 – 7 illustrate, the density matrix distributions sampled for $\boldsymbol{r} - \boldsymbol{r'}$ in our algorithm are significantly more complex than the Gaussian distribution sampled conventionally. The discrete inverse-transform sampling method we presented can accurately sample these heavy-tailed distributions, but there remain theoretical questions about these distributions. One key question is whether the infinite variance (for $\alpha < 2$) and infinite mean (for $\alpha \leq 1$) of the fractional density matrix require the use of other notions of central tendency (such as median) for certain observables. In this direction, it may be fruitful to explore "tempered-fractional quantum mechanics," which has not been studied to our knowledge. Tempered Lévy processes enjoy many of the same properties as Lévy processes, but avoid theoretical issues related to infinite variance [**147, 118**].

It may also be of interest to consider the physics of the time-fractional Schrodinger equation [**157**], and even the space-and-time-fractional Schrodinger equation [**218**]. These equations introduce waiting times in addition to long jumps. However, unlike the space-fractional equation, the properties of the time-fractional Schrodinger equation suggest that it cannot be used as a probabalistic theory of Quantum Mechanics [**62, 132**]. Thus, more work is needed before any implementation of a time-fractional model is justified.

In summary, we have proposed a novel fractional Path Integral Monte Carlo algorithm. Our algorithm provides a clear numerical path toward unraveling the fractional physics of interacting systems, much of which could only be approximated analytically in the past. We look forward to employing this algorithm to explore where our fully interacting predictions differ from previous approximate analytical solutions and to the study of such novel phenomena as fractional superfluidity.

CHAPTER 5

Machine Learning of Space-Fractional Differential Equations using Physics-Informed Gaussian Processes

5.1 Introduction

A novel use of machine learning, which has potential both for modeling with large or high-frequency data sets as well as advancing fundamental science, is the discovery of governing differential equations from data. Unlike highly specialized algorithms used to refine existing models, these novel methods are distinguished by comparatively limited assumptions, and the ability to produce various types of equations from a wide variety of data.

We now give a very brief (and incomplete) overview of a few proposed algorithms. Key differences between various works include the techniques used to generate candidate equations and the technique used to select equations. A fundamental problem that all these work address is that, if such algorithms are to mimic a human scientist, while generating accurate models, they must also avoid or penalize spurious "overfitted" models. In [189], a symbolic regression method was developed to learn conservation laws of physical systems. The laws, which could be nonlinear, were created using genetic programming and evaluated concurrently on predicative ability and parsimony (number of terms) in order to prevent overfitting. Earlier, in [27] in a dynamical system context, the equations were evaluated using "probing" tests while the overfitting was addressed using a separate "snipping" process. In [37], a more parametric method for learning nonlinear autonomous systems was developed in which the candidate equation is build from a linear combination of elements from a user-defined "dictionary". Parsimony translated to sparsity in the dictionary elements, so sparse regression was used to determine the coefficients. In [184], a similar approach was used to generate nonlinear partial differential evolution equations.

Building on an earlier work [172] where Gaussian process regression was used to infer solutions of equations, a Gaussian process framework was developed in [173]

for parametric learning of linear differential equations, of the form

$$\mathcal{L}^{p_1,...,p_k} u = f \tag{5.1}$$

given small data on f and u. Here $\mathcal{L}^{p_1,...,p_k}$ refers to a linear differential operator with parameters $p_1, ..., p_k$; for example, $\mathcal{L}^{p_1,...,p_k}$ could be a linear combination of k differential operators with coefficients $p_1, ..., p_k$. The method placed a Gaussian Process on the function u and used linearity of $\mathcal{L}^{p_1,...,p_k}$ to obtain a joint Gaussian Process on (u, f) in which the unknown parameters $p_1, ..., p_k$ were subsumed as hyperparameters (this is reviewed in detail in Section 5.2). This allowed the use of standard continuous optimization techniques to optimize the negative log-marginal likelihood, which effects an automatic trade-off between data-fit and model complexity, and thereby find $p_1, .., p_k$. Thus, in this approach, the problem of identifying the differential equation is "embedded" into the problem of interpolation/regression of data. Moreover, the Gaussian Process method only requires computation of the forward action of $\mathcal{L}^{\boldsymbol{p}}$ on the covariance kernel, rather than the solution of the differential equation. However, the method also required the user to select a "dictionary" of terms and assume a parametric form of the equation.

The inclusion of fractional-order operators in this framework, where the order itself is a parameter, allows for a single fractional-order operator to interpolate between derivatives of all orders. This allows the user to directly control the parsimony, by fitting a specified number of fractional derivatives to data, without making assumptions on the orders of derivatives to be discovered. Therefore, building on a basic example of a fractional-order operator treated in [**173**], we significantly extend the framework to treat other space-fractional differential operators and covariance kernels. The main problem that must be addressed is the efficient computation of the action of the unknown (fractional) linear operator $\mathcal{L}^{p_1,...,p_k}$ on covariance kernels.

At the same time, fractional-order derivatives are far more than a tool to interpolate between integer-order and facilitate data-driven discovery of PDEs using continuous optimization techniques. The advances in this chapter further improve the ability to discover fractional-order partial differential equations (FPDEs) from real-world data. It is now well understood that FPDEs have a profound connection with anomalous diffusions and systems driven by heavy-tailed processes ([**149**], [**152**]). While such heavy-tailed data abounds in the fields of, e.g., hydrology, finance, and plasma physics, FPDEs are currently underutilized as tools to model macroscopic properties of such systems. This can be attributed to the analytic difficulties of deriving FPDE models; not only is there an additional parameter, but the involved formulas and nonlocal nature of fractional-order derivatives make them significantly less attractive for specialists in other fields to work with.

Machine Learning is a natural tool for ameliorating this issue. As proof of this concept, we point to the work [**163**], which employed a multi-fidelity Gaussian Process method to discover fractional-order of the fractional advection-dispersion equation governing underground tritium transport through a heterogeneous medium at the Macrodispersion Experimental site at Columbus Air Force Base. This resulted in improved and highly efficient fitting of variable-order fractional equation to data. Along more theoretical lines, [**81**] explored the determination, using Gaussian processes, of the fractional-order of an elliptic problem involving a Spectral fractional Laplacian on a bounded domain with Neumann boundary condition. In addition, the authors also proved wellposedness of the inverse Bayesian formulation of this problem in the sense of [**205**]. Our work differs from [**163**] in that we do not repeatedly solve the forward problem, and from [**81**] in that we do not place a prior on the fractional order or on other parameters; rather, the parameters are inferred by placing a prior and training on the solution and right-hand side of the equation. This

allows for more flexibility with regard to the form of the equation and the inclusion of additional parameters.

In the aforementioned Gaussian Process framework of [**173**], it is possible to treat time-derivatives by considering the data and equation in space-time. Time may be treated as another dimension in the covariance kernel. An alternative method is suggested by the work of [**168**], in which learning of evolution equations is based on the numerical differentiation of Gaussian processes. In this method, the data is given at different "snap-shots" in time which are used to discretize the time-derivative. In this way, even nonlinear equations can be discovered using correspondence between nonlinear terms and specific linearizations. The training is similar technically to that of [**173**], and we extend this to more fractional operators and covariance kernels as well.

This chapter is organized as follows. In section 5.2, we review the Gaussian Process framework of [**173**] and [**168**]. In section 5.3, we review the Matérn family of covariance kernels and space-fractional operators and present new formulas for space-fractional derivatives of such covariance kernels. Such covariance kernels can be more suited to rough data in certain applications. The inclusion of these new formulas, which can be efficiently treated using generalized Gauss-Laguerre quadrature, allows the discovery of various fractional equations in a unified way. In section 5.4 we present basic synthetic examples to illustrate the methodology, and in section 5.5 we apply the methodology to the discovery and interpolation of integer-order advection and diffusion using the fractional-order framework. This includes an interesting problem of interpolating two-term advection-diffusion using a single fractional-order term, and an exploration of user-selected parsimony. After reviewing the relation between α-stable processes and fractional diffusion in section 5.6 and studying a synthetic example, in section 5.7 we apply the methodology to the modeling of relative stock

performance (Intel to S&P 500) by α-stable processes via an associated fractional-order diffusion equation.

5.2 The Gaussian Process Framework

We review the framework developed by [173] for parametric learning of linear differential equations, of the form

$$\mathcal{L}^{\boldsymbol{p}}u = \mathcal{L}^{p_1,\dots,p_k}u = f$$

given data on f and u. Here, $\mathcal{L}^{p_1,\dots,p_k}$ is a linear operator with unknown parameters $p_1, \dots p_k$. Here, and throughout the chapter, we use boldface characters (such as $\boldsymbol{x}$) to denote vector-valued variables, and capital boldface characters (such as $\boldsymbol{X}$) to denote data vectors.

Assume $u(\boldsymbol{x})$ to be Gaussian process with mean 0 and covariance function $k_{uu}(\boldsymbol{x}, \boldsymbol{x'}; \boldsymbol{\theta})$ with hyperparameters $\boldsymbol{\theta}$:

$$u(\boldsymbol{x}) \sim \mathcal{GP}(0, k_{uu}(\boldsymbol{x}, \boldsymbol{x'}; \boldsymbol{\theta})). \tag{5.2}$$

We shall be vague about the form of the covariance kernel until Section 5.3; for now, it suffices to say that it describes how the correlation between the values of u at two points $\boldsymbol{x}$ and $\boldsymbol{x'}$ falls off with $|\boldsymbol{x} - \boldsymbol{x'}|$ or otherwise behaves with the two points, and that it must be a symmetric, positive semidefinite function [177]. Then, the linear transformation $f = \mathcal{L}^{\boldsymbol{p}}u$ of the Gaussian process u implies a Gaussian Process for $f(\boldsymbol{x})$,

$$f(\boldsymbol{x}) \sim \mathcal{GP}(0, k_{ff}(\boldsymbol{x}, \boldsymbol{x'}; \boldsymbol{\theta}, \boldsymbol{p})),$$

with covariance kernel

$$k_{ff}(\boldsymbol{x}, \boldsymbol{x'}; \boldsymbol{\theta}, \boldsymbol{p}) = \mathcal{L}^{\boldsymbol{p}}_{\boldsymbol{x}} \mathcal{L}^{\boldsymbol{p}}_{\boldsymbol{x'}} k_{uu}(\boldsymbol{x}, \boldsymbol{x'}; \boldsymbol{\theta}). \tag{5.3}$$

Moreover, the covariance between $u(\boldsymbol{x})$ and $f(\boldsymbol{x'})$, and between $f(\boldsymbol{x})$ and $u(\boldsymbol{x'})$ is

$$\begin{aligned} k_{uf}(\boldsymbol{x}, \boldsymbol{x'}; \boldsymbol{\theta}, \boldsymbol{p}) &= \mathcal{L}^{\boldsymbol{p}}_{\boldsymbol{x'}} k_{uu}(\boldsymbol{x}, \boldsymbol{x'}; \theta) \\ k_{fu}(\boldsymbol{x}, \boldsymbol{x'}; \boldsymbol{\theta}, \boldsymbol{p}) &= \mathcal{L}^{\boldsymbol{p}}_{\boldsymbol{x}} k_{uu}(\boldsymbol{x}, \boldsymbol{x'}; \theta), \end{aligned} \tag{5.4}$$

respectively. By symmetry of k_{uu},

$$k_{fu}(\boldsymbol{x}, \boldsymbol{x'}; \boldsymbol{\theta}, \boldsymbol{p}) = k^T_{uf}(\boldsymbol{x}, \boldsymbol{x'}; \boldsymbol{\theta}, \boldsymbol{p}) \stackrel{\text{def}}{=} k_{uf}(\boldsymbol{x'}, \boldsymbol{x}; \boldsymbol{\theta}, \boldsymbol{p}).$$

The hyperparameters $(\boldsymbol{\theta}, \boldsymbol{p})$ of the joint Gaussian Process

$$\begin{bmatrix} u(\boldsymbol{x}) \\ f(\boldsymbol{x}) \end{bmatrix} \sim \mathcal{GP}\left(\boldsymbol{0}, \begin{bmatrix} k_{uu}(\boldsymbol{x}, \boldsymbol{x'}; \boldsymbol{\theta}) & k_{uf}(\boldsymbol{x}, \boldsymbol{x'}; \boldsymbol{\theta}, \boldsymbol{p}) \\ k_{fu}(\boldsymbol{x}, \boldsymbol{x'}; \boldsymbol{\theta}, \boldsymbol{p}) & k_{ff}(\boldsymbol{x}, \boldsymbol{x'}; \boldsymbol{\theta}, \boldsymbol{p}) \end{bmatrix} \right). \tag{5.5}$$

are then learned by training on the data $\boldsymbol{Y}_u$ of u given at points $\boldsymbol{X}_u$ and $\boldsymbol{Y}_f$ of f given at points $\boldsymbol{X}_f$. This is done with a Quasi-Newton optimizer L-BFGS to minimize the negative log marginal likelihood ([177]):

$$\begin{aligned} \mathcal{NLML}(\boldsymbol{\theta}, \boldsymbol{p}, \sigma^2_{n_u}, \sigma^2_{n_f}) &= -\log p(\boldsymbol{Y} | \boldsymbol{\theta}, \boldsymbol{p}, \sigma^2_{n_u}, \sigma^2_{n_f}) \\ &= \frac{1}{2} \boldsymbol{Y}^T \boldsymbol{K}^{-1} \boldsymbol{Y} + \frac{1}{2} \log |\boldsymbol{K}| + \frac{N}{2} \log(2\pi), \end{aligned} \tag{5.6}$$

where $\boldsymbol{Y} = \begin{bmatrix} \boldsymbol{Y}_u \\ \boldsymbol{Y}_f \end{bmatrix}$, $p(\boldsymbol{Y} | \boldsymbol{\theta}, \boldsymbol{p}, \sigma^2_{n_u}, \sigma^2_{n_f}) = \mathcal{N}(\boldsymbol{0}, \boldsymbol{K})$, and $\boldsymbol{K}$ is given by

$$\boldsymbol{K} = \begin{bmatrix} k_{uu}(\boldsymbol{X}_u, \boldsymbol{X}_u; \boldsymbol{\theta}) + \sigma^2_{n_u} \boldsymbol{I}_{n_u} & k_{uf}(\boldsymbol{X}_u, \boldsymbol{X}_f; \boldsymbol{\theta}, \boldsymbol{p}) \\ k_{fu}(\boldsymbol{X}_f, \boldsymbol{X}_u; \boldsymbol{\theta}, \boldsymbol{p}) & k_{ff}(\boldsymbol{X}_f, \boldsymbol{X}_f; \boldsymbol{\theta}, \boldsymbol{p}) + \sigma^2_{n_f} \boldsymbol{I}_{n_f} \end{bmatrix}. \tag{5.7}$$

The additional noise parameters $\sigma_{n_u}^2$ and $\sigma_{n_f}^2$ are included to learn noise in the data; their inclusion above corresponds to the assumption that

$$\boldsymbol{Y}_u = u(\boldsymbol{X}_u) + \boldsymbol{\epsilon}_u$$

$$\boldsymbol{Y}_f = f(\boldsymbol{X}_f) + \boldsymbol{\epsilon}_f$$

with $\boldsymbol{\epsilon}_u \sim \mathcal{N}(\boldsymbol{0}, \sigma_{n_u}^2 \boldsymbol{I}_{n_u})$ and independently $\boldsymbol{\epsilon}_f \sim \mathcal{N}(\boldsymbol{0}, \sigma_{n_f}^2 \boldsymbol{I}_{n_f})$.

Next we review the time-stepping Gaussian Process method of [**168**] for learning linear (in our case) equations of the form

$$u_t + \mathcal{L}^{p_1,\ldots,p_k} u = 0,\ x \in \mathbb{R}^d,\ t \in [0, T].$$

For our purposes, we consider two "snapshots" $\{\boldsymbol{x}^{n-1}, \boldsymbol{u}^{n-1}\}$ and $\{\boldsymbol{x}^n, \boldsymbol{u}^n\}$ of the system at two times t^{n-1} and t^n, respectively, such that

$$t^n - t^{n-1} = \Delta t \ll 1.$$

We perform, in the case of two snapshots, a backward Euler discretization

$$u^n + \Delta t \mathcal{L}^{p_1,\ldots,p_k} u^n = u^{n-1}. \tag{5.9}$$

Then we assume a Gaussian Process, but for u^n:

$$u^n(\boldsymbol{x}) \sim \mathcal{GP}(0, k(\boldsymbol{x}, \boldsymbol{x'}, \boldsymbol{\theta})). \tag{5.10}$$

As before, the linearity of $\mathcal{L}^{p_1,\ldots,p_k}$ leads to a Gaussian Process for u^{n-1}. We obtain the joint Gaussian process

$$\begin{bmatrix} u^n(\boldsymbol{x}) \\ u^{n-1}(\boldsymbol{x}) \end{bmatrix} \sim \mathcal{GP}\left(\boldsymbol{0}, \begin{bmatrix} k^{n,n}(\boldsymbol{x}, \boldsymbol{x'}; \boldsymbol{\theta}) & k^{n,n-1}(\boldsymbol{x}, \boldsymbol{x'}; \boldsymbol{\theta}, \boldsymbol{p}) \\ k^{n-1,n}(\boldsymbol{x}, \boldsymbol{x'}; \boldsymbol{\theta}, \boldsymbol{p}) & k^{n-1,n-1}(\boldsymbol{x}, \boldsymbol{x'}; \boldsymbol{\theta}, \boldsymbol{p}) \end{bmatrix}\right). \tag{5.11}$$

where, denoting the identity operator by Id,

$$
\begin{aligned}
(5.12)\quad & k^{n,n} = k, && k^{n,n-1} = (\mathrm{Id} + \Delta t \mathcal{L}^{\boldsymbol{p}}_{\boldsymbol{x}'})k, \\
& k^{n-1,n} = (\mathrm{Id} + \Delta t \mathcal{L}^{\boldsymbol{p}}_{\boldsymbol{x}})k, && k^{n-1,n-1} = (\mathrm{Id} + \Delta t \mathcal{L}^{\boldsymbol{p}}_{\boldsymbol{x}})(\mathrm{Id} + \Delta t \mathcal{L}^{\boldsymbol{p}}_{\boldsymbol{x}'})k.
\end{aligned}
$$

Equation (5.11) can be compared to equation (5.5), and equation (5.12) to (5.3) and (5.4). The set-ups are very similar, and again, $\boldsymbol{p}$ has been merged into the hyperparameters of this joint Gaussian Process. Given data at spacial points $\boldsymbol{X}^n$ and $\boldsymbol{X}^{n-1}$ for the functions u^n and u^{n-1}, represented by the vectors $\boldsymbol{U}^n$ and $\boldsymbol{U}^{n-1}$, respectively, the new hyperparameters $(\boldsymbol{\theta}, \boldsymbol{p})$ are trained by employing the same Quasi-Newton optimizer L-BFGS as before to minimize the $\mathcal{NLML}$ given by equation (5.6). In this case, $\boldsymbol{Y} = \begin{bmatrix} \boldsymbol{U}^n \\ \boldsymbol{U}^{n-1} \end{bmatrix}$, $p(\boldsymbol{y}|\boldsymbol{\theta}, \boldsymbol{p}, \sigma^2) = \mathcal{N}(\boldsymbol{0}, \boldsymbol{K})$, and $\boldsymbol{K}$ is given by

$$
(5.13)\qquad \boldsymbol{K} = \begin{bmatrix} k^{n,n}(\boldsymbol{X}^n, \boldsymbol{X}^n) & k^{n,n-1}(\boldsymbol{X}^n, \boldsymbol{X}^{n-1}) \\ k^{n-1,n}(\boldsymbol{X}^{n-1}, \boldsymbol{X}^n) & k^{n-1,n-1}(\boldsymbol{X}^{n-1}, \boldsymbol{X}^{n-1}) \end{bmatrix} + \sigma_n^2 \boldsymbol{I}.
$$

Here, σ_n^2 is an additional parameter to learn noise in the data, under the assumption

$$
\begin{aligned}
\boldsymbol{u}^n &= u^n(\boldsymbol{X}^n) + \boldsymbol{\epsilon}^n \\
\boldsymbol{u}^{n-1} &= u^{n-1}(\boldsymbol{X}^{n-1}) + \boldsymbol{\epsilon}^{n-1}
\end{aligned}
$$

with $\boldsymbol{\epsilon}^n \sim \mathcal{N}(0, \sigma_n^2 \boldsymbol{I})$ and $\boldsymbol{\epsilon}^{n-1} \sim \mathcal{N}(0, \sigma_n^2 \boldsymbol{I})$ being independent.

5.3 Fractional Derivatives of Covariance Kernels

Many properties of a Gaussian Process are determined by the choice of covariance kernel $k(\boldsymbol{x}, \boldsymbol{x'})$. In particular, the covariance kernel encodes an assumption about the smoothness of the field that being interpolated. Stein, in [200], writes

> "...properties of spatial interpolants depend strongly on the local behavior of the random field. In practice, this local behavior is not known and must be estimated from the same data that will be used to do the interpolation. This state of affairs strongly suggests that it is critical to select models for the covariance structures that include at least one member whose local behavior accurately reflects the actual local behavior of the spatially varying quantity under study. A number of commonly used models for the covariance structure, including the spherical, the exponential and the Gaussian, provide no flexibility with regard to this local behavior and essentially assume it is known *a priori*. An alternative model that I recommend for general adoption is the Matérn model. This model includes a parameter that allows for any degree of differentiability for the random field and includes the exponential model as a special case and the Gaussian model as a limiting case."

Matérn kernels M_ν (defined below), a family of stationary kernels which includes the exponential kernel for $\nu = 1/2$, and the squared-exponential kernel in the limit $\nu \to \infty$, have been widely used for this reason. A Gaussian Process with Matérn covariance kernel M_ν is n-times mean square differentiable for $n > \nu$. We have developed a computational methodology that allows for Matérn kernels of arbitrary real order $\nu > 0$ to be used in our Gaussian Process, namely in (5.2) and (5.10). In

fact, the parameter ν itself can be treated and optimized as a hyperparameter of the Gaussian Process, just as the equation parameters were in Section 5.2. We employ such an algorithm to explore the effect of the parameter ν when working with rough time series histogram data in section 5.6.

The main problem that arises when using Matérn kernels is the actual computation of the fractional derivatives of such kernel, as required by equations (5.3) and (5.4) for the time-independent case and (5.12) for the time-dependent case. Fractional derivatives, whether in $\mathbb{R}^d$, $\mathbb{R}^+$, or on bounded subsets with boundary conditions, are nonlocal operators often defined by singular integrals or eigenfunction expansions that are expensive to evaluate [**137**], [**149**]. However, space-fractional derivatives in $\mathbb{R}^d$ enjoy representations as Fourier multiplier operators. In other words, they are equivalent to multiplication by a function $m(\boldsymbol{\xi})$ in frequency space. This representation suggests a computational method that avoids any singular integral operators or the solution of extension problems in $\mathbb{R}^{d+1}$. The downside to Fourier methods is that, if used to compute the fractional derivative of a function u on $\mathbb{R}^d$, they may require quadrature of a $2d$ (forward and inverse) Fourier integral. Thus, if one wishes to compute the fractional derivative $\mathcal{L}$ of a covariance kernel $k(\boldsymbol{x}, \boldsymbol{y})$, as in (5.3), (5.4), or (5.12), this may entail $2d$ quadrature for $\mathcal{L}_{\boldsymbol{x}}k$ and $\mathcal{L}_{\boldsymbol{y}}k$, and $4d$ quadrature for $\mathcal{L}_{\boldsymbol{x}}\mathcal{L}_{\boldsymbol{y}}k$. These dimensions for quadrature can be cut in half provided the (forward) Fourier transforms of these kernels were known analytically. Moreover, if the covariance kernel k_{uu} is stationary, we see in Theorem 5.18 below that $\mathcal{L}_{\boldsymbol{x}}\mathcal{L}_{\boldsymbol{y}}k$ can further be reduced from a $2d$-dimensional integral to d-dimensional one.

Thus, the entire problem of kernel computation is reduced to d-dimensional quadrature if the following three conditions are satisfied:

(1) *The spacial differential operator $\mathcal{L}$ is a Fourier multiplier operator*:

$$\mathcal{F}\{\mathcal{L}f\}(\boldsymbol{\xi}) = m(\boldsymbol{\xi}) \cdot \mathcal{F}\{f\}(\boldsymbol{\xi}).$$

This is true for a variety of fractional space derivatives:

$$\begin{aligned} &\text{Fractional Laplacian}: \ \mathcal{F}\{(-\Delta)^{\alpha/2} f\}(\boldsymbol{\xi}) = |\boldsymbol{\xi}|^{\alpha} \mathcal{F}\{f\}(\boldsymbol{\xi}) \\ &\text{Left-sided Riemann-Louiville}: \ \mathcal{F}\{{}^{RL}_{-\infty}D^{\alpha}_{\boldsymbol{x}} f\}(\boldsymbol{\xi}) = (-i\boldsymbol{\xi})^{\alpha} \mathcal{F}\{f\}(\boldsymbol{\xi}) \\ &\text{Right-sided Riemann-Louiville}: \ \mathcal{F}\{{}^{RL}_{\boldsymbol{x}}D^{\alpha}_{\infty} f\}(\boldsymbol{\xi}) = (i\boldsymbol{\xi})^{\alpha} \mathcal{F}\{f\}(\boldsymbol{\xi}). \end{aligned} \tag{5.14}$$

Here, and throughout this chapter, we use the Fourier transform convention

$$\mathcal{F}f = \frac{1}{(2\pi)^{d/2}} \int_{\mathbb{R}^d} e^{-i\boldsymbol{\xi}\cdot\boldsymbol{x}} f(\boldsymbol{x}) d\boldsymbol{x}, \quad \mathcal{F}^{-1}\hat{f} = \frac{1}{(2\pi)^{d/2}} \int_{\mathbb{R}^d} e^{i\boldsymbol{\xi}\cdot\boldsymbol{x}} \hat{f}(\boldsymbol{\xi}) d\boldsymbol{\xi}$$

(2) *The covariance kernel k is stationary*:

$$k(\boldsymbol{x}, \boldsymbol{y}) = K(\boldsymbol{x} - \boldsymbol{y}).$$

This is true of the squared-exponential kernel in one-dimension

$$G(\sigma, \theta; x, y) = \sigma^2 \exp\left(-\frac{1}{2}\frac{(x-y)^2}{\theta^2}\right)$$

as well as frequently used multivariate squared-exponential kernels, formed by multiplication

$$G^{\times}(\sigma, \theta_1, \theta_2, ..., \theta_d; \boldsymbol{x}, \boldsymbol{y}) = \sigma^2 \prod_{i=1}^{d} \exp\left(-\frac{1}{2}\frac{(x_i - y_i)^2}{\theta_i^2}\right)$$

or addition

$$G^{+}(\sigma, \theta_1, \theta_2, ..., \theta_d; \boldsymbol{x}, \boldsymbol{y}) = \sigma^2 \sum_{i=1}^{d} \exp\left(-\frac{1}{2}\frac{(x_i - y_i)^2}{\theta_i^2}\right)$$

of the one-dimensional kernel. The same is true for the Matérn kernels M_ν, which have one-dimensional form

$$M_\nu(\sigma,\theta;x,y) = \frac{\sigma^2 2^{1-\nu}}{\Gamma(\nu)}\left(\frac{\sqrt{2\nu}}{\theta}(x-y)\right)^\nu K_\nu\left(\frac{\sqrt{2\nu}}{\theta}(x-y)\right) \tag{5.15}$$

and the corresponding multidimensional kernels

$$\begin{aligned} M^\times_{\nu_1,\dots,\nu_d}(\boldsymbol{x},\boldsymbol{y}) &= \prod_{i=1}^d M_{\nu_i}(x_i-y_i), \\ M^+_{\nu_1,\dots,\nu_d}(\boldsymbol{x},\boldsymbol{y}) &= \sum_{i=1}^d M_{\nu_i}(x_i-y_i). \end{aligned} \tag{5.16}$$

The notation K_ν refers to the modified Bessel function, which is potentially confusing, but will not be an issue as we will focus on Fourier representation of M_ν in what follows.

(3) *The (forward) Fourier transform $\hat{K}(\boldsymbol{\xi}) = \mathcal{F}\{K\}(\boldsymbol{\xi})$ of the stationary covariance kernel K is known analytically.* This is satisfied by the squared exponential kernel $G(\sigma,\theta;x)$ and the Matérn kernel[‡] $M_\nu(\sigma,\theta;x)$:

$$\begin{aligned} &\text{S. E. kernel: } \mathcal{F}\{G\}(\xi) = \theta\sigma^2 e^{-\frac{\theta^2}{2}\xi^2} \\ &\text{Matérn kernel: } \mathcal{F}\{M_\nu\}(\xi) = \frac{\theta\sigma^2\Gamma(\nu+1/2)}{\sqrt{\nu}\Gamma(\nu)}\left(1+\frac{\theta^2\xi^2}{2\nu}\right)^{-(\nu+1/2)} \end{aligned} \tag{5.17}$$

The same is true for the multidimensional kernels G^+ and M^+_ν by linearity of the Fourier transform, and for $G^\times$ and $M^\times_\nu$ by Fubini's theorem.

THEOREM 5.18. *Suppose conditions (1)-(3) on the covariance kernel k and the operator $\mathcal{L}$ and are satisfied. Then the fractional derivatives of the covariance kernel*

[‡]In the machine learning literature, authors such as [177] describe this Fourier transform as the *spectral density* in the context of Bochner's theorem on stationary kernels, and write it in the equivalent form, up to Fourier transform convention: $\hat{M}_\nu(\xi) = \sigma^2\frac{\sqrt{2}\Gamma(\nu+1/2)(2\nu)^\nu}{\Gamma(\nu)\theta^{2\nu}}\left(\frac{2\nu}{\theta^2}+\xi^2\right)^{-(\nu+1/2)}$.

$\mathcal{L}_{\boldsymbol{x}}k$, $\mathcal{L}_{\boldsymbol{y}}k = [\mathcal{L}_{\boldsymbol{x}}k]^T$, and $\mathcal{L}_{\boldsymbol{y}}\mathcal{L}_{\boldsymbol{x}}k$ can be computed by d-dimensional integrals

$$\begin{cases} \mathcal{L}_{\boldsymbol{x}}k = \dfrac{1}{\sqrt{2\pi}} \displaystyle\int_{\mathbb{R}^d} e^{i\langle \boldsymbol{x}-\boldsymbol{y},\boldsymbol{\xi}\rangle} m(\boldsymbol{\xi})\hat{K}(\boldsymbol{\xi}) d\boldsymbol{\xi} \\ \mathcal{L}_{\boldsymbol{y}}\mathcal{L}_{\boldsymbol{x}}k = \dfrac{1}{\sqrt{2\pi}} \displaystyle\int_{\mathbb{R}^d} e^{i\langle \boldsymbol{x}-\boldsymbol{y},\boldsymbol{\xi}\rangle} m(\boldsymbol{\xi})m(-\boldsymbol{\xi})\hat{K}(\boldsymbol{\xi}) d\boldsymbol{\xi}. \end{cases} \tag{5.19}$$

As for derivatives of the objective function (5.6) with respect to the expanded hyperparameters, we note in the above formulas that such derivatives pass into the integrand and through the complex exponential factor.

Proof. Recall the shift property of the Fourier transform:

$$\mathcal{F}\{f(\boldsymbol{x}-\boldsymbol{a})\}(\boldsymbol{\xi}) = e^{-i\boldsymbol{a}\cdot\boldsymbol{\xi}}\mathcal{F}\{f(\boldsymbol{x})\}(\boldsymbol{\xi})$$

By the stationarity of k,

$$\mathcal{F}_{\boldsymbol{x}}\{k(\boldsymbol{x},\boldsymbol{y})\} = \mathcal{F}_{\boldsymbol{x}}\{K(\boldsymbol{x}-\boldsymbol{y})\} = e^{-i\boldsymbol{y}\cdot\boldsymbol{\xi}}\hat{K}(\boldsymbol{\xi})$$

By the multiplier property of $\mathcal{L}$, in Fourier space, $\mathcal{L}_{\boldsymbol{x}}k$ is given by multiplying $\mathcal{F}_{\boldsymbol{x}}\{k\}$ by the symbol $m(\boldsymbol{\xi})$:

$$\mathcal{F}_{\boldsymbol{x}}\{\mathcal{L}_{\boldsymbol{x}}k\} = e^{-i\boldsymbol{y}\cdot\boldsymbol{\xi}}m(\boldsymbol{\xi})\hat{K}(\boldsymbol{\xi})$$

Taking the inverse Fourier transform gives

$$\begin{aligned} \mathcal{L}_{\boldsymbol{x}}k &= \mathcal{F}_{\boldsymbol{x}}^{-1}\left\{\mathcal{F}_{\boldsymbol{x}}\{\mathcal{L}_{\boldsymbol{x}}k\}\right\} \\ &= \mathcal{F}_{\boldsymbol{x}}^{-1}\left\{e^{-i\boldsymbol{y}\cdot\boldsymbol{\xi}}m(\boldsymbol{\xi})\hat{K}(\tilde{\boldsymbol{x}})\right\} \\ &= \frac{1}{\sqrt{2\pi}}\int_{\mathbb{R}^d} e^{i\boldsymbol{x}\cdot\boldsymbol{\xi}}e^{-i\boldsymbol{y}\cdot\boldsymbol{\xi}}m(\boldsymbol{\xi})\hat{K}(\boldsymbol{\xi})d\boldsymbol{\xi} \end{aligned} \tag{5.20}$$

This is the first of formulas (5.19). As for $\mathcal{L}_{\boldsymbol{y}}k$, define the transpose operator by $F^T(\boldsymbol{x},\boldsymbol{y}) = F(\boldsymbol{y},\boldsymbol{x})$. Then $\mathcal{L}_{\boldsymbol{y}}F = \left[\mathcal{L}_{\boldsymbol{x}}F^T\right]^T$ and symmetry of k implies

$$\mathcal{L}_{\boldsymbol{y}}k = \left[\mathcal{L}_{\boldsymbol{x}}k^T\right]^T = [\mathcal{L}_{\boldsymbol{x}}k]^T.$$

In other words, $\mathcal{L}_{\boldsymbol{y}} k(\boldsymbol{x}, \boldsymbol{y}) = \mathcal{L}_{\boldsymbol{x}} k(\boldsymbol{y}, \boldsymbol{x})$, and does not require a separate computation (this is true for any covariance kernel). So far, only a single d-dimensional integation is required, which is the benefit of knowing the Fourier transform $\hat{K}$ of K analytically. Next, we see how the stationary property gives the formula for $\mathcal{L}_{\boldsymbol{y}} \mathcal{L}_{\boldsymbol{x}} k$. By the multiplier property of $\mathcal{L}$, we have

$$\mathcal{L}_{\boldsymbol{y}} \mathcal{L}_{\boldsymbol{x}} k = \mathcal{F}_{\boldsymbol{y}}^{-1} \left\{ \mathcal{F}_{\boldsymbol{y}} \left\{ \mathcal{L}_{\boldsymbol{y}} \left[\mathcal{L}_{\boldsymbol{x}} k(\boldsymbol{x}, \boldsymbol{y}) \right] \right\} (\boldsymbol{\xi'}) \right\} = \mathcal{F}_{\boldsymbol{y}}^{-1} \left\{ m(\boldsymbol{\xi'}) \mathcal{F}_{\boldsymbol{y}} \{ \mathcal{L}_{\boldsymbol{x}} k(\boldsymbol{x}, \boldsymbol{y}) \} (\boldsymbol{\xi'}) \right\}.$$

Let us examine the inner term $\mathcal{F}_{\boldsymbol{y}} \{ \mathcal{L}_{\boldsymbol{x}} k(\boldsymbol{x}, \boldsymbol{y}) \} (\boldsymbol{\xi'})$. The Fourier transform $\mathcal{F}_{\boldsymbol{y}}$ passes through the integral over $\boldsymbol{\xi}$ in the final formula (5.20) for $\mathcal{L}_{\boldsymbol{x}} k(\boldsymbol{x}, \boldsymbol{y})$. Inside that integral, $\mathcal{F}_{\boldsymbol{y}}$ only sees a constant term (independent of $\boldsymbol{y}$) times the complex exponential $e^{-i\boldsymbol{y} \cdot \boldsymbol{\xi}}$. Thus, $\mathcal{F}_{\boldsymbol{y}} \{ \mathcal{L}_{\boldsymbol{x}} k(\boldsymbol{x}, \boldsymbol{y}) \} (\boldsymbol{\xi'})$ reduces to a δ-function in $\boldsymbol{\xi'}$:

$$\begin{aligned} \mathcal{F}_{\boldsymbol{y}} \{ \mathcal{L}_{\boldsymbol{x}} k(\boldsymbol{x}, \boldsymbol{y}) \} (\boldsymbol{\xi'}) &= \frac{1}{\sqrt{2\pi}} \int_{\mathbb{R}^d} \left[\sqrt{2\pi} \delta(\boldsymbol{\xi} + \boldsymbol{\xi'}) \right] e^{i\boldsymbol{x} \cdot \boldsymbol{\xi}} m(\boldsymbol{\xi}) \hat{K}(\boldsymbol{\xi}) d\boldsymbol{\xi} \\ &= \int_{\mathbb{R}^d} \delta(\boldsymbol{\xi} + \boldsymbol{\xi'}) e^{i\boldsymbol{x} \cdot \boldsymbol{\xi}} m(\boldsymbol{\xi}) \hat{K}(\boldsymbol{\xi}) d\boldsymbol{\xi} \end{aligned}$$

Therefore, we obtain the second of formulas (5.19):

$$\begin{aligned} \mathcal{L}_{\boldsymbol{y}} \mathcal{L}_{\boldsymbol{x}} k &= \mathcal{F}_{\boldsymbol{y}}^{-1} \left\{ m(\boldsymbol{\xi'}) \int_{\mathbb{R}^d} \delta(\boldsymbol{\xi'} + \boldsymbol{\xi}) e^{i\boldsymbol{x} \cdot \boldsymbol{\xi}} m(\boldsymbol{\xi}) \hat{K}(\boldsymbol{\xi}) d\boldsymbol{\xi} \right\} \\ &= \frac{1}{\sqrt{2\pi}} \int_{\mathbb{R}^d} e^{i\boldsymbol{y} \cdot \boldsymbol{\xi'}} \left\{ m(\boldsymbol{\xi'}) \int_{\mathbb{R}^d} \delta(\boldsymbol{\xi'} + \boldsymbol{\xi}) e^{i\boldsymbol{x} \cdot \boldsymbol{\xi}} m(\boldsymbol{\xi}) \hat{K}(\boldsymbol{\xi}) d\boldsymbol{\xi} \right\} d\boldsymbol{\xi'} \\ &= \frac{1}{\sqrt{2\pi}} \int_{\mathbb{R}^d} \int_{\mathbb{R}^d} e^{i\boldsymbol{y} \cdot \boldsymbol{\xi'}} \delta(\boldsymbol{\xi'} + \boldsymbol{\xi}) e^{i\boldsymbol{x} \cdot \boldsymbol{\xi}} m(\boldsymbol{\xi}) m(\boldsymbol{\xi'}) \hat{K}(\boldsymbol{\xi}) d\boldsymbol{\xi'} d\boldsymbol{\xi} \\ &= \frac{1}{\sqrt{2\pi}} \int_{\mathbb{R}^d} e^{-i\boldsymbol{y} \cdot \boldsymbol{\xi}} e^{i\boldsymbol{x} \cdot \boldsymbol{\xi}} m(\boldsymbol{\xi}) m(-\boldsymbol{\xi}) \hat{K}(\boldsymbol{\xi}) d\boldsymbol{\xi}. \end{aligned}$$

□

When training a Gaussian process, it is advantageous to *standardize* the data [**223**] so that $\boldsymbol{x}, \boldsymbol{y}, \theta \sim \mathcal{O}(1)$ when possible. In the framework discussed here, this

reduces the difficulty of computing the kernel functions in (5.19) by restricting the frequency and support of the integrands. When necessary, standardization for the applications considered here can be performed by rescaling the values and positions of the data point by appropriate constants. Once the differential equation is learned for the scaled solution $u_{\text{scaled}} = Au(Bx)$, the true coefficients can be obtained via inverse scaling. This is discussed in detail for an example in Section 5.7.

Although numerical calculation of the above integrals can be performed using Gauss-Hermite quadrature, this is not optimal as the fractional-order monomial $m(\boldsymbol{\xi})$ is not smooth at the origin. To obtain faster convergence with the number of quadrature points, a superior choice is generalized Gauss-Laguerre quadrature, involving a weight function of the form $x^{\alpha_{\text{gGL}}}e^{-x}$ for $\alpha_{\text{gGL}} > -1$:

$$\int_0^\infty f(x)dx = \int_0^\infty x^{\alpha_{\text{gGL}}}e^{-x}\left[e^x x^{-\alpha_{\text{gGL}}}f(x)\right]dx = \sum_i^n w_i e^{x_i} x_i^{-\alpha_{\text{gGL}}} f(x_i).$$

In practice, it is essential for α_{gGL} to match the fractional part of the power of the monomial in the integrand f, as the remainder yields a smooth function. We use the Golub-Welsch algorithm to find the nodes, but compute the weights by evaluating the generalized Gauss-Laguerre polynomial at these nodes for higher relative accuracy.

We describe two examples and discuss the convergence of the numerical Gauss-Laguerre quadrature in each one. First, consider the left-sided Riemann-Louiville derivative $\mathcal{L}_x = {}_{-\infty}^{RL}D_x^\alpha$ in one dimension, which involves $m(\xi) = (-i\xi)^\alpha$ in the above

formulas. Owing to the symmetry of $\hat{K}(\xi)$, one can write

$$\begin{aligned}
{}^{RL}_{-\infty}D^{\alpha}_{x}k &= \frac{1}{\sqrt{2\pi}}\int_{-\infty}^{\infty} e^{i(x-y,\xi)}(-i\xi)^{\alpha}\hat{K}(\xi)d\xi \\
&= \frac{1}{\sqrt{2\pi}}\left[\int_{0}^{\infty} e^{i(x-y,\xi)}(-i\xi)^{\alpha}\hat{K}(\xi)d\xi + \int_{-\infty}^{0} e^{i(x-y,\xi)}(-i\xi)^{\alpha}\hat{K}(\xi)d\xi\right] \\
&= \frac{1}{\sqrt{2\pi}}\left[\int_{0}^{\infty} e^{i(x-y,\xi)}(-i\xi)^{\alpha}\hat{K}(\xi)d\xi + \int_{0}^{\infty} \overline{e^{i(x-y,\xi)}(-i\xi)^{\alpha}}\hat{K}(\xi)d\xi\right] \\
&= \frac{2}{\sqrt{2\pi}}\int_{0}^{\infty} \mathrm{Re}\left[e^{i(x-y,\xi)}(-i\xi)^{\alpha}\hat{K}(\xi)\right]d\xi
\end{aligned}$$

Similarly,

$${}^{RL}_{-\infty}D^{\alpha}_{y}\left[{}^{RL}_{-\infty}D^{\alpha}_{x}k\right] = \frac{2}{\sqrt{2\pi}}\int_{0}^{\infty} \mathrm{Re}\left[e^{i(x-y,\xi)}(-i\xi)^{\alpha}(i\xi)^{\alpha}\hat{K}(\xi)\right]d\xi.$$

These integrals call for generalized Gauss-Laguerre quadrature to be performed with $\alpha_{\mathrm{gGL}} = \alpha$ for ${}^{RL}_{-\infty}D^{\alpha}_{x}k$ and $\alpha_{\mathrm{gGL}} = 2\alpha$ for ${}^{RL}_{-\infty}D^{\alpha}_{y}\left[{}^{RL}_{-\infty}D^{\alpha}_{x}k\right]$. Using the Matérn kernel with $\nu = 5/2$ as an example, the convergence of the error with the number of quadrature points is shown in Table 1. The MATLAB `integral` function is used for reference when computing the error. The setup for working with the right-sided Riemann-Louiville derivative, or for the one-dimensional fractional Laplacian, is entirely similar.

Function, with $\mathcal{L}_x =_x^{RL} D_\infty^{1/2}$	θ^2	$L^\infty[-1,1]$-norm of error as function of $(x-y)$ @ number of quadrature points			
		8	16	32	64
$M_{\frac{5}{2}}(x-y)$	$\frac{1}{10}$	1.190e-02	3.468e-04	2.917e-06	2.876e-07
	1	5.126e-03	8.029e-06	3.741e-07	3.204e-07
	10	8.163e-02	1.446e-02	2.378e-04	4.188e-06
$\mathcal{L}_x M_{\frac{5}{2}}(x-y)$	$\frac{1}{10}$	4.752e-02	1.991e-03	2.822e-05	3.315e-06
	1	6.179e-03	9.528e-05	2.524e-07	1.634e-07
	10	6.937e-02	9.915e-03	3.456e-04	2.828e-06
$\mathcal{L}_x\mathcal{L}_y M_{\frac{5}{2}}(x-y)$	$\frac{1}{10}$	1.624e-01	8.980e-03	2.277e-04	3.449e-06
	1	1.006e-03	1.515e-04	9.092e-07	9.642e-07
	10	6.571e-02	4.774e-03	3.370e-04	1.217e-06

TABLE 1. L^∞ error in computing the Matérn kernel $M_{\frac{5}{2}}(x-y)$ and the kernel blocks $\mathcal{L}_x M_{\frac{5}{2}}(x-y)$ and $\mathcal{L}_x\mathcal{L}_y M_{\frac{5}{2}}(x-y)$, with $\mathcal{L}_x =_x^{RL} D_\infty^{1/2}$, on $[-1,1]$ using generalized Gauss-Laguerre quadrature.

Next we consider the fractional Laplacian $\mathcal{L} = (-\Delta)^{\alpha/2}$ in two dimensions. This involves the multiplier $m(\boldsymbol{\xi}) = |\boldsymbol{\xi}|^\alpha = |\xi_1^2 + \xi_2^2|^{\alpha/2}$. We transform the integrals into polar coordinates:

$$(-\Delta_x)^{\alpha/2}k = \frac{1}{\sqrt{2\pi}}\int_0^{2\pi}\int_0^\infty e^{i\langle \boldsymbol{x}-\boldsymbol{y},(r\cos\theta, r\sin\theta)\rangle} r^\alpha \hat{K}(r\cos\theta, r\sin\theta) r dr d\theta.$$

$$(-\Delta_y)^{\alpha/2}(-\Delta_x)^{\alpha/2}k = \frac{1}{\sqrt{2\pi}}\int_0^{2\pi}\int_0^\infty e^{i\langle \boldsymbol{x}-\boldsymbol{y},(r\cos\theta, r\sin\theta)\rangle} r^{2\alpha} \hat{K}(r\cos\theta, r\sin\theta) r dr d\theta.$$

The quadrature of these integrals is performed using the trapezoid rule in θ and generalized Gauss-Laguerre quadrature in r, using $\alpha_{\text{gGL}} = \alpha + 1$ for $(-\Delta_x)^{\alpha/2}k$ and $\alpha_{\text{gGL}} = 2\alpha + 1$ for $(-\Delta_y)^{\alpha/2}(-\Delta_x)^{\alpha/2}k$. Using the product multivariate Matérn kernel $M_{\frac{5}{2}}M_{\frac{7}{2}}$ as an example, convergence with respect to the number of quadrature points in r is show in in Table 2, where 64 quadrature points in θ and 8, 16, 32, 64

quadrature points in r are used. Reference answers were generated by nesting the MATLAB `integral` function.

The examples in the following sections are built by defining the Matern kernels in Mathematica and performing derivatives with respect to the hyperparameters symbolically. The expressions are ported into MATLAB code where Gauss-Laguerre quadrature with appropriate α_{gGL} is used to compute the $\mathcal{NLML}$ (5.6) as well as the derivatives of the $\mathcal{NLML}$ with respect to the parameters. For our purposes, 64 quadrature points in one dimension and 64x64 quadrature points (as described above) in two dimensions is sufficient.

Function, with $\mathcal{L}_x = (-\Delta_x)^{\alpha/2}$	θ^2	$L^\infty[-1,1]^2$-norm of error as function of $(\boldsymbol{x}-\boldsymbol{y})$ @ number of quadrature points			
		8	16	32	64
$M_{\frac{5}{2}}M_{\frac{7}{2}}$	$\frac{1}{10}$	5.406e-02	6.201e-04	8.248e-06	9.939e-05
	1	1.368e-02	3.611e-04	2.659e-06	2.955e-06
	10	7.955e-01	8.385e-02	3.873e-03	2.006e-05
$\mathcal{L}_x\left[M_{\frac{5}{2}}M_{\frac{7}{2}}\right]$	$\frac{1}{10}$	2.025e-01	3.922e-03	6.705e-05	3.842e-05
	1	2.769e-02	9.611e-04	8.921e-06	8.977e-06
	10	3.717e-01	2.013e-02	3.340e-03	1.515e-05
$\mathcal{L}_x\mathcal{L}_y\left[M_{\frac{5}{2}}M_{\frac{7}{2}}\right]$	$\frac{1}{10}$	4.759e-01	2.644e-02	5.154e-04	7.347e-05
	1	8.117e-02	1.449e-03	8.740e-06	9.848e-06
	10	8.713e-02	4.553e-02	1.535e-03	8.209e-06

TABLE 2. L^∞ error in computing the Matérn kernel $M_{\frac{5}{2}}M_{\frac{7}{2}}(\boldsymbol{x}-\boldsymbol{y})$ and the kernel blocks $\mathcal{L}_{\boldsymbol{x}}M_{\frac{5}{2}}M_{\frac{7}{2}}(\boldsymbol{x}-\boldsymbol{y})$ and $\mathcal{L}_{\boldsymbol{x}}\mathcal{L}_{\boldsymbol{y}}M_{\frac{5}{2}}M_{\frac{7}{2}}(\boldsymbol{x}-\boldsymbol{y})$ on the square $[-1,1]^2$. The same correlation parameter θ is used for both kernels. Quadrature is performed generalized Gauss-Laguerre quadrature in the polar variable r with 8, 16, 32, and 64 quadrature points, with a fixed number of 64 trapezoid rule quadrature points in θ.

5.4 A Basic Example

5.4.1 One Dimension

In this section, we will illustrate the methodology to discover the parameters C and α in the fractional elliptic equation

$$C(-\Delta)^{\alpha/2}u = f$$

in one and two space dimensions from data on u and f.

Following the time-independent framework, this means that we must optimize the negative log marginal likelihood (5.6), where in the covariance matrix (5.7), the kernels are given by the integral formulas (5.19). In the latter formulas, the multiplier m and the Fourier transform $\hat{K}$ of the stationary prior kernel must be specified; the multiplier m corresponding to the operator $C(-\Delta)^{\alpha/2}$ is $m(\xi) = C|\xi|^{\alpha}$ in one dimension, and $m(\xi_1, \xi_2) = C|\xi_1^2 + \xi_2^2|^{\alpha/2}$ in two dimensions. We choose to use the Matérn kernel $k_{uu} = K = M_\nu$, given by (5.15) in one dimension, with a tensor product (5.16) of Matérn kernels $M^{\times}_{\nu_1,\nu_2}$ in two dimensions. Thus, by equations (5.17), $\hat{K} = \hat{M}_\nu(\xi)$ in one dimension, and $\hat{K} = \hat{M}_{\nu_1}(\xi_1)\hat{M}_{\nu_1}(\xi_2)$ in two dimensions. This completes the description of the covariance kernel.

In the one-dimensional case the solution/RHS pair

$$u = e^{-x^2}, \quad f = \frac{C}{\sqrt{2\pi}} \int_{-\infty}^{\infty} e^{ix\xi} |\xi|^{\alpha} \frac{e^{-\xi^2/4}}{\sqrt{2}} d\xi$$

is used. Three data sets are generated for three experiments. In all three experiments, we use the above solution/RHS pair to generate data with exact $C = 1.25, \quad \alpha = \sqrt{2} \approx 1.4142$. The Matérn kernel with fixed $\nu = 11/2$ is used to discover the parameters, and the initial parameters for the optimization are taken to be $\theta = 1, \sigma = 1, \alpha = 1.0, C = 0.5$.

(1) In the first experiment, 7 data points at $\boldsymbol{X}_u$ for u and 11 data points $\boldsymbol{X}_f$ for f are generated via latin hypercube sampling. No noise is added. The GP regression for the first experiment is shown in Figure 1. The equation parameters recovered are $\alpha = 1.40158$ and $C = 1.25840$, which are within 1% of the true values.

(2) The second experiment involves greater noise in the data. 20 data points for each of u and f are generated in the same way, but normal random noise of standard deviation 0.1 for u and 0.2 for f is added to the data. The parameters learned in the second experiment are $\alpha = 1.51151$ and $C = 1.18099$, which are within 7% and 6% of the true values, respectively. The regression is shown in Figure 2. There, we have also plotted the twice the standard deviation of the Gaussian process plus twice the standard deviation of the learned noise, $2\sigma_{n_u}$ and $2\sigma_{n_f}$ (in the previous experiment, these learned parameters were miniscule).

(3) The third experiment involves noiseless data spread over a wider window in featureless regions of the solution pair u/f. 10 data points for each of u and f are used. The parameters learned are $\alpha = 1.63138, C = 0.93670$, which are within 16% and 7% of the true values, respectively. The regression is shown in Figure 3.

The second and third experiments, respectively, demonstrate the effect of noise and overfitting on the learned parameters, with significantly greater discrepancies from the values used to generate data compared to the first experiment. Both are well-known hazards in the interpolation of spatial data. As the discovery of parameters is encoded into a problem of interpolation, all inaccuracies of spatial interpolation can be expected to affect the accuracy of the learned parameters.

REMARK 5.21. All reported wall times in this Chapter were obtained using four threads (default MATLAB vectorization) on an Intel i7-6700K at stock settings.

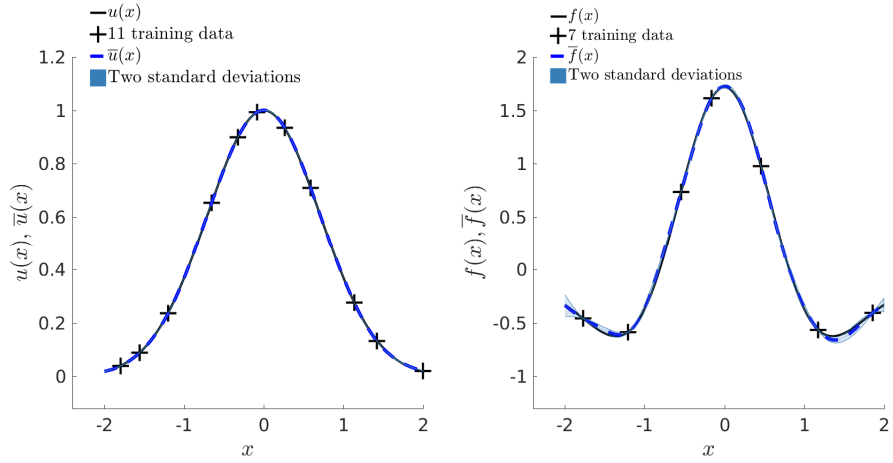

FIGURE 1. Result of training the GP in the one-dimensional example on 7 noise-free data points for u and 11 data points for f on $[-2, 2]$. The trained parameters are are within 1% of the true values. *Optimization wall time: 7 minutes. Roughly 1400 function evaluations.*

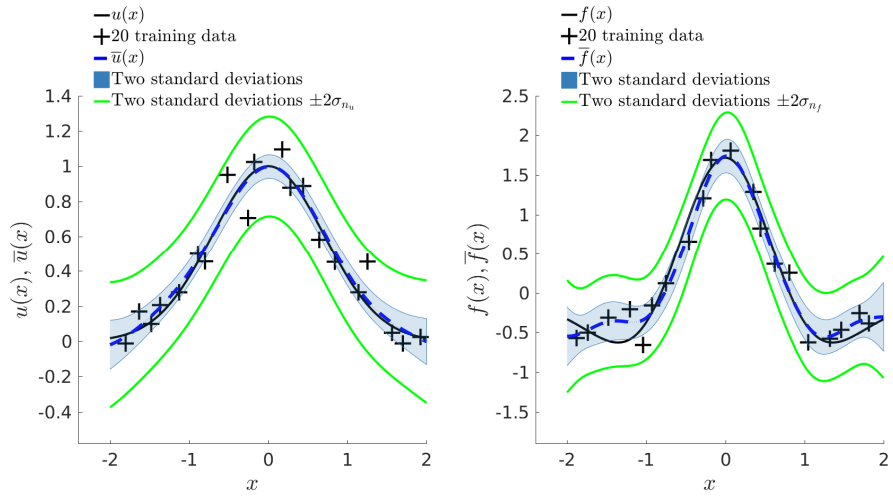

FIGURE 2. Result of training the GP on 20 noisy data points for each of u and f on $[-2, 2]$. The trained parameters are within 7% percent of the true values. For this example, we have also plotted in green two standard deviations of the GP, *plus* two times the learned noise parameter $\sigma_{n_u}/\sigma_{n_f}$. *Optimization wall time: 38 seconds. Roughly 100 function evaluations.*

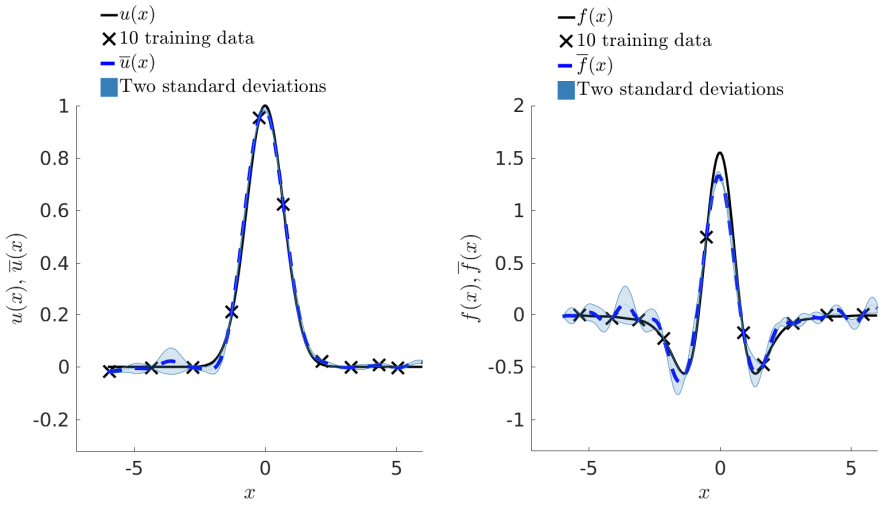

FIGURE 3. Overfitting. 10 noiseless data points on $[-6, 6]$; the poor choice of window and abundance of zero data results in high standard deviation and inaccurate parameters. The trained parameters are within 16% of the true values. Note the poor fitting of the peaks of f and the high standard deviation near the areas of zero data, despite the noiseless data. This problematic regression results in less accurate α. *Wall time: 80 seconds.*

5.4.2 Two Dimensions

Next, we study the effect of the number of data points on the learned parameters. In this two dimensional example, the exact solution pair used to generate data is now

$$u = e^{-x_1^2 - x_2^2}, \quad f = \frac{C}{2\pi} \int_{-\infty}^{\infty} \int_{-\infty}^{\infty} e^{ix_1\xi_1} e^{ix_2\xi_2} |\xi_1^2 + \xi_2^2|^{\alpha/2} \frac{e^{-\xi_1^2/4 - \xi_2^2/4}}{2} d\xi_1 d\xi_2$$

with exact $C = 1, \alpha = \sqrt{3} \approx 1.7321$. Again, the Matérn parameter

$$\nu = \nu_1 = \nu_2 = 11/2$$

is used. The initial parameters for the optimization are

$$\sigma = 1, \theta_1 = 1, \theta_2 = 1, \alpha = 2, C = 1.5.$$

We generate the same number of data for each of u and f, at positions given by using latin hypercube sampling on $[-2,2] \times [-2,2]$. The parameters

$$\alpha = \sqrt{3} \approx 1.7321 \text{ and } C = 1$$

were used to generate data. In the first experiment, 20 points for each of f and u were used to train; in the second experiment, 40 points for each of f and u were used. The setup and results of the training are shown in Figures 4, 5, and 6.

In the 20/20 data point experiment (wall time 11 minutes), the learned parameters are $\alpha = 1.76516$ and $C = 0.81762$, with hyperparameters $\sigma = 0.02813$, $\theta_1 = 1.73731$, and $\theta_2 = 1.42719$. This value of α is quite accurate, but the value of C has an error of 20%. In the 40/40 data point experiment (wall time 74 minutes), the learned parameters are $\alpha = 1.72888$ and $C = 0.99977$, within 1% of the true values, with hyperparameters $\sigma = 0.0213$, $\theta_1 = 1.581$, and $\theta_2 = 1.586$.

These examples in one- and two-dimensions demonstrate the feasiblity of implementing the fractional kernels as described in the previous sections and the accuracy of discovered parameters, even with noise or small data.

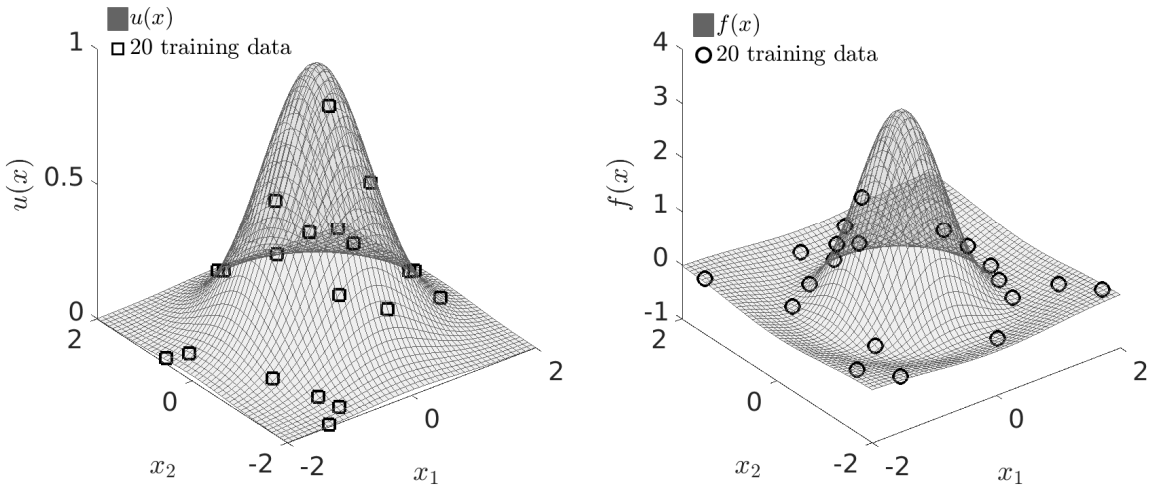

(A) 20 data points for u and f

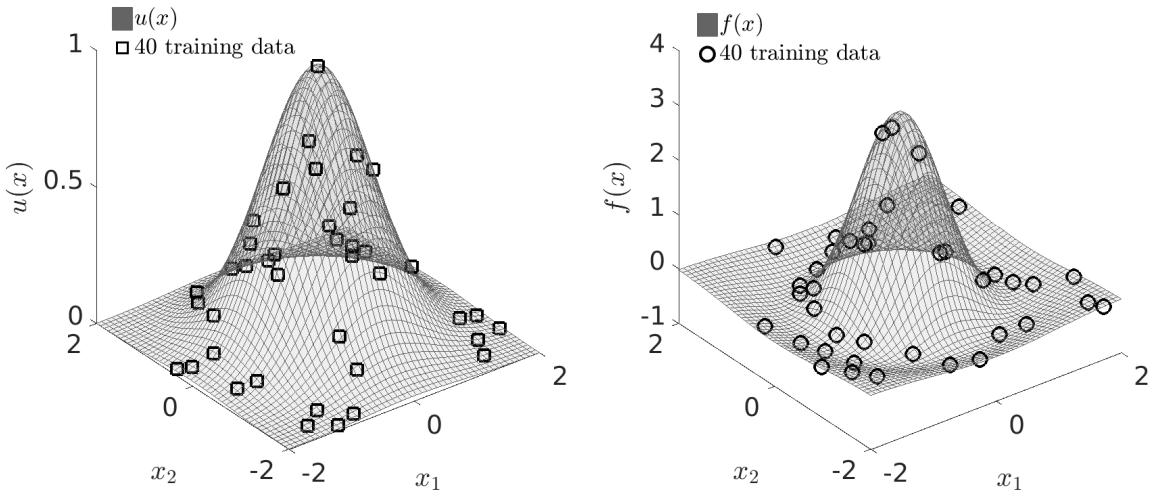

(B) 40 data points for u and f

FIGURE 4. Surface plots of the exact u (left) and f (right), which solve the equation with parameters $C = 1$ and $\sqrt{3} \approx 1.7321$, that are used to generate data. Data points on each of u (squares) and f (circles) are shown on these surface plots. The top row (A) shows the data points on u/f for the 20/20 data point simulation, and the bottom row (B) shows the data points for the 40/40 data point simulation.

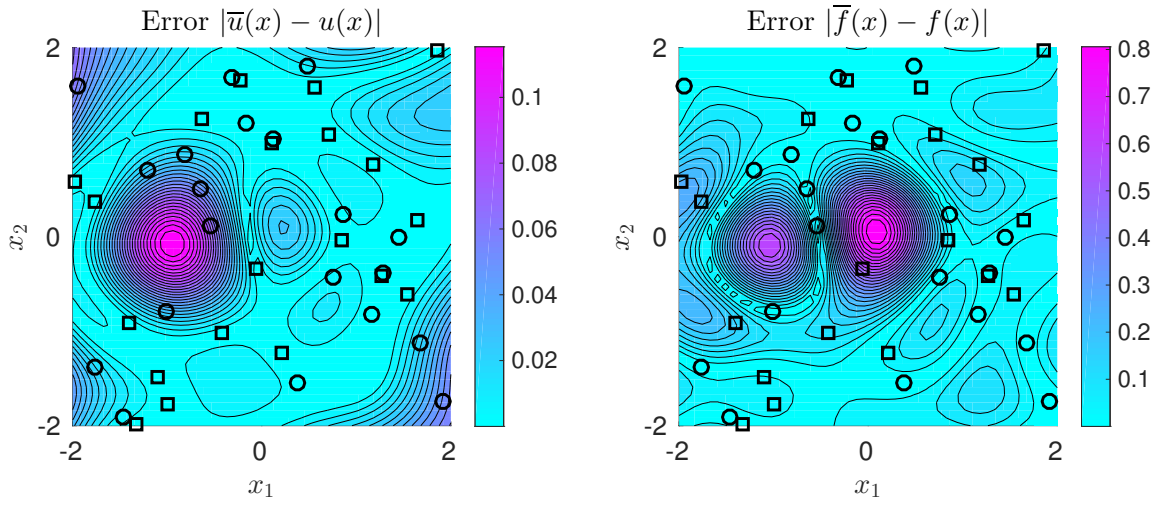

(A) 20 data points for u and f

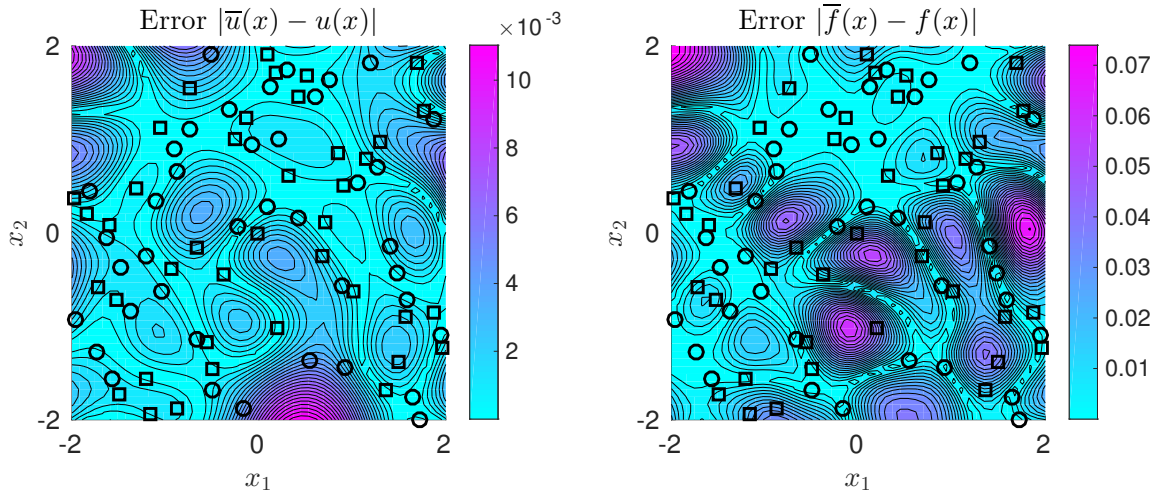

(B) 40 data points for u and f

FIGURE 5. Error between the mean of the trained GP for u (left) and f (right) and the exact u, f used to generate data. The top row (A) shows the error for u/f for the 20/20 data point simulation, and the bottom row (B) shows the error for the 40/40 data point simulation. Note that the positions of data points for u are illustrated by squares, while data points for f are illustrated by circles.

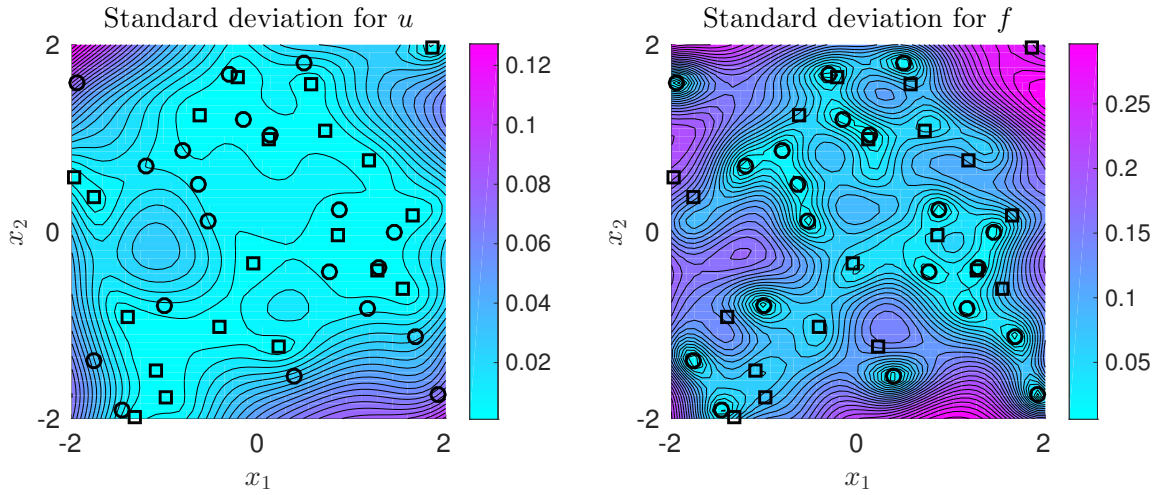

(A) 20 data points for u and f

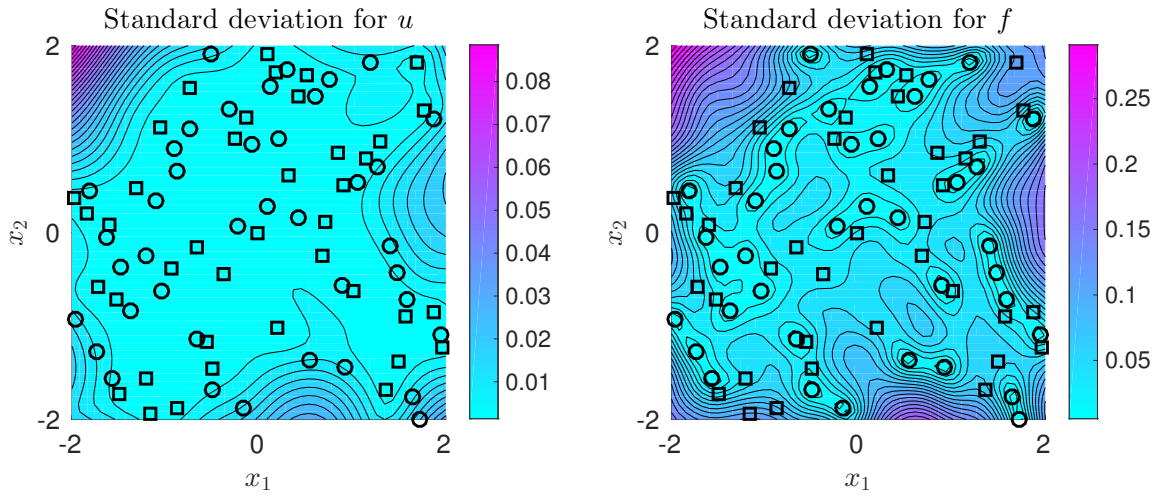

(B) 40 data points for u and f

FIGURE 6. Standard deviation of the trained GP for u (left) and f (right) and the exact u, f used to generate data. The top row (A) shows the standard deviation for u/f for the 20/20 data point simulation, and the bottom row (B) shows the standard deviation for the 40/40 data point simulation. The positions of data points for u are illustrated by squares, while data points for f are illustrated by circles.

5.5 Discovering and Interpolating Integer Order Models

As discussed in the introduction, fractional-order differential operators interpolate between classical differential operators of integer order, reducing the task of choosing a "dictionary" of operators of various orders and the assumptions that this entails. The user controls the parsimony directly, by choosing the number of fractional terms in the candidate equation. For example, the model in Section 5.4 was constrained to be of parsimony one, since it includes a single differential operator of fractional order. This raises several questions, such as: Can the method be used to discover integer-order operators when they drive the true dynamics? What can be expected if the user-selected parsimony is lower than the parsimony of the "true" model driving the data? Can lower-parsimony models still be used to model dynamics? To explore these questions, we consider the parametrized model

$$\frac{\partial u}{\partial t} - C\left({}^{RL}_{-\infty}D^{\alpha}_{x}\right)u = 0, \tag{5.22}$$

for $u(t,x), t \in \mathbb{R}^+, x \in \mathbb{R}$. where the left-sided Riemann-Louiville derivative ${}^{RL}_{-\infty}D^{\alpha}_{x}u$ was defined in (5.14). Note that

$$\alpha = 1 \implies {}^{RL}_{-\infty}D^{\alpha}_{x}u = -\partial u/\partial x, \quad \alpha = 2 \implies {}^{RL}_{-\infty}D^{\alpha}_{x}u = \partial^2 u/\partial x^2.$$

For $\alpha = 1, C = 1$, (5.22) reduces to the advection equation (with speed $C = 1$)

$$\frac{\partial u}{\partial t} + \frac{\partial u}{\partial x} = 0, \tag{5.23}$$

and for $\alpha = 2, C = 1$, to the diffusion equation (with diffusion coefficient $k = 1$)

$$\frac{\partial u}{\partial t} - \frac{\partial^2 u}{\partial x^2} = 0. \tag{5.24}$$

We perform four experiments. Importantly, we learn these equations using the time-stepping methodology, optimizing (5.6), where the kernel blocks are given by (5.12) and (5.13). We take $k = M_{\frac{19}{2}}$ (effectively a squared-exponential kernel) and again use (5.19) with generalized Gauss-Laguerre quadrature to evaluate the action of the fractional derivatives on k. In all of experiments, we generate data that satisfies the initial condition $u_0 = \sin(x)$. We choose $\Delta t = 0.1$ and $n = 3$; thus, $u^n = u(t = 0.3, x), u^{n-1} = u(t = 0.2, x)$. The GP is trained on 30 data points for each of these time slices. The experiments are

(1) Data generated from $u(t, x) = \sin(x - t)$, the solution to the advection equation (5.23). We learn the order α and coefficient C in (5.22); the exact $\alpha = 1$.

(2) Data generated from $u(t, x) = e^{-t}\sin(x)$, the solution to the heat equation (5.24). We learn the order α and coefficient C in (5.22); the exact $\alpha = 2$.

(3) Data generated from $u(t, x) = e^{-t}\sin(x-t)$, the solution to the integer order advection-diffusion equation

$$\frac{\partial u}{\partial t} + \frac{\partial u}{\partial x} - \frac{\partial^2 u}{\partial x^2} = 0.$$

We learn the order α and coefficient C in (5.22). Note that this archetype is limited to only one space-differential operator; we will see that the algorithm will select best order $1 < \alpha < 2$ to capture both the advection and diffusion in the data.

(4) The same advection-diffusion data as in experiment 3, but with the two term, four parameter candidate equation

$$\frac{\partial u}{\partial t} - C_1 \left({}^{RL}_{-\infty}D^{\alpha_1}_x\right) u - C_2 \left({}^{RL}_{-\infty}D^{\alpha_2}_x\right) u = 0$$

We note that all of these experiments call for only a *single* fractional-order dictionary term; even Experiment 4 uses two copies of the same archetype. Experiments 1-3 use initial parameters $\alpha = 0.5$ and $C = 1.25$, and Experiment 4 uses $\alpha_1 = 0.5$, $\alpha_2 = 1.5, C_1 = 1.25, C_2 = 0.75$.

In Experiments 1 and 2, we note that fractional-order parameters are discovered close to (within 5% of) the true integer-order parameters. In this sense, the true dynamics can be considered recovered. The numerical difference from the true parameters despite the high number of data points (30 per slice) is likely due to approximation error from the backwards Euler approximation (5.9), and may be resolved by using higher-order differentiation with more time slices [**169**], as simply taking Δt to be extremely small may cause the optimization to be dominated by numerical error in computing the kernels.

Experiment 3 shows what occurs when the user-defined parsimony is less than the true dynamics used to generate data. The optimizer still converges, and to a sensible answer – the result can be interpreted as an interpolation of the two integer-order operators in the true dynamics. Moreover, as shown in Figure 7, near the time of the data used to train the model, and even much later, the fractional dynamics are a good approximation to the true dynamics, while being simpler in the sense of being driven by only one spatial derivative. This leads to potential applications of interpolating complex systems using lower-parsimony fractional models.

In Experiment 4, the parsimony was increased with the inclusion of an additional indepedent copy of the fractional archetype. The advection-diffusion equation is recovered with parameters within 5% of the true values. Thus, with a single fractional archetype and user-controlled parsimony, it is possible to discover advection, diffusion, advection-diffusion, as well as a single-term fractional interpolation of advection-diffusion.

Exp.	Data	Candidate	Parameters Learned
1	Advection: $\frac{\partial u}{\partial t} + \frac{\partial u}{\partial x} = 0$	$\frac{\partial u}{\partial t} - C\left({}^{RL}_{-\infty}D^{\alpha}_{x}u\right) = 0$	$C = 1.01$ $\alpha = 0.97$
2	Diffusion: $\frac{\partial u}{\partial t} - \frac{\partial^2 u}{\partial x^2} = 0$	$\frac{\partial u}{\partial t} - C\left({}^{RL}_{-\infty}D^{\alpha}_{x}u\right) = 0$	$C = 1.05$ $\alpha = 2.00$
3	Advection-Diffusion: $\frac{\partial u}{\partial t} + \frac{\partial u}{\partial x} - \frac{\partial^2 u}{\partial x^2} = 0$	$\frac{\partial u}{\partial t} - C\left({}^{RL}_{-\infty}D^{\alpha}_{x}\right)u = 0$	$C = 1.49$ $\alpha = 1.47$
4	Advection-Diffusion: $\frac{\partial u}{\partial t} + \frac{\partial u}{\partial x} - \frac{\partial^2 u}{\partial x^2} = 0$	$\frac{\partial u}{\partial t} - C_1\left({}^{RL}_{-\infty}D^{\alpha_1}_{x}\right)u - C_2\left({}^{RL}_{-\infty}D^{\alpha_2}_{x}\right)u = 0$	$C_1 = 1.05$ $\alpha_1 = 0.98$ $C_2 = 1.03$ $\alpha_2 = 1.96$

TABLE 3. Results of the four experiments. *Wall times: roughly 11/14/13/21 minutes.*

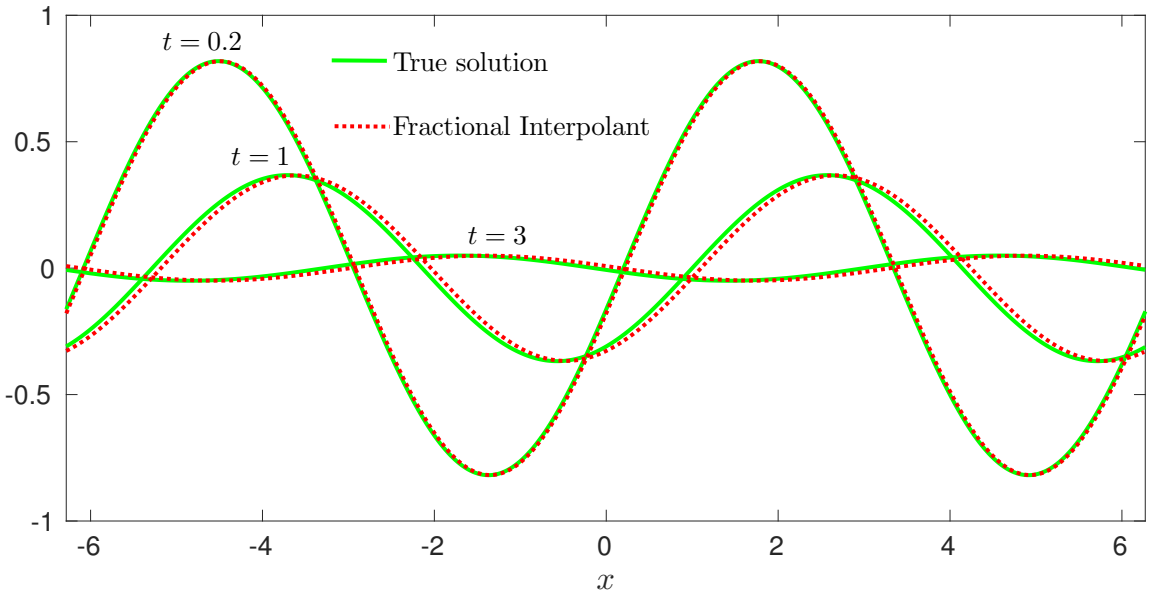

FIGURE 7. Comparison of the true advection-diffusion dynamics with the fractional-order dynamics learned in Experiment 3. Near the time ($t = 0.2$) when the equation was learned, the fractional-dynamics are a good approximation, although for later time t the dynamics are increasingly out-of-phase.

5.6 Learning Fractional Diffusion from α-stable Time Series

We now consider an example that will set up our application to financial time series data and explore the effect of the Matérn parameter ν. The example will involve identification of α-stable Lévy processes parameters from time series data. Equivalently, the same data is used to identify a fractional-order diffusion equation governing the transition density of the process, of the form

$$\frac{\partial u}{\partial t} = \frac{\gamma^\alpha}{|\cos(\pi\alpha/2)|}\left[p({}_{-\infty}^{RL}D_x^\alpha u) + (1-p)({}_x^{RL}D_\infty^\alpha u)\right], \quad t > 0.$$

where

$$0 < \gamma, \quad 0 < p < 1, \quad 0 < \alpha < 2.$$

The exact solution to this equation (technically, with intial condition a point distribution at zero) is in fact the α-stable probability density

$$S_\alpha(2p-1, \gamma t^{1/\alpha}, 0)$$

with stability parameter α, skewness parameter $2p-1$, scale parameter $\gamma t^{1/\alpha}$, and position parameter 0. See Proposition 5.8 in Meerschaert and Sikorskii [**149**].

Under the ansatz that the increments are drawn from a transition density, a time series X_i, $i = 1, ..., i_{\max}$ can be used to recover the transition densities in the following way. Suppose that the increments occur in units of time Δt. To approximate the transition density $\rho_{n\Delta t}$ at times $n\Delta t$, $n \in \mathbb{N}$, first the collection of increments

$$\{X_{(i+n)\Delta t} - X_{i\Delta t}\}_{i=1,2,...,i_{\max}-k}.$$

is assembled. A histogram of such increments is created and normalized; the result is an empirical probability distribution, and as the number of samples increases, the empirical distribution converges to the probability density function [**212**]. Therefore, if X_t is a time series in which, at each time increment Δt, a space increment is drawn from the α-stable density with parameters skewness $2p-1$, scale $\gamma(\Delta t)^{1/\alpha}$, and position 0, then these empirical histograms $\rho_{n\Delta t}$ will approximate the same density $S_\alpha(2p-1, \gamma(n\Delta t)^{1/\alpha}, 0)$. In other words, $\rho_{n\Delta t}$ will approximate the time-slices $u(t = n\Delta t, x)$ of the solution to equation 5.6. This setup is shown in Figure 8, which illustrates empirical distributions using 1,200 and 120,000 samples.

In preparation for the next section, we will use the much noiser data generated from an α-stable time series of 1,200 steps and parameters $\alpha = \sqrt{2}, p = 0.8$, $\gamma = 1$ and $\Delta t = 0.01$, at times $t = 0.03$ and $t = 0.04$. This is the data shown in the bottom panel of Figure 8. Because we are only seeking an equation that can be associated with an α-stable process, we enforce $0 \leq p \leq 1$ and $0 < \alpha \leq 2$ by placing these variables in sigmoids:

$$p = \frac{1}{1 + \exp[-\tilde{p}]}, \quad \alpha = \frac{2}{1 + \exp[-\tilde{\alpha}]}.$$

The optimization is then over $\tilde{p}$ and $\tilde{\alpha}$. The parameters are initialized as $\alpha = 1.8$, $p = 0.5$, and $\gamma = 1$. Because the data appears quite rough, we have also allowed for variable order ν, optimizing it as an extra hyperparameter, initializing with $\nu = 9/2$.

The result of the training is shown in 9. The trained parameters are $\alpha = 1.38415, p = 0.87519, \gamma = 0.89166, \sigma = 0.05576, \theta = 0.16287$, and $\nu = 14.82891$. First, we note that the equation parameters are roughly within 10% of the values used to generate the data, despite the low number of samples and roughness of the histogram. Next, the learned value of ν, which is much higher than the starting value of 4.5, shows that the Gaussian process was able to learn the noise parameter

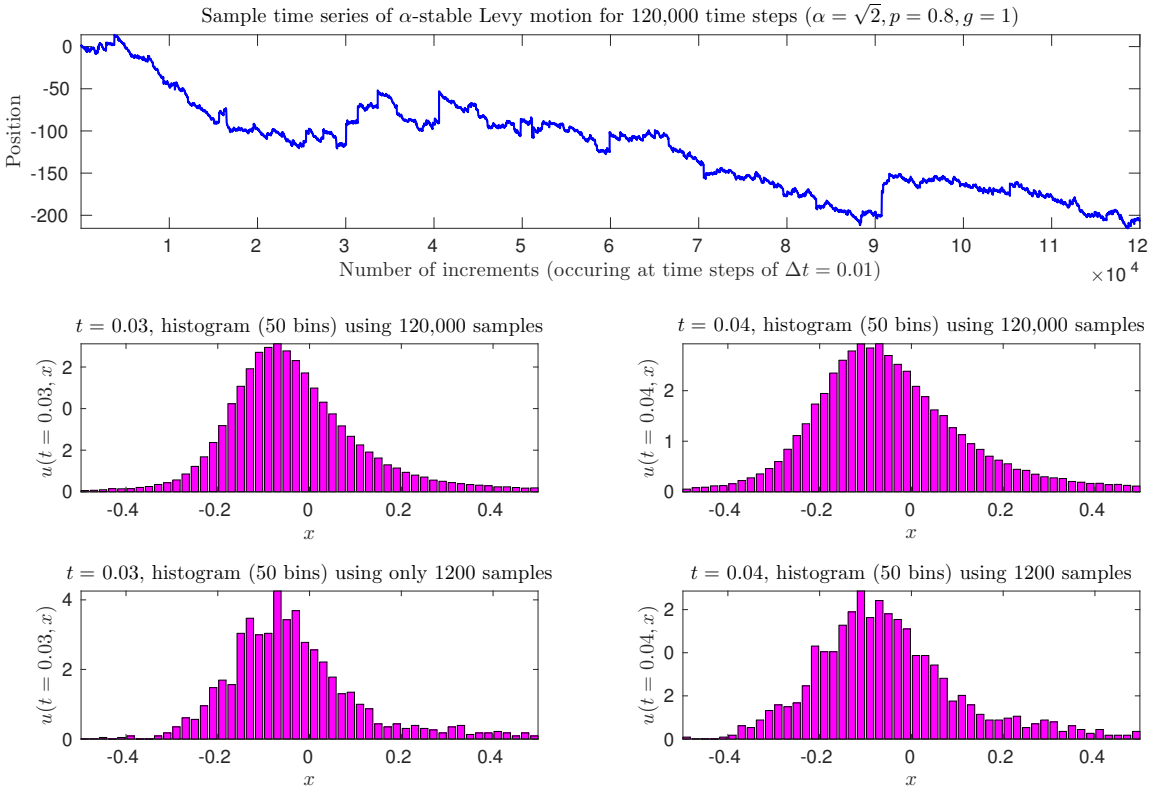

FIGURE 8. Illustration of how data is produced to discover a fractional-order diffusion equation using time series data. The top shows an example α-stable time series with $\alpha = \sqrt{2}, p = 0.8, \gamma = 1$ at time increments of $\Delta t = 0.01$. To approximate the solution at $t = 0.03$, as on the left, a histogram is made of the spatial increments in three units of time along the time series, and normalized. The longer the time series, the more accurate the empirical density will approximate the true density/solution. The middle row shows histograms made with a time series of 120,000 increments, while the bottom shows histograms made with a time series of 1,200 increments.

σ and write off the roughness of the histogram as not intrinsic to the data, so that a low ν value was not required. As higher Matérn kernel M_ν are for practical purposes the same as the squared-exponential kernel and with each other [**177**], we conclude that for such data it is not necessary to utilize a variable-order Matérn kernel, as it prolongs the optimization needlessly. Indeed, performing the same simulation with ν fixed as $9/2$ yields parameters $\alpha = 1.32148, p = 0.80294, \gamma = 0.98273$, which are

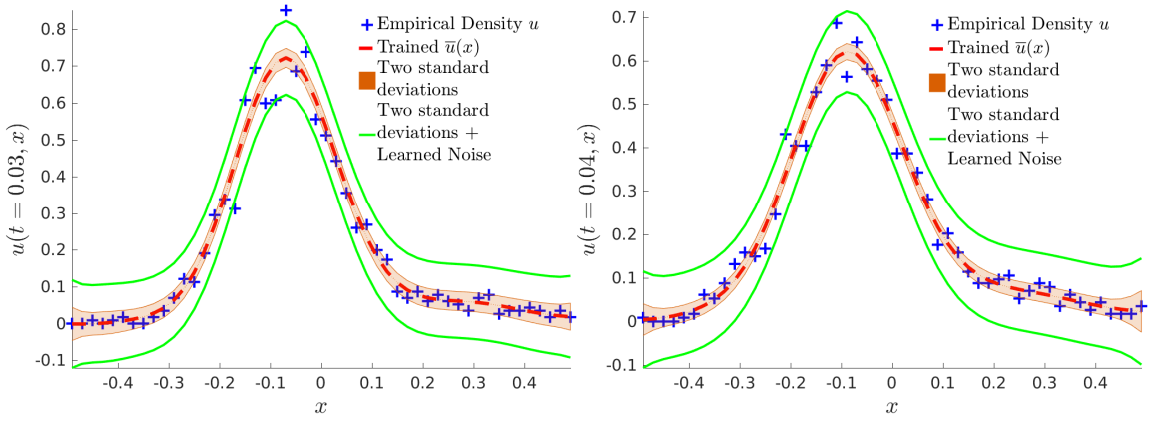

FIGURE 9. Result of training the GP on the synthetic 1200-step α-stable time series data. The blue crosses are the normalized histogram/empirical distribution function data. The red curve/orange bars show the mean/two standard deviations of the trained GP, while the green curve shows two standard deviations $\pm$ the learned noise $2\sigma_n$.

arguably slightly closer to the true values. However, we do not claim this to be true for all applications; in particular, in cases where enough data is available to resolve local behavior clearly, variable-order ν optimization may be critical in training the Gaussian process [**200**].

5.7 Fractional Diffusion for Relative Stock Performance

Many types of Lévy processes – such as α-stable processes – are well known and heavily used in financial modeling due to their heavy tails [**207**, **96**, **35**]. This began with the work of Mandelbrot in 1963 [**141**], who showed that returns of cotton prices are more accurately modeled by an α-stable density with $\alpha = 1.7$ than with a normal density, followed by the work of Fama in 1965 [**73**] arriving at a similar conclusion for daily returns of the Dow Jones Industrial Average. More recent investigations include

α-stable behavior in Mexican financial markets [**10**], as well as financial modeling by more general Lévy processes [**143, 75**]. The implications of heavy tailed behavior in financial processes cannot be underestimated in practice; Wilmott [**222**] gives the following example based on daily data of the S&P 500 from 1980-2004. While a 20% fall in the S&P 500 occured once in this interval of 24 years (the stock market crash of October 19th, 1987) a normal distribution for S&P 500 returns (based on an average volatility of 16.9%) would imply such an event would occur only once in every 2×10^{76} years.

A number of methods have been used to determine the parameters of an α-distribution from empirical data (see Chapter 7 of [**207**] for a summary, as well as [**188**]). A naive approach would be to plot the empirical densities in log-log scale, where the power-law tail would appear linear, and read the stability parameter α from the slope the curve for large argument. This can be misleading because it is not clear for what arguments an α-stable distribution is converged to a power law, nor is the answer simple; it depends on the parameter α, and the density enters into a transitory power law decay with power > 2 before settling into the "true" power law decay with $\alpha < 2$ (see [**33**]). Much more reliable methods include maximum likelihood estimation [**159**] and the generalized method of moments [**44**], which have had good success in practice.

We propose using machine learning of fractional diffusion equations outlined in section 5.6, with empirical distributions as data, to calibrate the parameters of the corresponding α-stable Lévy process. We have demonstrated that such a method can reliably recover the parameters of synthetic data, and can handle very noisy or rough data in Section 5.6. The following simulations use the exact same setup, only with empirical (rather than synthetic) data, to learn the parameters of the equation

$$\frac{\partial u}{\partial t} = \frac{\gamma^\alpha}{|\cos(\pi\alpha/2)|}\left[p({}^{RL}_{-\infty}D^\alpha_x u) + (1-p)({}^{RL}_{x}D^\alpha_\infty u)\right], \quad t > 0.$$

The raw data we take for illustration is the relative stock performance of Intel vs S&P 500. We use the daily closing values of each stock in a 5-year period from 2013/02/27 to 2018/02/26. We normalize each stock to the "initial" value on 2013/02/27, then take ratio of the two stocks (Intel/SP500) to yield the time series that will be trained on. The time series used in the procedure are illustrated in Figure 10.

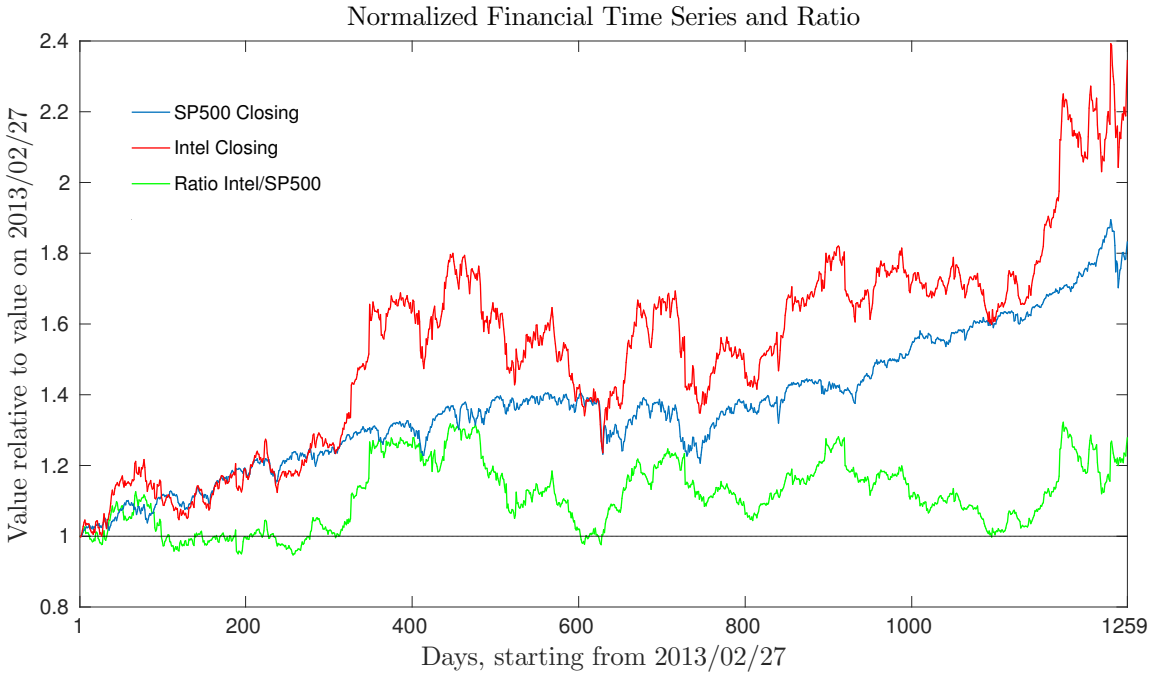

FIGURE 10. The financial time series data used to calibrate the model. The blue curve shows the daily closing values of the S&P 500, normalized to the value on 2013/02/27, while the red curve shows the same for Intel. The ratio (which measures the performance of Intel relative to the S&P 500 index in the same time period) is shown in green.

The natural time intervals here are $\Delta t = 1$ days. Thus, in (5.9) and in the kernels, $\Delta t = 1$, and $t = n$, where $n \in \mathbb{N}$. The parameter γ can, in principle, capture any space-time scaling relation for the diffusion. However, very small or very large values of γ cause optimization instability. Thus, the time series values are rescaled by a constant factor factor $\sqrt{i_{\max}}$ – the scaling for Brownian motion – prior to fine

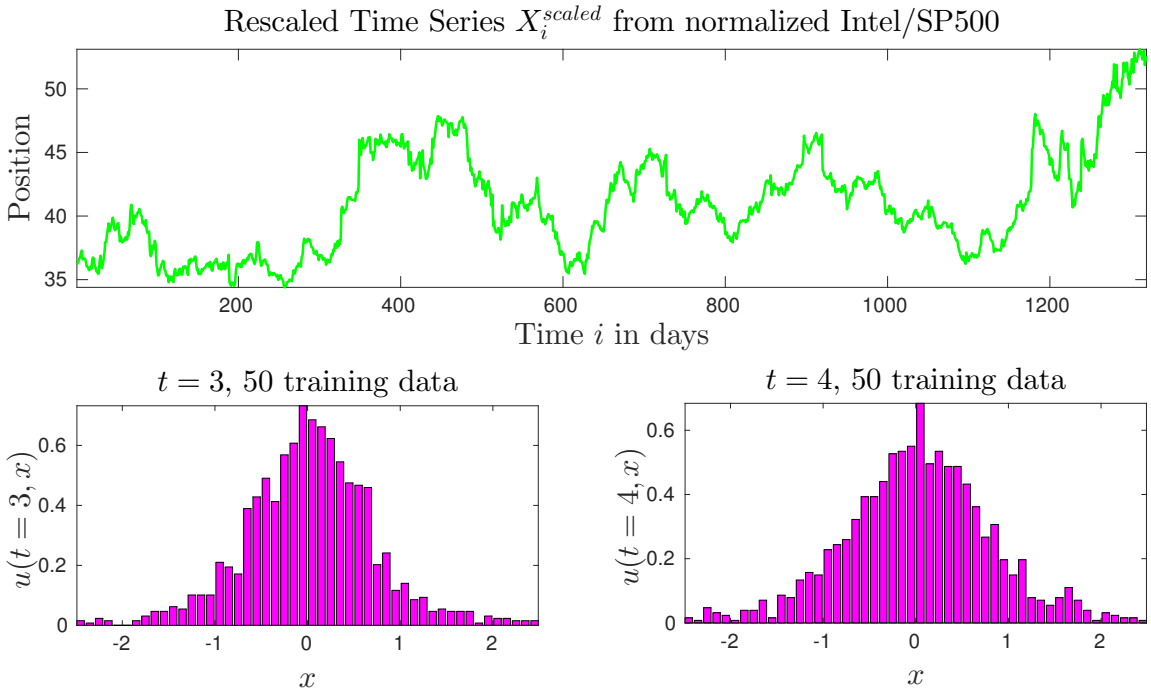

FIGURE 11. (top) The rescaled time series given by (5.25). The relative (normalized) Intel/SP500 stock is multiplied by $\sqrt{1259}$ to put it in the same window as standard Brownian motion. (bottom) The empirical histograms to be used as data to discover the fractional-order diffusion equation.

tuning with γ:

$$X_i^{\text{scaled}} = \sqrt{i_{\max}} X_i = \sqrt{1259} X_i. \tag{5.25}$$

This ensures $\gamma = \mathcal{O}(1)$, because it places X_i in roughly the same window as a standard 2-stable process (Brownian Motion) with the same number of steps. After this preprocessing, a value of γ^{scaled} will be learned for the scaled diffusion. The original diffusion then has true scaling parameter

$$\gamma = \gamma^{\text{scaled}} / \sqrt{i_{\max}} = \gamma^{\text{scaled}} / \sqrt{1259}.$$

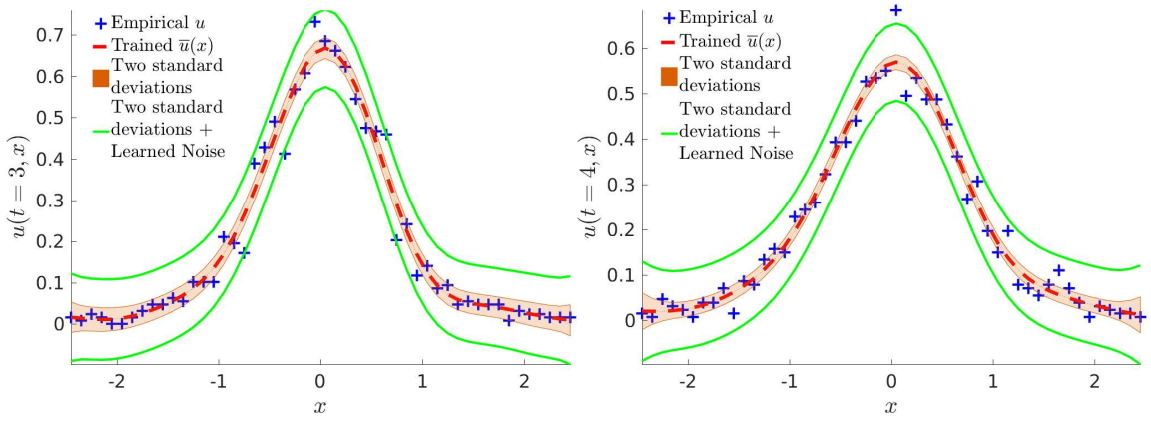

FIGURE 12. The result of training the GP using the histogram data in Figure 11. The blue crosses are the normalized histogram/empirical distribution function data. The red curve/orange bars show the mean/two standard deviations of the trained GP, while the green curve shows two standard deviations ± the learned noise $2\sigma_n$.

This is shown in Figure 11, and the result of the training is shown in Figure 12. Following the discussion in Section 5.6, a fixed Matern parameter $\nu = 9/2$ was used. The initial parameters were $\alpha = 1.8, p = 0.5, \gamma^{\text{scaled}} = 1, \sigma = 0.1, \theta = 0.2$. The trained parameters were $\alpha = 1.667$, $p = 0.422$, $\gamma^{\text{scaled}} = 0.235$, and hyperparameters $\sigma = 0.0617$, $\theta = 1.173$ and learned noise $\sigma_n = 0.0344$. The true $\gamma = 0.0066$. The optimization wall time was 6 minutes and 31 seconds.

The conclusion of this training is that, in this model, the transition density $u(t,x)$ of the original Intel(normalized)/SP500(normalized) process is governed by the fractional diffusion equation

$$\begin{aligned}\frac{\partial u}{\partial t} &= \frac{0.0066^{1.667}}{|\cos(1.667\pi/2)|}\left[0.422({}^{RL}_{-\infty}D_x^{1.667}u) + 0.578({}^{RL}_{x}D_{\infty}^{1.667}u)\right] \\ &= 0.000113({}^{RL}_{-\infty}D_x^{1.667}u) + 0.000155({}^{RL}_{x}D_{\infty}^{1.667}u).\end{aligned}$$

Equivalently, the time series may be described as an α-stable process,

$$X_{i+n} - X_i \sim S_{1.667}(-0.156, 0.0066(n^{1/1.667}), 0). \tag{5.26}$$

However, for modeling purposes, it should be kept in mind that the training was performed using data in the interval $[-2.5, 2.5]/\sqrt{1259}$ with $n = 3$ and $n = 4$; increments greater than $2.5/\sqrt{1259}$ in four units of time were excluded. Thus, for consistency, the stable densities should be truncated to this interval as well, and renormalized. If increments in four units of time are drawn from the 1.667-stable density (5.26) with $n = 4$ truncated to $[-2.5, 2.5]/\sqrt{1259}$, increments in one unit of time should be drawn as from the appropriate ($n = 1$) density truncated to $[-2.5, 2.5]/(\sqrt{1259} \times 4^{1/1.667}) = [-0.031, 0.031]$ and normalized:

$$X_{i+1} - X_i \sim C_{\text{norm}} \mathbb{1}_{[-0.031, 0.031]} S_{1.667}(-0.156, 0.0066, 0) \tag{5.27}$$

Sampling of this distribution can be performed by sampling $S_{1.667}(-0.156, 0.0066, 0)$ and rejecting draws greater in magnitude than 0.031. Backtesting with this model, shown in Figure 13, yields good agreement with both the trend and volatility of the historical data.

Fitting α-stable densities to financial data is important for risk management and is of relevance to trading strategies based on assumptions of underlying α-stable random behavior. In this direction, fractional Black-Scholes equations have been introduced ([**40**], [**120**]) as appropriate models for hedging, since standard Black-Scholes theory is based on assumptions of normality/log-normality of the underlying processes. The example here can serve as a building block to applying fractional Black-Scholes theory to financial data.

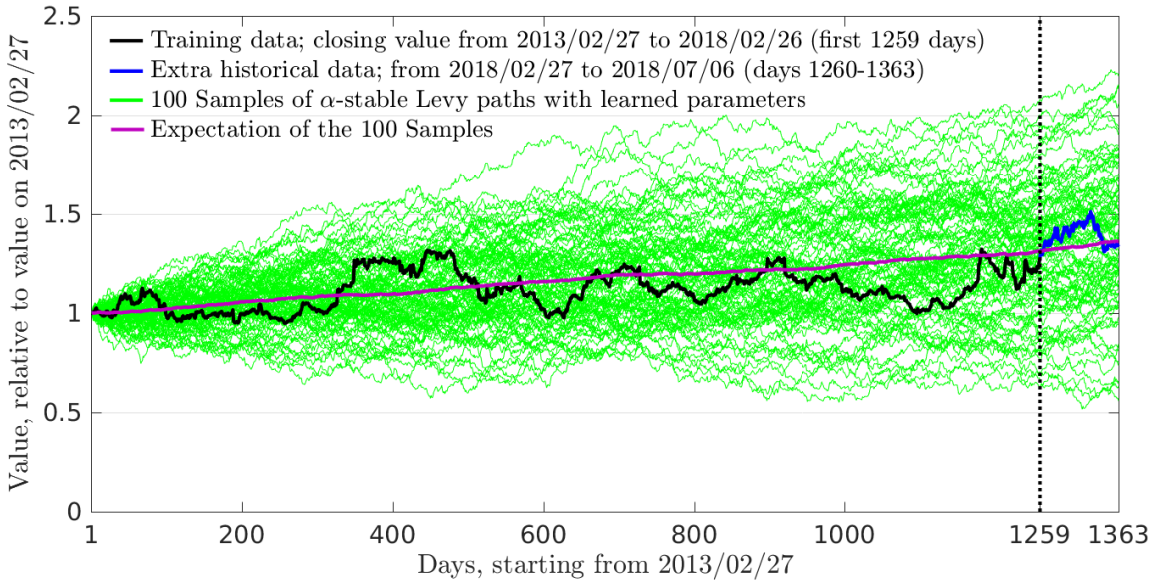

FIGURE 13. Backtesting/validation of the trained α-stable parameters. The black curve shows the training data of normalised Intel / normalized S&P 500 for 1259 days starting Feb. 27, 2013. The blue curve shows extra historical time series data, from Feb. 26, 2018 until July 26, 2018 (not used to train). Each of the 100 green curves is a sample path of the truncated α-stable process (5.27). The dark/filled region of the envelope of samples contains the historical data, providing a fairly sharp estimate of volatility in the first year. The purple curve is the expectation of the samples, which is accurate initially but does not take into account the mean-reverting behavior of the stock over five years.

5.8 Chapter Conclusion

The Gaussian processes methodology based on the implementation of fractional derivatives and stationary covariance kernels in Theorem 5.18 allows for the effective and efficient discovery of linear space-fractional equations in $\mathbb{R}^d$. We have demonstrated the feasibility, robustness, and accuracy of this methodology. Due to the versatilty of fractional archetypes and user-controlled parsimony, we demonstrated the appeal of the method even for discovering integer-order equations, and discussed

a novel approach to interpolating multi-term linear PDEs. The methodology allows for versatile discovery of linear space-fractional differential equations in $\mathbb{R}^d$ in many applications where fractional or anomalous behavior is expected, as illustrated by the discovery of a fractional diffusion equation for relative stock performance. This can be used to calibrate α-stable parameters from time series, and has potential impact in risk management and fractional Black-Scholes theory.

Regarding extensions of this work, one potential drawback of the methodology is that Gaussian processes may not scale well to large datasets. In this regard, remedies proposed in [**99, 170**] may be worth exploring. On the other hand, neural networks are intrinsically suited to larger data sets. Moreover, unlike Gaussian processes, neural networks do not require a linear relationship of the form (5.1), and can be freely used to discover parametrized nonlinear differential equations. Neural networks were used to solve and discover (integer-order) PDEs in [**174, 175**]. The methodology therein was further utilized in [**176**] and [**171**] to train neural networks to distill the actual dynamics of nonlinear dynamical systems and nonlinear partial differential equations, respectively. See also [**138**] for a different approach. However, direct extension of these methods to allow for fractional-order differential operators would require *fractional automatic differentiation* of neural networks, which remains a major conceptual and numerical challenge due to a lack of classical chain rule for fractional-order operators.

CHAPTER 6

Thesis Conclusion and Future Work

One of the contributions of this thesis is a unified discussion of boundary conditions for fractional Laplacians and a proof that the various proposed extensions of the spectral fractional Laplacian to nonzero boundary conditions are equivalent. We have also shown that the same operator can be defined using the spectral theorem to directly define the inverse operator, justifying the lifting of the boundary condition by more general nonharmonic functions, and that these definitions, too, are equivalent. Moreover, we have validated this operator from a stochastic perspective by establishing Feynman-Kac formulas that involve subordinate stopped Brownian motion. Thus, we conclude that the problem of defining the spectral fractional Laplacian with nonzero boundary conditions has largely been solved, and we can speak of *the* spectral fractional Laplacian for nonzero boundary conditions in a bounded domain.

The stochastic solution formulas proven and tested in this thesis are highly parallelizable and offer advantages for local solution of boundary value problems. A pertinent application of the formulas is to boundary value problems in high dimensions (as illustrated by the 16-dimensional benchmark problem in Section 3.10.4) or in complex domains. Solving using these formulas involves successively generating a normal random number, using it to increment the Brownian motion, and then checking if the new endpoint of the path is still in the domain. Methods for normal random number generation have shown significant speedup on GPUs compared to CPUs [**3**]. Assuming that the boundary of the domain can be approximated by a polyhedron, the test of whether the path endpoint remains in the domain reduces to the classical point-in-polyhedron problem. One method of solution is to cast a single long ray (say, longer than the increment plus the diameter of the domain) in any direction and compute the number of intersections with all the polygonal faces of the domain. The point is inside the domain if and only if this number of intersections is odd. This is parallelizable over the triangulation of the domain and is essentially

a problem of computer graphics. Clearly, it is also highly amenable to GPU implementation. Thus, a GPU implementation of the discretized Feynman-Kac formula as described in Chapter 3 is a priority for future work by the author.

One method of accelerating the stochastic solution methods of Chapter 3 that may be explored is Walk-on-Spheres, as discussed in Sections 2.4.3 and 3.11. Classically, this method is highly advantageous for the homogeneous problem $\Delta u = 0, u|_{\partial\Omega} = g$, since the stochastic solution formula reduces to an expectation over exit points of Brownian motion, which may be sampled quickly by generating a sequence of maximally-inscribed spheres rather than exact paths. The Poisson problem $\Delta u = r, u|_{\partial\Omega} = g$ with nonzero right-hand side r may be reduced to the homogeneous problem by subtracting a particular solution to the Poisson equation that need not satisfy the boundary condition, leading to a new boundary condition. However, this reduction is difficult to apply to the fractional problem of Chapter 3, since boundary conditions are "built into" fractional operators and the computation of the new boundary condition in the fractional case may be just as difficult as solving the boundary value problem itself. On the other hand, the stochastic solution formula for the general Poisson problem involves path integration of the right-hand side which, in the Walk-on-Spheres method, must be replaced by integration of the right-hand side over the occupation measures of the spheres [**125**]. The cost of performing such integrals (using quadrature rules or Monte Carlo integration) should be compared to the direct path-integration implementation of the stochastic solution formulas. Moreover, the distribution for exit points of subordinate stopped Brownian motion within a domain must be understood as well, since it is required to sample this to implement Walk-on-Spheres [**125**].

Another priority in this direction is the stochastic solution formula for the Neumann problem. The author conjectures that this will involve subordinate *reflected* Brownian motion, and that the boundary local time process that appears in the

classical stochastic solution formula [**36, 136, 23, 103**] will in turn be subordinated for the fractional formula. Thus, it will not be necessary to solve the Skorokhod problem "from scratch" for the fractional problem. Looking beyond the spectral fractional Laplacian, the stochastic viewpoint is appealing for understanding reflecting boundary conditions for the Riesz fractional Laplacian and other operators, which is currently a poorly understood area with many open problems.

Continuing the development of Monte Carlo methods for FPDEs, in this thesis we have developed a Path Integral Monte Carlo method for the fractional Schrödinger equation with periodic boundary conditions. Although the subject of fractional quantum mechanics has attracted theoretical debate for years, there had been few studies of realistic quantum systems in fractional regimes. This thesis contains the first method (Fractional Path Integral Monte Carlo) that can study quantum systems in fractional regimes with arbitrary, realistic potentials. For future work, in addition to exploring novel properties of condensates in the fractional regime, we aim to use this method to generate a synthetic database of fractional quantum systems that can be compared with experimental data to potentially identify fractional behavior in applications.

To accelerate the discovery of FPDE models in applications from field data, we have developed a fractional physics-informed Gaussian process method for discovering linear space-fractional PDEs. The method is compatible with a wide variety of stationary kernels including the Matérn family. We illustrated how the use of fractional derivatives within a physics-informed Gaussian process framework allows continuous regression to be performed over the orders of differential operators themselves, providing a powerful tool for discovering both fractional and integer-order PDEs. The author is currently collaborating with the group of Prof. Hong Wang of the University of South Carolina to develop frameworks for time-fractional physics-informed Gaussian processes. The behavior of the data in time calls for a large

variety of covariance kernels, the choice of which is essential to successfully train the Gaussian process. Such kernels include Matérn, rational quadratic, periodic, and locally periodic. For example, a Gaussian process trained on *seasonal* data requires periodic kernels and will fail when used with a stationary kernel such as the squared-exponential or Matérn [**69, 156**]. Thus, it is required to develop a library of robust and fast methods to compute time-fractional Gaussian process kernels for a range of hyperparameters.

Compared to Gaussian processes, physics-informed neural networks scale favorably to larger data, and can be freely used to discover parametrized *nonlinear* differential equations. They were used to solve and discover (integer-order) PDEs in [**174, 175**] and further utilized in [**176**] and [**171**], but fractional differentiation of neural networks poses a new challenge. This is the means by which the candidate equation is encoded into the neural network (just as in the Gaussian process framework). While classical derivatives of neural networks exploit the structure of neural networks as layered compositions of affine functions and activation functions to perform *automatic differentiation* or *backpropagation* based on repeated use of the chain rule, fractional and nonlocal derivatives generally do not satisfy a tractable chain rule. Recently, in [**162**], a hybrid method for fractional physics-informed neural networks was proposed that involves automatic differentiation for the integer-order operators and numerical discretization for the fractional operators. This represents a promising approach to the problem, and may provide a basis for future work on fractional physics-informed neural networks.

It is now clear that all potential frameworks for machine learning of FPDEs reduce to efficient and robust subroutines for the computation of the action of fractional operators (on Gaussian process kernels or neural networks) or for the solution of associated equations/boundary value problems. The Fourier transform based numerical algorithms developed in Chapter 5, while sufficient for discovering many types of

linear space-fractional PDEs, cannot be used in bounded domains or for certain inhomogeneous coefficients or fractional orders. A robust library of fast direct solvers for the wide variety of fractional and nonlocal operators and boundary value problems would prove extremely useful for further development of physics-informed learning machines. Due to nonlocality of fractional derivatives, discretization of such operators and problems leads to fully dense matrices. For such linear systems, N degrees of freedom therefore requires $\mathcal{O}(N^2)$ memory for storage and $\mathcal{O}(N^3)$ operations for solution. When the underlying mesh is uniform, the resulting Toeplitz-like nature of coefficient matrices has been exploited to alleviate this [**217, 216**]. Hierarchical-matrix ($\mathcal{H}$-matrix) methods, based on approximations of dense matrices by low-rank "data-sparse"' matrices of rank k, allow for a similar reduction in storage requirements and complexity to $\mathcal{O}(Nk \log N)$, but do not require uniform meshes. Thus, they allow for geometric multigrid methods to be utilized, further increasing the efficiency [**231**]. Using an $\mathcal{H}$-matrix preconditioner, [**134**] reduced the computational cost of solving a benchmark FPDE by a factor of 11 orders of magnitude. An $\mathcal{H}$-matrix method was developed to solve equations involving generators of general Lévy processes in [**224**]. For future work, therefore, we aim to develop fast linear algebra subroutines to consistently and directly address the numerical challenges involved with data-driven discovery of FPDEs within a variety of machine learning frameworks.

APPENDIX A

Classical Sobolev Spaces, Hölder Spaces, and Dirichlet Eigenfunction Decomposition

A.1 $H^k(\Omega)$ and $H_0^1(\Omega)$

Let $\Omega \subset \mathbb{R}^d$ be a domain with Lipschitz continuous boundary. The Sobolev space $H^k(\Omega)$ for integer $k \geq 0$ is defined to be the set of all functions $u \in L^2(\Omega)$ such that all weak partial derivatives $D^\beta u$ of order $|\beta| \leq k$ belong to $L^2(\Omega)$. Here, $\beta = (\beta_1, ..., \beta_d)$ is a multi-index, with $\beta_i \in \mathbb{N} = \{0, 1, 2, ...\}$ and $|\beta| = \beta_1 + ...\beta_d$. The space $H^k(\Omega)$ is equipped with the inner product

$$(u, v)_{H^k(\Omega)} = \sum_{|\beta| \leq k} \int_\Omega D^\beta u D^\beta v dx$$

and norm

$$\|u\|_{H^k(\Omega)} = (u, v)^{1/2}_{H^k(\Omega)} = \left(\sum_{|\alpha| \leq k} \int_\Omega (D^\beta u)^2 dx \right)^{1/2}.$$

The space $H^k(\Omega)$ forms a Hilbert space with the above norm. For the space $H^1(\Omega)$, we introduce the following seminorm:

$$[u]_{H_0^1(\Omega)} = \|\nabla u\|_{L^2(\Omega)}.$$

Thus,

$$\|u\|_{H^1(\Omega)} = \|u\|_{L^2(\Omega)} + [u]_{H_0^1(\Omega)}.$$

By the trace theorem (Theorem B.3 in Appendix B), for a bounded domain Ω with Lipschitz continuous boundary, the trace operator $|_{\partial\Omega}$ exists and is a bounded linear mapping from $H_0^1(\Omega)$ into $L^2(\partial\Omega)$. Thus, the set

$$H_0^1(\Omega) = \left\{ u \in H^1(\Omega) \text{ such that } \ u|_{\partial\Omega} = 0 \right\}$$

is a well-defined linear subspace of $H_0^1(\Omega)$. It may be equipped with the same norm $\|\cdot\|_{H^1(\Omega)}$ as $H^1(\Omega)$. However, by Poincare's inequality, the seminorm $[\cdot]_{H_0^1(\Omega)}$ is a norm on $H_0^1(\Omega)$ equivalent to the norm $\|\cdot\|_{H^1(\Omega)}$. See [**127**].

A.2 Hölder Spaces

For integer $k \geq 0$, the space of k-times differentiable functions $C^k(\Omega)$ is equipped with norm

$$\|u\|_{C^k(\Omega)} = \sum_{|\beta| \leq k} \sup_{x \in \Omega} |D^\beta u(x)|.$$

The derivatives $D^\beta u(x)$ are required to exist in the classical (pointwise) sense. Here $\beta = (\beta_1, ..., \beta_d)$ is a multi-index as before. The Hölder coefficient, for $0 < \rho \leq 1$, is defined as

$$[u]_{C^{0,\rho}(\Omega)} = \sup_{x \in \Omega} \frac{|u(x) - u(y)|}{|x - y|^\rho}.$$

The Hölder Space $C^{k,\rho}(\Omega)$ is defined to be the space of all functions $u \in C^k(\Omega)$ such that the Hölder norm

$$\|u\|_{C^{k,\rho}(\Omega)} = \|u\|_{C^k(\Omega)} + \max_{|\beta|=k} \left[D^\beta u\right]_{C^{0,\rho}(\Omega)}$$

is finite. The space $C^{k,0}(\Omega)$ is taken to mean $C^k(\Omega)$.

Grubb [**89**] uses the following notation for Hölder spaces, which is very convenient for stating fractional regularity results: for nonnegative real number $r \geq 0$, the space $C^r(\Omega)$ is defined as

$$C^r(\Omega) = C^{\lfloor r \rfloor, \rho}(\Omega), \quad r = \lfloor r \rfloor + \rho, \quad 0 \leq \rho < 1.$$

Here, $\lfloor r \rfloor$ denotes the largest integer $\leq r$, and the space $C^{\lfloor r \rfloor, \rho}(\Omega)$ is the standard Hölder space defined above.

A.3 Inequalities

The Sobolev inequality that we use is stated in the appendix of [127]:

THEOREM A.1. *Let $k > d/2 + r$. There exists a constant C such that*

$$\|v\|_{C^r(\Omega)} \leq C\|v\|_{H^k(\Omega)}.$$

Thus, $H^k(\Omega) \subset C^r(\Omega)$.

This holds for domains Ω with Lipschitz boundary [13] or which satisfy the cone condition [6]. Finally, we require the following elliptic regularity estimate, transcribed from Chapter 3.7 of [127]:

THEOREM A.2. *Let Ω be a smooth domain. Then for $u \in H^{k+2}(\Omega) \cap H_0^1(\Omega)$, there exists a constant C such that*

$$\|u\|_{H^{k+2}(\Omega)} \leq C\|(-\Delta)u\|_{H^k(\Omega)}.$$

A.4 Basic Facts about Dirichlet Eigenfunction Decomposition

The following results about the spectrum of $-\Delta$ and eigenfunction decomposition are transcribed from Chapter 6.1 of [127]. In that text, $\Omega \subset \mathbb{R}^d$ is taken to be a domain with smooth boundary, although in general Ω can have piecewise smooth

boundary [54]. Consider the Dirichlet eigenvalue problem

$$-\Delta e_\lambda = \lambda e_\lambda \quad \text{in } \Omega, \quad e_\lambda|_{\partial\Omega} = 0, \tag{A.3}$$

defining eigenvalues λ with corresponding eigenfunctions e_λ.

THEOREM A.4. *The eigenvalues λ of (A.3) are real, positive, and can be ordered in a nondecreasing sequence λ_k such that*

$$\lambda_k \to \infty \quad as \quad k \to \infty.$$

Two eigenfunctions e_{λ_1} and e_{λ_2} corresponding to different eigenvalues $\lambda_1 \neq \lambda_2$, are orthogonal in L^2 and H_0^1.

THEOREM A.5. *The sequence of eigenfunctions $\{e_k\}$ corresponding to the nondecreasing sequence of eigenvalues $\{\lambda_k\}$ forms an orthonormal basis for $L_2(\Omega)$. Moreover, $v \in H_0^1(\Omega)$ if and only if the series*

$$\sum_{k=0}^{\infty} \lambda_k \left(v, e_k\right)^2 \quad converges.$$

The following identity holds:

$$[v]_{H_0^1}^2 = \|\nabla v\|_{L^2}^2 = \sum_{k=1}^{\infty} \lambda_k \left(v, e_k\right)^2.$$

APPENDIX B

Fractional Sobolev Spaces

In this appendix, we assemble the commonly-used Sobolev spaces for the fractional Laplacian. These spaces are discussed in [88, 89], but we have more closely followed the exposition and notation of [11].

DEFINITION B.1 ([11]). *For $0 < s < 1$ and domain Ω with Lipschitz continuous boundary, we define the fractional Sobolev space*

$$H^s(\Omega) := \left\{ u \in L^2(\Omega) : \int_\Omega \int_\Omega \frac{|u(x) - u(y)|^2}{|x-y|^{n+2s}} dxdy < \infty \right\},$$

with the semi-norm and norm

$$|u|^2_{H^s(\Omega)} := \int_\Omega \int_\Omega \frac{|u(x) - u(y)|^2}{|x-y|^{n+2s}} dxdy,$$
$$\|u\|_{H^s(\Omega)} := \left(\|u\|^2_{L^2(\Omega)} + |u|^2_{H^s(\Omega)} \right)^{1/2}.$$

DEFINITION B.2 ([59]). *For any $u \in C^\infty(\Omega)$, define the trace operator $\gamma\big|_{\partial\Omega}$ by*

$$\gamma\big|_{\partial\Omega} u(x) = u(x), \quad x \in \partial\Omega.$$

THEOREM B.3. *Trace Theorem [59]. Let Ω be a bounded, simply connected Lipschitz domain and $1/2 < s < 3/2$. Then the trace operator $\gamma\big|_{\partial\Omega}$ is a bounded linear operator from $H^s(\Omega)$ to $H^{s-\frac{1}{2}}(\partial\Omega)$.*

This range for s, $1/2 < s < 3/2$, is sufficient for the discussion of traces in this article. Now we can define the subspace $H^s_0(\Omega)$ of $H^s(\Omega)$.

DEFINITION B.4. *For $s > 1/2$,*

$$H^s_0(\Omega) := \left\{ u \in H^s(\Omega) : \gamma\big|_{\partial\Omega} u(x) = 0 \right\}.$$

In the case $s = 1/2$, we must define another fractional Sobolev space, denoted $H^{1/2}_{00}(\Omega)$.

DEFINITION B.5 ([11]).

$$H_{00}^{1/2}(\Omega) := \left\{ u \in H^{1/2}(\Omega) : \int_\Omega \frac{u^2(x)}{\operatorname{dist}(x, \partial\Omega)} dx < \infty \right\}.$$

The associated norm is defined

$$\|u\|_{H_{00}^{1/2}(\Omega)} := \left(\|u\|^2_{H^{1/2}(\Omega)} + \int_\Omega \frac{u^2(x)}{\operatorname{dist}(x, \partial\Omega)} dx \right)^{1/2}.$$

REMARK B.6. The space $H_{00}^{1/2}$ is known as the Lions-Magenes space, and there is an important reason why it is introduced. As noted in [209], for bounded open set Ω with Lipschitz boundary and $0 < s < 1$, Lions and Magenes [135] showed that the L^2-interpolation of $H_0^1(\Omega)$ and $L^2(\Omega)$ gives

$$(H_0^1(\Omega), L^2(\Omega))_{1-s,2} = \begin{cases} H_0^s(\Omega) & \text{if } 0 < s < 1/2, \\ H_{00}^{1/2}(\Omega) & \text{if } s = 1/2, \\ H^s(\Omega) & \text{if } 1/2 < s < 1. \end{cases}$$

In other words, the interpolation space $(H_0^1(\Omega), L^2(\Omega))_{1-s,2}$ for $s = 1/2$ gives not $H^{1/2}(\Omega)$ but rather $H_{00}^{1/2}(\Omega)$. This suprising fact causes $H_{00}^{1/2}(\Omega)$ to play a more important role than the space $H^{1/2}(\Omega)$ in certain theoretical results for the fractional Laplacian. Note that the interpolation space $(H_0^1(\Omega), L^2(\Omega))_{1-s,2}$ can be identified with the space $\mathbb{H}^s(\Omega)$ that follows and which will be used throughout this thesis.

We define the space $\mathbb{H}^s(\Omega)$, which is used to characterize the regularity properties of the spectral fractional Laplacian.

DEFINITION B.7 ([11]). *For any $s \geq 0$,*

$$\mathbb{H}^s(\Omega) := \left\{ u = \sum_{k=1}^\infty u_k \phi_k \in L^2(\Omega) : \|u\|^2_{\mathbb{H}^s(\Omega)} := \sum_{k=1}^\infty \lambda_k^s u_k^2 < \infty \right\}$$

where (λ_k, ϕ_k) are the eigenpairs of the integer Laplacian $-\Delta$ on Ω with zero Dirichlet boundary conditions.

As noted in Ref. [11], the following relationship exists between the fractional Sobolev spaces presented in Defs. B.1, B.4, B.5, and B.7

$$\mathbb{H}^s(\Omega) = \begin{cases} H^s(\Omega) = H_0^s(\Omega) & \text{if } 0 < s < 1/2, \\ H_{00}^{1/2}(\Omega) & \text{if } s = 1/2, \\ H_0^s(\Omega) & \text{if } 1/2 < s < 1. \end{cases}$$

REMARK B.8. As indicated above, we occasionally use the notation $H_0^s(\Omega)$ even for $0 < s \leq 1/2$. In some cases, this allows us to simplify statements of results. Strictly speaking, $H_0^s(\Omega)$ was defined only for $s > 1/2$. Since the trace operator does not exist for $s \leq 1/2$, we identify $H_0^s(\Omega)$ with $H^s(\Omega)$. The case $s = 1/2$ is the distinction between this usage of $H_0^s(\Omega)$ and $\mathbb{H}^s(\Omega)$.

DEFINITION B.9. *The space $\mathbb{H}^{-s}(\Omega)$, for $s \geq 0$, is defined to be the dual space of $\mathbb{H}^s(\Omega)$.*

Note that for $s < 1/2$, $\mathbb{H}^{-s}(\Omega)$ is equivalent to the dual of $H^s(\Omega)$, denoted in this thesis by $(H^s(\Omega))^*$. However, $\mathbb{H}^{-s}(\Omega)$ is distinct from $(H^s(\Omega))^*$ for $s > 1/2$; in fact, since $H_0^s(\Omega) \subset H^s(\Omega)$, we have $(H^s(\Omega))^* \subset \mathbb{H}^{-s}(\Omega)$ for $s \geq 1/2$.

DEFINITION B.10. $H_{loc}^s(\Omega) = \{u \in H^s(K)$ *for all compact sets* $K \subseteq \overline{\Omega}\}$.

APPENDIX C

Example MATLAB Implementation of the Stochastic Solution of the Cauchy Problem for the Spectral Fractional Laplacian

Here, we include a MATLAB implementation for the method described in Section 3.10.1. The script below (which calls `subordinator_killed_any_dimension`, also shown below) computes the stochastic solution of the parabolic problem (3.51) in time at a single point in the unit hypercube in dimension d, and plots this curve along with the exact solution for comparison (similar to Figures 6 and 8).

```
tic;
d = 16;
dt = 10^(-5);
t = 0.03;
alpha = sqrt(3);
point = (4/5)*ones(d,1);

g = @(X) ones(1,size(X,2))+0.5*(1/d)*sum(X);
r = @(X) (1/(d*pi^2)^(-alpha/2))*prod(sin(pi*X));
f = @(X)  1+0.5*(1/d)*sum(X) + prod(sin(pi*X)) + prod(sin(2*pi*X));
u = @(t,X) 1+0.5*(1/d)*sum(X) + prod(sin(pi*X)) + ...
                    exp(-(4*d*pi^2)^(alpha/2).*t).*prod(sin(2*pi*X));

% The following function should be f on the interior, g on
% the boundary. Since prod(sin(2*pi*X)) = 0 on the boundary,
% may as well just set this to f rather than coding a case.
% For other data, this might not be true!
gorf = @(X) f(X);

Npaths = 1000;
paths = cell(Npaths,1);

for n = 1:Npaths
    fprintf('Path %i out of %i. \n', n, Npaths)
    % Make a Brownian path until it exits the domain.
    X = point;
    while max(X(:,end) < 0 | X(:,end) > 1) == 0
        X = [X X(:,end) + ...
            sqrt(2)*(dt^0.5)*transpose(mvnrnd(zeros(d,1),eye(d)))];
    end
    % Modify the endpoint; "pull" it back to the boundary.
    X(:,end) = X(:,end) - (X(:,end) > 1).*(X(:,end)-1) - ...
        (X(:,end) < 0).*X(:,end);
    % Now we have killed BM. Make time vector, starting at zero,
    % same length as path.
```

```
34      T = 0:dt:dt*(length(X(1,:))-1);
35      % Subordinate the path.
36      [Tsub Xsub] =  ...
            subordinator_killed_any_dimension(T,X,dt,T(end),alpha);
37      % Now add the path to the cell of paths.
38      paths{n} = Xsub;
39  end
40
41  % All the paths are completed and stored.
42  % Now we compute the solution.
43  pathlength = @(x) size(x,2);
44  maxlength = round(t/dt)+1;
45  rintegral_to_size = zeros(maxlength,Npaths);
46  gorfvec_to_size = zeros(maxlength,Npaths);
47  % The following gets us the path integrals at
48  % the discrete times until the final time.
49  for n = 1:Npaths
50      path = paths{n};
51      rvec = r(path);
52      rintegral = cumsum(rvec)*dt;
53      gorfvec = gorf(path);
54      % Some paths will be longer than maxlength.
55      % This means that the path did not exit within the
56      % final time. So we trim the vectors.
57      if pathlength(path) > maxlength
58          rintegral = rintegral(1:maxlength);
59          gorfvec = gorfvec(1:maxlength);
60      % Other paths exit by the final time.
61      % To prevent integrating over the
62      % constant exit point and getting the wrong answer,
63      % we keep the solution over that path constant.
64      else
65          rintegral = [rintegral rintegral(end)*ones(1, ...
                maxlength-pathlength(path))];
66          gorfvec = [gorfvec gorfvec(end)*ones(1, ...
                maxlength-pathlength(path))];
67      end
68      rintegral_to_size(:,n) = rintegral;
69      gorfvec_to_size(:,n) = gorfvec;
70  end
71  average = sum(rintegral_to_size+gorfvec_to_size,2)/Npaths;
72  toc;
73  % Plot stochastic solution and exact solution to compare:
74  T = [0:dt:t]; figure; plot(T,average, 'r-');
75  hold on; plot(T, u(T, point), 'black');
```

```
function [Tsub, Xsub] = ...
    subordinator_killed_any_dimension(T,X,dt,tau,alpha)

% Takes a stopped path X, at times T in steps of dt,
% with stopping time tau. Returns the subordinated
% times rounded up to the dt-ceiling of tau, and the
% corresponding path positions.
% These returned variables are of random length!

% Parameters of the standard alpha-stable in the
% Taqqu and Samorodinsky parametrization
% (this is used in the stblrnd function).
a2 = alpha/2;
skewness = 1;
scaleg = (cos(pi*a2/2))^(1/a2);
center = 0;

% Generate a sample path of the subordinator until
% exit time is exceeded.
sub = [0];
while sub(end) < tau
    sub = [sub sub(end) + ...
        (dt^(1/a2))*stblrnd(a2, skewness,scaleg, center)];
end
% Round the subordinator values up to nearest multiples of dt.
Tsub = dt*(ceil(sub*(1/dt)));
% Get the indices of the vector T at which the values of Tsub
% appear (e.g, if sub = [0 0.33 0.66] and dt = 0.1, then
% Tsub = [0 0.4 0.7], and the next command will give [ 1 5 8 ].
indices = ceil(sub*(1/dt))+1;
% Trim the last index, which exceeds the length of T and X.
indices = indices(1:end-1);
% Get final subordinated time and positions.
% Also, attach the final time/position.
Tsub = [T(indices)-dt Tsub(end)];
Xsub = [X(:,indices) X(:,end)];
```

Note: that for maximum simplicity, we used MATLAB features such as cells and dynamic array sizing. To separate the path sampling from the solution evaluation, we store all the paths in an array and vectorize the evaluation of the data on each path vector, which incurs higher memory cost. For a high performance implementation, especially in C++ or Fortran, these features may be avoided.

APPENDIX D

Convolution of Density Matrices and Suzuki-Trotter Factorization

In order to use the Path Integral Monte Carlo algorithm for the fractional case, it is essential to first demonstrate that the fractional density matrices obey the density matrix convolution principle given by Equation (4.5). First, we consider the case of a single particle in $\mathbb{R}^d$. Using formula (4.13), we have

$$\begin{aligned}
&\int_{\mathbb{R}^d} d\boldsymbol{R}_2 \rho(\boldsymbol{R}_1, \boldsymbol{R}_2; \beta_1)\rho(\boldsymbol{R}_2, \boldsymbol{R}_3; \beta_2) \\
&\qquad = \int_{\mathbb{R}^d} d\boldsymbol{R}_2 \frac{1}{(2\pi)^d} \int_{\mathbb{R}^d} d\boldsymbol{C} e^{-i\langle \boldsymbol{C}, \boldsymbol{R_1}-\boldsymbol{R_2}\rangle} e^{-\beta_1 D_\alpha \hbar^\alpha |\boldsymbol{C}|^\alpha} \\
&\qquad\qquad \times \frac{1}{(2\pi)^d} \int_{\mathbb{R}^d} d\boldsymbol{C'} e^{-i\langle \boldsymbol{C'}, \boldsymbol{R_2}-\boldsymbol{R_3}\rangle} e^{-\beta_2 D_\alpha \hbar^\alpha |\boldsymbol{C'}|^\alpha} \\
&\qquad = \frac{1}{(2\pi)^{2d}} \int_{\mathbb{R}^d} \int_{\mathbb{R}^d} d\boldsymbol{C} d\boldsymbol{C'} e^{-i\langle \boldsymbol{C}, \boldsymbol{R_1}\rangle} e^{-i\langle \boldsymbol{C'}, -\boldsymbol{R_3}\rangle} \\
&\qquad\qquad \times \left[\int_{\mathbb{R}^d} d\boldsymbol{R}_2 e^{i\langle \boldsymbol{R_2}, \boldsymbol{C}-\boldsymbol{C'}\rangle} \right] e^{-\beta_1 D_\alpha \hbar^\alpha |\boldsymbol{C}|^\alpha} e^{-\beta_2 D_\alpha \hbar^\alpha |\boldsymbol{C'}|^\alpha} \\
&\qquad = \frac{1}{(2\pi)^{2d}} \int_{\mathbb{R}^d} \int_{\mathbb{R}^d} d\boldsymbol{C} d\boldsymbol{C'} e^{-i\langle \boldsymbol{C}, \boldsymbol{R_1}\rangle} e^{-i\langle \boldsymbol{C'}, -\boldsymbol{R_3}\rangle} \\
&\qquad\qquad (2\pi)^d \delta(\boldsymbol{C}-\boldsymbol{C'}) e^{-\beta_1 D_\alpha \hbar^\alpha |\boldsymbol{C}|^\alpha} e^{-\beta_2 D_\alpha \hbar^\alpha |\boldsymbol{C'}|^\alpha}.
\end{aligned}$$

To obtain the final line above, we used $\int_{\mathbb{R}^d} d\boldsymbol{R}_2 e^{i\langle \boldsymbol{R_2}, \boldsymbol{C}-\boldsymbol{C'}\rangle} = (2\pi)^d \delta(\boldsymbol{C}-\boldsymbol{C'})$. Simplifying, we have

$$\begin{aligned}
\int_{\mathbb{R}^d} d\boldsymbol{R}_2 \rho(\boldsymbol{R}_1, \boldsymbol{R}_2; \beta_1)\rho(\boldsymbol{R}_2, \boldsymbol{R}_3; \beta_2) &= \frac{1}{(2\pi)^d} \int_{\mathbb{R}^d} d\boldsymbol{C} e^{-i\langle \boldsymbol{C}, \boldsymbol{R_1}-\boldsymbol{R_2}\rangle} e^{-(\beta_1+\beta_2) D_\alpha \hbar^\alpha |\boldsymbol{C}|^\alpha} \\
&= \rho(\boldsymbol{R}_1, \boldsymbol{R}_3; \beta_1+\beta_2).
\end{aligned}$$

This demonstrates that the single-particle fractional kinetic density matrix at a large imaginary time, β, may be factored into a convolution over short imaginary time density matrices. That the same property holds for the N-particle kinetic density matrix follows from the factorization (4.15), Fubini's theorem, and the same result for the single-particle case.

In order to factor the full short time propagators into kinetic and potential propagators, it must moreover be verified that Suzuki-Trotter factorization [**211**] can be performed on the fractional Laplacian. As discussed by Simon [**193**], Suzuki-Trotter factorization is valid as long as the kinetic and potential operators are self-adjoint [**131**] and bounded from below. This holds by the definition of the (negative) fractional Laplacian [**137**].

APPENDIX E

Analytical Form for the One-Dimensional Free Particle Fractional Density Matrix

In Chapter 4, we have focused on the sampling of $3N$-dimensional density matrices, which are based on the three-dimensional fractional Laplacian. This operator cannot be separated into independent one-dimensional fractional Laplacians and necessitates a fully numerical approach. However, in order to make a connection with previous works on the fractional Schrödinger equation, we describe how in one dimension, the fractional density matrix derived in this work for periodic boundary conditions possesses an analytical form.

In one dimension, denoting $\boldsymbol{r} = x$, equation (4.13) becomes

$$\rho^{\mathrm{per},L}(x,x',\tau) = \frac{1}{2\pi}\int_{-\infty}^{\infty} dC e^{-iC(x-x')} e^{-\tau D_\alpha \hbar^\alpha |C|^\alpha}. \tag{E.1}$$

For general values of α, it is impossible to compute this integral in closed form, but it can be represented as a special function defined by a power series. The integral may be identified as the characteristic function of the generalized normal random variable X_{GN}. This is the random variable given by the probability density function

$$f_\kappa(\mu,\sigma;x) = \xi(\kappa) = \frac{\kappa}{2\sigma\Gamma(1/\kappa)} e^{-\left|\frac{x-\mu}{\sigma}\right|^\kappa}.$$

The characteristic function of $\xi(\kappa)$ for $\kappa > 1$ was first computed explicitly in terms of special functions by Pogany and Nadarajah in 2006 [**165**]. It may be expressed as

$$E\{e^{itX_{GN}}\} = \frac{\sqrt{\pi}e^{it\mu}}{\Gamma(1/\kappa)} \Psi_1^1\left[(1/\kappa, 2/\kappa); (1/2, 1); -\frac{(\sigma t)^2}{4}\right],$$

where Ψ_1^1 denotes the Fox-Wright generalized hypergeometric function. It is specified by an arbitrary number, $p+q$, of parameters, and is defined as the series

$$\Psi_q^p\left[(\alpha_1, A_1), ..., (\alpha_p, A_p); (\beta_1, B_1), ..., (\beta_q, B_q); z\right] = \sum_{n=0}^{\infty} \frac{\prod_{j=1}^p \Gamma(\alpha_j + A_j n)}{\prod_{j=1}^q \Gamma(\beta_j + B_j n)} \frac{z^n}{n!}.$$

Comparing the generalized normal distribution in the expression for the density matrix given by Equation (4.13) with the definition of the generalized normal distribution given by Equation (E.1), we have $|x-\mu| = |C|$, $\sigma = \frac{1}{\tau^{1/\alpha} D_\alpha^{1/\alpha} \hbar}$, and $\mu = 0$. Making these substitutions, we obtain

$$\begin{aligned}
\rho^{\mathrm{per},L}(x,x',\tau) &= \frac{1}{2\pi}\int_{-\infty}^{\infty} dC e^{-iC(x-x')} e^{-\tau D_\alpha \hbar^\alpha |C|^\alpha} \\
&= \frac{1}{2\pi}\frac{2\Gamma(1/\alpha)}{\tau^{1/\alpha} D_\alpha^{1/\alpha}\hbar\alpha}\frac{\sqrt{\pi} e^{i(x-x')\mu}}{\Gamma(1/\alpha)} \\
&\qquad \times \Psi_1^1\left[(1/\alpha, 2/\alpha); (1/2,1); \frac{-(x-x')^2}{4\beta^{2/\alpha} D_\alpha^{2/\alpha}\hbar^2}\right] \\
&= \frac{1}{\sqrt{\pi}\beta^{1/\alpha} D_\sigma^{1/\alpha}\hbar\alpha} \\
&\qquad \times \sum_{n=0}^{\infty} \frac{\Gamma(1/\alpha + (2/\alpha)\, n)}{\Gamma(1/2+n)} \frac{\left[\frac{-(x-x')^2}{4\tau^{2/\alpha} D_\alpha^{2/\alpha}\hbar^2}\right]^n}{n!}.
\end{aligned}$$

The generalized expression for the fractional kinetic density matrix is therefore proportional to the Fox-Wright function of argument $(x-x')^2$. Similar representations were obtained by Laskin [**131**] for the free-particle density matrix on $\mathbb{R}^d$ without boundary conditions. Laskin used the more general Fox H-function in his representation, which for the given indices reduces to the Fox-Wright function shown here. In another context, similar results were derived by Mainardi and Pagnini [**139**], where the integral form of Equation (E.2) arises as the fundamental solution to the space-fractional diffusion equation.

In principle, one-dimensional observables that depend on the density matrices may be derived from the power series given by Equation (E.2). For example, the

kinetic energy may be written as

$$\left\langle \hat{K} \right\rangle_{\text{link}} = \left\langle \frac{3N}{\tau\alpha} + \frac{2N}{\tau\alpha}\left[-C_\alpha (x-x')^2\right] \right. \\ \left[\sum_{n=0}^{\infty} \frac{\Gamma(1/\alpha + (2/\alpha)(n+1))}{\Gamma(1/2+(n+1))}\left[-C_\alpha(x-x')^2\right]^n /n!\right] / \\ \left.\left[\sum_{n=0}^{\infty} \frac{\Gamma(1/\alpha + (2/\alpha)n)}{\Gamma(1/2+n)}\left[-C_\alpha(x-x')^2\right]^n /n!\right]\right\rangle_{\text{link}} \tag{E.2}$$

where $C_\alpha = \frac{2^{2/\alpha} m^{2/\alpha}}{4\tau^{2/\alpha}\hbar^2}$ and $\langle\rangle_{\text{link}}$ denotes the average over links between beads. We omit the derivation, which involves differentiation of the series given in Equation (E.2) term by term as prescribed by Equation (4.20). Such formulas are the analogue of Equation (4.21) for the $\alpha = 2$ case, although they are limited in validity to the one-dimensional case. In all of our many-dimensional PIMC computations, we have therefore used the fully numerical approach detailed in Section 4.3.2, which is valid in all dimensions and considerably easier and more stable to implement.

Bibliography

[1] ALCF Aurora 2021 Early Science Program: Data and Learning Call For Proposals. https://www.alcf.anl.gov/alcf-aurora-2021-early-science-program-data-and-learning-call-proposals. Accessed: 2018-11-29.

[2] Argonne hints at future architecture of Aurora exascale system. https://www.nextplatform.com/2018/03/19/argonne-hints-at-future-architecture-of-aurora-exascale-system/. Accessed: 2018-11-29.

[3] GPU Gems 3. Chapter 37. Efficient Random Number Generation and Application using CUDA. https://developer.nvidia.com/gpugems/GPUGems3/gpugems3_ch37.html. Accessed: 2018-12-09.

[4] Gabriel Acosta, Francisco M. Bersetche, and Juan Pablo Borthagaray. A Short FE implementation for a 2D Homogeneous Dirichlet problem of a Fractional Laplacian. *Comput. Math. Appl.*, 74(4):784–816, August 2017.

[5] Gabriel Acosta and Juan Pablo Borthagaray. A fractional Laplace equation: Regularity of solutions and finite element approximations. *SIAM J. Numer. Anal.*, 55:472–495, 2017.

[6] Robert Adams and John Fournier. *Sobolev Spaces*. Elsevier, Second edition, 2003.

[7] Mark Ainsworth and Christian Glusa. Aspects of an adaptive finite element method for the fractional Laplacian: A priori and a posteriori error estimates, efficient implementation and multigrid solver. *Computer Methods in Applied Mechanics and Engineering*, 327:4 – 35, 2017.

[8] Mark Ainsworth and Christian Glusa. Hybrid finite element–spectral method for the fractional Laplacian: approximation theory and efficient solver. *SIAM J. Sci. Comput.*, 40(4):A2383–A2405, 2018.

[9] Mark Ainsworth and Christian Glusa. Towards an efficient finite element method for the integral fractional Laplacian on polygonal domains. In *Contemporary computational mathematics—a celebration of the 80th birthday of Ian Sloan. Vol. 1, 2*, pages 17–57. Springer, Cham, 2018.

[10] L. Alfonso, R. Mansilla, and C. A. Terrero-Escalante. On the scaling of the distribution of daily price fluctuations in the Mexican financial market index. *Physica A Statistical Mechanics and its Applications*, 391:2990–2996, May 2012.

[11] H. Antil, J. Pfefferer, and S. Rogovs. Fractional operators with inhomogeneous boundary conditions: Analysis, control, and discretization.

[12] D. Applebaum. *Lévy Processes and Stochastic Calculus*. Cambridge University Press, 2 edition, 2009.

[13] Thierry Aubin. *Nonlinear analysis on manifolds. Monge-Ampere equations*, volume 252. Springer Science & Business Media, 1982.

[14] R. A. Aziz, V. P. S. Nain, J. S. Carley, W. L. Taylor, and G. T. McConville. An accurate intermolecular potential for helium. *The Journal of Chemical Physics*, 70(9):4330–4342, 1979.

[15] Louis Bachelier. *Théorie de la spéculation*. Gauthier-Villars, 1900.

[16] Boris Baeumer, Mihály Kovács, Mark M. Meerschaert, and Harish Sankaranarayanan. Boundary conditions for fractional diffusion. *Journal of Computational and Applied Mathematics*, 336:408 – 424, 2018.

[17] Boris Baeumer and Mark M. Meerschaert. Stochastic solutions for fractional Cauchy problems. *Fractional Calculus and Applied Analysis*, 4(4):481–500, 2001.

[18] A. V. Balakrishnan. Fractional powers of closed operators and the semigroups generated by them. *Pacific J. Math.*, 10:419–437, 1960.

[19] R. Balescu. Anomalous transport in turbulent plasmas and continuous time random walks. *Physics Review E*, 51(5):4807–4822, 1995.

[20] J. A. Barker. A quantum-statistical Monte Carlo method; path integrals with boundary conditions. *The Journal of Chemical Physics*, 70(6):2914–2918, 1979.

[21] Ole E. Barndorff-Nielsen and Neil Shephard. Econometrics of testing for jumps in financial economics using bipower variation. *Journal of financial Econometrics*, 4(1):1–30, 2006.

[22] Richard F. Bass and Pei Hsu. Some potential theory for reflecting Brownian motion in Holder and Lipschitz domains. *The Annals of Probability*, pages 486–508, 1991.

[23] A. Benchérif-Madani and É. Pardoux. A probabilistic formula for a Poisson equation with Neumann boundary condition. *Stochastic Analysis and Applications*, 27(4):739–746, 2009.

[24] David Benson, Rina Schumer, Mark M. Meerschaert, and Stephen Wheatcraft. Fractional dispersion, Lévy motion, and the MADE tracer tests. *Transport in Porous Media*, 42(1–2):211–240, 2001.

[25] Krzysztof Bogdan, Krzysztof Burdzy, and Zhen-Qing Chen. Censored Stable Processes. *Probab. Theory Relat. fields*, 127:89–152, 2003.

[26] Krzysztof Bogdan, Tomasz Byczkowski, Tadeusz Kulczycki, Michal Ryznar, Renming Song, and Zoran Vondraček. *Potential analysis of stable processes and its extensions*. Springer Science & Business Media, 2009.

[27] Josh Bongard and Hod Lipson. Automated reverse engineering of nonlinear dynamical systems. *Proceedings of the National Academy of Sciences*, 104(24):9943–9948, 2007.

[28] Massimo Boninsegni. Permutation sampling in path integral monte carlo. *Journal of Low Temperature Physics*, 141(1):27–46, Oct 2005.

[29] Andrea Bonito, Juan Pablo Borthagaray, Ricardo H. Nochetto, Enrique Otarola, and Abner J. Salgado. Numerical methods for fractional diffusion. *Computing and Visualization in Science*, pages 1–28, 2018.

[30] Andrea Bonito, Wenyu Lei, and Joseph E. Pasciak. The approximation of parabolic equations involving fractional powers of elliptic operators. *Journal of Computational and Applied Mathematics*, 315:32–48, 2017.

[31] Andrea Bonito, Wenyu Lei, and Joseph E. Pasciak. On sinc quadrature approximations of fractional powers of regularly accretive operators. *Journal of Numerical Mathematics*, 2017.

[32] Andrea Bonito and Joseph E. Pasciak. Numerical approximation of fractional powers of elliptic operators. *Math. Comp.*, 84(295):2083–2110, 2015.

[33] Szymon Borak, Wolfgang Härdle, and Rafał Weron. Stable distributions. SFB 649 Discussion Papers SFB649DP2005-008, Humboldt University, Collaborative Research Center 649, 2005.

[34] Jean-Philippe Bouchaud and Antoine Georges. Anomalous diffusion in disordered media: Statistical mechanisms, models and physical applications. *Physics Reports*, 195(4–5):127–293, 1990.

[35] Brendan O. Bradley and Murad S. Taqqu. Financial risk and heavy tails. In Svetlozar T. Rachev, editor, *Handbook of Heavy Tailed Distributions in Finance*, volume 1 of *Handbooks in Finance*, pages 35 – 103. North-Holland, Amsterdam, 2003.

[36] G. A. Brosamler. A Probabilistic solution of the Neumann problem. *Math. Scand.*, 38:137–147, 1967.

[37] Steven L. Brunton, Joshua L. Proctor, and J. Nathan Kutz. Discovering governing equations from data by sparse identification of nonlinear dynamical systems. *Proceedings of the National Academy of Sciences*, 113(15):3932–3937, 2016.

[38] Luis Caffarelli and Luis Silvestre. An extension problem related to the fractional Laplacian. *Communications in Partial Differential Equations*, 32(8):1245–1260, 2007.

[39] Luis Caffarelli and Pablo Raúl Stinga. Fractional elliptic equations, Caccioppoli estimates and regularity. In *Annales de l'Institut Henri Poincare (C) Non Linear Analysis*, volume 33, pages 767–807. Elsevier, 2016.

[40] Alvaro Cartea and Diego del Castillo-Negrete. Fractional diffusion models of option prices in markets with jumps. *Physica A: Statistical Mechanics and its Applications*, 374(2):749 – 763, 2007.

[41] D. M. Ceperley. Path integrals in the theory of condensed helium. *Rev. Mod. Phys.*, 67:279–355, Apr 1995.

[42] D. M. Ceperley and E. L. Pollock. Path-integral computation of the low-temperature properties of liquid ^{4}He. *Physical Review Letters*, 56(4):351–354, 1986.

[43] J.M. Chambers, C.L. Mallows, and B.W. Stuck. A method for simulating stable random variables. *Journal of the American Statistical Association*, 71(354):340–344, 1976.

[44] Pierre Chaussé. Computing generalized method of moments and generalized empirical likelihood with R. *Journal of Statistical Software, Articles*, 34(11):1–35, 2010.

[45] Wen Chen and Guofei Pang. A new definition of fractional Laplacian with application to modeling three-dimensional nonlocal heat conduction. *Journal of Computational Physics*, 309:350 – 367, 2016.

[46] Zhen-Qing Chen. Time fractional equations and probabilistic representation. *Chaos, Solitons & Fractals*, 102:168–174, 2017.

[47] Zhen-Qing Chen, Mark M. Meerschaert, and Erkan Nane. Space–time fractional diffusion on bounded domains. *Journal of Mathematical Analysis and Applications*, 393(2):479 – 488, 2012.

[48] Zhen-Qing Chen and Renming Song. Two-sided eigenvalue estimates for subordinate processes in domains. *Journal of Functional Analysis*, 226(1):90–113, 2005.

[49] Kai Lai Chung and Zhong Xin Zhao. *From Brownian motion to Schrödinger's equation*, volume 312 of *Grundlehren der Mathematischen Wissenschaften [Fundamental Principles of Mathematical Sciences]*. Springer-Verlag, Berlin, 1995.

[50] Óscar Ciaurri, Luz Roncal, Pablo Raúl Stinga, José L. Torrea, and Juan Luis Varona. Nonlocal discrete diffusion equations and the fractional discrete Laplacian, regularity and applications. *Advances in Mathematics*, 330:688–738, 2018.

[51] Raimondas Čiegis, Vadimas Starikovičius, Svetozar Margenov, and Rima Kriauzienė. A comparison of Accuracy and Efficiency of Parallel Solvers for Fractional Power Diffusion Problems. In Roman Wyrzykowski, Jack Dongarra, Ewa Deelman, and Konrad Karczewski, editors, *Parallel Processing and Applied Mathematics*, pages 79–89, Cham, 2018. Springer International Publishing.

[52] Rama Cont and Peter Tankov. *Financial Modelling with Jump Processes*. Chapman & Hall/CRC Financial Mathematics Series. Chapman & Hall/CRC, Boca Raton, FL, 2004.

[53] P. B. Corkum. Anomalous diffusion in a magnetized plasma. *Physical Review Letters*, 31(13):809–811, 1973.

[54] R. Courant and D. Hilbert. *Methods of Mathematical Physics, Vol. I*. Interscience Publishers, New York and London, First English edition, 1953.

[55] N. Cusimano, F. del Teso, L. Gerardo-Giorda, and G. Pagnini. Discretizations of the spectral fractional Laplacian on general domains with Dirichlet, Neumann, and Robin boundary conditions. *SIAM Journal on Numerical Analysis*, 56(3):1243–1272, 2018.

[56] Edmundo Capelas de Oliveira, Felix Silva Costa, and Jayme Vaz Jr. The fractional Schrödinger equation for delta potentials. *Journal of Mathematical Physics*, 51(12):123517, 2010.

[57] R. DeBlassie. The First Exit Time of a Two-Dimensional Symmetric Stable Process from a Wedge. *Ann. Probab.*, 18:1034–1070, 1990.

[58] Ozlem Defterli, Marta D'Elia, Qiang Du, Max Gunzburger, Rich Lehoucq, and Mark M. Meerschaert. Fractional diffusion on bounded domains. *Fractional Calculus and Applied Analysis*, 18(2):342–360, 2015.

[59] Zhonghai Ding. A proof of the trace theorem of Sobolev spaces on Lipschitz domains. *Proc. Amer. Math. Soc.*, 124(2):591–600, 1996.

[60] Serena Dipierro, Xavier Ros-Oton, and Enrico Valdinoci. Nonlocal problems with Neumann boundary conditions. *Rev. Mat. Iberoam*, 33:377–416, 2017.

[61] J. D. Doll, Rob D. Coalson, and David L. Freeman. Fourier path-integral Monte Carlo methods: Partial averaging. *Phys. Rev. Lett.*, 55:1–4, Jul 1985.

[62] Jianping Dong and Mingyu Xu. Space–time fractional Schrödinger equation with time-independent potentials. *Journal of Mathematical Analysis and Applications*, 344:1005 – 1017, 2008.

[63] William Drummond and Marshall Rosenbluth. Anomalous diffusion arising from microinstabilities in a plasma. *Physics of Fluids*, 5(12):1507–1513, 1962.

[64] Maolin Du, Zaihua Wang, and Haiyan Hu. Measuring memory with the order of fractional derivative. *Nature Scientific Reports*, 3(3431), 2013.

[65] Qiang Du, Max Gunzburger, Richard B. Lehoucq, and Kun Zhou. Analysis and approximation of nonlocal diffusion problems with volume constraints. *SIAM review*, 54(4):667–696, 2012.

[66] Qiang Du, Zhan Huang, and Richard B. Lehoucq. Nonlocal convection-diffusion volume-constrained problems and jump processes. *Discrete & Continuous Dynamical Systems-Series B*, 19(4), 2014.

[67] Qiang Du, Lorenzo Toniazzi, and Zhi Zhou. Stochastic representation of solution to nonlocal-in-time diffusion. *arXiv preprint arXiv:1810.08788*, 2018.

[68] Siwei Duo, Hong Wang, and Yanzhi Zhang. A comparative study on nonlocal diffusion operators related to the fractional Laplacian. *Discrete & Continuous Dynamical Systems - B*, 24:231, 2019.

[69] David Duvenaud. The kernel cookbook: Advice on covariance functions. https://www.cs.toronto.edu/~duvenaud/cookbook/. Accessed: 2018-10-15.

[70] Albert Einstein. *Investigations on the Theory of the Brownian Movement*. Dover publications, 1956.

[71] Brenden P. Epps and Benoit Cushman-Roisin. Turbulence Modeling via the Fractional Laplacian. *arXiv preprint arXiv:1803.05286*, 2018.

[72] Stewart N. Ethier and Thomas G. Kurtz. *Markov Processes: Characterization and Convergence*, volume 282. John Wiley & Sons, 2009.

[73] Eugene F. Fama. The behavior of stock-market prices. *The Journal of Business*, 38(1):34–105, 1965.

[74] Patricio Felmer, Alexander Quaas, and Jinggang Tan. Positive solutions of the nonlinear schrödinger equation with the fractional laplacian. *Proceedings of the Royal Society of Edinburgh: Section A Mathematics*, 142(6):1237–1262, 2012.

[75] L. Feng and X. Lin. Pricing Bermudan options in Lévy process models. *SIAM Journal on Financial Mathematics*, 4(1):474–493, 2013.

[76] D. L. Freeman, R. D. Coalson, and J. D. Doll. Fourier path integral methods: A model study of simple fluids. *Journal of Statistical Physics*, 43(5):931–934, Jun 1986.

[77] Mark Freidlin. *Functional Integration and Partial Differential Equations*, volume 109 of *Annals of Mathematics Studies*. Princeton University Press, Princeton, NJ, 1985.

[78] F. Friedlander and M. Joshi. *Introduction to The Theory of Distributions*. Cambridge University Press, 2 edition, 1999.

[79] Masatoshi Fukushima, Yoichi Oshima, and Masayoshi Takeda. *Dirichlet forms and symmetric Markov processes*, volume 19. Walter de Gruyter, 2010.

[80] José E. Galé, Pedro J. Miana, and Pablo Raúl Stinga. Extension problem and fractional operators: semigroups and wave equations. *Journal of Evolution Equations*, 13(2):343–368, 2013.

[81] N. García Trillos and D. Sanz-Alonso. The Bayesian formulation and well-posedness of fractional elliptic inverse problems. *Inverse Problems*, 33(6):065006, June 2017.

[82] Paolo Gatto and Jan S. Hesthaven. Numerical approximation of the fractional Laplacian via *hp*-finite elements, with an application to image denoising. *J. Sci. Comput.*, 65(1):249–270, October 2015.

[83] Yuval Gefen, Amnon Aharony, and Shlomo Alexander. Anomalous diffusion on percolating clusters. *Phys. Rev. Lett.*, 50(1):77–80, 1983.

[84] Klaus Geissler. Classical and anomalous diffusion of an afterglow plasma. *Physical Review*, 171(1):179–180, 1968.

[85] R. Getoor. First Passage Times for Symmetric Stable Processes in Space. *Transactions of the American Mathematical Society*, 101:75–90, 1961.

[86] David Gilbarg and Neil S. Trudinger. *Elliptic partial differential equations of second order*. Springer, 2015.

[87] A. G. O. Goulart, M. J. Lazo, J. M. S. Suarez, and D. M. Moreira. Fractional derivative models for atmospheric dispersion of pollutants. *Physica A: Statistical Mechanics and its Applications*, 477:9–19, 2017.

[88] Gerd Grubb. Fractional Laplacians on domains, a development of Hörmander's theory of μ-transmission pseudodifferential operators. *Advances in Mathematics*, 268:478–528, 2015.

[89] Gerd Grubb. Regularity of spectral fractional Dirichlet and Neumann problems. *Mathematische Nachrichten*, 289(7):831–844, 2016.

[90] Qing-Yang Guan and Zhi-Ming Ma. Boundary problems for fractional Laplacians. *Stochastics and Dynamics*, 05(03):385–424, 2005.

[91] Qing-Yang Guan and Zhi-Ming Ma. Reflected symmetric α-stable processes and the regional fractional Laplacian. *Probab. Theory Relat. Fields*, 134:649–694, 2006.

[92] Mamikon Gulian and Guofei Pang. Stochastic solution of elliptic and parabolic boundary value problems for the spectral fractional laplacian. *arXiv preprint arXiv:1812.01206*, 2018.

[93] Mamikon Gulian, Maziar Raissi, Paris Perdikaris, and George Karniadakis. Machine learning of space-fractional differential equations. *arXiv preprint arXiv:1808.00931*, 2018.

[94] Mamikon Gulian, Haobo Yang, and Brenda M. Rubenstein. Fractional Path Integral Monte Carlo. *arXiv preprint arXiv:1709.09089*, 2017.

[95] Xiaoyi Guo and Mingyu Xu. Some physical applications of fractional Schrödinger equation. *Journal of Mathematical Physics*, 47(8):082104, 2006.

[96] Markus Haas and Christian Pigorsch. *Financial Economics, Fat-Tailed Distributions*, pages 308–339. Springer New York, New York, NY, 2011.

[97] Roy Haggerty, Steven M. Wondzell, and Matthew A. Johnson. Power-law residence time distribution in the hyporheic zone of a 2nd-order mountain stream. *Geophysical Research Letters*, 29(13):18–1–18–4.

[98] Emmanuel Hanert, Eva Schumacher, and Eric Deleersnijder. Front dynamics in fractional-order epidemic models. *Journal of theoretical biology*, 279(1):9–16, 2011.

[99] James Hensman, Nicolo Fusi, and Neil D. Lawrence. Gaussian processes for big data. *arXiv preprint arXiv:1309.6835*, 2013.

[100] Richard Hermann. *Fractional Calculus: An Introduction for Physicists*. World Scientific, 2nd edition, 2014. 500pp.

[101] Einar Hille and Ralph S. Phillips. *Functional analysis and semi-groups*. American Mathematical Society, Providence, R. I., 1974. Third printing of the revised edition of 1957, American Mathematical Society Colloquium Publications, Vol. XXXI.

[102] L. Hörmander. *The Analysis of Linear Partial Differential Operators I: Distribution Theory and Fourier Analysis*. Springer-Verlag, 2nd edition, 2003.

[103] (Elton) P. Hsu. Reflecting Brownian motion, boundary local time and the Neumann problem. *Dissertation Abstracts International Part B: Science and Engineering*, 45(6), 1984.

[104] K. D. Humbird, J. L. Peterson, and Ryan G. McClarren. Deep jointly-informed neural networks. *arXiv preprint arXiv:1707.00784*, 2017.

[105] Nicolas E. Humphries, Henri Weimerskirch, Nuno Queiroz, Emily J. Southall, and David W. Sims. Foraging success of biological Lévy flights recorded in situ. *Proceedings of the National Academy of Sciences*, 2012.

[106] Fritz John. *Partial differential equations, Volume 1 of Applied Mathematical Sciences*. Springer-Verlag, New York,, 1982.

[107] Mark Kac. On Distributions of certain Wiener functionals. *Transactions of the American Mathematical Society*, 65:1–13, 1949.

[108] Mark Kac. On some connections between probability theory and differential and integral equations. In *Proceedings of the Second Berkeley Symposium on Mathematical Statistics and Probability*, pages 189–215. University of California Press, Berkeley and Los Angeles, 1951.

[109] Shizuo Kakutani. Two-dimensional Brownian Motion and Harmonic Functions. *Proceedings of the Imperial Academy*, 20(10):706–714, 1944.

[110] Aharon Kapitulnik and Guy Deutscher. Percolation characteristics in discontinuous thin films of Pb. *Phys. Rev. Lett.*, 49(19):1444–1448, 1983.

[111] Tosio Kato. On the Trotter-Lie product formula. *Proc. Japan Acad.*, 50(9):694–698, 1974.

[112] James F. Kelly, Cheng-Gang Li, and Mark M. Meerschaert. Anomalous diffusion with ballistic scaling: A new fractional derivative. *Journal of Computational and Applied Mathematics*, 339:161–178, 2018.

[113] James F. Kelly, Harish Sankaranarayanan, and Mark M. Meerschaert. Boundary conditions for two-sided fractional diffusion. *Journal of Computational Physics*, 376:1089 – 1107, 2019.

[114] Panki Kim, Renming Song, and Zoran Vondraček. On the boundary theory of subordinate killed Lévy processes. *arXiv preprint arXiv:1705.02595*, 2017.

[115] Panki Kim, Renming Song, and Zoran Vondraček. Potential theory of subordinate killed Brownian motion. *Transactions of the American Mathematical Society*, 2018.

[116] Kay Kirkpatrick, Enno Lenzmann, and Gigliola Staffilani. On the continuum limit for discrete NLS with long-range lattice interactions. *Commun. Math. Phys.*, 317:563–591, 2013.

[117] Joseph Klafter and Igor M. Sokolov. Anomalous diffusion spreads its wings. *Physics World*, 18(8):29–32, August 2005.

[118] Hagen Kleinert. *Path Integrals in Quantum Mechanics, Statistics, Polymer Physics, and Financial Markets*. EBL-Schweitzer. World Scientific, 2009.

[119] Hagen Kleinert. Fractional quantum field theory, path integral, and stochastic differential equation for strongly interacting many-particle systems. *EPL (Europhysics Letters)*, 100(1):10001, 2012.

[120] Hagen Kleinert and Jan Korbel. Option pricing beyond black-scholes based on double-fractional diffusion. *Physica A: Statistical Mechanics and its Applications*, 449(Supplement C):200 – 214, 2016.

[121] Vassili N. Kolokoltsov. *Markov Processes, Semigroups and Generators*, volume 38 of *De Gruyter Studies in Mathematics*. Walter de Gruyter & Co., Berlin, 2011.

[122] Ismo Koponen. Analytic approach to the problem of convergence of truncated Lévy flights towards the Gaussian stochastic process. *Phys. Rev. E*, 52:1197–1199, Jul 1995.

[123] W. Krauth. *Statistical Mechanics: Algorithms and Computations*. EBSCO ebook academic collection. OUP Oxford, 2006.

[124] M. Kwaśnicki. Ten equivalent definitions of the fractional Laplace operator. *Fractional Calculus and Applied Analysis*, 20(1):7 – 51, Feb 2017.

[125] Andreas E. Kyprianou, Ana Osojnik, and Tony Shardlow. Unbiased "walk-on-spheres" Monte Carlo methods for the fractional Laplacian. *IMA Journal of Numerical Analysis*, 38(3):1550–1578, 2018.

[126] N. Landkof. *Foundations of Modern Potential Theory*. Springer-Verlag, 1972.

[127] Stig Larsson and Vidar Thomée. *Partial differential equations with numerical methods*, volume 45. Springer Science & Business Media, 2008.

[128] Nick Laskin. Fractional Quantum Mechanics. *Physical Review E*, 62(3):3135–3145, 2000.

[129] Nick Laskin. Fractional Schrödinger Equation. *Physical Review E*, 66:056108, 2002.

[130] Nick Laskin. Fractional Quantum Mechanics. *arXiv preprint arXiv:0811.17693*, 2008.

[131] Nick Laskin. Principles of Fractional Quantum Mechanics. *arXiv preprint arXiv:1009.5533*, 2010.

[132] Nick Laskin. Time fractional quantum mechanics. *Chaos, Solitons & Fractals*, 102:16–28, 2017.

[133] K. A. Lazopoulos. Non-local continuum mechanics and fractional calculus. *Mechanics Research Communications*, 33(6):753–757, 2006.

[134] Xianjuan Li, Zhiping Mao, Fangying Song, Hong Wang, and George Em Karniadakis. A fast solver for spectral element approximation applied to fractional differential equations using hierarchical matrix approximation. *arXiv preprint arXiv:1808.02937*, 2018.

[135] J. L. Lions and E. Magenes. *Problemes aux limites non homogenes et applications*. Dunod, 1968.

[136] P. L. Lions and A. S. Sznitman. Stochastic differential equations with reflecting boundary conditions. *Communications on Pure and Applied Mathematics*, 37(4):511–537, 1984.

[137] Anna Lischke, Guofei Pang, Mamikon Gulian, Fangying Song, Christian Glusa, Xiaoning Zheng, Zhiping Mao, Wei Cai, Mark M. Meerschaert, Mark Ainsworth, and George Em Karniadakis. What Is the Fractional Laplacian? *arXiv preprint arXiv:1801.09767*, 2018.

[138] Zichao Long, Yiping Lu, Xianzhong Ma, and Bin Dong. PDE-Net: Learning PDEs from Data. *arXiv preprint arXiv:1710.09668*, 2017.

[139] Francesco Mainardi and Gianni Pagnini. The role of the Fox-Wright functions in fractional sub-diffusion of distributed order. *Journal of Computational and Applied Mathematics*, 207:245–257, 2007.

[140] Andrew Majda and Peter Kramer. Simplifed models for turbulent diffusion: Theory, numerical modelling, and physical phenomena. *Physics Reports*, 314(4–5):237–574, 1999.

[141] Benoît Mandelbrot. The variation of certain speculative prices. *The Journal of Business*, 36, 1963.

[142] N.H. March, W.H. Young, and S. Sampanthar. *The Many-body Problem in Quantum Mechanics*. Dover books on physics. Dover Publications, 1967.

[143] Ana-Maria Matache, Christoph Schwab, and Thomas P. Wihler. Fast numerical solution of parabolic integrodifferential equations with applications in finance. *SIAM J. Scientific Computing*, 27(2):369–393, 2005.

[144] Mark M. Meerschaert, David A. Benson, and Boris Bäumer. Multidimensional advection and fractional dispersion. *Physical Review E*, 59(5):5026, 1999.

[145] Mark M. Meerschaert, David A Benson, Hans-Peter Scheffler, and Boris Baeumer. Stochastic solution of space-time fractional diffusion equations. *Physical Review E*, 65(4):041103, 2002.

[146] Mark M. Meerschaert, Jeff Mortensen, and Stephen W. Wheatcraft. Fractional vector calculus for fractional advection–dispersion. *Physica A: Statistical Mechanics and its Applications*, 367:181 – 190, 2006.

[147] Mark M. Meerschaert, Farzad Sabzikar, and Jinghun Chen. Tempered fractional calculus. *Journal of Computational Physics*, 293:14–28, 2015.

[148] Mark M. Meerschaert and Hans-Peter Scheffler. Limit theorems for continuous-time random walks with infinite mean waiting times. *Journal of Applied Probability*, 41:623–638, 2004.

[149] Mark M. Meerschaert and Alla Sikorskii. *Stochastic models for fractional calculus*, volume 43 of *De Gruyter Studies in Mathematics*. Walter de Gruyter & Co., Berlin, 2012.

[150] Nicholas Metropolis, Arianna W. Rosenbluth, Marshall N. Rosenbluth, Augusta H. Teller, and Edward Teller. Equation of state calculations by fast computing machines. *The Journal of Chemical Physics*, 21(6):1087–1092, 1953.

[151] Nicholas Metropolis and Stanislaw Ulam. The Monte Carlo method. *Journal of the American statistical association*, 44(247):335–341, 1949.

[152] Ralf Metzler and Joseph Klafter. The random walk's guide to anomalous diffusion: a fractional dynamics approach. *Physics Reports*, 339(1):1 – 77, 2000.

[153] S. Molchanov and E. Ostrovskii. Symmetric Stable Processes as Traces of Degenerate Diffusion Processes. *Theory Probab. Appl.*, 14(1):128–131, 1968.

[154] Bradley Moskowitz and Russel E. Caflisch. Smoothness and dimension reduction in quasi-Monte Carlo methods. *Mathematical and Computer Modelling*, 23(8):37–54, 1996.

[155] Mervin E. Muller. Some Continuous Monte Carlo methods for the Dirichlet problem. *Ann. Math. Statist.*, 27(3):569–589, 09 1956.

[156] Kevin P. Murphy. *Machine Learning: A Probabilistic Perspective*. The MIT Press, 2012.

[157] Mark Naber. Time fractional Schrödinger equation. *Journal of Mathematical Physics*, 45(8):3339–3352, 2004.

[158] Ricardo H. Nochetto, Enrique Otàrola, and Abner J. Salgado. A PDE approach to fractional diffusion in general domains: A priori error analysis. *Foundations of Computational Mathematics*, 15(3):733–791, 2015.

[159] John P. Nolan. *Maximum Likelihood Estimation and Diagnostics for Stable Distributions*, pages 379–400. Birkhäuser Boston, Boston, MA, 2001.

[160] Ryan Nora, Jayson Luc Peterson, Brian Keith Spears, John Everett Field, and Scott Brandon. Ensemble simulations of inertial confinement fusion implosions. *Statistical Analysis and Data Mining: The ASA Data Science Journal*, 10(4):230–237, 2017.

[161] Guofei Pang, Wen Chen, and K. Y. Sze. Gauss–Jacobi-type quadrature rules for fractional directional integrals. *Computers and Mathematics with Applications*, 66(5):597–607, 2013.

[162] Guofei Pang, Lu Lu, and George Em Karniadakis. fPINNs: Fractional physics-informed neural networks. *arXiv preprint arXiv:1811.08967*, 2018.

[163] Guofei Pang, Paris Perdikaris, Wei Cai, and George Em Karniadakis. Discovering variable fractional orders of advection–dispersion equations from field data using multi-fidelity Bayesian optimization. *Journal of Computational Physics*, 348:694 – 714, 2017.

[164] J. L. Peterson, K. D. Humbird, J. E. Field, S. T. Brandon, S. H. Langer, R. C. Nora, B. K. Spears, and P. T. Springer. Zonal flow generation in inertial confinement fusion implosions. *Physics of Plasmas*, 24(3):032702, 2017.

[165] Tibor K. Pogany and Saralees Nadarajah. On the characteristic function of the generalized normal distribution. *Comptes Rendus Mathematique*, 348(3):203 – 206, 2010.

[166] E. L. Pollock and D. M. Ceperley. Simulation of quantum many-body systems by path-integral methods. *Phys. Rev. B*, 30:2555–2568, Sep 1984.

[167] Nicolas Privault. Potential theory in classical probability. In *Quantum potential theory*, volume 1954 of *Lecture Notes in Math.*, pages 3–59. Springer, Berlin, 2008.

[168] M. Raissi and G. E. Karniadakis. Hidden physics models: Machine learning of nonlinear partial differential equations. *Journal of Computational Physics*, 357:125–141, March 2018.

[169] M. Raissi, P. Perdikaris, and G. Karniadakis. Numerical Gaussian Processes for Time-Dependent and Nonlinear Partial Differential Equations. *SIAM Journal on Scientific Computing*, 40(1):A172–A198, 2018.

[170] Maziar Raissi. Parametric Gaussian Process Regression for Big Data. *arXiv preprint arXiv:1704.03144*, 2017.

[171] Maziar Raissi. Deep hidden physics models: Deep learning of nonlinear partial differential equations. *arXiv preprint arXiv:1801.06637*, 2018.

[172] Maziar Raissi, Paris Perdikaris, and George Em Karniadakis. Inferring solutions of differential equations using noisy multi-fidelity data. *Journal of Computational Physics*, 335:736 – 746, 2017.

[173] Maziar Raissi, Paris Perdikaris, and George Em Karniadakis. Machine learning of linear differential equations using Gaussian processes. *Journal of Computational Physics*, 348:683 – 693, 2017.

[174] Maziar Raissi, Paris Perdikaris, and George Em Karniadakis. Physics informed deep learning (Part I): Data-driven solutions of nonlinear partial differential equations. *arXiv preprint arXiv:1711.10561*, 2017.

[175] Maziar Raissi, Paris Perdikaris, and George Em Karniadakis. Physics informed deep learning (Part II): data-driven discovery of nonlinear partial differential equations. *arXiv preprint arXiv:1711.10566*, 2017.

[176] Maziar Raissi, Paris Perdikaris, and George Em Karniadakis. Multistep neural networks for data-driven discovery of nonlinear dynamical systems. *arXiv preprint arXiv:1801.01236*, 2018.

[177] C. E. Rasmussen and C. K. I. Williams. *Gaussian Processes for Machine Learning*. Adaptive Computation and Machine Learning. MIT Press, Cambridge, MA, USA, January 2006.

[178] M. Reed and B. Simon. *Methods of Modern Mathematical Physics I: Functional Analysis*. Academic Press, Revised and enlarged edition edition, 1980.

[179] Lewis Richardson. Atmospheric diffusion shown on a distance-neighbour graph. *Proceedings of the Royal Society A*, 110(756):709–737, 1926.

[180] Luz Roncal and Pablo Raúl Stinga. Transference of fractional Laplacian regularity. In *Special functions, partial differential equations, and harmonic analysis*, pages 203–212. Springer, 2014.

[181] Luz Roncal and Pablo Raúl Stinga. Fractional Laplacian on the torus. *Communications in Contemporary Mathematics*, 18(03):1550033, 2016.

[182] X. Ros-Oton and J. Serra. The Dirichlet problem for the fractional Laplacian: Regularity up to the boundary. *Journal de Mathematiques Pures et Appliquees*, 101:275–302, 2014.

[183] W. Rudin. *Functional Analysis*. McGraw-Hill, 2nd edition, 1991.

[184] Samuel H. Rudy, Steven L. Brunton, Joshua L. Proctor, and J. Nathan Kutz. Data-driven discovery of partial differential equations. *Science Advances*, 3(4), 2017.

[185] S. G. Samko, A. A. Kilbas, and O. I. Maričev. *Fractional integrals and derivatives*. Gordon and Breach Science Publ., 1993.

[186] Gennady Samoradnitsky and Murad Taqqu. *Stable non-Gaussian random processes: stochastic models with infinite variance*. Routledge, 2017.

[187] Ken-iti Sato. *Lévy processes and infinitely divisible distributions*, volume 68 of *Cambridge Studies in Advanced Mathematics*. Cambridge University Press, Cambridge, 2013. Translated from the 1990 Japanese original, Revised edition of the 1999 English translation.

[188] Enrico Scalas and Kyungsik Kim. The Art of Fitting Financial Time Series with Lévy Stable Distributions. *Journal of the Korean Physical Society*, 50, 09 2006.

[189] Michael Schmidt and Hod Lipson. Distilling free-form natural laws from experimental data. *Science*, 324(5923):81–85, 2009.

[190] Rina Schumer, David A. Benson, Mark M. Meerschaert, and Boris Baeumer. Fractal mobile/immobile solute transport. *Water Resources Research*, 39(10), 2003.

[191] Simone Secchi. Ground state solutions for nonlinear fractional Schrödinger equations in $\mathbb{R}^n$. *Journal of Mathematical Physics*, 54(3):031501, 2013.

[192] Tony Shardlow. A walk outside spheres for the fractional Laplacian: fields and first eigenvalue. *arXiv preprint arXiv:1803.03921*, 2018.

[193] B. Simon. *Functional Integration and Quantum Physics*. American Mathematical Society, second edition, 2005.

[194] T. H. Solomon, E. R. Weeks, and H. L. Swinney. Chaotic advection in a two-dimensional flow: Lévy flights and anomalous diffusion. *Physica D*, 76:70–84, 1994.

[195] Fangying Song, Chuanju Xu, and George Em Karniadakis. Computing fractional Laplacians on complex-geometry domains: algorithms and simulations. *SIAM Journal on Scientific Computing*, 39(4):A1320–A1344, 2017.

[196] Renming Song and Zoran Vondraček. Potential theory of subordinate killed Brownian motion in a domain. *Probability Theory and Related Fields*, 125(4):578–592, 2003.

[197] Renming Song and Zoran Vondraček. On the relationship between subordinate killed and killed subordinate processes. *Electronic Communications in Probability*, 13:325–336, 2008.

[198] Brian K. Spears, James Brase, Peer-Timo Bremer, Barry Chen, John Field, Jim Gaffney, Michael Kruse, Steve Langer, Katie Lewis, Ryan Nora, Jayson Luc Peterson, Jayaraman Jayaraman Thiagarajan, Brian Van Essen, and Kelli Humbird. Deep learning: A guide for practitioners in the physical sciences. *Physics of Plasmas*, 25(8):080901, 2018.

[199] Michiel Sprik, Michael L. Klein, and David Chandler. Staging: A sampling technique for the monte carlo evaluation of path integrals. *Phys. Rev. B*, 31:4234–4244, Apr 1985.

[200] Elias M. Stein. *Singular Integrals and Differentiability Properties of Functions*. Princeton University Press, 1971.

[201] Elias M. Stein and Guido Weiss. *Introduction to Fourier Analysis on Euclidean Spaces (PMS-32)*. Princeton University Press, 1971.

[202] Pablo Raúl Stinga. *Fractional powers of second order partial differential operators: extension problem and regularity theory*. PhD thesis, Universidad Autonoma de Madrid, 2010.

[203] Pablo Raúl Stinga and José Luis Torrea. Extension problem and Harnack's inequality for some fractional operators. *Communications in Partial Differential Equations*, 35(11):2092–2122, 2010.

[204] Pablo Raúl Stinga and Bruno Volzone. Fractional semilinear Neumann problems arising from a fractional Keller–Segel model. *Calculus of Variations and Partial Differential Equations*, 54(1):1009–1042, 2015.

[205] A. M. Stuart. Inverse problems: A Bayesian perspective. *Acta Numerica*, 19:451–559, 2010.

[206] Nassim Nicholas Taleb. *The black swan: The impact of the highly improbable*. Random house, 2007.

[207] P. Tankov and R. Cont. *Financial Modelling with Jump Processes, Second Edition*. Chapman and Hall/CRC Financial Mathematics Series. Taylor & Francis, 2015.

[208] Vasily E. Tarasov. Fractional vector calculus and fractional Maxwell's equations. *Annals of Physics*, 323(11):2756–2778, 2008.

[209] Luc Tartar. *An introduction to Sobolev spaces and interpolation spaces*, volume 3. Springer Science & Business Media, 2007.

[210] Lorenzo Toniazzi. Stochastic solutions for space-time fractional evolution equations on bounded domain. *arXiv preprint arXiv:1805.02464*, 2018.

[211] H. F. Trotter. On the product of semi-groups of operators. *Proceedings of the American Mathematical Society*, 10:545–551, 1959.

[212] A. W. van der Vaart. *Asymptotic Statistics*. Cambridge Series in Statistical and Probabilistic Mathematics. Cambridge University Press, 1998.

[213] Petr N. Vabishchevich. Numerically solving an equation for fractional powers of elliptic operators. *Journal of Computational Physics*, 282:289 – 302, 2015.

[214] Mark Veillette. Alpha-Stable distributions in MATLAB. http://math.bu.edu/people/mveillet/html/alphastablepub.html#17. Accessed: 2018-11-29.

[215] Loukas Vlahos, Heinz Isliker, Yannis Kominis, and Kyriakos Hizanidis. Normal and anomalous diffusion: A tutorial. *arXiv preprint arXiv:0805.0419*, 2008.

[216] Hong Wang and Ning Du. A superfast-preconditioned iterative method for steady-state space-fractional diffusion equations. *J. Comput. Phys.*, 240:49–57, May 2013.

[217] Hong Wang, Kaixin Wang, and Treena Sircar. A direct $O(N \log^2 N)$ finite difference method for fractional diffusion equations. *Journal of Computational Physics*, 229(21):8095 – 8104, 2010.

[218] Shaowei Wang and Mingyu Xu. Generalized fractional Schrödinger equation with space-time fractional derivatives. *Journal of Mathematical Physics*, 48:043502–1 – 043502–10, 2007.

[219] Mahamadi Warma. The fractional relative capacity and the fractional Laplacian with Neumann and Robin boundary conditions on open sets. *Potential Analysis*, 42(2):499–547, Feb 2015.

[220] E. R. Weeks, J. S. Urbach, and H. L. Swinney. Anomalous diffusion in asymmetric random walks with a quasi-geostrophic flow example. *Physica D*, 97:291–310, 1996.

[221] Aleksander Weron and Rafal Weron. Computer simulation of Lévy α-stable variables and processes. In *Chaos – The Interplay Between Stochastic and Deterministic Behaviour*, pages 379–392. Springer, 1995.

[222] Paul Wilmott. *Paul Wilmott Introduces Quantitative Finance*. Wiley-Interscience, New York, NY, USA, 2nd edition, 2007.

[223] Ian H. Witten, Eibe Frank, and Mark A. Hall. *Data Mining: Practical Machine Learning Tools and Techniques*. Morgan Kaufmann Publishers Inc., San Francisco, CA, USA, 3rd edition, 2011.

[224] Kailai Xu and Eric Darve. Efficient numerical method for models driven by Lévy process via hierarchical matrices. *arXiv preprint arXiv:1812.08324*, 2018.

[225] Chanhao Yan, Wei Cai, and Xuan Zeng. A parallel method for solving Laplace equations with Dirichlet data using local boundary integral equations and random walks. *SIAM Journal on Scientific Computing*, 35(4):B868–B889, 2013.

[226] Qianqian Yang, Fawang Liu, and Ian Turner. Numerical methods for fractional partial differential equations with Riesz space fractional derivatives. *Applied Mathematical Modelling*, 34(1):200–218, 2010.

[227] S. Yoshikawa and D. J. Rose. Anomalous diffusion of a plasma across a magnetic field. *Physics of Fluids*, 5(3):334–340, 1962.

[228] Kôsaku Yosida. *Functional Analysis*, volume 123 of *Grundlehren der Mathematischen Wissenschaften [Fundamental Principles of Mathematical Sciences]*. Springer-Verlag, Berlin-New York, Sixth edition, 1980.

[229] G. M. Zaslavsky. Chaos, fractional kinetics, and anomalous transport. *Physics Reports*, 371:461–580, 2002.

[230] Zhijiang Zhang, Weihua Deng, and George Em Karniadakis. A Riesz basis Galerkin method for the tempered fractional Laplacian. *SIAM Journal on Numerical Analysis*, 56(5):3010–3039, 2018.

[231] Xuan Zhao, Xiaozhe Hu, Wei Cai, and George Em Karniadakis. Adaptive finite element method for fractional differential equations using hierarchical matrices. *Computer Methods in Applied Mechanics and Engineering*, 325:56–76, 2017.

[232] Yijing Zhou and Wei Cai. Numerical Solution of the Robin problem of Laplace Equations with a Feynman–Kac Formula and Reflecting Brownian motions. *Journal of Scientific Computing*, 69(1):107–121, Oct 2016.

[233] Yijing Zhou, Wei Cai, and Elton Hsu. Computation of the local time of reflecting Brownian motion and the probabilistic representation of the Neumann problem. *Commun. Math. Sci.*, 15(1):237–259, 2017.